New Approaches For Evaluation and Controlling Alkali-Silica Reaction Damage In Deteriorated Concrete

Sameh Hassan

A Thesis

In the Department

of

Building, Civil and Environmental Engineering

Presented in Partial Fulfillment of the Requirements

For the Degree of

Doctorate of Philosophy (Civil Engineering) at

Concordia University

Montreal, Quebec, Canada

February 2019

CONCORDIA UNIVERSITY

SCHOOL OF GRADUATE STUDIES

This is to certify that the thesis prepared

By: Sameh Hassan

Entitled: New Approaches for Evaluation and Controlling Alkali-Silica Reaction Damage in Deteriorated Concrete

and submitted in partial fulfillment of the requirements for the degree of

Doctor of Philosophy (Civil Engineering)

Complies with the regulations of the University and meets the accepted standards with respect to originality and quality.

Signed by the final examining committee:

_____ Chair
Dr. Chun-Yi Su

_____ External Examiner
Dr. Medhat Shehata

_____ External to Program
Dr. Amin Hammad

_____ Examiner
Dr. Ashutosh Bagchi

_____ Examiner
Dr. Khaled Galal

_____ Thesis Co-Supervisor
Dr. Michelle Nokken

_____ Thesis Co-Supervisor
Dr. Ahmed Soliman

Approved by

Dr. Fariborz Haghighat, Graduate Program Director

March 29, 2019

_____
Dr. Amir Asif, Dean
Gina Cody School of Engineering & Computer Science

Abstract

New Approaches For Evaluation and Controlling Alkali-Silica Reaction Damage In Deteriorated Concrete

Sameh Hassan, Ph.D.

Concordia University, 2019

Alkali-Silica Reaction (ASR) is considered one of the most significant critical internal deterioration mechanisms for concrete. ASR produces internal stresses that causes expansion and extended cracks threatening the country's wealth of existing infrastructure. Since ASR recognition in 1940 by Stanton, many studies had been conducted to evaluate the degree of reactivity for different types of gravel. However, limited research has focused on studying the effect of specimens' shape and size, and casting direction on the accuracy of measured ASR expansion and find a correlation between cylindrical and standard prismatic specimens. Moreover, few studies have attempted to evaluate the optimum expansion level for controlling ASR expansion by strengthening ASR-damaged concrete.

An experimental work divided into three phases was conducted to evaluate; (1) The effect of these new approaches on ASR expansion using fused silica (FS) as a fast-acting material, (2) The selection of a suitable jacketing materials based on target performance rather than focusing only on the achieved strength investigating concrete mixtures incorporating four types of fibre and fine crumb rubber aggregates (FCRA) with and without silica fume, (3) The effectiveness of six different strengthening materials as CFRP, BFRP, mortar with GG mesh, mortar with BFRP mesh, FRC, and CRC with BFRP to suppress ASR expansion, and evaluate sensitivity of

strengthening time and testing time vs. the strengthening types on the concrete mechanical properties.

The results exhibited addition of FS caused a drastic increase in the expansion, and plays a crucial role to adversely affect concrete mechanical properties and durability index until age 180 day, then the effectiveness decreased until 548 days. Specimen geometry and size, and casting direction had a significant effect on the rate of expansion. Cylindrical specimens expanded at a higher rate than the prisms until 56 days in the range from 43% to 37%, and from 9% to 15% at 90 days until test termination at 548 days. Specimens cast vertically exhibited an increase in expansion over the others cast horizontally in the range from 2.63% to 8.41%. Specimens Ø100×200mm reveal lower expansion in the range from 5.89% to 9.52% than specimens Ø75×285mm.

Concrete mixtures incorporating steel, macro, and micro polypropylene, micro nylon fibres, and FCRA with and without SF were examined. Based on balancing between mechanical properties, durability indices, and electrical resistivity, FRC incorporating micro polypropylene with SF, and CRC contained FCRA with silica were selected as FRC and CRC jacketing.

Strengthening type, strengthening time, and testing time after applying strengthening materials showed a significant effect to control ASR expansion and enhanced the damaged concrete properties. For instance, CFRP exhibited a significant reduction in expansion compared to that with control specimens and followed by BFRP, CRC with BFRP, Mortar with GG, Mortar with BFRP, and FRC, respectively. Moreover, strengthening at early ages revealed decreases mechanical properties as a result of high residual expansion. However, testing at early ages

showed higher results proved the exposure conditions had an adverse effect on the strengthening materials.

ACKNOWLEDGMENTS

This dissertation has been carried out under the supervision of Dr. Michelle Nokken, and Dr. Ahmed Soliman. I would like to thank my professors for all guidance, academic support, and positively believing in my work during research. Moreover, I would like to thank all Concordia staff especially technician team.

Furthermore, I would like to express my sincere gratitude and appreciation to all companies supporting me and research with materials as a donation: Lafarge CA, Sika CA, BSAF Corp., Saint Gobain ADFORS-USA, Forta-Ferro-USA, Arcelor metal, Precision Electro Minerals Co. (PEMCO)-USA, Englobe laboratory, and Ministry of Transportation - Ontario (MTO).

.

DEDICATION

TO THE SOUL OF MY MARVELOUS AND LOVELY PARENTS

"FATHY DIAB AND SABAH HASSAN"

THEY SANCTIFIED THE FAMILY LIFE AND CONSECRATED ALL THEIR LIFE TO THEIR CHILDREN

TO ALL OF MY SISTERS AND BROTHERS

"MERFAT, ASHRAF, MOHAMED, NAGLAA, NABILA"

TO THE GREATEST IN MY WORLD;

MY WIFE AND KIDS;

"HEND AHMED"

"REMAS, BARAA, EBAA, AND RETAL"

TO MY TEACHERS

AND

FRIENDS

Table of Contents

List of Figures

List of Tables

NOMENCLATURE

%	*Percentage*
µm	*Micro Millimeter*
A	*Cross-Sectional Area*
a	*Area (mm^2)*
AAR	*Alkali Aggregate Reaction*
AASHTO	*American Association of State Highway and Transportation Officials*
AC	*Alternating Current*
ACI	*American Concrete Institute*
AEA	*Air Entraining Admixture*
AMBT	*Accelerated Mortar Bar Test*
ASG	*Alkali-Silica Gel*
ASR	*Alkali-Silica Reaction*
ASTM	*American Society for Testing and Materials*
BCS	*Brass Coated Steel*
BD	*Bulk Diffusion*
BFM	*Basalt Fabric Mesh*
BFRP	*Basalt Fibre Reinforced Polymer*
BR	*Bulk Resistivity*
Ca^2+	*Calcium Ions*
CFRP	*Carbon Fibre Reinforced Polymer*
CPT	*Concrete Prism Test*
CRC	*Crump Rubber Concrete*
CS	*Compressive Strength*
CSA	*Canadian Standard Association*
D	*Diameter*
d	*Water Density (gm/mm^3)*
D1	*Plastic Deformation*
D1+D2	*Total Deformation*
DT_s	*Destructive Tests*

ERT_s	*Electrical Resistivity Tests*
$f\acute{c}$	*Compressive Strength*
FCRA	*Fine Crumb Rubber Aggregate*
FHAW	*Federal Highway Administration*
FRC	*Fibre Reinforcement Concrete*
FRP	*Fibre Reinforcement Polymer*
FS	*Fused Silica*
f_t	*Tensile Strength*
g	*Gramm*
GFRP	*Glass Fibre Reinforced Polymer*
GGBS	*Ground granulated blast-furnace slag*
GGM	*Glass Grid Mesh*
GU	*General Use Cement*
HA	*Hysteresis Area*
HE	*Hooked End Steel Fibres*
HRA	*High Reactive Aggregate*
HRM	*High Reactive Metakaolin*
HRWRA	*High Range Water Reducing Admixture*
HS	*Hooked Steel*
I	*Current by Amperes*
I	*Absorption (mm)*
J/m^3	*Jole Per Qubic Meter*
K+	*Potassium Ions*
K_2O	*Potassium oxide*
kHz	*Kilo Hertz*
KN	*Kilo Newton*
l	*Length*
L_{eff}	*Effective Length*
L_i	*Initial Length*
Li_2CO_3	*Lithium Carbonate*
Li_2O	*Lithium oxide*

Li_2SO_4	*Lithium Sulfate*
LiCl	*Lithium Chloride*
$LiNO_3$	*Lithium Nitrate*
LiOH	*Lithium Hydroxide*
L_n	*Length Measured at (n) Day*
LRA	*Low Reactive Aggregate*
mm	*Millimeter*
MOE	*Modulus Of Elasticity*
MOR	*Modulus Of Rupture*
MPa	*Mega Pascal*
m_t	*Mass in Grams at Time (t)*
MTO	*Ministry of Transportation - Ontario*
Na+	*Sodium ions*
Na_2O	*Sodium Oxide*
Na_2Oe	*Total Equivalent Alkaline*
NaCl	*Sodium Chloride*
NaOH	*Sodium Hydroxide*
NCA	*Natural Coarse Aggregate*
NDT_s	*Non-Destructive Tests*
NFA	*Natural Fine Aggregate*
NiCl	*Nickel Chloride*
NRA	*Non-Reactive Aggregate*
Ø	*Diameter*
^oC	*Temperature in Celsius*
OH^-	*hydroxyl ions*
P	*Maximum Applied Load*
PC	*Plain Concrete*
PDI	*Plasticity Deformation Index*
pH	*Logarithmic Scale Used to Specify The Acidity or Basicity of An Aqueous Solution*
PVA	*Polyvinyl Alcohol*

Q	***Charge by Coulombs***
RA	***Reactive Aggregate***
RC	***Reinforced Concrete***
RCPT	***Rapid Chloride Permeability Test***
RH	***Relative Humidity***
S	***Sorptivity***
s	***Second***
S1	***Irreversible Energy of Concrete (Hysteresis Area)***
S2	***Elastic Deformation Energy***
SRCA	***Spratt Reactive Coarse Aggregate***
SCMs	***Supplementary Cementitious Materials***
SDI	***Stiffness Damage Index***
SDT	***Stiffness Damage Test***
SF	***Silica Fume***
Si¯O¯	***Silanol***
SMF	***Steel Micro fibre***
SR	***Surface Resistivity***
SRFA	***Spratt Reactive Fine Aggregate***
SSD	***Saturated Surface Dry***
TS	***Tensile Strength***
UPV	***Ultrasonic Pulse Velocity***
V	***Volt***
W/C	***Water Cement Ratio***
Wi	***Initial Mass***
Wn	***Mass Measured at (n) Day***
υ	***Poison Ratio***

Chapter

1

Introduction

1.1 General Background and Problem Definition

The existing infrastructure is considered a significant part of social wealth. It should have special care and periodic maintenance to protect from the attack of various types of aggressive materials and harsh environmental conditions. Alkali-silica reaction (ASR) is one of the most significant critical internal deterioration mechanisms and undesirable for concrete. It can lead to premature and unforeseen deterioration, loss of serviceability and obsolescence many, if not all, types of infrastructure and roads around the world.

The first publication related to the ASR degradation was in 1940 through the discussion of the cracked structures in California highways (Stanton, 1940). However, many of the existing infrastructures that have been built since that time reveal the typical symptoms of rapid deterioration due to ASR. These infrastructures require proper techniques for rehabilitation and external strengthening to counteract the produced internal stresses resulting from ASR. Many variables govern the selection of these methods and materials such as; susceptibility of forming Alkali-Silica gel, degree, and rate of deterioration, the structural element (shape and location), weathering condition, and cost.

On the other side, the new concrete can design to mitigate ASR by; Identifying the primary sources that trigger ASR before preparing concrete such as; sufficient moisture, alkali, and reactive silica. Moreover, the utilization of suitable materials that can control ASR as; using of

Supplementary Cementitious materials (SCMs), Lithium, and various types of fibres have been recommended.

This research covered the examination and evaluation of the deteriorated concrete specimens performance before and after strengthening at different ages. These strengthening techniques will include wrapping by carbon and basalt fibre reinforced polymer (CFRP, and BFRP), basalt fabric mesh (BFM), and glass grid mesh (GGM) with mortar. In addition, two different types of concrete mixtures were used for jacketing; (1) polypropylene fibre with silica fume, and (2) fine crumb rubber aggregate (FCRA) with silica fume.

1.2 Scope and Objectives of The Dissertation Research

The primary goal of the dissertation is to examine the convenience and efficiency of the integration of numerous techniques and materials for strengthening and to mitigate the deleterious effect of ASR on existing concrete infrastructure.

The main objectives are:

Through an experimental work:

1. Identify the most appropriate strengthening materials for jacketing including SCMs as silica fume (SF), and;
    - Different types of fibre as; steel, polypropylene (macro and micro), and nylon.
    - Fine Crumb Rubber Aggregate (FCRA).
2. Evaluate the performance of various externally strengthening methods to counteract the internal stresses produced by ASR including:
    - Carbon Fibre Reinforcement Polymers (CFRP),
    - Basalt Fibre Reinforcement Polymers (BFRP),

- Basalt Fabric Mesh (BFM),
- Glass Grid Mesh (GGM),
- Concrete jacketing prepared with micro Polypropylene fibre and silica fume (SF),
- Concrete jacketing prepared with Fine Crumb Rubber aggregate (FCRA) and SF.

3. Investigate the correlation between time of applied strengthening and different strengthening methods under harsh environmental conditions.
4. Compare the conventional evaluation techniques including, compressive strength, and modulus of elasticity with Stiffness Damage Test (SDT).
5. Rank repair method based on concrete properties enhancement, and ease.

1.3 Organization of The Dissertation

The dissertation covering state of the art for materials used for strengthening the existing concrete suffered from the deleterious effect of alkali-silica reaction, and the suggesting methodology plan for achieving an adequate strengthening technique. A total of seven chapters in addition to references will be presented in this dissertation.

Chapter 1, traces the problem definition and the primary objective of the research. **Chapter 2**, begin with an introduction to defining the ASR and its mechanism, description the factors govern the reaction development in concrete. In addition, reviewed ASR common symptoms and deleterious effect on the concrete properties. Moreover, presents the materials used to mitigate or relief the ASR in existing concrete. **Chapter 3**, dealt with the description in details the three main phases of the experimental work plan, including the materials, tests procedure, devices (machines), and specimens. **Chapter 4**, provides the evaluation and detection of the degree of damage in concrete and mortar specimens contain Spratt aggregate Type #3 and fused silica (FS) as fastening material including; experimental work, results, and analysis. **Chapter 5**, presents the

quantification of concrete and mortar mixtures properties contains SCMs as silica fume (SF), fine crumb rubber aggregate, and four different types of fibres as steel, polypropylene (macro and micro) and nylon fibres. This chapter, includes the experimental work, results, and analysis. **Chapter 6** discusses the remedy methods of strengthening for deteriorated concrete specimens using six different methods, testing, results, and analysis. Finally, **Chapter 7** describes the conclusion of the dissertation, contribution, the recommendation based on the results (i.e. future work), and list of publications.

Chapter

2

Literature review

2.1 Alkali-Silica Reaction

2.1.1 Alkali-Silica Definition

Alkali-silica reaction (ASR) is defined as; a chemical reaction between reactive silica presented in aggregate particles, and alkalis (Na_2O and K_2O) contained into the cement paste (Neville2002, Hou, et al., 2004, and Mehta and Montiero 2006). The product of ASR is alkali-silica gel (ASG), this gel has the ability to absorb water from its surrounding hydrated cement past and external sources and expands (Forster et al., 1998, Neville2002, and Mehta and Montiero 2006). The internal pressure results from expansion (i.e. volume increase), ASG induces internal stresses. Once these stresses exceed the concrete tensile strength limit, aggregate particles and the surrounding paste start to crack (Mehta and Montiero 2006).

2.1.2 Alkali-Silica Reaction Mechanism

Most types of concrete aggregates contain various forms of silica, which reacts chemically with the hydroxide ions present in the concrete pore fluid. The higher concentration of hydroxide leads to a higher pH and increases the probability for the attack of the reactive silica (Forster et al., 1998, Swamy 2002, Mehta and Montiero 2006, and U.S. (FHWA 2013)). Based on the microstructure (micropores) of concrete, the increase in pH of pore water occurs due to the migration of water and hydroxyl ions (OH^-) released from the water-soluble alkalis. At high pH,

dissolution of silica occurs, and rupture in the siloxane bridge occurs and forms a silanol Si–O^- bond. The dissolution of silica is affected by pore solution pH, the concentration of cations (i.e. Na^+, K^+, Ca^{2+}), temperature, and the particle size of the silica.

Alkali-silica gel starts to swell after absorbing moisture and produces internal stresses. These stresses are considered the main reasons for the cracks into the aggregate particles and the surrounding cement paste. These cracks can expose the concrete members to different forms of damage as corrosion, stiffness loss, and ingress of deleterious substances (Forster et al., 1998, Swamy 2002, and Mehta and Montiero 2006). Formation of Alkali-silica Gel illustrated in **Fig. (2.1).**

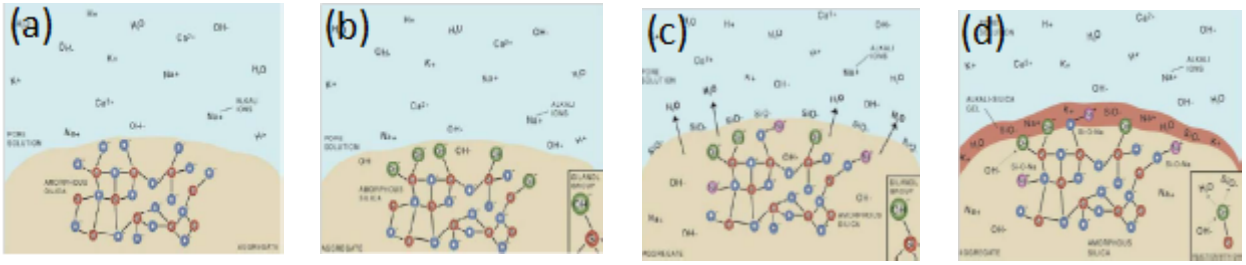

Figure (2.1) Formation of alkali-silica gel

(a) Amorphous siliceous aggregate, (b) OH^- ions penetration into aggregate, (c) Formation of Si−O^-, and (d) Formation of ASR gel

[Collins et al., 2015]

2.1.3 Factors affecting Alkali-Silica Reaction

The primary factors govern ASR are sufficient moisture, sufficient alkali, and reactive silica from the aggregate particles (Forster et al., 1998, Neville2002, United States Federal Aviation Administration 2004, and Montiero 2006, and U.S. (FHWA 2013)) as shown in **Fig. (2.2)**. In addition, the selected materials to prepare different concrete mixtures, the environmental and

exposure conditions, test conditions, and specimens (type, shape, and size) plays a crucial role in the expansion rate.

For instance, the temperature affects the expansion rate and level. According to the standards used as a reliable reference to quantify and evaluate the ASR, the typical temperature condition used in laboratory test are 38 ^{o}C and 80 ^{o}C for the concrete prism test (CPT), and accelerated mortar bar test (AMBT), respectively. Some of the experimental works exhibit, the higher the temperature, the higher the expansion rate (Fournier et al., 2009, and Gautam and Panesar 2017).

For example, raising the temperature of CPT prisms contains the same reactive aggregate by 12 ^{o}C from 38 ^{o}C to 50 ^{o}C, accelerated the expansion by about 3.22 times (Gautam and Panesar 2017). However, sometimes the increasing of temperature can cause a reduction in expansion due to a reduction of the hydroxyl ion concentration, increased leaching of alkalies, use of non-reactive aggregate, and dry the prisms at a higher temperature (Ideker et al., 2010). Moreover, the experimental and outdoor specimens carried out by utilized different aggregate types with various degree of reactivity reveals; the warmer environmental accelerate the expansion in a range from 4 to 5 times than the cooler climatic condition (Fournier et al., 2009). In addition, the expansion of CPT increased by increasing the temperature for the same type of aggregate as shown in **Fig. (2.3)** (Latifee et al., 2014).

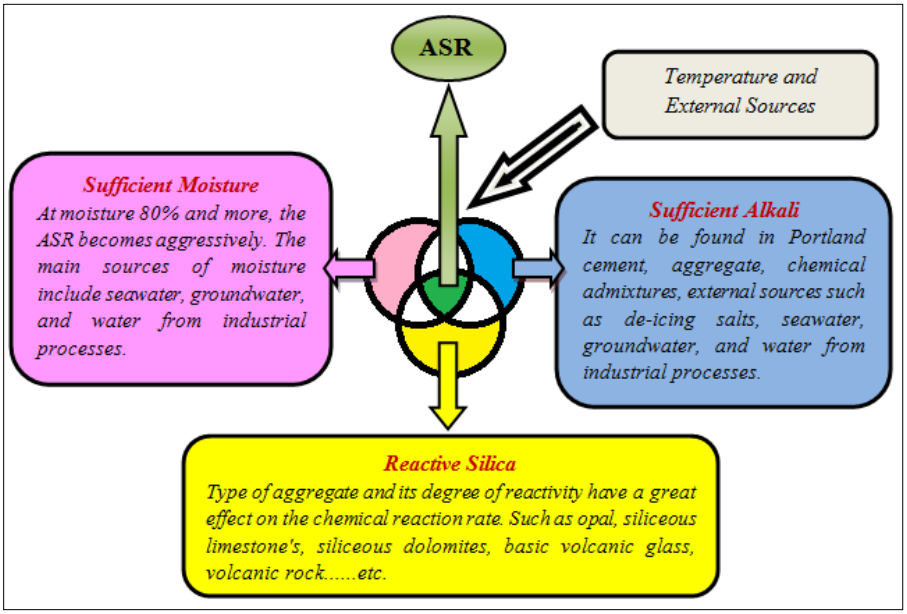

Figure (2.2) Primary factors govern ASR

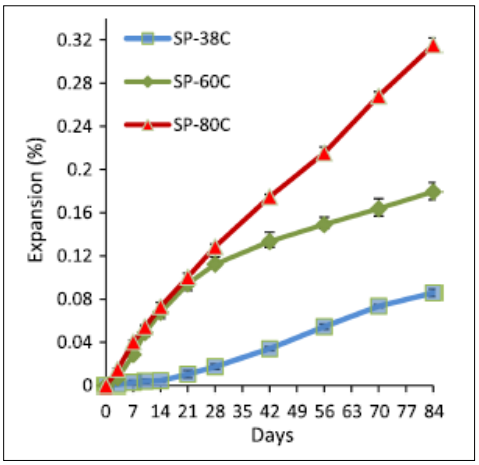

Figure (2.3) Effect of temperature increase on the expansion rate for Spratt aggregate [Latifee et al., 2014]

Moreover, the studies conducted to evaluate the effect of specimens size on the expansion concluded the large specimens would expand less than the small specimens (Ahmed et al., 1999, and Gautam and Panesar 2017). As a result; the concrete bearing strength reduced by about 3%, and 35% in large and small Reinforced concrete (RC) specimens, respectively (Ahmed et al., 1999).

Furthermore, the concrete type considered a significant factor effect on expansion. RC reveals the lower level of both expansion and loss of the mechanical properties than Plain concrete (PC) due to the presence of reinforcement bars and stirrups (Ahmed et al., 1999, Smaoui et al., 2007, Haddad et al., 2008, and Musaoglu et al., 2014). These due to the cracks produced at the surface of PC prisms were extensive and continuous, while cracks of short length, small in width, and discontinuous formed on RC beams surface (Haddad et al., 2008). As a result of these cracks; both compression and splitting strength recorded a higher deduction by about 42% and 35% respectively into the PC concrete specimens (Haddad et al., 2008). Moreover, The RC reveal less reduction in bearing capacity than the PC (Ahmed et al., 1999).

In addition, the final expansion and mechanical properties of concrete specimens contain reactive aggregate govern by the curing method. The steam is curing exhibit higher expansion and less compression strength more than the typical curing (Shayan et al., 2006).

2.1.4 Common Symptoms of Alkali-Silica Reaction

The deleterious effect of ASR on concrete is known as a long-term that takes several years with slow rate (Pan et al., 2012). Where its associated with different defects such as displacement, closure of joints, Joint misalignment, Blow up/buckling/heaving, cracking ranging from 0.1mm to 10mm in the extreme cases, network of cracks (map) in plain concrete, cracks parallel to the reinforcement bars in RC concrete, corner break, D-cracking, aggregate pop-out, reaction rims around aggregate particles, open or gel-filled cracks in aggregate particles, efflorescence and exudation (Forster et al., 1998, Neville2002, US. Federal Aviation Administration 2004, Mehta and Montiero 2006, and US. (FHWA 2013)).

2.1.5 Alkali-Silica Reaction Deleterious Effect

ASR had an adverse effect on the mechanical and hydraulic index of concrete and mortar. The development of cracks over time due to ASR results in the decrease of strength (compressive, tensile, and bond), modulus of elasticity, stiffness (Fan and Hanson 1998, Ben Haha, 2006, Haddad, et al.,2008, and Na et al., 2016). Moreover, this reaction can cause an increase in permeability and porosity. While, many factors govern the degree and rate of the adverse effect such as expansion level, the induced (micro and macro) cracks, and deterioration (degree & rate), test (type, procedure, and time) (Forster et al., 1998, Neville2002, US. Federal Aviation Administration 2004, and Montiero 2006, and U.S. (FHWA 2013)). In addition, the test method used to hasten the reaction over time, and the type of reactive aggregate govern the degree and rate of deterioration caused by ASR. From the previous researches carried out to quantify the adverse effects of ASR on concrete properties, there is no evidence of the concrete elements of the same structure that suffering from ASR can deteriorate to the same degree. In addition, the previous researches conducted to study the effect of ASR on the mechanical properties of concrete using different types of reactive aggregate at different exposure conditions exhibited a different adverse effect on the mechanical properties and durability index of concrete and mortar.

Compressive strength decrease in the range from 30% to 40% at 0.6 expansion, while this reduction was changed to be in the range from 10% to 60% depends primarily on the expansion level (i.e. type of reactive aggregate and fastening materials) (Swamy and Asali 1988). Fan and Hanson (1998) found no effect occurs until 90 days, while cracks start to develop with slightly effect on mechanical properties at 125 days. In addition, at 180 days, reduction occurs by about 24%, 38%, and 31% in the compressive, tensile strengths, and dynamic modulus, respectively. Other studies exhibited the less sensitivity of compressive strength compared with tensile

strength and modulus of elasticity (MOE) especially at expansion level of 0.12% and above (Shayan et al. 2008). While, compressive strength and modulus of elasticity decreased by about 28%, and 80% with high reactive aggregate, respectively (Marzouk et al., 2003). However, with moderate reactive, no adverse effect occurs in compressive strength, but the modulus of elasticity decreased by about 20% (Marzouk et al., 2003). Ben Haha, (2006) reported; with three different types of aggregate, and depends on the degree of alkaline; (1) The maximum deduction in compressive strength reached 10% for mortar and concrete specimens at 90 and 240 days, respectively. (2) Flexure strength of mortar reduced in the range from 18% to 24% after 90 days. (3) The tensile strength of concrete reduced in the range from 5% to 20% at 365 days, and (4) modulus of elasticity of concrete decreased by about from7% to 25% at 365 days. While, compressive and splitting strength of PC reduced by about 42% and 35%, respectively (Haddad et al., 2008). Contradictory data on the sensitivity of Poisson ratio to ASR produced from reactive aggregate has been reported (Larive 1997, Fan and Hanson 1998, Multon et al.,2003, Giaccio et al., 2008, and Yurtdas et al., 2013).

2.2 Mitigation of Alkali-Silica Reaction

Based on understanding the factors caused and fastening ASR, the new concrete structures can easily protect from the deleterious effect of ASR. The protection can be accomplished by selecting the proper concrete ingredients such as; non-reactive aggregates, the cement of low alkalinity, and limiting moisture and total alkali content. In addition, using pozzolanic materials like fly ash, silica fume, granulated blast furnace, metakaolin, and binary or ternary blend. Moreover can use silane, and lithium nitrate-based admixtures (US Federal Aviation Administration 2004, and U.S. (FHWA 2013)).

On the other hand, ASR into the existing concrete cannot completely suppress, especially at the presence of the main factors caused ASR. So, the stresses induced from the ASR should be neutralized with external strengthening materials. The strengthening depends mainly on the type of structural elements and its location. Various materials and techniques can accomplish the strengthening as Fibre Reinforcement Polymer (FRP), Fibre Reinforcement Concrete (FRC), concrete jacketing, packing strap, external post-tensioning, and overlay (Haddad et al., 2008, Talley et al., 2009, and Markus et al., 2013).

2.2.1 ASR - Mitigation Techniques

The strengthening of existing infrastructure aiming to increase the service life and enhance the structure element properties such as ductility and stiffness with low cost, fast method of casting, and applying the strengthening materials.

2.2.1.1 Lithium Nitrate

Lithium has been used successfully as an admixture to control the expansion in new concrete since discovered in 1951 until now (McCoy and Caldwell 1951, and Barborak 2005). Addition of Lithium changes the nature of the reaction products (i.e. lithium–silica complex is less soluble, more stable, hardly swells and dissolves), In addition, the capability of lithium to decrease silica dissolution and limit ASR gel repolymerization (Feng et al., 2005 and 2010). Many studies have been accomplished to investigate the effectiveness of lithium in different forms to control ASR. Some of these forms included lithium hydroxide (LiOH), lithium carbonate (Li_2CO_3), lithium chloride (LiCl), lithium nitrate ($LiNO_3$), and lithium sulfate (Li_2SO_4). The studies reveal the effectiveness of each lithium forms was primarily governed by some factors such as lithium dosage, alkali content, and type of reactive aggregate. For instance; the dosage of total lithium to

the total alkali (Li_2O)/(Na_2Oe) should be adopted. The studies exhibited, 0.6LiOH, 0.8$LiNO_3$, and 0.9NiCl were enough to keep the expansion of mortar bars below 0.05% after 56 days (Collins et al., 2004). Moreover, 0.6Li_2CO_3 was the appropriate ratio. These results prove the amount of lithium is related to the alkali content (Mo et al., 2010). However, the increase in the dosage had an adverse effect on the mechanical properties especially the compressive strength (Mo 2005, and Mo et al., 2010).

For existing concrete, the thickness of the concrete penetrated by lithium was the most significant problem. Many applications such as topical, electrochemical, and vacuum impregnation were used to examine the efficiency of lithium to mitigate ASR to increase the service life of the structure element (Thomas et al., 2007, Folliard et al., 2008, and Markus 2013). The topical application was conducted by using spraying system mounted on trucks or by hand pressurized spraying bottle as shown in **Fig. (2.4)** (Thomas et al., 2007, Folliard et al., 2008, and Giannini 2009). The authors found this method was not sufficient because the maximum depth of lithium was 4mm and this depth not enough to minimize the expansion (Folliard et al., 2008). This conclusion was reinforced, as the concrete slabs and columns treated by the topical application and did not showed a significant reduction in the concrete expansion (Markus 2013).

The vacuum impregnation application was used as an alternative technique for forcing the lithium into the existing concrete affected by ASR. The application starts by covering the cracked area with a plastic mesh fixed on the concrete surface by double face tape, then evacuated the air from the covered area. When the pressure reached 0.5 atmospheres, the lithium diffused into this area through a tube inserted in the plastic mesh as represented in **Fig. (2.5)**. This method in some cases reveals deep penetration of lithium into the concrete to reached about

8-10mm (Folliard et al., 2008). While other cases included bridge decks and columns, did not exhibit any observation to prove the effectiveness of vacuum impregnation to decrease ASR expansion (Markus 2013).

Figure (2.4) Topical application of lithium

(a) Spraying $LiNO_3$ on pavement surface using trucks, Idaho, USA [Folliard et al., 2008)]

(b) Hand spraying $LiNO_3$ on the concrete surface [Markus 2013]

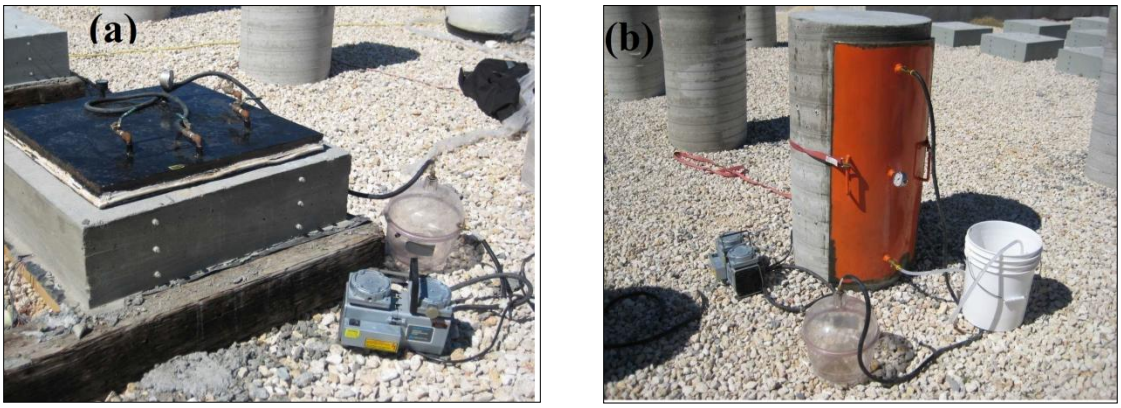

Figure (2.5) Vacuum impregnation treatment on ASR

(a,b) Using steel plates [Markus 2013]

The electrochemical application was used to forcing lithium deeply into the concrete by using an electrical current. On the concrete surface, a titanium mesh positioned between two layers of

felt was fixed and connected to a power supply to create an anode. The reinforcement steel works as a cathode connected by electrical wire through holes filled with crushed lead. Finally, plastic sheets were used to protect concrete surfaces (Thomas et al., 2007, and Markus 2013). The studies reveal this method was valid because the penetration of lithium reached 19-32mm (Thomas et al., 2007). This result reinforced by (Folliard et al., 2008), where the penetration depth was 50mm from the surface. However, the expansion measurements of the concrete columns treated by electrochemical application did not show the significant effect to reduce expansion of ASR (Markus 2013). Form the literature it is apparently, cracks characteristics as; (length, thickness, and depth) is considered a critical factor governing the efficiency of lithium to penetrate the deteriorated concrete.

2.2.1.2 Fibre Reinforcement Polymers

Composites are defined as: "materials created by a combination of two or more materials, on a macroscopic scale to form a new product with enhanced properties that are superior to those of the individual constituents alone" (ISIS educational module (6), 2006). These materials contain fibres and polymers; the polymers consider the main component in most common fibre composite matrices. Polymers play an important role such as; a binder material to collect the fibres, protective material to protect fibre from the environmental condition, and transferring forces between the fibres (ISIS educational module (6), 2006, and Täljsten et al.,2008). Fibres are available in different types such as aramid, glass, basalt, and carbon. Each type had different properties as; stiffness, tensile strength, durability, elastic modulus,…etc. These properties govern the selection of the strengthening material (Bakis et al., 2002, and Chhabra 2013).

Fibre Reinforcement Polymer (FRP) had been used in a wide range of industries due to its high efficiency and mechanical properties especially aerospace (Saafi, 2000).

Moreover, FRP characterized by high strength to weight ratio, durable against the effect of weathering conditions, non-magnetic, rapid installation, high resistance to corrosion, electronically non-conductive, and low thermal conductivity (De Lorenzis et al., 2007). FRP extended to use in the construction industries as a strengthening method to improve the strength, toughness, stiffness of the structural elements (Hensher, 2016). Typically, FRP can be applied on the structural elements with different techniques such as; wet lay-up (i.e. fibre sheets or fabrics saturated at the site), pre-preg (i.e. pre-impregnated fibre sheets of fabrics off-site) and pre-cured (i.e. composite sheets and shapes manufactured off-site). In addition, depends on FRP geometries, FRP becomes unidirectional when the fibres are oriented in one direction, and bi or multidirectional when the woven or bonded fibres in many directions.

Carbon Fibre Reinforcement Polymer (CFRP) was used to strengthening the concrete columns deteriorated by ASR of different shapes (square and cylindrical) (Shayan et al., 2008, and Shayan et al., 2009). The authors observed CFRP caused a reduction in the expansion rate, but not stop the deleterious expansion. Moreover, the cylindrical specimens reveal less expansion after strengthening than the square specimens when wrapped at the same age with the same no. of CFRP layers; this results reinforced by (Abdullah, 2012).

CFRP wrapping efficiency to control ASR governed by significant factors such as wrapping time and no. of layers. The columns wrapped at early ages produced increasing in ultimate loads and less expansion, and the increasing of CFRP layers from one to two layers caused an increase in the ultimate load as shown in **Fig. (2.6)** (Abdullah, 2012). Moreover, concrete beams strengthened by CFRP had a reduction in ductility by about 37% and 58% with one and two CFRP layers, respectively (Issa et al., 2014).

The selection of CFRP type plays a crucial factor to mitigate the ASR expansion and enhance the concrete properties after wrapping. The studies reveal, CFRP of high modulus was not effective and ruptured due to high expansion when wrapped after two months of exposure. However, the specimens wrapped after six months of exposure by one and two layers of normal CFRP showed an increase up to 30% and 50%, respectively in the loads carrying capacity (Abdullah et al., 2010).

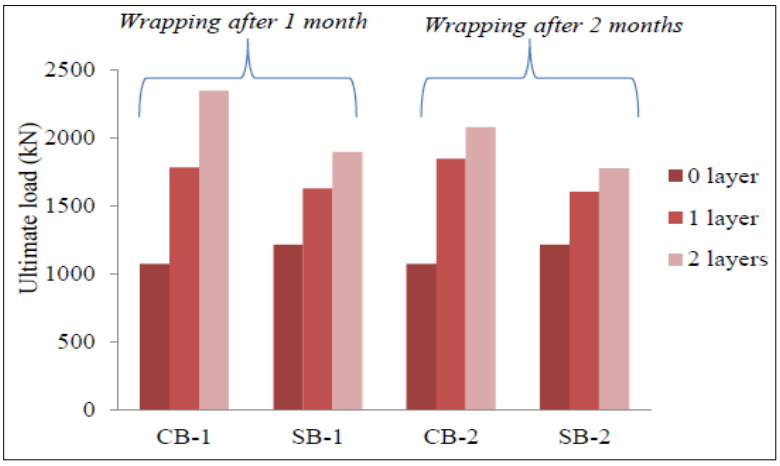

Figure (2.6) Ultimate loads of unwrapped and wrapped columns - wrapping by CFRP

(CB) Circular columns incorporating 7.5% FS and (S) Square columns incorporating 7.5% FS [Abdullah, 2012]

Moreover, the wrapping method is considered an essential factor that governs the efficiency of FRP. Qian et al., (2003), studied the effectiveness of wrapping of three different type FRP (i.e. carbon, glass, and hybrid) to restrain the alkali-aggregate expansion in concrete. The wrapping was accomplished on the radial and longitudinal direction with single and double layers. The author concluded; (1) wrapping with one layer of all FRP types reduced ASR when wrapping in both direction (i.e. radial and longitudinal). Moreover, the pulse velocity was higher than the reference specimens. In addition, the radial wrapping by one layer not improved the pulse

velocity. (2) Pulse velocity of specimens wrapped by two layers FRP was lower than the specimens wrapped in both direction, but it is higher than the specimens wrapped by one layer in the radial direction. (3) On the other hand, specimens coated with the epoxy resin did not reveal enough mitigation for ASR. (4) The higher the modulus of FRP, the better the effect of restraint. Hattori et al., (2003) found the spiral wrapping by CFRP at a pitch of 122mm increased the ductility of the concrete specimens with no rupture occurred in CFRP after two years of exposure to 40^{o}C and 100%.

Unidirectional CFRP was used to strengthening the bottom face of RC beams damaged by AAR, and the authors observed a contribution to limit the concrete expansion (i.e. slow down the effects of Alkali-Aggregate Reaction (AAR) on the face on which they were installed (Lacasse et al., 2003). It appears that the effects of AAR are "migrating" to areas that present less resistance to their actions. In addition, CFRP produced a significant increase in bending strength based on the exposure time, and the failure mode was de-bonding at the concrete/CFRP interface (Lacasse et al., 2003).

As mentioned above, FRP is durable against the effect of weathering conditions. CFRP confinement works as a barrier to reducing water infiltration by about 90% (Mohamed et al., 2005). Moreover, the load capacity of strengthened beams did not decrease after seven years of exposure to the long-term accelerated aging environment as wetting-and-drying cycles with 15% salt water solution. This proof CFRP sheets and epoxy materials are flexible to cyclic salt water exposure conditions (Issa et al., 2014). In addition, the fibre direction effect significantly on the expansion level, where the longitudinal expansion reached a level higher three times compared with the expansion reached in the transverse direction (Mohamed et al., 2005).

Moreover, an experimental work carried out to evaluate the long-term durability of the concrete beams after repair by different types FRP (i.e. carbon (C) and glass (G) under different environmental conditions (i.e. +20 ^{o}C at room temperature, 300 wet/dry cycles). The research exhibited wrapping by CFRP produced high value than the GFRP with all types of epoxy and both types of environmental condition (Toutanji and Gomez, 1997). In addition, the epoxy type had a high effect on the results of load capacity, and maximum deflection. Based on the FRP type and epoxy type; the specimens subjected to wet/dry conditions reveal less improvement than specimens kept at room temperature (Toutanji and Gomez, 1997).

Toutanji and Balaguru, (1998), extend the research to study the effect of different factors such as wet/dry and freezing/thawing on the performance of concrete columns after wrapping by FRP (C, G). The columns strengthening by CFRP was more effective than GFRP to withstand against the harsh environmental conditions, where the reduction in compressive strength was so small and no loss in ductility after exposed to wet/dry environments. Moreover, the more failure and loss of ductility occurs in specimens subjected to freezing/thawing cycling (Toutanji and Balaguru, 1998).

Finally, The bond between FRP and existing concrete considered a dominant parameter. The methods used to prepare the existing concrete before installed FRP affects mainly on the bond strength. Bond strength of FRP types (C, G) after preparing the surface by water jet and sandblast was examined. The author reported, for the CFRP, the higher the modulus, the higher the bonding with both techniques of treatment, and water get treatment produced the highest bond (Toutanji and Ortiz, 2001).

Evaluation of existing structure deteriorated by ASR was essential to select and evaluate the proper repair method. Structures damaged by ASR in Hokuriku district - Japan and subjected to three different types of repair {i.e. three types of continuous fibre sheet as a surface coating, polymer cement for section repair with shotcrete, and concrete jacketing} were evaluated. Cores drilled from these structures were accelerated in the expansion according to ASTM C1260 (2014). The analysis reveals the deterioration occurred when the andesite content and the alkali content were more than 4% and 2kg/m^3, respectively. Moreover, the increase of andesite and alkali content leads to more extensive cracks and severe deterioration (Masahiro et al., 2013). Regardless of the repair materials, the results can conclude as follow;

- Concrete jacketing was effective to suppress the residual expansion, although ASR potential of the structure was high.
- Sodium silicate was not effective in reducing ASR progress, and to fill the cracks even after 17 years of repair, because the coarse aggregate had cracks by about 0.5mm on the surface.
- Polymer cement mortar does not mitigate ASR; the cracks reoccurred on the surface of the repaired patch.
- Acrylic type of fibre sheet coating with low ASR potential was capable to suppress the residual expansion, and with high ASR potential, the urethane type of continuous fibre sheet performed well.
- The application of the epoxy type of fibre sheet coating was difficult although the core expansion reduced by 50%. This was because ASR would continue for long periods, and cracks occurred when the residual expansion was more than 0.2% due to the andesite ratio was high, and the alkali content was low (Masahiro et al., 2013).

2.2.1.3 Fibre Reinforcement Concrete

Nemours types of fibres were introduced with the concrete ingredient to enhance concrete properties. In addition, to overcome some concrete issues such as brittle behavior and cracks development (ACI 544.1 R-2009). For instance, the adding of steel fibre with 0.5% and 2% fraction increased tensile strength by about 19% to 98%, respectively, and modulus of rupture (MOR) increased by about 28.1% and 126.6%, respectively (Song and Hwang, 2004). Recently many types of fibres of different sizes, shapes, and colors are available such as steel, nylon, polypropylene, glass, and natural fibres. Many researchers have been conducted to study the FRC properties; there is an agreement, the mechanical properties of FRC much better than the normal concrete (Song et al., 2005, Bencardino et al., 2010, Khitab et al., 2013, and Tabatabaei et al.,2014).

Moreover, the effectiveness of fibre to minimize the effect of alkali-silica reaction were evaluated, there is conformity the use of fibres into the mortar, and concrete mixtures can reduce the expansion resulting from ASR. Haddad and Qudah, (2005) reported the use of brass-coated steel (BCS), hooked steel (HS), and polypropylene fibres reduced the adverse effect of ASR (i.e. expansion and cracks) in high-performance and normal-strength cement grouts.

The contribution of fibre mainly depends on the fibre type and content, exposure period and type of mixtures. For instance, the use of BCS and HS in high-performance grouts was most effective at a portion of 1% and 2% by volume, respectively. However, in normal strength grout, 0.15 vol.% from polypropylene and both of 1 and 2 vol.% from BCS fibres were effective to minify the expansion (Haddad and Qudah, 2005). In addition, the use of 0.7 vol. % steel microfibre (SMF) controlled the cracks induced by ASR by about 33.0% after 12

days, and diminish the loss of strength (Yi et al., 2005). These results were reinforced when the expansion of mortar specimens contains 2% brass coated steel fibre (BCS) reduced by about 65%, and 32% at 14 and 120 days respectively (Yazıcı, 2012). This fraction was effective in preventing flexural strength loss due to ASR at different ages and with different types of treatment as shown in **Fig. (2.7)** (Yazıcı, 2012).

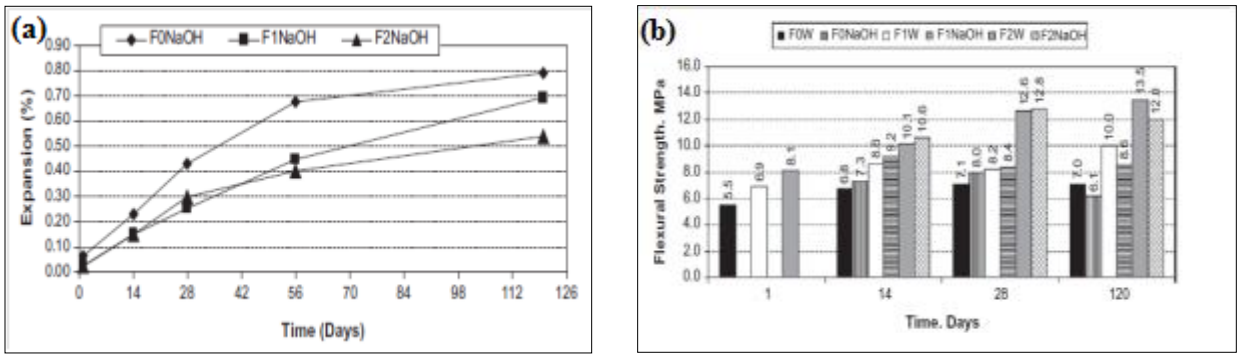

Figure (2.7) Mortar bars contained BCS fibre and treated with different types.

(a) Expansion and (b) Flexural strength

[Yazıcı, 2012]

Furthermore, the concrete mixtures contain different alkali content, types of fibres, and content reveals less damaged for cracks, highest values at all ages for compressive and bending tests, and improvement in the concrete characteristics related to the air permeability (Giaccio et al., 2015). Steel fibres were the most efficient followed by macro and micro fibres to decrease the ASR expansion after 150 days as shown in **Figure (2.8)** (Giaccio et al., 2015).

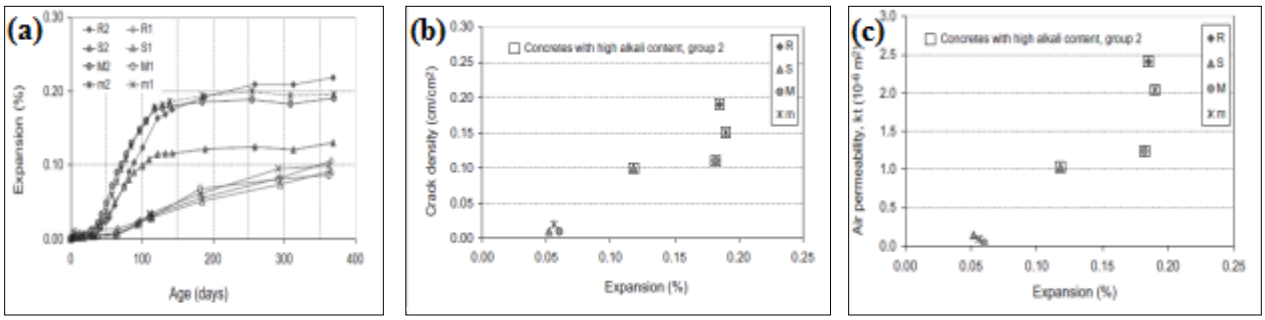

Figure (2.8) Concrete mixtures contain hooked-end steel, macro, and micro-fibres

(a) The expansion vs. time, (b) The expansion vs. crack density, and (c) The expansion vs. air permeability coefficient [Giaccio et al., 2015]

As mentioned above the characteristics of fibre and its content consider the significant factors that govern its effect. (de Carvalho et al., 2010) carried out a study to evaluate the effectiveness of steel fibre of different aspect ratio and content as; SF {(0.16mm diameter and 6.0mm length), and (0.20mm diameter and 13.0mm length)} with fibre volume contents of 1.0% and 2.0% in mortars subjected to AAR. The author concluded; the expansion reached a minimum level (i.e. 61% less) with SF13mm at 2 vol.%. On the other side, the mechanical properties (i.e. compressive strength and Young's modulus) influenced adversely at some ages as represented in **Fig. (2.9)**. The decrease in mechanical properties caused due to voids and presence of ASG in pores and interfaced paste/aggregate, moreover on the surface of the steel fibres plus the boundary of aggregate as shown in **Fig. (2.10)** (de Carvalho et al., 2010).

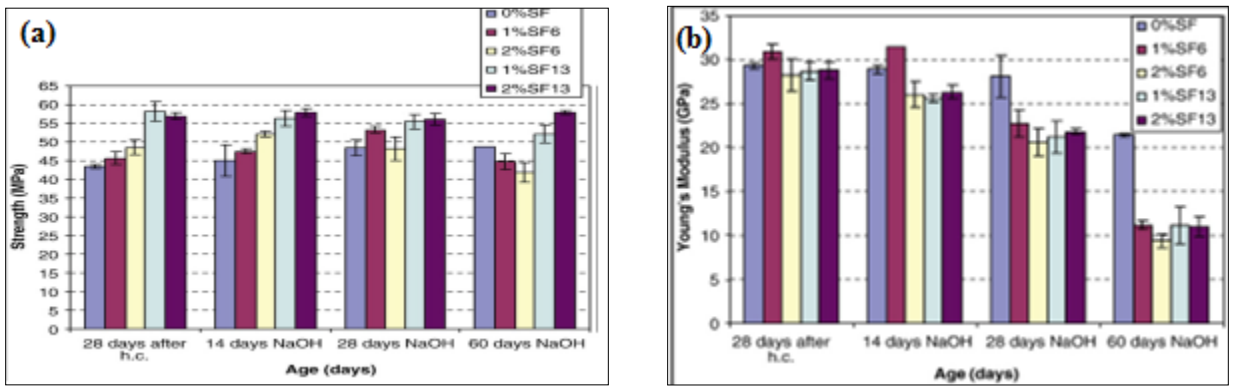

Figure (2.9) Concrete mixtures contain steel fibre

(a) Compressive strength and (b) Young's modulus [de Carvalho et al., 2010]

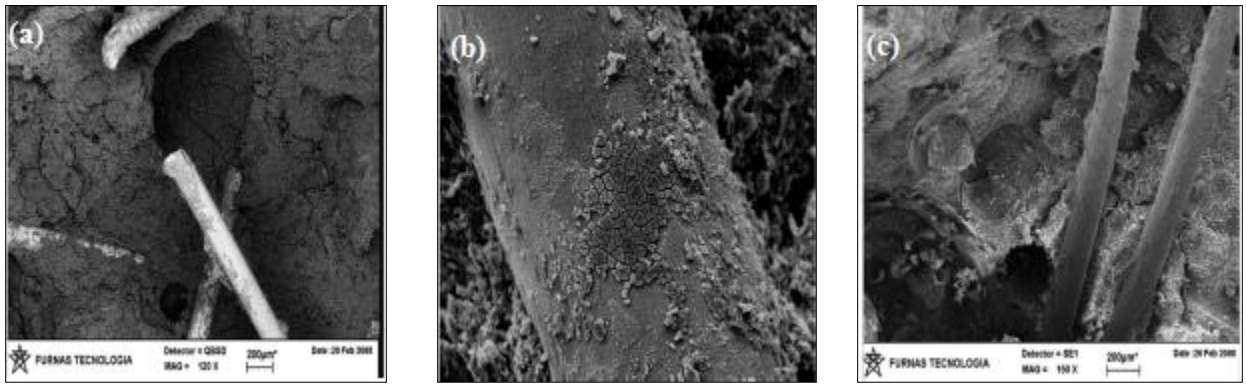

Figure (2.10) Pores and presence of alkali-silica gel (ASG)

(a) 1% SF6 Pore filled with cracked gel, and fibres around the pore, (b) ASG on fibre surface, and (c) Fibres close to the pores with cracked gel in its interior [de Carvalho et al., 2010]

Andiç et al., (2008) studied mortar mixtures contains basaltoid aggregate as a reactive material and different types of fibres such as carbon, polyvinyl-alcohol (PVA) and smooth brass coated steel microfibres. Mixtures treated traditionally according to ASTM C1260 (2014) and exposed to extended curing in water at 23 ^{o}C for 14 days, then in 80 ^{o}C water for one day, and the remaining period in 80 ^{o}C 1 N NaOH solution. Addition of fibres under the traditional curing did not significantly affect the expansion behavior of the mortars. Moreover, the steel micro-fibre increased expansions except for 3% S and 5% as shown in **Fig. (2.11)**.

However, the specimens exposed to extend curing reveal an improvement to decrease the expansion to be lower than the maximum approved limit 1% as shown in **Fig. (2.12)**.

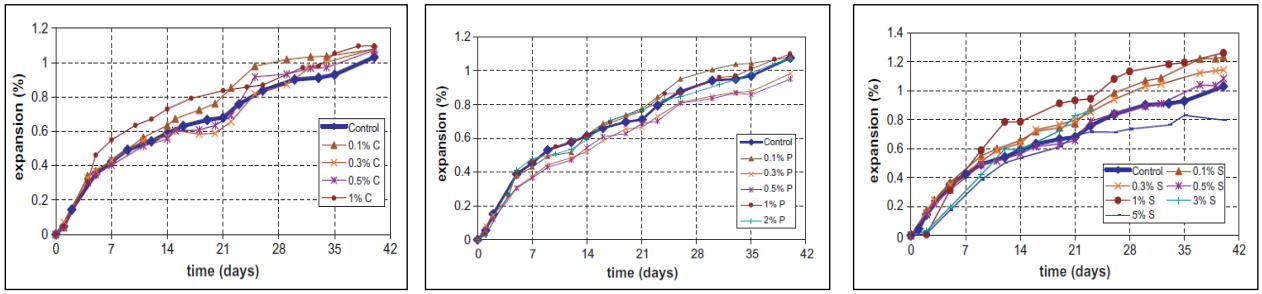

Figure (2.11) Expansion of mortar contains different types of fibres types and content treated traditionally according to ASTM C1260

(a) Carbon fibre, (b) PVA fibre, and (c) Brass coated Steel fibre [Andiç et al., 2008]

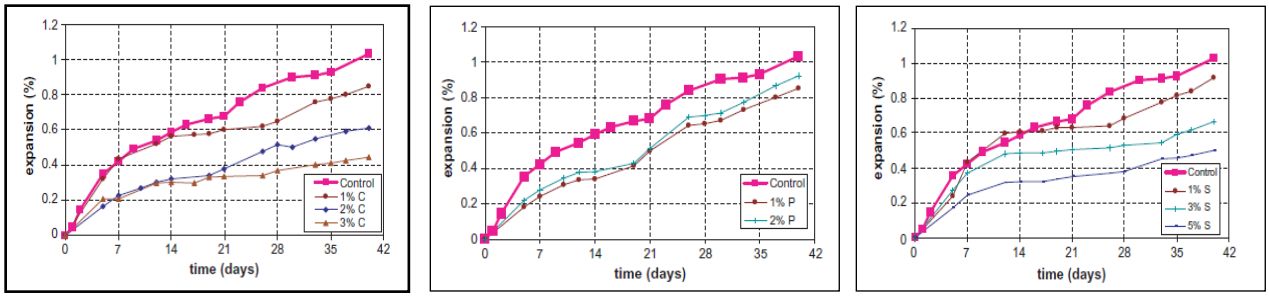

Figure (2.12) Expansion of mortar contains different types and content of fibres exposed to extended treatment

(a) Carbon fibre, (b) PVA fibre, and (c) Brass coated Steel fibre [Andiç et al., 2008]

U-shape high-strength FRC jackets contained different types of fibre content in the range from 1% to 2% fraction were used to suppress the expansion induced by ASR (Haddad et al., 2008). The study reveals the expansion changed to be lower at two stages (i.e. after 24 and 50 days, respectively). The expansion change occurred due to jacketing restrained, while expansion increased continuously in unrestrained specimens without change as represented in **Fig. (2.13)**. FRC jacketing causes an improvement in the ultimate load capacity, serviceable

load, stiffness, and rigidity as shown in **Fig. (2.14)**. The ultimate load capacity increased by about 19% and 10% when compared with the control RC beams (Haddad et al., 2008). These results reinforce the use of FRC was effective to restore the flexural capacity of ASR-damaged RC members.

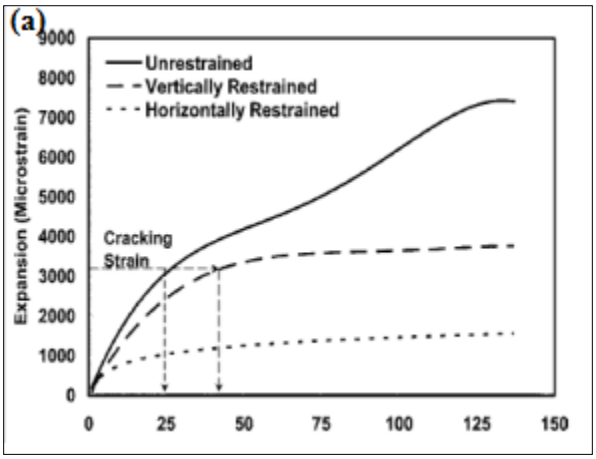

Figure (2.13) ASR expansion Vs. time for unrestrained and restrained concrete
[Haddad et al., 2008]

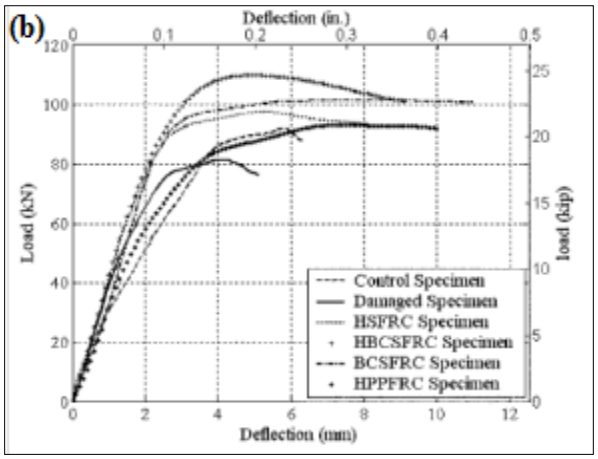

Figure (2.14) Load-deflection diagrams for control, damage, and repaired beams
[Haddad et al., 2008]

2.2.1.4 Enhancement of SCMs to Reduce ASR

Utilization of SCMs such as fly ash, silica fume, granulated blast furnace slag, and metakaolin are capable of reducing ASR expansion. The replacement of SCMs resulting in a reduction of concrete permeability and increase the chemical durability due to pozzolanic and densification effect of these materials. SCMs causes diminish the concentration of alkali and reduce the ability of alkali movement to reach the reactive aggregate (Mehta and Montiero, 2006, Fournier et al., 2001, Ukita et al., 1989, and Bouikni et al., 2009). However, SCMs effect mainly depends on material constituents {i.e. the degree of reactive aggregate and alkaline available with concrete}, exposure condition, and SCMs {type, chemical composition

and sufficient level of replacement} (Fournier and Malhotra, 1997, Thomas 2011, and U.S. (FHWA 2013)) as shown in **Fig. (2.15)**. The expansion resulting from ASR in the range 0.04% to 0.12% at one year could be controlled by using SCM at the level of partial replacement greater than 7.5%, 35%, and 20% for SF, GGBS, and Class F fly ash, respectively. However, to control an expansion higher than 0.12%, the level of replacement of SCM should greater than 10%, 50, and 30% for SF, GGBS, and Class F fly ash, respectively. This proves the high portion of SCMs are necessary to control expansion resulting by higher reactive aggregate (Fournier and Malhotra, 1997 and FHWA 2013).

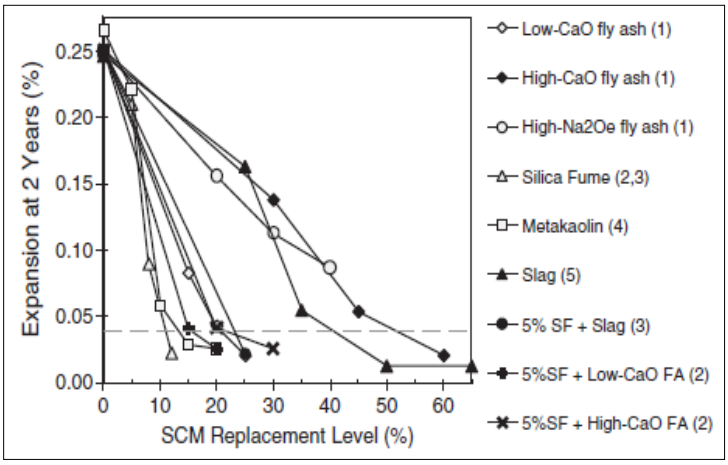

Figure (2.15) Effect of SCMs on the two-year expansion of concrete containing siliceous limestone - [Thomas, 2011]

Figure (2.16) represented with moderately reactive aggregate and moderate-alkali cement at replacement levels of about 10%; the expansion can eliminate with SCMs of the high level of reactive silica and negligible alkali content (Thomas, 2011). However, the use of highly reactive aggregate and high-alkali cement required SCMs of higher alkali and lower silica content at replacement levels in the range from 50% to 60% or higher as represented in **Fig. (2.16)** (Thomas, 2011). Moreover, (Thomas) carried out outdoor exposure specimens to

determine the efficacy of fly ash in controlling damaging ASR for a duration up to 18 years. The author found both expansion and cracks were reduced at replacement level of fly ash in the range from 25% to 40% (Thomas et al., 2011).

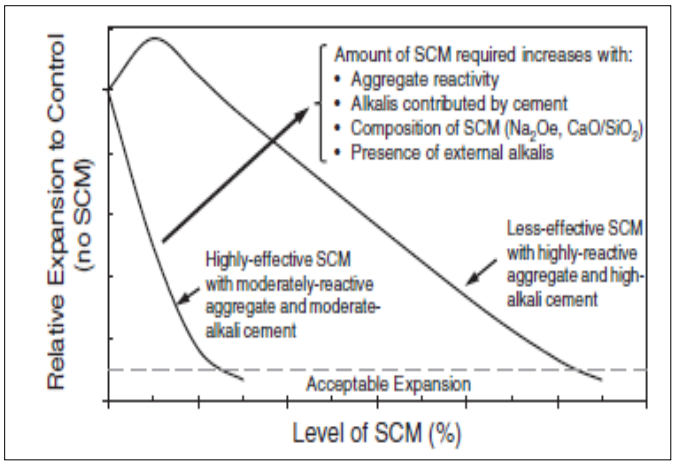

Figure (2.16) Conceptual relationship between the expansion of concrete and level of SCM - [Thomas, 2011]

The type and replacement level of SCMs as mentioned above plays a crucial role to control the expansion. For instance, high reactive metakaolin (HRM) with replacement portion in the range from 5% to 20% was added to concrete and mortar mixtures incorporated two different reactive aggregates (i.e. high and low reactive aggregate (HRA and LRA)). Its obvious, the HRM was effective to suppress ASR at replacement level ranging from 10% to 15% as represented in **Fig. (2.17)** (Ramlochan et al., 2000).

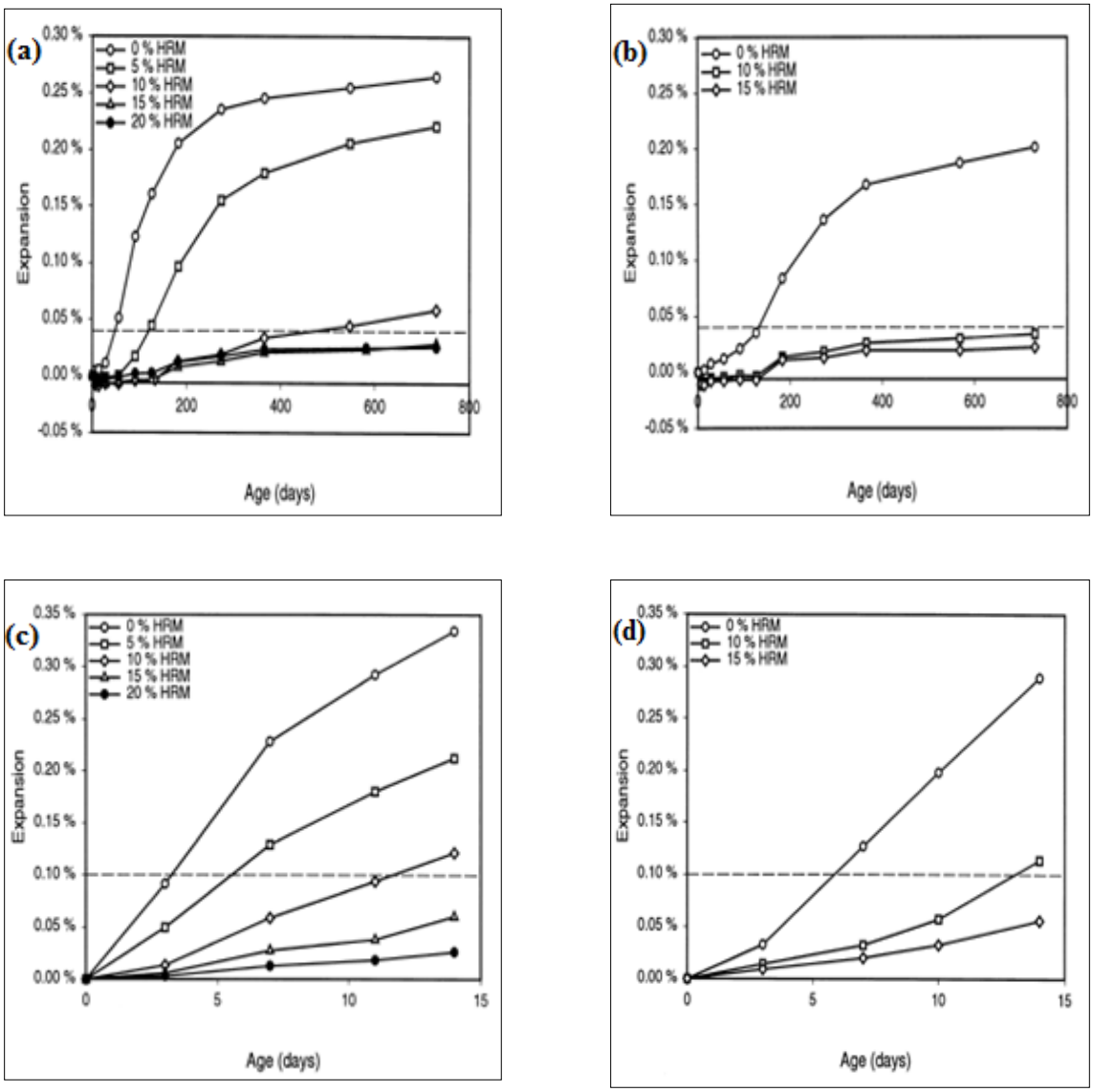

Figure (2.17) Expansion of concrete prisms and mortar bars

(a) Concrete prisms incorporated HRM and HRA, (b) Concrete prisms incorporated HRM and LRA, (c) Mortar bars contains HRM and HRA, and (d) Mortar bars contains HRM and LRA [Terrence Ramlochan et al., 2000]

Moreover, the use of ternary SCMs such as high-calcium fly ash with slag did not reveal real contribution than the binary blends at the same level of replacement to mitigate ASR as shown in **Fig. (2.18 and 2.19)**, this capability mainly depends on SCMs capacity to keep alkalis in its hydration products (Kandasamy and Shehata, 2014). In addition, the curing time has a tremendous effect on the expansion. The studies were exhibited at 30PFA10SF with seven days of curing period, the expansion was at the lowest level at 14 days and not exceed the standard limit (Fares and Khan, 2014).

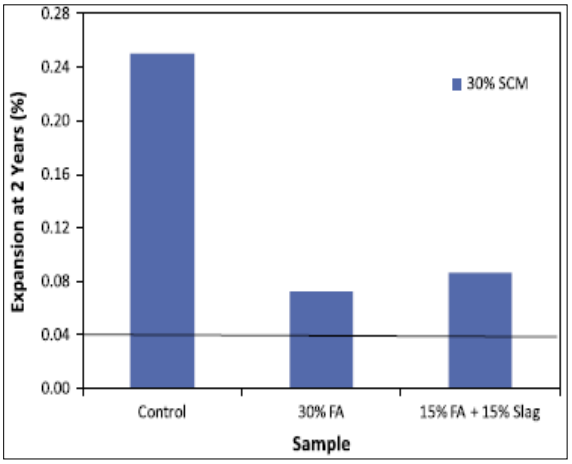

Figure (2.18) Expansion of concrete prisms at two years for samples with 30% total SCM
[Kandasamy and Shehata, 2014]

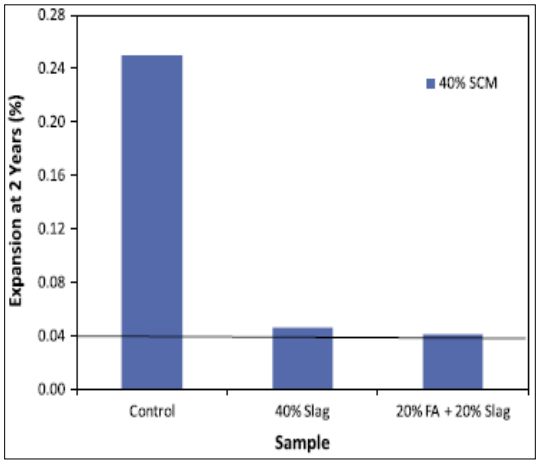

Figure (2.19) Expansion of concrete prisms at two years for samples with 40% total SCM
[Kandasamy and Shehata, 2014]

Chapter

3

Experimental Work & Methodology Plan

3.1 Introduction

This chapter details the methodology and experimental work plan involving the materials, laboratory equipment, tests, and procedures utilized in each phase to evaluate the concrete mixtures and strengthening techniques.

3.2 Experimental Work - Phases

The experimental plan comprised three main phases as represented in **Fig. (3.1 and 3.2)**.

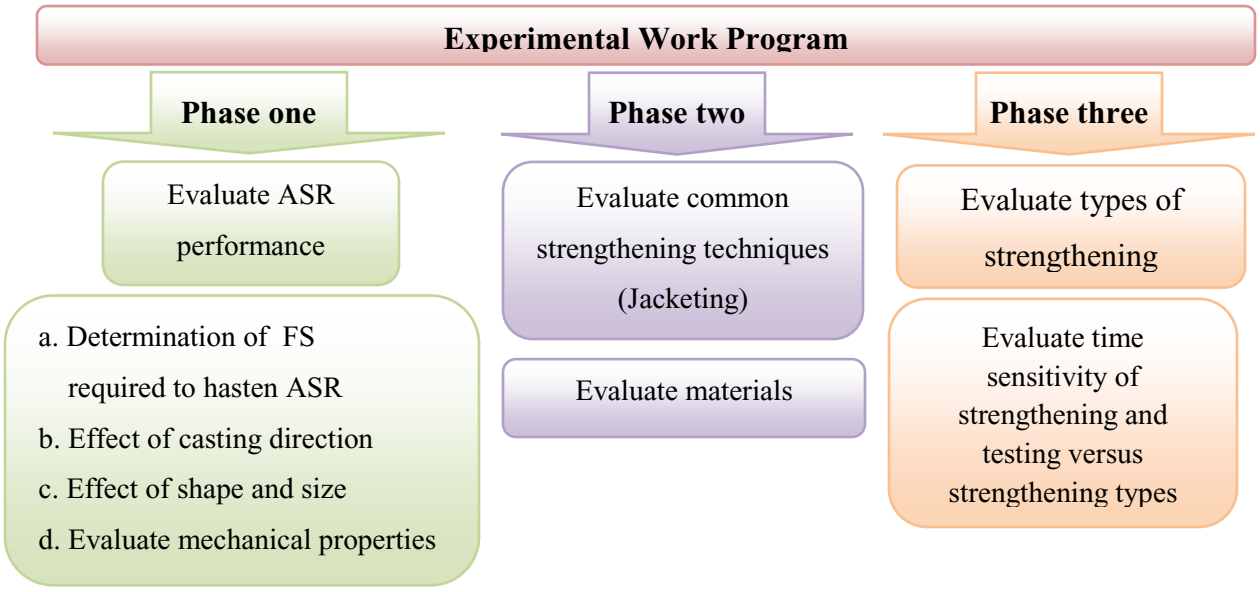

Figure (3.1) Three main phases of the experimental work plan

Phase One included the preparation of several concrete and mortar mixtures containing reactive aggregate (RA) obtained from the Spratt, ON quarry and different portions of fused silica (FS). The purpose of phase one was to determine the concrete mixture with the highest level of expansion within a reasonable timeframe to apply various strengthening methods in Phase three. Moreover, the casting direction, specimen shape and size, and the addition of different amounts of FS were investigated.

Phase One consists of casting six concrete and mortar mixtures as below and presented in details in **Chapter 4**:

A. Six mortar mixtures, each with 3 mortar bars of 25mm×25mm×285mm, were cast and measured for expansion according to ASTM C1260 (2014). All of the mixtures contained Spratt reactive fine aggregate and various portions of FS replacements (0%, 5%, 7.5%, 10%, 15%, and 20%).
B. Six concrete mixtures of total 54 specimens were used to evaluate the influence of shape and size, casting direction, and a portion of FS. Each mixture consists of:
    - Three concrete prisms of 75mm×75mm×285mm were cast in the horizontal direction.
    - Three concrete prisms of 75mm×75mm×285mm were cast in the vertical direction.
    - Three concrete cylinders of Ø75mm×285mm.

The six concretes mixtures contained Spratt reactive coarse aggregate, and the same replacements of FS mentioned for the mortar mixtures. The specimen preparation, curing, and monitoring length change and weight were conducted according to ASTM C1293 (2018).

Six concrete mixtures of total 522 specimens containing a different portion of FS were cast to evaluate expansion, changes in mechanical properties and durability indices of concrete undergoing ASR expansion. Each mixture consisted of:

- Seventy-two concrete cylinders of Ø100mm×200mm to measure mechanical properties at different times as compression and tensile strengths, stiffness loss, modulus of elasticity (MOE), Poison ratio (υ), and ultrasonic pulse velocity (UPV).
- Fifteen concrete cylinders of Ø100mm×50mm to measure durability indices properties such as permeability.

Phase two dealt with the preparation and evaluation of various concrete mixtures which included non-reactive aggregate (NRA), silica fume (SF) as supplementary cementing materials (SCMs), fibres (i.e. steel, macro and micro polypropylene, and micro nylon), and fine crumb rubber aggregate (FCRA). Moreover, the evaluation of mortar mixtures.

The purpose of phase two is to select the concrete mixture with a suitable level of mechanical properties and durability indices to be used as concrete jacketing for deteriorated specimens. Concrete mixtures were designed according to ACI 211.4R (2009). The specimens dimensions were adopted to meet the requirements of ASTM tests as; for compressive strength (CS), tensile strength (TS), rapid chloride permeability (RCPT), sorptivity (S), ultrasonic pulse velocity (UPV), bulk resistivity (BR), and surface resistivity (SR).

Details of **Phase Two** mix design represented in **Chapter 5**, this phase comprised three categories as follows:

A. Eight concrete mixtures containing various types of fibres with and without SCMs, and two concrete mixtures without fibres were prepared as a control. A total of 300

cylinders were cast, then subjected to tests according to ASTM requirements. Each mixture consisted of:

- Twelve concrete cylinders of Ø100mm×200mm to measure mechanical properties at 28 and 90 days, respectively. In addition, electrical resistivity at 28, 42, 56, 70, and 90 days, respectively.
- Eighteen concrete cylinders of Ø100mm×50mm to measure durability indices such as permeability and sorptivity at 28, 56, and 90 days, respectively.

B. Two concrete mixtures containing fine crumb rubber aggregate with and without SCMs, and two concrete mixtures without FCRA prepared as a control. A total of 144 cylinders were cast, then subjected to tests according to ASTM requirements. Each mixture consisted of:

- Twenty-seven concrete cylinders of Ø100mm×200mm to measure mechanical properties at 28, 56, and 90 days, respectively. In addition, to evaluate electrical resistivity at 28, 42, 56, 70, and 90 days, respectively.
- Nine concrete cylinders of Ø100mm×50mm to measure durability indices properties such as permeability at 28, 56, and 90 days, respectively.

C. One mortar mixture was prepared to evaluate the effect of harsh environmental conditions (i.e. 38^{o}C and 95±5% RH) compared with lab conditions (i.e. 22^{o}C and 50% RH) at different ages. A total of 54 specimens were cast, then subjected to compression and tensile tests according to ASTM requirements.

The mixture consisted of:

- Twenty-four cubes 5mm×5mm to evaluate the compressive strength,
- Thirty dog bone shape ASTM C307 (2018).

Phase Three was aimed to evaluate the effectiveness of six different repairing techniques and materials carried out at different times to mitigate deleterious effects in ASR-damaged concrete specimens. One mixture was selected from Phase one (i.e. mixture incorporating 15% FS). A total of 432 concrete cylinder specimens Ø100mm×200mm were cast and stored in an environmental room under harsh conditions of 38 ^{o}C and 95±5% humidity. After sandblasting, these specimens were subjected to strengthening after 28, 56, 90, 120, 150, and 182 days from casting date, respectively and tested after 2, 4, and 6 months from the strengthening time, respectively.

The method statement of strengthening was detailed in **Chapter 6**. The strengthening was started by applying lithium nitrate of 30% solution by "Topical application" approach at rates in the range from 0.12 to 0.24 L/m^2 on the concrete surface, then applying the treatments:

1- Strengthening:

- Uni-Directional carbon fibre reinforced polymer (CFRP), one layer applied directly on the surface of the deteriorated samples.
- Uni-Directional basalt fibre reinforced polymer (BFRP), one layer applied directly on the surface of the deteriorated samples.
- Basalt fabric mesh with mortar of thickness 25mm.
- Glass Grid mesh with mortar of thickness 25mm.

2- Jacketing

- Concrete jacketing containing micro polypropylene fibres with 10% silica fume
- Concrete jacketing containing fine crumb rubber aggregate with 10% silica fume, then strengthened using BFRP-one layer.

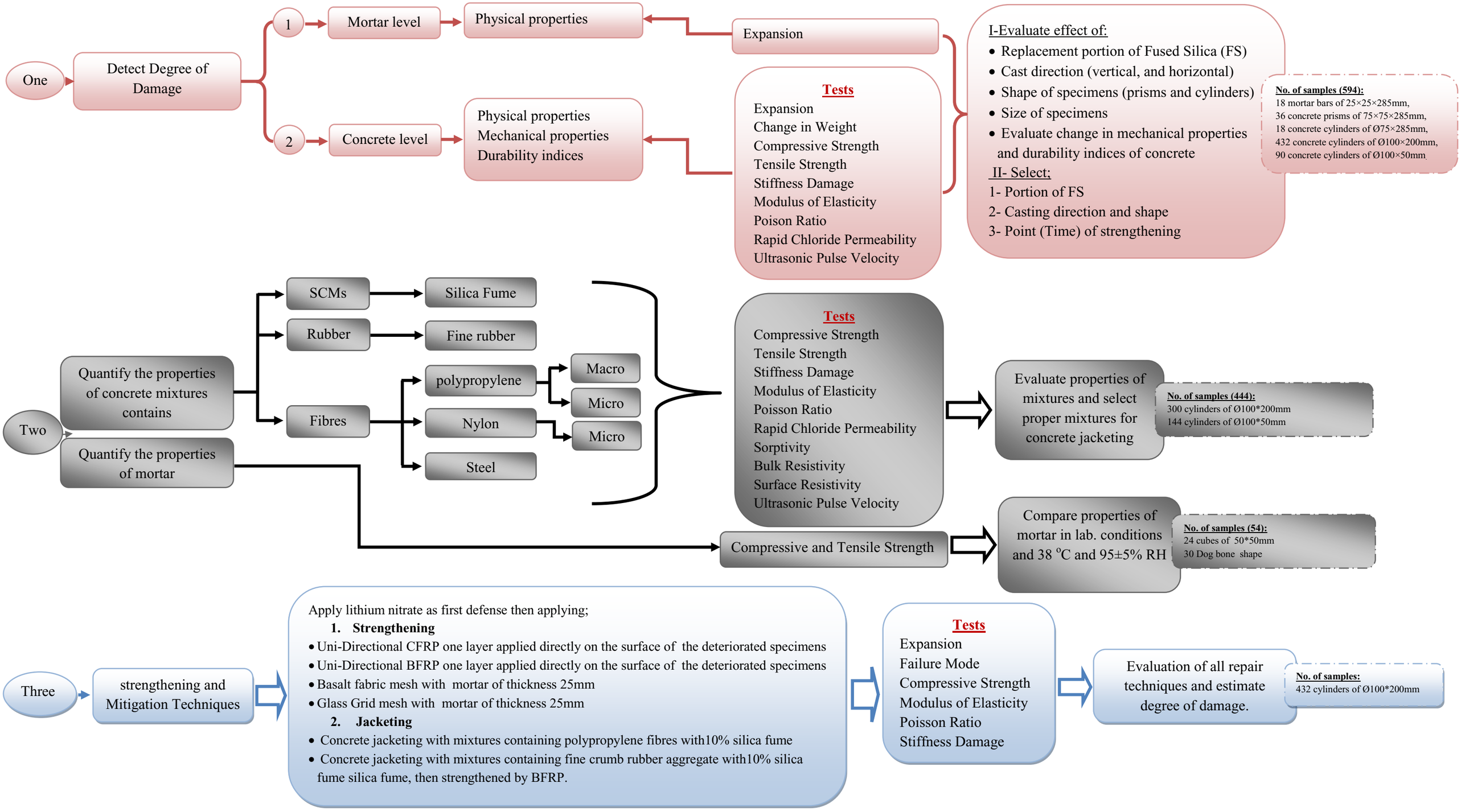

Figure (3.2) Flowchart of the experimental program, testing, and specimens number

3.3 Material Properties

To achieve the desired goals of this dissertation, the experimental work covered the evaluation of materials available in the region and nearby area to make its usage suitable for the industrial objectives.

3.3.1 Cement

General use cement (GU) produced according to Canadian Standard Association CSA-A3001 (CSA 2013) was used in all mixtures. The chemical composition, physical, and mechanical properties of GU cement presented in **Table (3.1)**.

3.3.2 Supplementary Cementing Materials

Silica fume (SF) produced by Master Build solutions (D-BASF) with an average 93.8% silicon dioxide was used in selected mixtures as a partial replacement of cement at a rate of 10%. The chemical synthesis and physical characteristics are given in **Table (3.1)**.

3.3.3 Natural Aggregate

The natural aggregate used through this research was obtained from Lafarge-Canada and subjected to various types of tests according to ASTM standards to recognize its properties as described below.

3.3.3.1 Fine Aggregate

Natural Fine Aggregate (NFA) properties before used in all mixtures were evaluated such as; fineness modulus was 2.70 according to ASTM C136 (2014). The specific gravity, apparent specific gravity, and sorptivity were 2.51, 2.69, and 2.73%, respectively determined by ASTM C 128 (2015). Moreover; the average loose bulk density, average rodded bulk density, and

percentage voids were 1718.98 kg/m3, 1785.55 kg/m^3, and 31.50%, respectively based on ASTM C29 (2017). Finally, the sieve analysis met ASTM C33 (2018) requirements as represented in **Fig. (3.3a)**. Moreover, silt content was 4.02 %.

Table (3.1) Chemical and physical properties of cement and silica fume

		OPC (1)	**SF (2)**
SiO_2	(%)	19.80	93.80
Al_2O_3	(%)	4.90	00.24
CaO	(%)	62.30	0.70
Fe_2O_3	(%)	2.30	0.16
SO_3	(%)	3.70	00.24
Na_2O	(%)	0.34	00.19
C_3S	(%)	57.00	--
C_2S	(%)	14.00	--
C_3A	(%)	9.00	--
C_4AF	(%)	7.00	--
SO_3	(%)	--	0.29
K_2O	(%)	0.81	0.61
Na2Oeq	(%)	0.87	0.17
MgO	(%)	2.80	0.29
P_2O_5	(%)	--	0.12
H_2O	(%)	--	0.53
C free	(%)	--	2.38
Cl	(%)	--	0.22
Fire loss	(%)	2.40	--
Insoluble Residue	(%)	0.94	--
Loss on ignition	(%)	1.90	2.79
Specific gravity	--	3.15	2.20
Bilk Density	(g/l)	--	174
Surface area (Finesse - Blaine)	(m^2/kg)	373	19500
Autoclave expansion	(%)	0.05	-0.010
Air content	(%)	5.00	
Retained on 45µm sieve	(%)	4.50	4.98
Set time	(minutes)	140	--
compressive strength	MPa	3- day--28.5 7- day--33.7 28-day--43.4	--

(1) GU cement produced by Lafarge cement plant, Factory at St. Constant

(2) SF "Master Life SF-100 (Rheomac SF 100)" produced by Master Builders Solutions (D-BASF)

3.1.3.2 Coarse Aggregate

Natural Coarse Aggregate (NCA) No.#8 of nominal size 9.5mm and sieve analysis meeting ASTM C33 (2018) requirements were utilized as illustrated in **Fig. (3.3b)**. According to ASTM C127 (2015); the specific gravity, apparent specific gravity, and sorptivity were 2.70, 2.83, and 1.3%, respectively. Moreover, the average loose bulk density, average rodded bulk density, and percentage voids were 1360.96 kg/m^3, 1512.91 kg/m^3, and 49.59%, respectively based on ASTM C29 (2017).

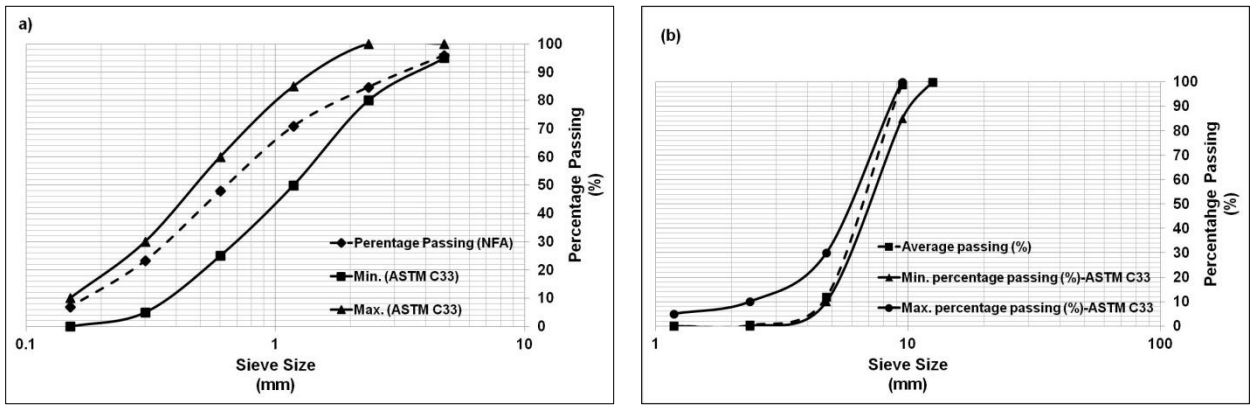

Figure (3.3) Sieve analysis of aggregate

(a) Natural fine aggregate, and (b) Coarse aggregate

3.3.4 Reactive Aggregate

Spratt reactive coarse aggregate (SRCA) type #3, obtained from the Ministry of Transportation - Ontario (MTO) used as a reactive aggregate. SRCA was sieved before it was added to concrete mixtures to avoid particles not meeting the conditions of ASTM C1260 (2014) and ASTM C1293 (2018). The chemical, physical, and Petro-graphical properties of SRCA are represented in **Table (3.2).** Moreover, SRCA was crushed into a small crusher at an external lab

"Englobe" to obtain the Spratt Reactive Fine Aggregate (SRFA), then sieved before used into the mortar mixtures to meet the standard conditions.

Table (3.2) Chemical and physical properties of Spratt reactive aggregate

Physical Property		
Absorption	(%)	0.72
Bulk Relative Density	--	2.712
Magnesium Sulphate Soundness	(%)	4
Los Angeles Abrasion and Impact	--	19
Material Wash Pass 75 um sieve	(%)	0.32
Petro-graphic Number	--	111
Acid Insoluble Residue	(%)	10.00
Petro-graphic Composition		
Good Limestone	(%)	96.30
Slightly Shaley Limestone	(%)	2.30
Cherty Limestone	(%)	0.50
Shaley Limestone	(%)	0.80
Shale	(%)	0.1

3.3.5 Fused Silica

Fused silica (FS) produced by **Precision Electro Minerals Co.** of size fraction 10/20 matching with the specified reactive sand was used to hasten the expansion rate for both mortar and concrete specimens. Chemical, physical, and petrographic properties for FS is summarized in **Tables (3.3)**.

Table (3.3) Chemical, physical, and petrographic properties of fused silica

Physical Property		
Magnetics	(%)	0.004
PH	Max	7.00
Specific Gravity	g/cc	2.21
Coeff. Therm. Exp.	Co	0.5×10^{-6}
Bulk Density	lb/ft3	65-75
Petro-graphic Composition		
SiO_2	(%)	99.80
Al_2O_3	(%)	0.05
Fe_2O3	(%)	0.015
Na_2O	(%)	0.007
K_2O	(%)	0.003
TiO_2	(%)	0.010
CaO	(%)	0.010
MgO	(%)	0.003

3.3.6 Fine Crumb Rubber Aggregate

Fine Crumb Rubber Aggregate (FCRA) was produced by tearing (i.e. manufacture process) the shabby scrap tire and then were sieved to get rubber particles that met the size fraction of fine aggregate in accordance with ASTM C33 (2018) as shown in **Fig. (3.4a).** Black FCRA of 1.16 gm/cm^3 specific gravity and a bulk density in the range from 0.37 to 0.44 gm/cm^3 according to ASTM D5603 (2015) as shown in **Fig. (4b)** were used in selected mixtures at a rate of 10% as a partial replacement of natural fine sand.

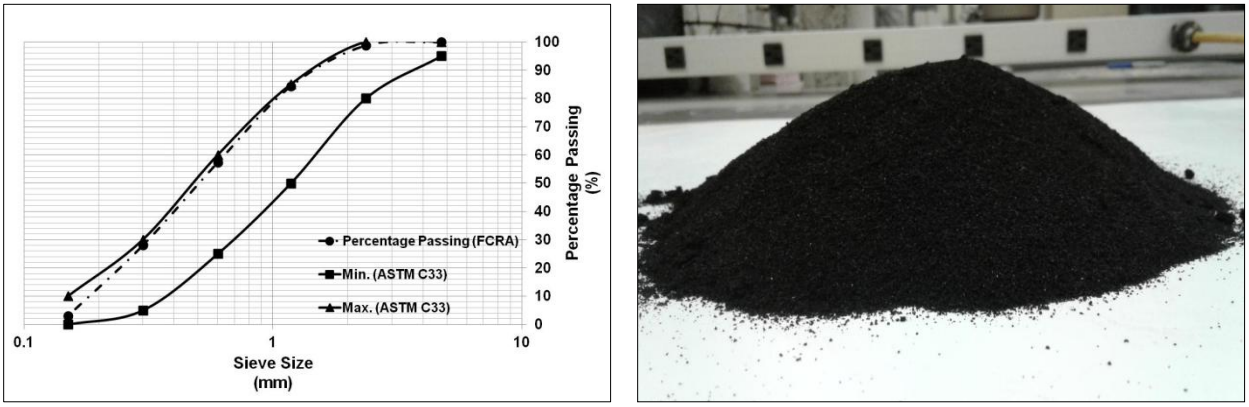

Figure (3.4) Black fine crumb rubber aggregate

(a) Size fraction after sieving according to ASTM C33, (b) Fine rubber aggregate texture

3.3.7 Fibres

Various types of fibre of an appropriate aspect ratio were used to avoid the balling phenomena, to prevent difficulty of fibre separation during the mixing, to allow proper distribution within the mixtures, and to enhance the concrete strength. Hooked-End Steel Fibres (HE 1/50) of aspect ratio 50 was used as a conductive fibre, while synthetic polypropylene and nylon fibres of different aspect ratios were used as non-conductive fibres. The geometry and properties of the fibres are given in **Table (3.4)** and **Fig. (3.5),** respectively.

Table (3.4) Properties of steel, polypropylene, and Nylon fibres

Fibre Code	Type of fibre	Shape	Length l (mm)	Diameter d (mm)	Aspect ratio (l/d)	Specific gravity	Elastic modulus (GPa)	Tensile strength (MPa)
S (1)	Steel	Hooked End	50	1.00	50	7.80	200	1150
P (2)	Polypropylene	Straight	39	0.78	50	0.91	3.6	570
MP (3)	Polypropylene	Straight	12	0.019	631	0.91	3.6	570
MN (4)	Nylon	Straight	19	0.03	633	1.14	5.17	966

(1) Steel Fibres (S) produced by ArcelorMittal, Canada, (2) Macro Polypropylene (P), (3) Micro Polypropylene (MP), and (4) Nylon (MN) produced by Forta-Ferro corporation, USA

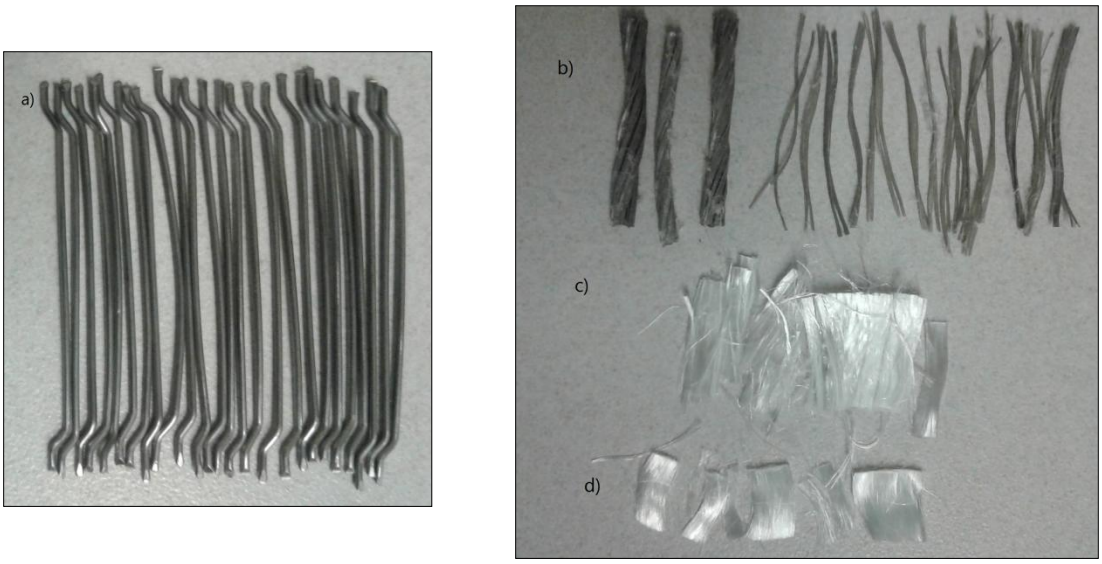

Figure (3.5) The shape of steel, polypropylene, and nylon fibres;
(a) Steel fibre (S), (b) macro polypropylene (P), (c) micro nylon (MN), and (d) micro polypropylene (MP)

3.3.8 Chemical Admixtures

Different types of chemical admixtures approved by the Ontario Ministry of Transportation and the Ministère des Transports du Québec produced by Sika-Canada were added to enhance the concrete properties based on the type of mixture and required properties.

A High Range Water Reducing and super plasticizing; admixture "SikaViscoCrete 2100" of specific gravity 1.08 were incorporated to increase workability and keep slump within the acceptable level (i.e. 90mm to 120mm). It met the requirements for ASTM C494 (2017) and AASHTO M-194 Type A and F (2006).

***Sika Top Armtec 110 EpoCem*;** Anti-corrosion coating, used as a bonding agent between the deteriorated concrete specimens and new mixtures used for strengthening (i.e. concrete and mortar).

***Sika Control ASR*;** lithium nitrate based admixture ($LiNO_3$) applied on the existing concrete surface by the most straightforward approach "Topical application". $LiNO_3$ used to be the first barrier before applying the strengthening materials to minimize the distress and enhance the concrete appearance prior start strengthening techniques.

***Sika Stabilizer 4R*;** is liquid based viscosity modified admixture added to the concretes mixtures contains rubber aggregate to avoid the segregation concern.

Sika Multi Air; is a multi-component synthetic, and detergent based air entraining admixture produced according to ASTM C260 (2016) introduced into concrete mixtures to control air content.

Sika Top 13 Plus; is polymer-modified, non-sag mortar, cementitious, and migration corrosion inhibitor. This admixture consists of two components (A and B) mixed by the specified weight ratio of 1A:4.8B (i.e. manufacture recommendation). Mainly designed with high early strength to repair the vertical surfaces of the deteriorated concrete.

3.3.9 Water

Potable water was used to prepare all concrete and mortar mixtures. However, different types of chemical solutions added to concrete and mortar mixtures, and solutions required during the testing procedures were prepared using distilled water.

3.3.10 Chemical Solutions

The experimental work required to prepare different solutions such as sodium hydroxide (0.3N NaOH and 1M NaOH), and sodium chloride (3% NaCl).

3.3.11 Fibre Reinforcement Polymer and Adhesive

Different types of fibre reinforced polymers (FRP) were used in the research to reinforce the deteriorated concrete specimens to mitigate the expansion resulting from ASR. The properties and features of all FRP types were represented in **Fig. (3.6)** moreover, **Table (3.5).**

Both carbon and basalt fibre reinforcement (CFRP and BFRP) were installed directly on the surface of concrete specimens after applying the epoxy adhesive (Sikadur 330). The adhesive contains two components that mixed mechanically in ratio 4A:1B using a drill at low speed for a continuous three minutes until obtaining a homogenous color without colored streaks. It was then remixed for one minute to minimize the air entrained. However, both of basalt fibre mesh (BFM) and glass grid (GG) installed on the concrete specimens and strengthening by a mortar layer of thickness 25mm prepared using Sika Top 13 Plus.

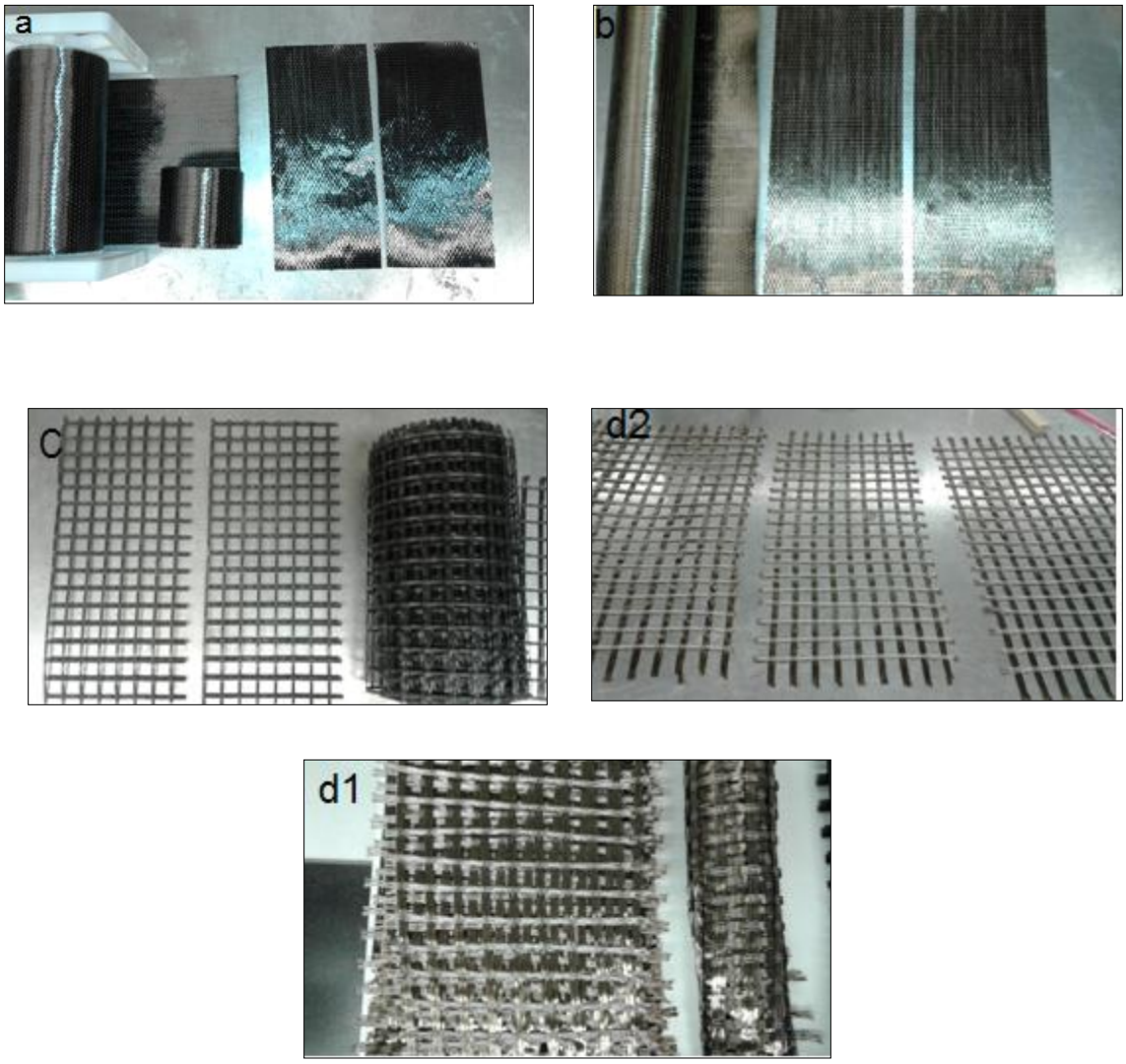

Figure (3.6) Types of fibre reinforcement polymer

(a) Carbon fibre reinforcement polymer (CFRP) produced by Sika, CA

(b) Basalt fibre reinforcement polymer (BFRP) produced by Smarter building systems LL, USA

(c) Glass grid (GG) produced by Tensar International Corporation, USA

(d1, d2) Basalt fibre mesh (BFM) Smarter building systems LL, USA

Table (3.5) Properties of fibre reinforcement polymers

	*CFRP	BFRP	BFM	GGM	Epoxy
Material	The black unidirectional fibre of 305mm×45.7m	Basalt fabric Uni-directional, smooth of width 60±1cm and wt.300gram ±8%	Basalt Geomesh 25mm x 25mm of 350 grams/sq. meter	Fibreglass reinforcement with a modified polymer coating and pressure-sensitive adhesive backing. grid size-center to center of strand 25mm×25mm and unit weight 405g/m^2	Sikadur 330 of two component
Tensile Strength	894 MPa	--	--	115×115 +/- 15 KN/m	30
Tensile Modulus	65402 MPa	--	--	73000 MPa	--
Elongation	1.33 %	--	6.67% +/- 5%	2.5 +/- 0.5%	1.5 %
Wrap break strength		> 2250 (N/25mm)	80,780 (N/meter)	--	--
Flexure modulus	--	--	--	--	3.8 GPa
Thickness (mm)	0.381	0.36±0.1	0.08-0.09	--	--

* Mechanical properties of the CFRP laminate were obtained experimentally from tensile testing of flat coupons and compared to the manufacturer's datasheet by Alotaibi (2018).

3.4 Tests and Testing Procedure

The experimental work comprised several types of tests included destructive, non-destructive, and durability indices tests. The tests were performed on both the fresh and hardened concrete and mortar specimens according to ASTM standards as represented in **Fig. (3.7)**.

3.4.1 Destructive Tests

Three destructive tests (DT_s) were used during research: compression, tension, and stiffness damage tests. DT_s were used to assess the effect of fused silica amount on the concrete mechanical properties, the efficacy of integrating various types of fibres and fine crumb rubber with and without silica fume, and evaluation the different strengthening methods, respectively.

The compression test is considered the most widely used and first technique to determine if the concrete mixtures meet the design and specification requirements. Moreover, because the concrete is sensitive and vulnerable to tensile cracks as subjected to different loads and concrete has low tensile strength compared with its compressive strength, the splitting tensile test was used to measure the concrete tensile strength. Finally, the stiffness damage test was considered an interesting tool to evaluate the concrete performance and assessing the degree of damage before and after applying the strengthening methods.

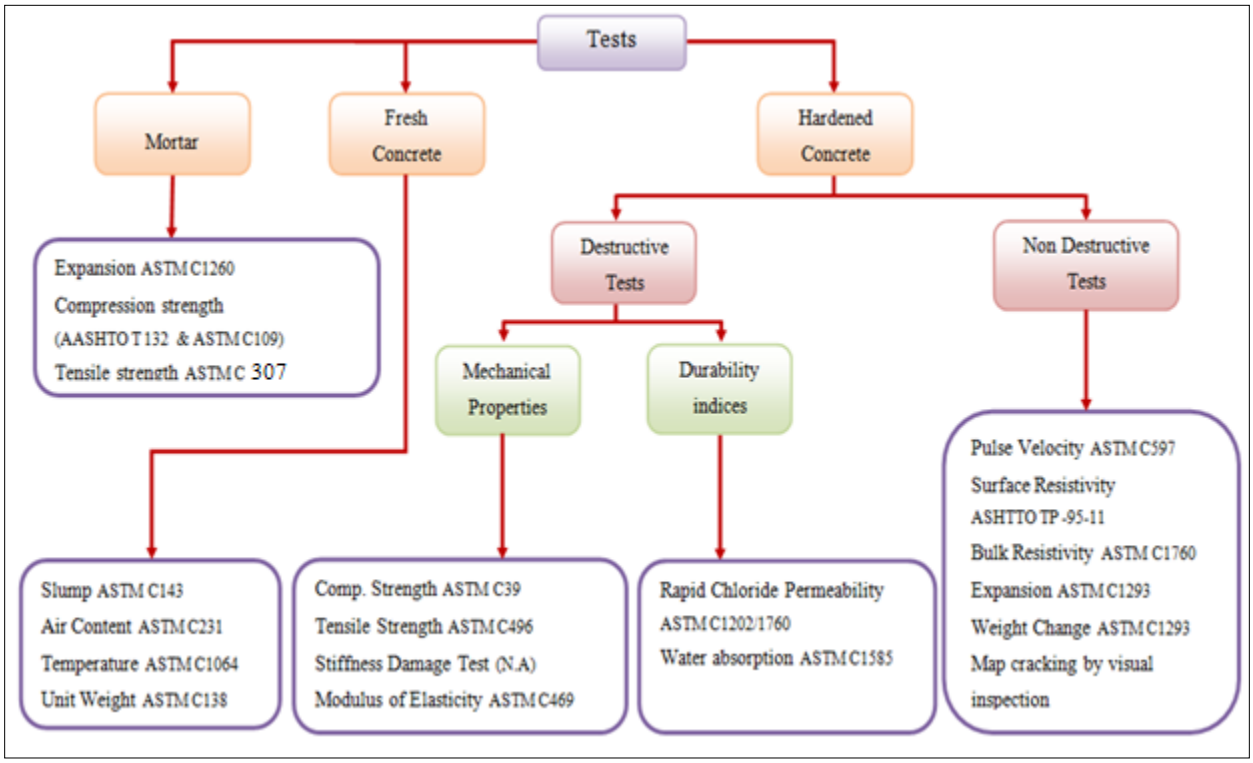

Figure (3.7) Tests accomplished on both the fresh and hardened concrete specimens

3.4.1.1 Compression and Splitting Tensile Test

The DTs were accomplished by using Forney digital compression machine of 1100 KN capacity. The compressive strength test was accomplished according to ASTM C39 (2018). The specimens subjected to uniaxial compression load at rate 0.25MPa/s. The splitting tensile test was completed according to ASTM C496 (2017), the standard cylinders placed horizontally between the compression loading plates of the same machine. Along the cylinder length, placed two strips of plywood above and below the specimens to; (1) Minimize the high compression stresses that closed to the points of applied loads, and (2) Ensure the subjected loads is distribute uniformly. Finally, the loads are applied to the specimens uniformly at rate1.15 MPa/min.

For all DTs, three or two cylinders of Ø100mm×200mm were tested for all mixtures and the failure loads recorded, where the result values presented the average of specimens. The compressive and tensile strengths calculated according to **Eq. (3.1)**, and **Eq. (3.1),** respectively.

$$f_{\acute{c}} = P/A \qquad \textbf{Eq. (3.1)}$$

$$f_t = 2P/\pi Dl \qquad \textbf{Eq. (3.2)}$$

Where P is Maximum load applied to the specimens at failure loads (N), A is a cross-sectional area (mm^2), D is Diameter (mm) and, *l* is Length (mm).

Moreover, the compressive and tensile strengths of mortar specimens were evaluated under two different conditions as; (1) Lab. conditions with normal curing by water, (2) Harsh environmental parameters as 38 ^oC & 95±5% RH, respectively. The compression test was conducted by using the same machine mentioned above on cube specimens 50mm×50mm according to ASTM C109 (2016). The tensile strength measured according to ASTM C307 (2018) on specimens prepared on briquette mold by using Com-Ten industries machine.

3.4.1.2 Stiffness Damage Test

The Stiffness damage test (SDT) was used previously by other researchers to evaluate rock specimens and concrete cylinders (Walsh 1965). It was extended to examine the plain concrete cores by Crouch (1987). SDT has been used recently as a new tool to quantify the mechanical properties and degree of damage into concrete under uniaxial compression cyclic loads (Smaoui et al., 2004, Giannini, et al., 2012, and 2018, Sanchez et al., 2014, 2015, and 2016). Despite the long use, SDT is not yet standardized.

Concrete suffering from ASR was examined under 10 MPa (Smaoui et al., 2004, and Giannini, et al., 2012). Then the test procedure was developed to include uniaxial compression cyclic loads as a percentage of the 28 days compressive strength of concrete specimens containing reactive aggregate (Sanchez et al., 2014, and 2016, and Giannini, et al., 2018). Moreover, SDT was used to evaluate the high performance concrete (HPC) comprising different replacement portion of fly ash and metakaolin at the elevated temperature in the range from 27 ^{o}C to 400 ^{o}C (Nadeem et al., 2013).

SDT results are affected by several parameters as; depth of the specimens, length to diameter ratio, environmental conditions, and moisture conditions of the specimens prior test, while the surface preparation by capping and grinding did not reveal any effect on the results (Sanchez et al., 2015). The primary outputs of SDT are the Modulus of Elasticity (MOE), Plastic Deformation, and Hysteresis Area (Sanchez et al., 2014).

Typically the loading rate used during the load cycles to evaluate the primary outputs is 241 ±34 kPa/s according to ASTM C469 (2014). Chrisp et al., (1989 and 1993) investigated concrete samples under a fixed cyclic uniaxial load and rate as 5.5 MPa and 0.1 MPa/sec, respectively. In this research, the rate recommended from the previous researches was kept at 0.1MPa/s

Concrete specimens of Ø100mm×200mm of different ingredients (i.e. specimens containing Spratt reactive aggregate with and without fused silica, specimens containing fine crumb rubber, and deteriorated specimens after applying strengthening methods) were subjected to five loading and unloading cycles. The cycles comprised loading of 40% of 28 days compressive strength. A digital compresometer/extensometer was fixed on all specimens before testing to record the vertical and horizontal deformation in concrete due to the applied loads as shown in **Fig. (3.8)**.

The loading was increased on all specimens with a fixed rate of 0.1MPa/s with a peak compressive strength of 40% from the final compressive strength. All test accomplished by using a Forney digital compression machine of 1100 kN capacity.

Figure (3.9) illustrates the primary output of SDT proposed from the previous research. The determination of the hysteresis area (HA) of the first load cycle (S1) was calculated by using a Matlab code and the total deformation over the five loading cycles (D1). Moreover, the indices of Stiffness Damage Index (SDI) and Plasticity Deformation Index (PDI) were calculated using **Eqs. (3.1 and 3.2),** respectively (Sanchez et al., 2014, and 2016, and Giannini, et al., 2018).

$$SDI = (S1)/(S1+S2) \qquad \textbf{Eq. (3.1)}$$

$$PDI = (D1)/(D1+D2) \qquad \textbf{Eq. (3.22)}$$

Where SDI is Stiffness Damage Index (%) represents the energy consumed by concrete specimens over uniaxial compression loading, S1 is irreversible energy of concrete (hysteresis area) (J/m^3), S2 is elastic deformation energy (J/m^3), PDI is the Plasticity Deformation Index (%), D1 is plastic deformation (μstrain), and (D1+D2) is total deformation (μstrain) after 5 loading cycles.

Figure (3.8) Setup of stiffness damage test (SDT) of

(a) SDT on Ø100mm×200mm specimens prior strengthening, and (b) SDT after strengthening

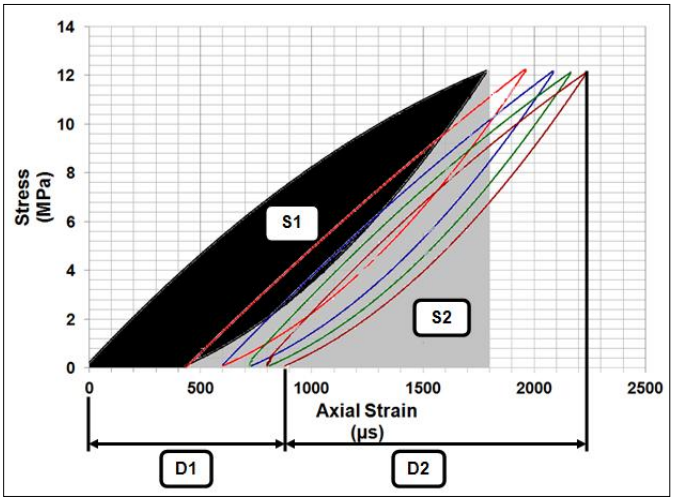

Figure (3.9) Illustration of the primary output of stiffness damage test (SDT)

3.4.2 Non - Destructive Tests

This part covered evaluation for all tested concrete mixtures by using Non-Destructive Tests (NDT_s) as Ultrasonic pulse velocity (UPV), Electrical Resistivity test (ER) (i.e. surface and bulk resistivity).

3.4.2.1 Ultrasonic Pulse Velocity Test

UPV is considered the most promising technique for assessing the concrete micro-cracks and examining matrix homogeneity (Toutanji, 2000, and Kirchhof et al., 2015). Furthermore, UPV can be used to provide information related to concrete quality (Toutanji, 2000). The fundamental concept of UPV test depends upon waves passing through a specimen of known length between transmitting and receiving transducers (Malhotra and Carino, 2003). The relationship between UPV test results and concrete strength is not unique and varies depending on many variables that affect the wave speed (Malhotra and Carino, 2003). These are the path length, material density, pore solution, and the characteristics of the specimens as dimensions, temperature, curing and moisture conditions (Malhotra and Carino, 2003).

In this research, UPV was conducted to explore its correlation, efficiency, and sensitivity to expansion due to ASR and rubber ingredient along time. Specimens Ø100mm×200mm were tested at three different locations as illustrated in **Fig. (3.10)**. A portable lab. device, the "Proceq Pundit", was used to test all specimens of Ø100mm×200mm. UPV test methodology was started by calibration of the device as shown in **Fig. (3.11a).** All specimens were tested directly after removal from the environmental room, and at saturated surface dry (SSD) condition for the deteriorated specimens and rubberized specimens, respectively to avoid the effect of the concrete moisture content as shown in **Fig. (3.11b)**. Finally, to avoid the roughness effect of the concrete

surface, an Aquasonic gel was applied on the surface of two transducers prior to testing the specimens. The frequency of 150 kHz was used during tests to follow the conditions of ASTM C597 (2016). The test was conducted as a function of time**.**

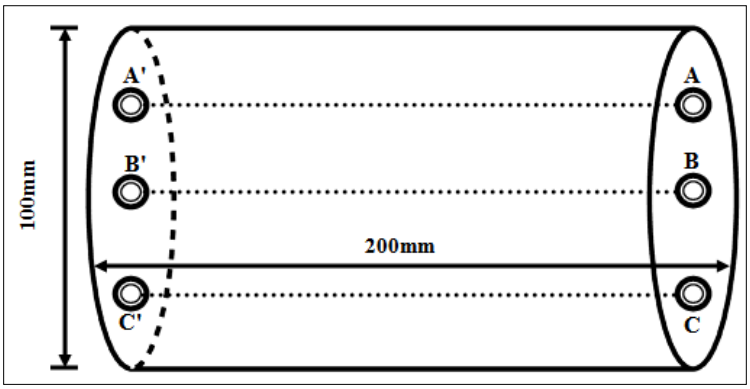

Figure (3.10) Schematic of UPV measurements location on cylinders Ø100×200mm

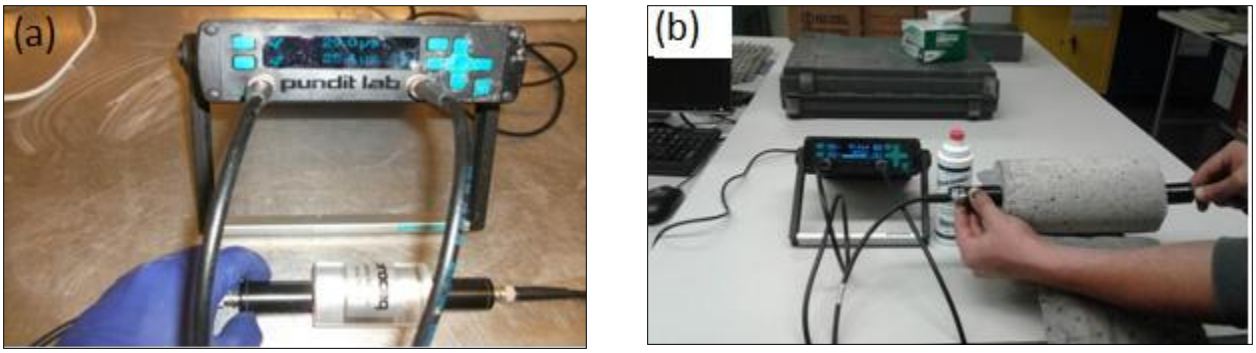

Figure. (3.11) Ultrasonic pulls velocity test (UPV)

(a) Device calibration, and (b) Testing specimens Ø100mm×200mm

3.4.2.2 Electrical Resistivity Tests

The concrete durability and quality control can be assessed by several tests and techniques, such as rapid chloride permeability (RCPT), Bulk Diffusion (BD), Freezing and Thawing. Electrical Resistivity Tests (ERT_s) requiring a minimum of technician, time, and cost so that it becomes widely used by investigators (Rupnow and Icenogle, 2012). ERTs evaluated by many researchers and approved as an electrical indicator of concrete permeability in Florida DOTs (Rupnow and Icenogle, 2011).

The fundamental theory of most electrical resistivity mechanisms mainly depends on quantifying the conductive properties of the concrete matrix and microstructure (Layssi et al., 2015, and Kevern et al., 2015). The conductivity is affected by many factors such as the volumes of pores, saturation degree, pore size, and its distribution in the concrete matrix, moisture conditions, and temperature of concrete specimens (Layssi et al., 2015). Because concrete can be considered as a composite material containing solids, voids, and liquid, this reveals the higher the liquid in pores, the lower the specimen's resistivity (Spragg et al., 2012). Typically, ERTs are used to evaluate the resistance to permeation of aggressive fluids through the concrete pore system causing deterioration that can be used to predict the risk of various types of damage as corrosion (Kevern et al., 2015).

3.4.2.2.1 Surface Resistivity Test

The Surface Resistivity Test (SR) was implemented on cylinders of Ø100mm×200mm at 4, 6, 8, 10, and 12 weeks according to ASHTTO TP -95-11 (2011). Commercially available 4 points Wenner probe surface resistivity meter was used for SR test. The device consists of four electrodes in the straight line and at equal distances of 3.8mm as represented in **Fig. (3.12)**. The

AC current induced from exterior probes to the concrete specimens and the potential drop, V, is measured by the two inner probes. Details about the device, illustration, and test set up can be found in (Spragg et al., 2013, Layssi et al., 2015, and Kevern et al., 2015).

Figure (3.12) Surface resistivity test (SRT);

(a) Wenner probe and measurements, and (b) Specimens marks on the top surface according to ASHTTO TP -95-11

3.4.2.2.2 Bulk Resistivity Test

Bulk resistivity tests (BR) were completed by using the same Wenner probe "Resipod Proceq" device according to ASTM C1760 (2012). This device is linked with two plate electrodes placed on either end of the specimens as represented in **Fig. (3.13)**. These plates cause a uniform distribution of the electrical current flow throughout the specimens (Spragg et al., 2013).

All cylinders of Ø100mm×200mm and Ø100mm×50mm were tested under SSD conditions and at laboratory temperature directly after removal from the curing room. The proper electrical contact was produced by placing two wet sponge between the electrode plates and the specimens (Spragg et al., 2013).

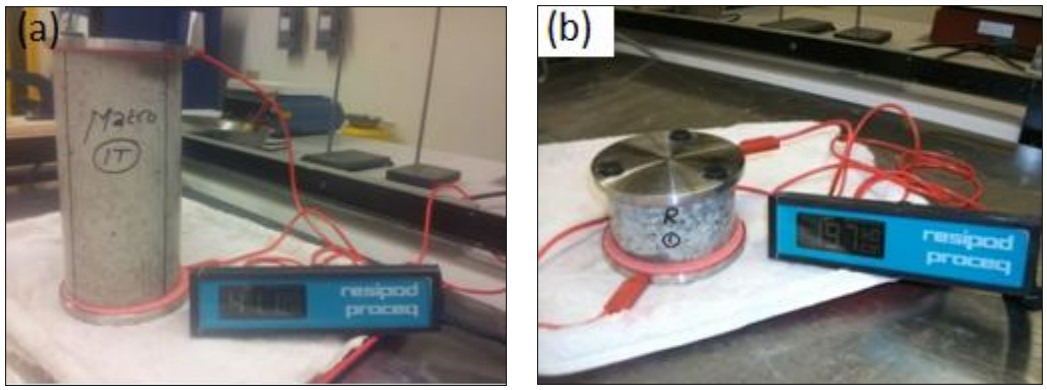

Figure (3.13) Bulk resistivity test (BRT) and measurements

(a) Specimen 100mm×200mm, and (b) Specimen 50mm×100mm

3.4.2.2.3 Expansion

Expansion measurements were conducted on the concrete and mortar specimens included in **Phase One** by using a digital comparator of accuracy 0.002mm as shown in **Fig. (3.14)**. The measurements started after de-molding the specimens to record the initial readings according to ASTM C1260 (2014). The mortar bars readings were recorded every day for a continuous 14 days, then weekly until three months. However, the concrete prism and cylinder readings were recorded at 7, 28, and 56 days, respectively, then at 3, 6, 9, 12, 15, and 18 months, respectively according to ASTM C1293 (2018). The expansion (i.e. Length change) was measured using **Eq. (3.3)**

$$\text{Expansion} = (L_n - L_i)/L_{eff.} \qquad \textbf{Eq. (3.3)}$$

Where L_n is Length measured at (n) day, L_i is Initial length measured after de-mold the specimens, and $L_{eff.}$ is the effective length.

The expansion of concrete specimens included into **Phase Three** was monitored by using two different methods; (1) 150mm digital demec mechanical strain gauge as shown in **Fig. (3.15a)**, and (2) strain gauges were fixed on the specimens adhesive and protected from the harsh

environmental conditions and process of strengthening by using a rubber tap of 10mm wide and 3mm thickness. Then connected to data acquisition system (DAS) as shown in **Fig. (3.15b).**

Figure (3.14) Expansion measurements by using digital comparator of accuracy 0.002mm

(a) Mortar bar, (b) Concrete prism, and (c) Concrete cylinders

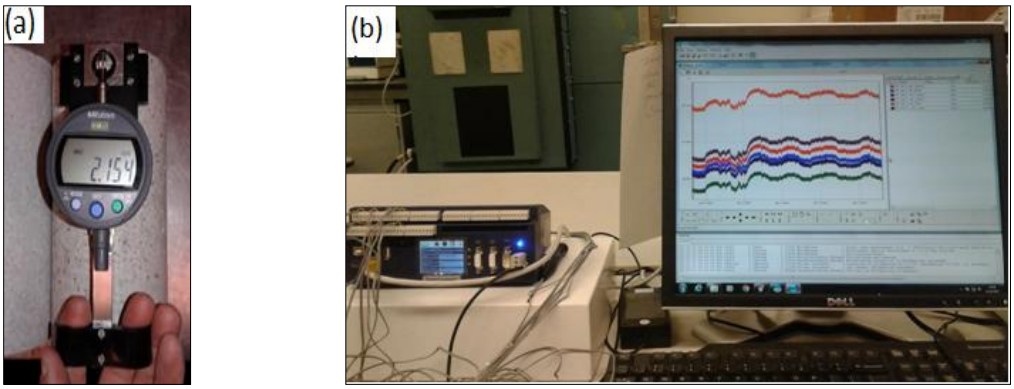

Figure (3.15) Expansion measurements using;

(a) The 150mm digital demec mechanical strain gauge, and (b) Strain gauges connected to DAS

3.4.2.2.4 Mass change

The mass change of deteriorated concrete prisms and cylinders were monitored according to ASTM C1293 (2018) at 7, 28, and 56 days, then at 3, 6, 9, 12, 15, and 18 months, respectively. The change in mass was calculated using **Eq. (3.4)**

$$\text{mass change} = (W_n - W_i)/W_i \qquad \textbf{Eq. (3.4)}$$

Where W_n is the mass measured at (n) day, W_i is the initial mass measured after de-molding the specimens.

Moreover, the mass change due to sorptivity was measured based on ASTM C1585 (2013) by using a balance of accuracy 0.01gram as shown in **Fig. (3.16)**.

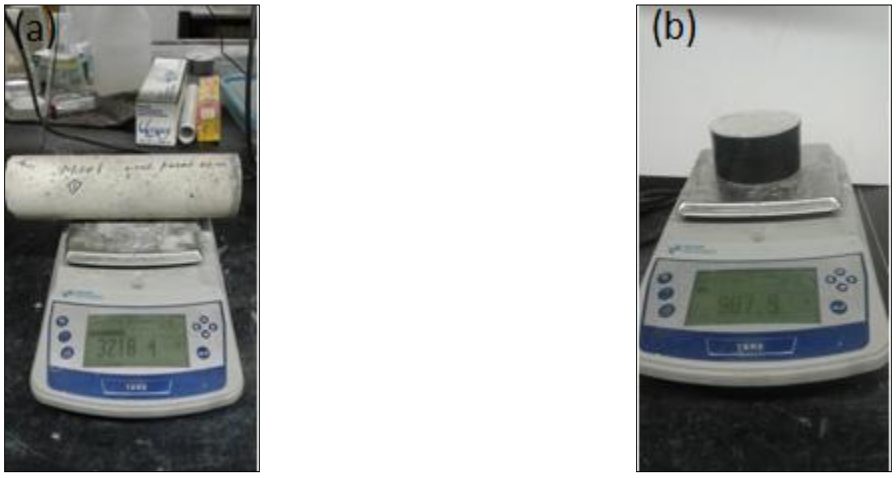

Figure (3.16) Weight change measurements according to;
(a) ASTM C1293, (b) ASTM C1585

3.4.3 Durability Index Tests

Concrete durability typically defined as "The ability of concrete to withstand the harsh environmental conditions and resist the attack of aggressive materials" (Mehta and Montiero 2006). It mainly depends upon the pore system, which governs the fluid transport and causes deterioration. The main causes of deterioration can be classified into physical and chemical causes. The former includes abrasion, erosion, cavitation, cracks, freezing and thawing, salt attack, and fire. The latter includes steel corrosion, alkali-aggregate reaction, sulfate attack, delayed ettringite formation, acid attack, and leaching (Mehta and Montiero 2006).

Increasing the concrete service life and minimizing the maintenance cost primarily governed by factors such as; (1) The selection of most appropriate concrete ingredients (i.e. concrete ingredients in new structures plays an important role). (2) Evaluation of concrete deterioration degree, plus durability becomes more necessitate. Therefore the evaluation of concrete surface (i.e. cover) considered one of the most critical indicators that express resistance of material transportation.

The research covered measuring the durability of various concrete mixtures by used the Rapid chloride penetration test, and the sorptivity test.

3.4.3.1 Chloride Permeability and Water Absorption

The Rapid Chloride Permeability Test (RCPT) was used according to the ASTM C1202 (2017) as a measure of durability in this research. The test consists of placing concrete specimens of dimensions Ø100mm×50mm between two electrodes, applying a DC voltage of 60V and measuring the current. RCPT was conducted on cylinders Ø100mm×50mm at different ages by using the Germann "PROOVE'it" device as shown in **Fig. (3.17a)**.

The test procedure was conducted by extracting the air from the pore system of concrete specimens after placing into a vacuum desiccator. The desiccators were connected to a vacuum pump which ran for three continuous hours as shown in **Fig. (3.17b)**. Then de-aired water from the second desiccator was transferred to fully cover the specimens, followed by an extra one hour of vacuum. Finally, the vacuum was released, and the specimens left fully saturated in the water for a continuous eighteen hours.

After completing the specimen preparation as mentioned above, the specimens were removed from the desiccators and the "PROOVE'it" jackets placed at both ends of the specimens. Then used grease to ensure the specimens were in good contact with the cells and fully sealed. The specimen was fixed carefully at the middle point of the two acrylic cells and tightened evenly to prevent any leakage.

The two reservoirs (i.e. negative and positive) were filled only up to 5mm below the center of the bottom fill hole by 3% NaCl and 0.3N NaOH solutions, respectively. The reservoir cells connected to the channel and a current of 60V was applied from the power supply for 6 hours. Finally, the total charge passing through the tested concrete specimens was calculated according to **Eq. (3.5**).

$$Q=900\ (I_0+2I_{30}+2I_{60}+\ldots\ldots+2I_{300}+2I_{330}+I_{360}) \qquad \textbf{Eq. (3.5)}$$

Where Q is the charge passed by coulombs; Io is a current (Amperes) immediately after voltage is applied; It is the current (amperes) at the time (t) after the voltage is applied.

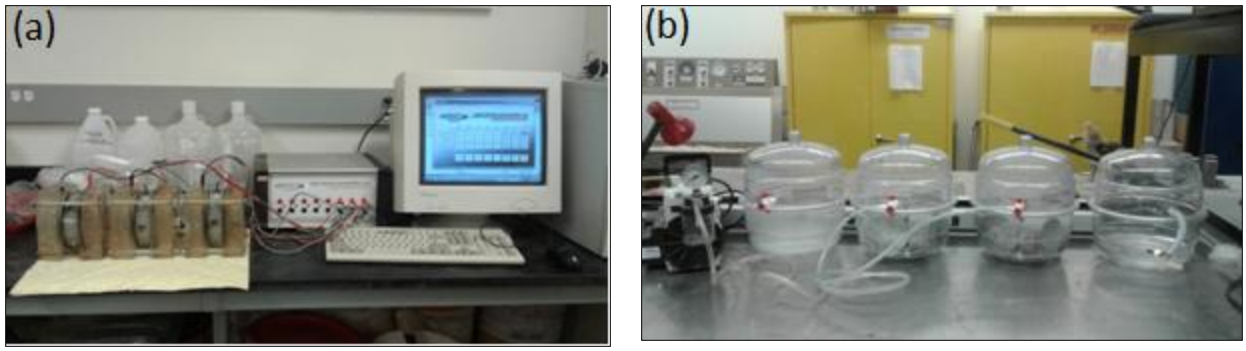

Figure (3.17) Rapid chloride permeability test (RCPT)

(a) Set up during test running, (b) Set up of air extraction from concrete specimens

3.4.3.2 Sorptivity

Sorptivity (S) defined as; "the capability of water/fluid to transport through the unsaturated pore system into the concrete matrix under the capillary suction and with no external pressure" (Mehta and Montiero 2006). The concrete sorptivity is considered one of the transport mechanisms used to represent the concrete quality and its durability. Sorptivity is strongly affected by many factors such as curing period, W/C, pores volume and connectivity, tortuosity and relative humidity into the concrete matrix (Mehta and Montiero 2006, Hosseini et al., 2009, Shahroodi et al., 2010, and Castro et al., 2011)

Sorptivity measures the rate of water penetration into concrete specimens due to the capillary force during a specified time according to ASTM C1585 (2013). The test was applied to concrete specimens of Ø100mm×50mm. These specimens were subjected to 50±2 ^{o}C and 80±3% RH for consecutive three days as shown in **Fig. (3.18)**, to obtain an internal 50-70% RH that match the RH of most structures concrete cover (DeSouza et al., 1997). Moreover, to ensure the good distribution of moisture within the specimens (Bentz et al., 2001), each specimen was stored in a sealed container at 23±2 ^{o}C for consecutive two weeks.

Directly after removal of the specimens from the sealed container, the mass of each specimen was recorded. Then the outer surface of each specimen sealed by a vinyl electrical tap to grantee the uni-directional flow rate of water throughout the specimens, and a plastic sheet was used to cover the top surface. The specimens were placed onto a plastic grid into a pan filled with tap water, where the unsealed bottom surface touched the tap water, and the water level was kept constant during the test duration. Finally, the mass change of each specimen was recorded by using a balance of accuracy 0.01gram according to ASTM 1508 (2013) as shown in **Fig. (3.19)**.

Figure (3.18) Storage concrete specimens under 50±2 ^{o}C and 80±3% RH

Figure (3.19) Samples preparation before starting sorptivity test

The initial and secondary sorptivity was determined at a specified interval according to ASTM C1585 (2013). The initial Sorptivity measured during the first 6 hours representing the filling of cracks and larger pores by water at a higher rate. The secondary Sorptivity represents the saturation of gel pores with slower rate measured throughout the next eight days (Yang et al., 2006).

The absorption was calculated by **Eq. (3.6).** Finally, the Sorptivity obtained by calculating the slope of the best line fit, which represents the relation between the calculated absorption, I, and square root of time as shown in **Fig. (3.20)**.

$$I = (m_t)/(a.d) \qquad \textbf{Eq. (3.6)}$$

Where I is the absorption (mm), m_t is the specimens mass in grams at a time (t), a is the specimens exposed area (mm^2), and d is the water density (gm/mm^3).

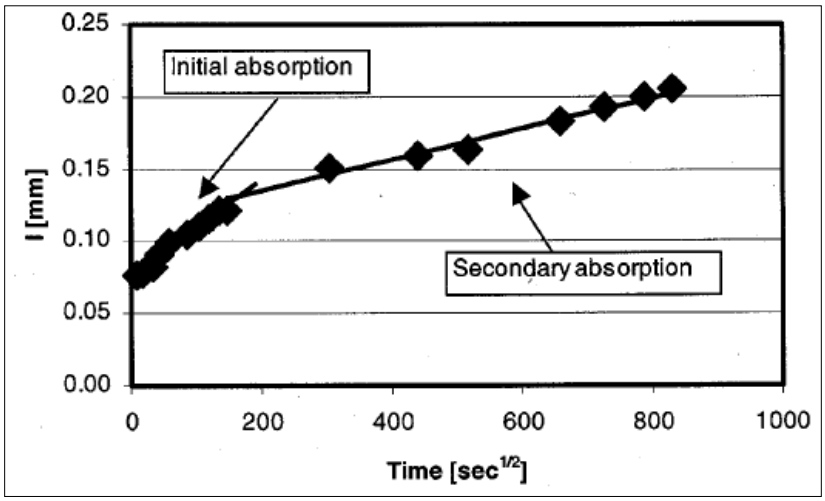

Figure (3.20) Initial and secondary absorption

[ASTM C1585]

Chapter

4

Evaluation ASR Performance

(Phase One)

4.1 Introduction

This chapter examines concrete and mortar mixtures containing Spratt reactive aggregate and fused silica. It provides a comprehensive understanding of the effect of different parameters as specimens shape, casting direction of concrete, specimens size, and different degree of reactivity on ASR performance. Moreover, evaluate the effect of the degree of damage and its extent on the different properties of concrete using the destructive and nondestructive tests.

4.2 Literature Review

Since ASR recognition in 1940 (Stanton, 1940), many studies had been conducted to evaluate the degree of reactivity for different types of rocks (Alderman 1943, Mielenz et al., 1947, Kelly et al., 1948, Bérubé, et al, 2000, Roy and Morrison, 2000, and Smaoui et al., 2004 and 2007). Simply, Alkali-silica reaction (ASR) is defined as; a chemical reaction between reactive silica presented in aggregate particles, and alkalis (Na_2O and K_2O) contained into the cement paste (Neville2002, Hou, et al., 2004, and Mehta and Montiero 2006). The product of this reaction is alkali-silica gel (ASG), this gel has the ability to absorb water from its surrounding hydrated cement past and/or external sources and expands (Forster et al., 1998, Neville2002, and Mehta and Montiero 2006). The internal pressure results from expansion (i.e. volume increase), ASG

induces internal stresses. Once these stresses exceed the concrete tensile strength limit, aggregate particles and the surrounding paste start to crack (Mehta and Montiero 2006).

Most studies follow the standardized tests to assess the ASR in concrete including; concrete prism test (CPT) as ASTM C1293 (2018), CSA A23.2-14A (2014), and RILEM AAR-3 (2000) for concrete. However, the concrete prism specimens need to be tested for a consecutive two years according to ASTM C1293 (2018). To shorten the testing time, other standard tests are focused on testing mortar instead of concrete. For instance, accelerated mortar bar test (AMBT), requires two weeks of test monitoring and can be extended for several weeks according to ASTM C1260 (2014).

Other researchers attempt to use various materials to accelerate the expansion rate including; Pyrex glass, quartz, opal, chert, and fused silica (FS). Pyrex glass was found effective in the mortar expansion (McConnell and Irwin, 1945). Under room temperature, both opal and FS were reported to induce excessive expansion (Gaskin et al., 1955). Moreover, 4.5% Opal was reported to produce a higher expansion than 15% FS replaced fine aggregate by weight at cured temperature 20^{o}C and 96% relative humidity (RH) as shown in **Fig. (4.1)** (Swamy and Asali 1988, and Ahmed et al., 2003). Conversely, macro and micro quartz did not reveal an appreciable reactivity (Gaskin et al., 1955).

The effect of FS with 15% replacement ratio of the total aggregate weight was evaluated earlier on concrete prisms 75mm×75mm×300mm by (Swamy and Asali 1988). The authors reported the expansion measured at 28, 100, and 365 days were 0.023, 0.259, and 0.623, respectively. While, with the same replacement level of fused silica (i.e. 15% FS) the expansion measured on concrete prisms 100mm×100mm×500mm was 0.009, 0.122, and 0.166, at 28, 100,

and 365 days, respectively (Ahmed et al., 2003). Recently, the effect of FS with different fine aggregate replaced ratios on the expansion of concrete prisms 75mm×75mm×300mm when exposed to 38 °C and 100% RH was investigated, the author reported 15% FS produced an expansion of about 0.46, 0.88, 1.022 at 28, 100, and 336 days, respectively (Abdullah, 2013). The author used 7.5% FS as a replacement for fine aggregate by weight because that portion resulted in the highest expansion by about 1.22% at 48 weeks (Abdullah, 2013). The same FS content (i.e. 7.5%) was used based on the previous research to triggering the ASR into RC columns (Kubat et al., 2014, and 2016).

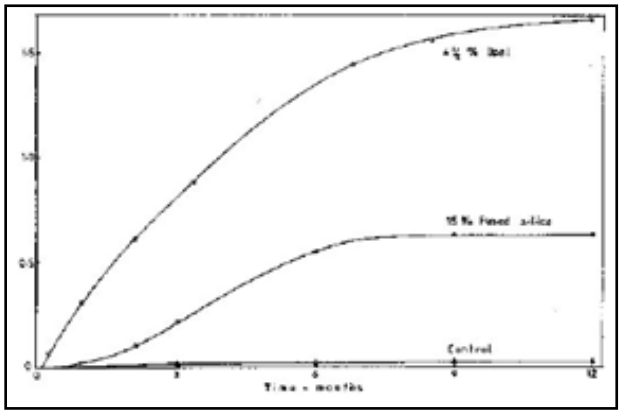

Figure (4.1) Expansion of concrete specimens (control, 15% FS, 4.5% opal) cured at 20 °C and 96% RH

[Swamy and Asali 1988]

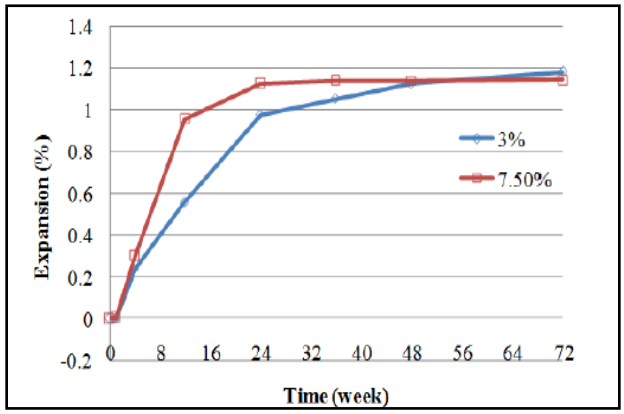

Figure (4.2) Expansion of concrete specimens contains 3% and 7.5% FS Cured at 38 °C and 100% RH

[Abdullah, 2013]

Many points had been raised about concrete prism standard test, it requires long-term monitoring. However, it underestimates expansion due to alkalis leaching (Thomas et al., 2006, and Lindgård et al., 2013). The leaching of alkalis of specimens exposed to 38 °C and 100% RH

was about 20% and 35% within the first 90, and 365 days, respectively due to convective air current (Thomas et al., 2006).

On the other hand, In laboratory testing, prisms are cast horizontally and subsequently tested for expansion in the vertical direction. These tests may not adequately relate to actual cast-in-place concrete structures. In addition, core samples extracted from defective structures to evaluate ASR were tested usually in the same casting direction. However, CPT specimens are tested perpendicular to the casting direction.

Researchers conducted on studying the effect of specimens shape on ASR expansion reported that cylindrical specimen exhibit higher expansion than that of the prismatic specimens (Smaoui et al., 2004, Multon et al., 2005, Latifee et al., 2014, and Piersanti, 2015). In addition, the casting direction may also contribute to the measure expansion value.

Latifee et al., (2014) carried out a rapid test named miniature concrete prism test (MCPT), to compare the expansion of MCPT and CPT specimens at 56 and 365 days, respectively. Two shapes of specimens included four different types of aggregate tested at 38, 60, and 80 ^{o}C, respectively. However, through assessing the effect of specimens shape, the authors modified some of the standard test parameters as standard prism dimension to be 50mm×50mm×285mm, and cylinder mold of Ø50mm×285mm.

Moreover, the degree of temperature increased from 38 ^{o}C to 60 ^{o}C, the maximum particle size changed to be 12.5mm instead of 19.5mm, and all specimens soaked in 1N NaOH solution during test duration (i.e. 84 days). The results exhibit a higher expansion of cylinders than the prisms after 84 days for the four different types of aggregate. **Figure (4.3)** represents the difference in expansion of cylinders and prisms specimens containing Spratt aggregate.

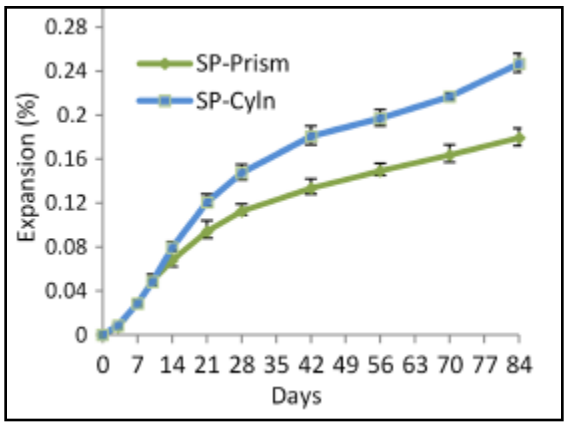

Figure (4.3) Expansion comparison of concrete specimens prisms and cylinders contains Spratt aggregate at 84-day soaked in 1N NaOH at 60 ^{o}C. [Latifee et al., 2014]

Alkali-silica reaction expansion for concrete has been evaluated extensively for a long time with different methods. However, limited research has focused on the effect of tested specimens' shape, size and casting direction on the evaluated ASR expansion value. In addition, contradictory data on the effective ratio of FS were reported in the literature. Therefore, the experimental work - **Phase One** explores the effect of specimens' shape and size on the accuracy of measured ASR expansion and find a correlation between cylindrical and standard prismatic specimens. In addition, it highlights the effect of casting direction concerning ASR expansion. Finally, covered the effect of these factors on the mechanical properties and durability indices of concrete. It is anticipated that the outcome of this phase would contribute to enhancing existed standards test methods.

4.3 Specimens, Mixtures, Casting, and Curing

4.3.1 Concrete and Mortar Specimens

As detailed in section 3.2, a total of 594 specimens were cast through **Phase One** to evaluate ASR performance, mechanical properties, and durability indices for concrete and mortar mixtures in accordance with ASTM standards as shown in **Fig. (4.4)** and **Table (4.1).**

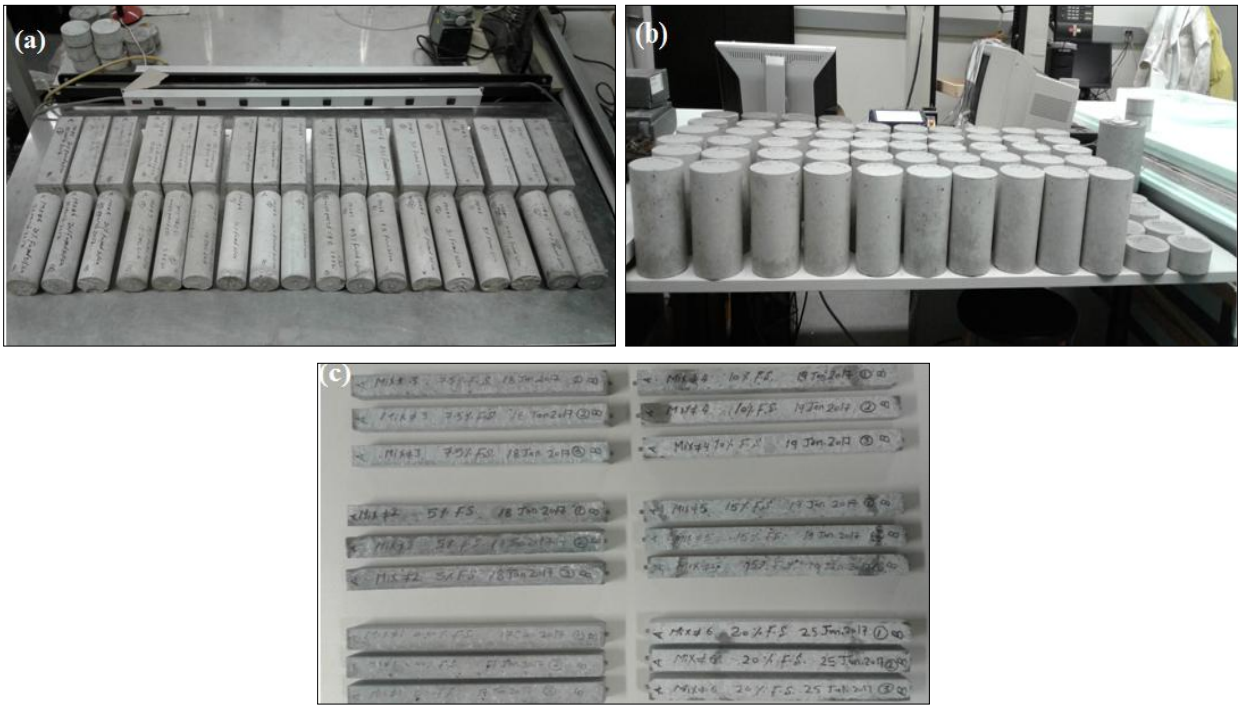

Figure (4.4) Concrete and mortar specimens

(a) Prisms 75mm×75mm×285mm, and cylinders Ø75mm×285mm, (b) Concrete Cylinders Ø100mm×200mm and Ø100mm×50mm, and (c) Mortar bars 25mm×25mm×285mm

Table (4.1) Phase One concrete mixture proportions, specimen (shape, dimensions, and number), and tests performed (measurements, duration, and specifications)

Mix ID	Mixture ingredients												Specimens				Test		
	Water (kg/m^3)	W/C	Cement (kg/m^3)	Aggregate (kg/m^3)		Fused Silica (%) The ratio from total aggregate weight							Shape		Dimension (mm)	No	Measurements	Duration (day/week)	Standard
				Fine	Coarse	0.0	5	7.5	10	**15[(1)]**	20		Prisms	Cylinders					
1	189	0.45	420	793	927	0.0	-	-	-	-	-		✓	-	75×75×285	6	Expansion	1,3,7,15,28,56,90,180,270,365, 456 and 548 days	ASTM C1293
													-	✓	Ø75×285	3			
													✓	-	25×25×285	3		Daily from 1 to14-day and Weekly till 12 week	ASTM C1260
																	Expansion	Monthly from 1 to 12	ASTM C1293
																	Compression Strength	Monthly from 1 to 12	ASTM C39
													-	✓	Ø100×200	72	Tensile Strength	Monthly from 1 to 12	ASTM C496
																	MOE, υ, and SDT	Monthly from 1 to 12	ASTM C469, and N.A.
																	Ultrasonic Pulse Velocity	Weekly till 365s days	ASTM C597
													-	✓	Ø100×50	15	Permeability	28, 56,90, 180 and 365 days	ASTM C1202
2	189	0.45	420	707	927	-	86	-	-	-	-								
3	189	0.45	420	664	927	-	-	129	-	-	-								
4	189	0.45	420	621	927	-	-	-	172	-	-						As mentioned above in Mix#1		
5*	**189**	**0.45**	**420**	**535**	**927**	**-**	**-**	**-**	**-**	**258**									
6	189	0.45	420	459	927	-	-	-	-	-	334								
Total number of concrete specimens																	**594 specimens of different size and shape**		

*Concrete mixture selected to prepare deteriorated concrete mixture in experimental work - Phase three

4.3.2 Mixtures

Five concrete mixtures included Spratt reactive aggregate and different portions of FS, and one mixture without FS as a control were prepared according to ASTM C192 (2016). The FS was added as a replacement fine aggregate by mass at rates; 0%, 5%, 7.5%, 10%, 15%, and 20% as shown in **Table (4.1)**. The total alkali content for all mixtures was adapted at level 1.25% Na_2O equivalent by adding NaOH solution to mixing water; the solution prepared according to ASTM C1293 (2018). All concrete mixtures of total weight 2329 kg/m^3 were cast with a ratio of 1:1.9:2.2 (i.e. cement: fine agg.: coarse agg.). All mixtures had a constant 0.45W/C, and proportions of 189 Kg/m^3 water, 420 kg/m^3 GU cement type #10 of total alkali content 0.87% Na_2O equivalent. In addition, 927 kg/m^3 Spratt aggregate Type #3 meeting the requirements of ASTM C1260 (2014) of nominal size 19mm and gradation as shown in **Table (4.2)**, and 793 kg/m^3 natural fine non-reactive aggregate of fineness modulus 2.7.

Moreover, a portion of Spratt aggregate Type #3 was crushed and sieved to obtain a fine reactive aggregate according to ASTM C1260 (2014) for mortar mixtures. Six mortar mixtures were cast using fine reactive aggregate with the same various portions of FS used in the concrete mixtures for testing according to ASTM C1260 (2014). Chemical, physical, and petrographic properties for used aggregate and fused silica are summarized in **Chapter 3, Tables (3.2a,3.3).**

Table (4.2) Reactive coarse aggregate from Spratt after sieve

Sieve Size		Weight (%)	
Passing	Retained	ASTM C1293	Sample used in mixtures
19.0$_{mm}$ (3⁄4 in.)	12.5$_{mm}$ (1⁄2 in.)	33	33
12.5$_{mm}$ (1⁄2 in.)	9.5$_{mm}$ (3⁄8 in.)	33	33
9.5$_{mm}$ (3⁄8 in.)	4.75$_{mm}$ (No. 4)	33	33

4.3.3 Mixing, Casting, and Curing

The mortar ingredients were measured by the balance of accuracy 0.01gram, and small mortar mixer used to prepare all mixtures according to ASTM C305 (2014). Mortar bars immersed in 1M NaOH solution into plastic containers, then covered by plastic sheets and placed inside an oven at 80 ^{o}C satisfying the requirements of ASTM C1260 (2014) as represented in **Fig. (4.5)**.

Figure (4.5) Storage of mortar bars in an oven at 80 ^{o}C

On the other hand, all concrete ingredients were measured by the balance of accuracy 5gram, then mixed in the pan type small mixer of bowl capacity 0.1m^3 according to ASTM C192 (2016). Concrete specimens were cast in the specified prism molds (i.e. 75mm×75mm×285mm) in two different directions (i.e. vertically and horizontally) as illustrated in **Fig. (4.6a)**. Moreover, The concrete was cast in plastic cylinder molds prepared for that purpose by Ø75mm×285mm, where the custom cylinder molds were sized to be the dimensions of the prisms as illustrated in **Fig. (4.6b and 4.7)**. As well as cast concrete in commercial cylinder molds Ø100mm×200mm as shown in **Fig. (4.8).**

Metal demec points were fixed on the concrete prisms, cylindrical specimens Ø75mm×285mm according to ASTM C1293 (2018). However, metal demec points were fixed on concrete cylinders Ø100mm×200mm at 25±3mm from each end linearly (i.e. parallel to the longitudinal axis) at four different lines matching angles $^{o}0$, $^{o}90$, $^{o}180$, and $^{o}270$, respectively as illustrated in **Fig. (4.8).** The concrete cast was started by fixing the different molds on the vibrating table after oiled and installed the studs, then placed the concrete in the molds at two and three layers in the prisms cast horizontally and vertically, respectively. In addition, placed the concrete into the cylindrical molds of Ø100mm×200mm and Ø75mm×285mm in two and three layers, respectively. Each layer was vibrated. Finally, the top surface of the last layer was finished smoothly by trowel before covered the mold.

All concrete specimens were stored in plastic containers with 20±5mm water at the bottom. Specimens were placed above light grid panels made of polystyrene to prevent any direct contact with water. Containers with the specimens were stored in an environmental chamber (i.e. prepared with dimension 2.4m×1.2m×1.2m) under 38 ^{o}C and 95±5% RH to meet ASTM C1293 (2018) requirements as shown in **Fig. (4.9)**.

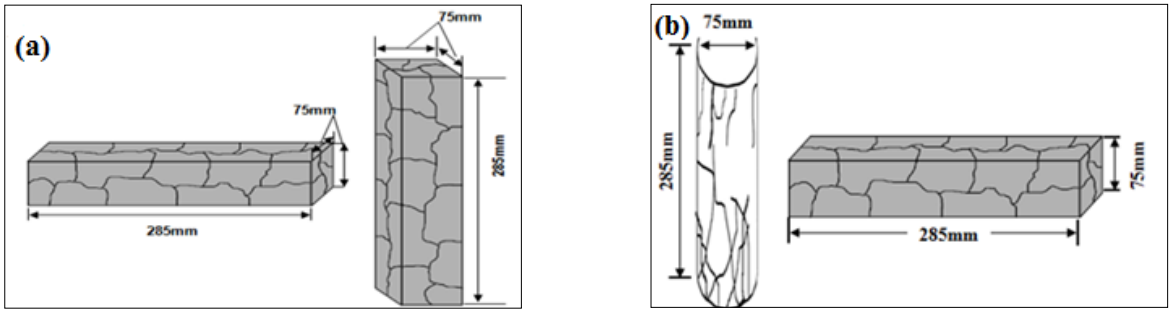

Figure (4.6) Illustrate the different geometry of specimens

(a) prismatic specimens cast vertically Vs. horizontally, (b) prismatic Vs. cylindrical

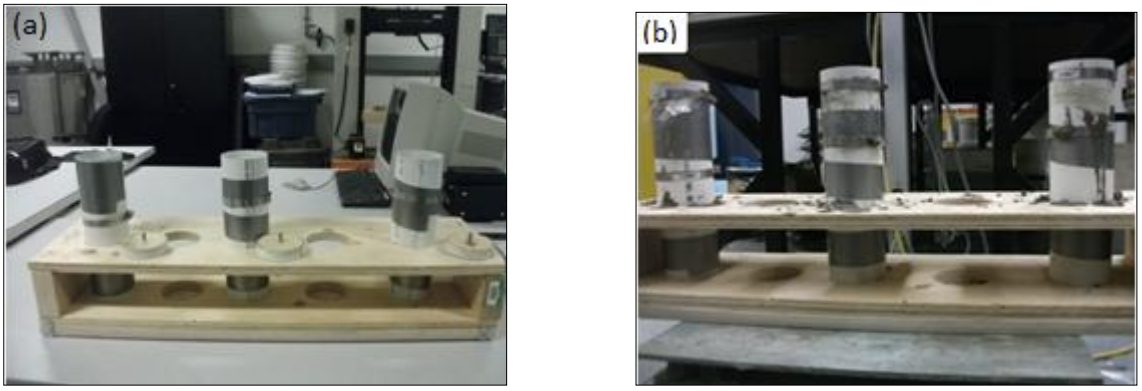

Figure (4.7) Preparation of concrete cylinder specimens (Ø75mm×285mm)

(a) Mold of cylinders Ø75mm×285mm, and (b) Mold after casting concrete

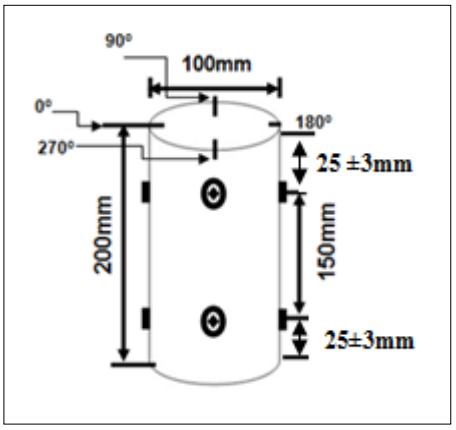

Figure (4.8) Illustration of the demec fixation on concrete specimens Ø100mm×200mm

Figure (4.9) Storage of concrete specimens in the environmental room at 38 ^{o}C and 95±5% RH

The environmental room walls and bottom were fabricated from gypsum board sheets covered by plastic to be protected from high relative humidity (i.e. vapor barrier), then fix the chamber on a wood sheet. The columns fabricated from wood 1000mm×100mm×50mm covered by the same plastics sheets. The vinyl tiles installed to protect the floor from any debris materials. Two heaters of 50.8cm, 500Watts, and 240V were installed and connected to a controller with thermocouples to keep the temperature at 38 ^{o}C. The chamber cover prepared from a plastic sheet of doubled layers and fix Velcro tap to open and close the room quickly. Finally, the Styrofoam 50mm thickness was used to cover all sides externally and the top of the chamber to prevent heat loss. To maintain the uniformity of relative humidity and temperature inside the environmental chamber as shown in **Fig. (4.9)**, two small fans were placed inside. Four sensors connected to data acquisition system (DAS) and computer were inserted in the containers to collect the temperature and relative humidity data.

Expansion measurements were conducted on concrete prisms, cylindrical specimens Ø75mm×285mm, and mortar specimens using a digital comparator of the accuracy of 0.002mm at ages met ASTM C1260 (2014) and C1293 (2018). While expansion measured on cylindrical concrete specimens Ø100mm×200mm by using150mm digital demec mechanical strain gauge. The expansion measured on cylindrical concrete specimens Ø100mm×200mm after de-molding the specimens to record the initial readings, then continue data recording daily at 1, 3, 7, 15, 28 days, and monthly until 12 months.

Fresh properties for the examined concrete mixtures were evaluated in conformity to ASTM standards ASTM C143 (2015), ASTM C231 (2017), and ASTM C138 (2017). The slump was in the range from 95mm to 130mm, the air content was in the range from 2.0 to 2.2%, and unit weight was in the range from 2375 to 2415 kg/m^3.

4.4 Measurements and Results

The measurements and results are divided into three different categories: expansion, mechanical properties, UPV (i.e. nondestructive test), and durability indices. The first category included measuring of expansion and mass variation. The second category dealt with measurements of compressive and tensile strengths, modulus of elasticity (MOE), Poisson ratio (υ), loss of stiffness, plasticity deformation, and UPV sensitivity to the degree of damage over time. The third category comprised measuring of durability index. All of these measurements accomplished according to ASTM requirements.

4.4.1 Category I - Change in Physical Properties

4.4.1.1 Expansion

4.4.1.1.1 Effect of Triggering Material

The expansion measurements as a function of time for all tested concrete mixtures containing Spratt aggregate with and without different portions of FS are shown in **Fig. (4.10)**. The standard deviation of the expansion results was in the range of 0.001% to 2.65%. Generally, expansion increased with time for all tested specimens. Mixtures incorporating FS exhibited a higher increase in expansion compared to that with reactive aggregate only. All mixtures containing FS reveals a drastic increase in expansion until age 180 days, then the rate of expansion became stable until the end of the investigated period (i.e. 548 days). So, the expansion rate can be divided into two main parts concerning to time, part A (i.e. initial part) represent the drastic expansion from day 0 to 182 days and part B (i.e. secondary part) in the range from 182 days to 548 days represent the steadiness of expansion.

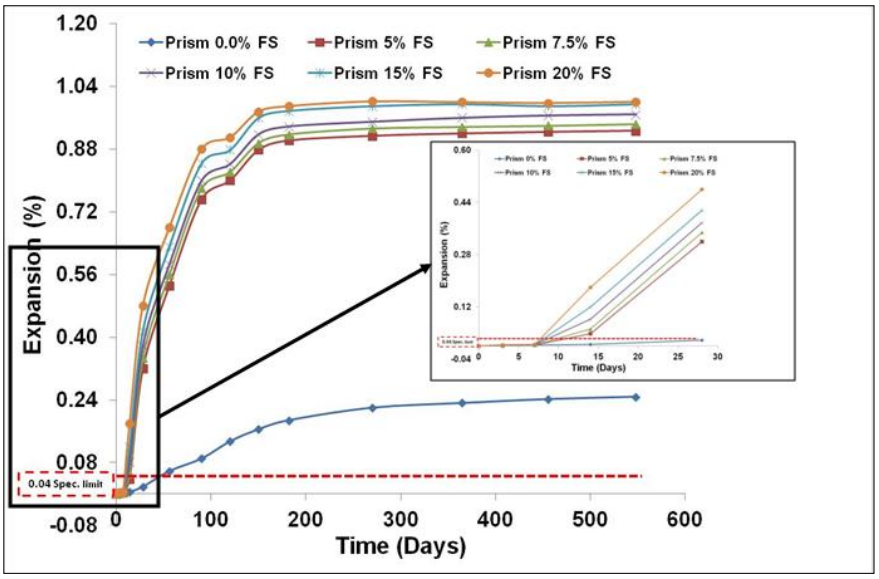

Figure (4.10) Expansion of concrete specimens – standard horizontal prisms (75mm×75mm×285mm)

Comparing the results with the previous researches conducted using 15%FS replaced the fine aggregate. The results exhibited a higher expansion a long time than the expansion reported by (Swamy and Asali 1988) by about 94%, 70%, and 37%, at 28, 100, and 365 days, respectively. In addition, higher than the expansion reported by (Ahmed et al., 2003) by about 98%, 86%, and 83% at 28, 100, and 365 days, respectively. While it was lower than the expansion reported by (Abdullah, 2013) by about 11%, 74%, 2.7% at 28, 100, and 336 days, respectively. It is clear the type and source of FS play a crucial effect on the measured expansion. Concerning the level of replacement of FS, 7.5% FS showed a higher expansion than 15% and 20% FS (Abdullah, 2013). While the results exhibited the higher the FS, the higher the expansion.

For instance, all prismatic specimens containing greater than 7.5% FS exceed the standard expansion limit (i.e. 0.04%) after 14 days. Based on the visual inspection, the first cracks were detected after two weeks on the surface of concrete prisms contains 7.5% FS and more. The

cracks started as hair cracks then propagated and connected to cover the surface of all concrete prisms as shown in **Fig. (4.11a,b).** Cracks developed as a result of the increase in the internal stresses at an early age, while the concrete tensile strength was still low.

From the above explanation, it is clear, the rate of expansion under the standard condition (i.e. 38 ^{o}C and 100% RH) was primarily affected by the replacement level of FS in concrete mixtures. For instance, the expansion at 90 days of prismatic specimens were recorded 0.090, 0.752, 0.780, 0.800, 0.844, and 0.880 for mixtures contains 0%, 5%, 7.5%, 10%, 15%, and 20% FS, respectively.

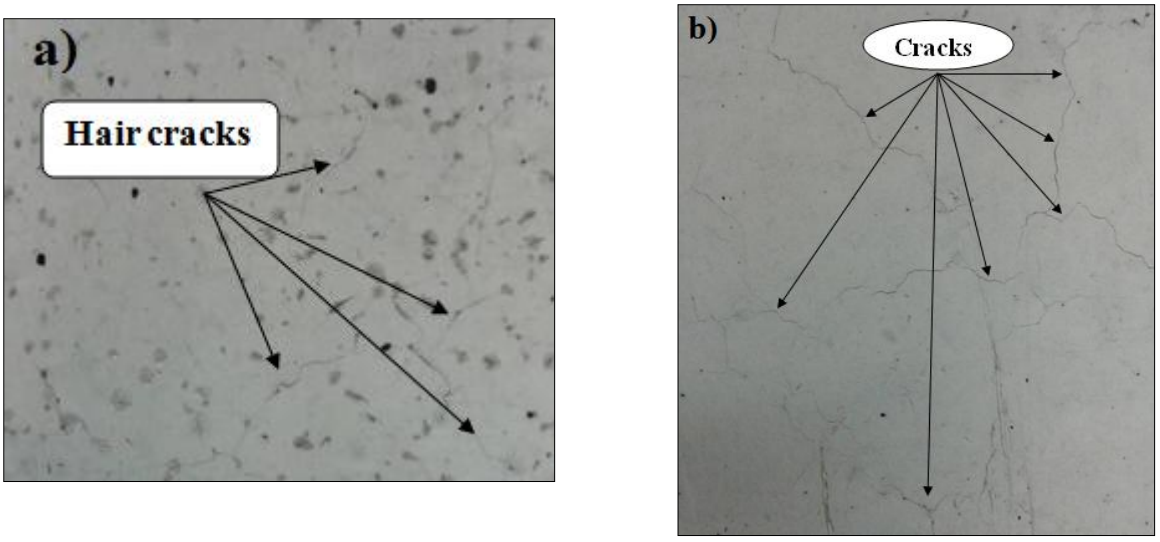

Figure (4.11) Cracks development on the concrete surface of mixture incorporating 15% FS

(a) Hair cracks after two weeks, (b) Cracks growing up at 56 days

The mortar mixtures followed the same general trend as the concrete expansion as represented in **Fig. (4.12)**. The standard deviation of the expansion results was in the range of 0.001% to 0.174%. All mixtures exhibited an extreme increase in expansion with time during the test duration. Moreover, mixtures incorporating FS exhibited a higher increase in expansion

compared to that with fine Spratt reactive aggregate only. The expansion can be a feature of the high alkali content and the harsh environmental condition with the presence of high amount of silica present in the mortar mixtures from FS without any restrained due to no aggregate particles (Haddad et al., 2008, Berra, et al., 2010, and Yurtdas, et al., 2013). As a result, the cracks become more extensive as FS portion increase as shown in **Fig. (4.13).**

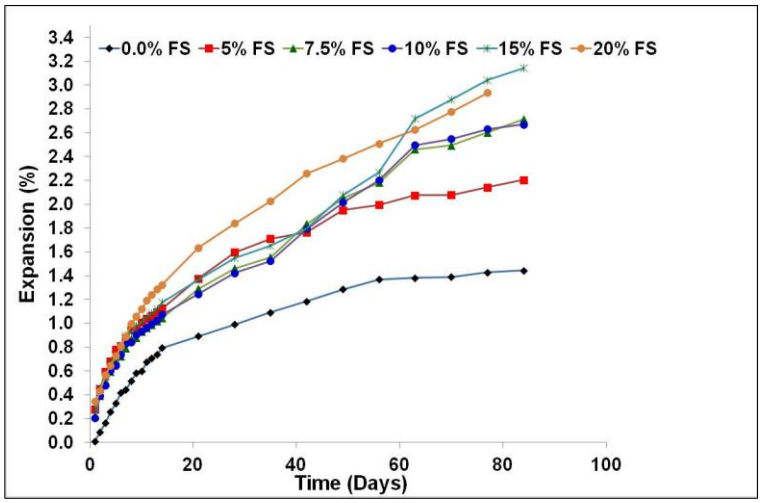

Figure (4.12) Expansion of mortar specimens contains Spratt aggregate and a different portion of fused silica (FS)

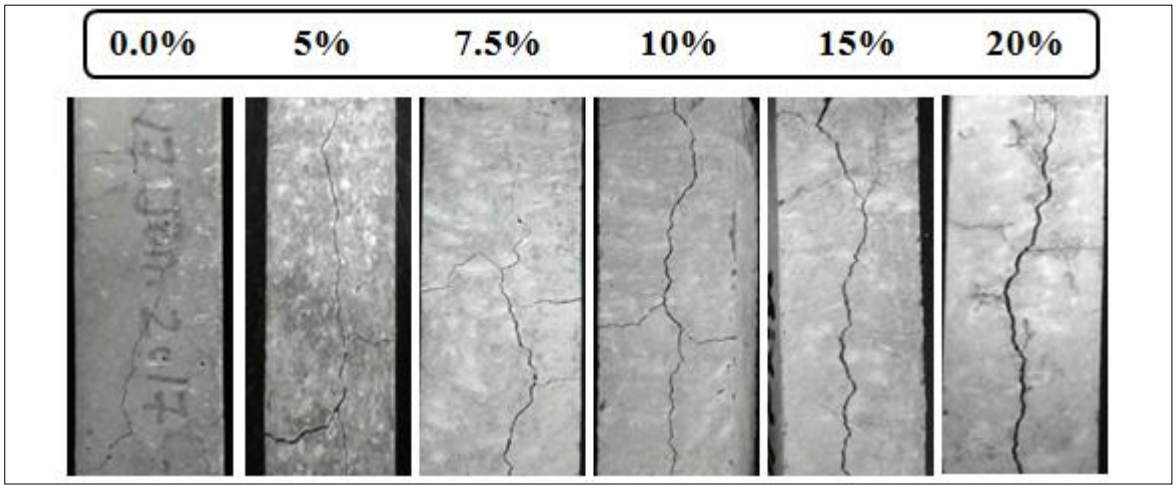

Figure (4.13) Cracks in mortar bars incorporating different portions of FS at ten weeks

Despite there is good agreement between CPT and AMBT (i.e. all mixtures incorporated FS revealed a higher expansion than the mixture not contained FS a long 548 days of measurements). The measurements conducted on the mortar mixtures incorporating different levels of replacement of FS did not reinforce the conclusion of the concrete mixtures (i.e. the higher the fused silica, the higher the expansion). For instance, at four days the mixture incorporated 5% FS was 0.682% higher than the expansion of mixtures contained 7.5% and 10% FS (i.e. 0.596% and 0.603% respectively). Moreover, expansion of mixture contains 15%FS was 0.676% while the expansion of mixture incorporated 20% FS was 0.648% on the same day (i.e. four days).

The relationship between the CPT and AMBT was plotted by a power trend line with a regression coefficient in the range from 0.85 to 0.96 distinguished based on the FS portion as represented in **Fig. (4.14)**. The results reveal the presence of FS with high replacement portion consumed faster at early ages causing dramatically increase in expansion rate. So that, selection of the replacement amount of FS or any fastening materials should govern by the type and portion of this materials.

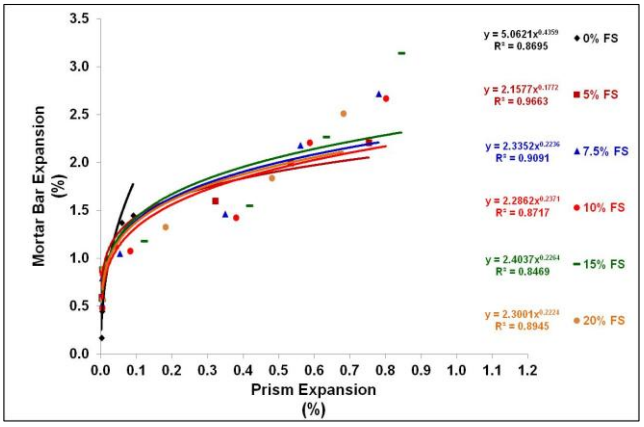

Figure (4.14) Expansion relationship between mortar bars and concrete prisms

4.4.1.1.2 Effect of Specimen Shape

For instance, at replacement portion of 15% FS, cylinders had an increase in expansion over the prisms by about 40% at 28 days. Moreover, at the same time (i.e. 28 days) all mixtures had the same increase as shown in **Fig. (4.15 and 4.16)**. The increase in the expansion of cylinders continued with higher expansion than the prisms until 56 days with the same trend by about 37.93% to 40.23% for all replacement portions of FS. While at 90 days until 548 days the increase in expansion between cylindrical and prismatic specimens was decreased to be in the range from 15% to 9%.

Comparing with the literature, The average expansion measured on concrete specimens using four different types of aggregate (i.e. Texas sand, new Mexico gravel, potassium sandstone, and Quebec city limestone) show an equal or quite similar expansion for both cylinders Ø150mm×200mm (i.e. expansion measured vertically in the same cast direction) and standard prisms (Smaoui et al., 2004). While the expansion measured on cylinders Ø160mm×320mm (i.e. cast and measured in the vertical direction) was twice higher than the expansion measured on prisms 140mm×140mm×280mm (i.e. cast in the horizontal direction) (Multon et al., 2005).

Finally, the relationship between the standard prismatic specimens (i.e. cast horizontally) and cylindrical specimens Ø75mm×285mm for examined mixtures (i.e. 6 mixtures) was represented in **Fig. (4.17)**. The coefficient of determination values for linear trend line is close to unity (i.e. R^2=0.98) at all level of replacement of FS. Despite the points referred to the relationship at 28 and 56 days laying above the linear trend line, the slope of the linear trend line is 1.09. These points exhibit the increased ratio of cylindrical specimens than the standard prismatic specimens for all tested mixtures have the same trend a long time but with a varied portion as mentioned above (i.e. in the range from 43% to 37% at 28 and 56 days, and from 15% to 9% until 548

days). The relationship indicates the expansion measurements on the standard prisms and cylindrical specimens at different ages (i.e. along 548 days) are well correlated linearly and confirming the ASR expansion is related to the geometry of the tested specimens.

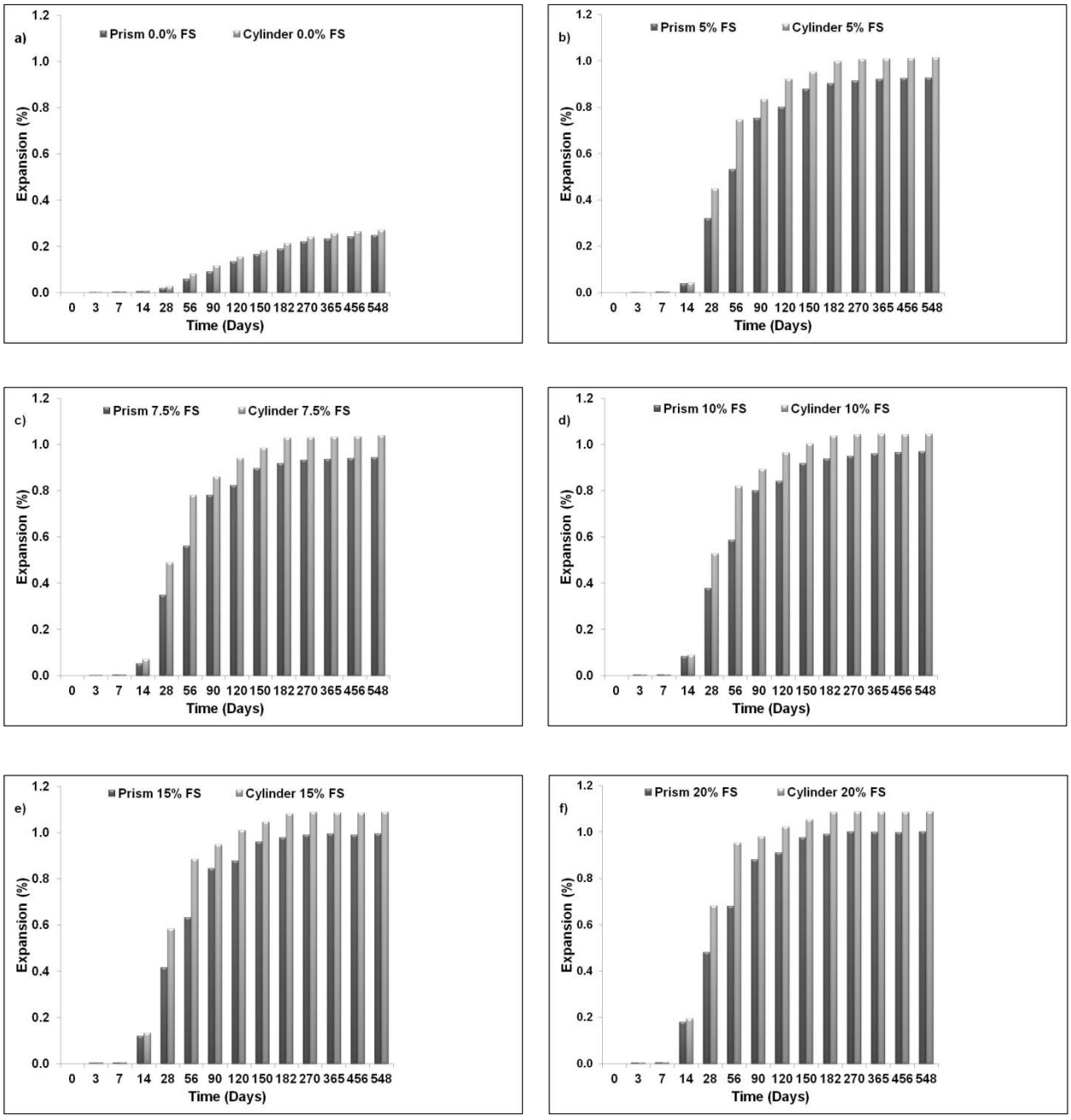

Figure (4.15) Expansion in cylindrical (Ø75mm×285mm) Vs. standard prismatic (75mm×75mm×285mm) specimens contains Spratt aggregate with different portions of fused silica

(a) 0%, (b) 5%, (c) 7.5%, (d) 10%, (e) 15%, and (f) 20%

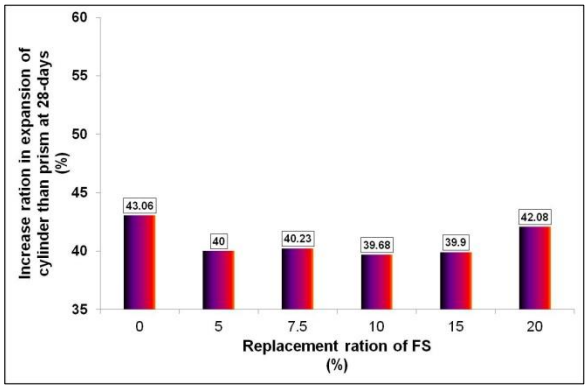

Figure (4.16) Increased ratio of expansion at 28 days for cylindrical (Ø75mm×285mm) Vs. standard prismatic specimens

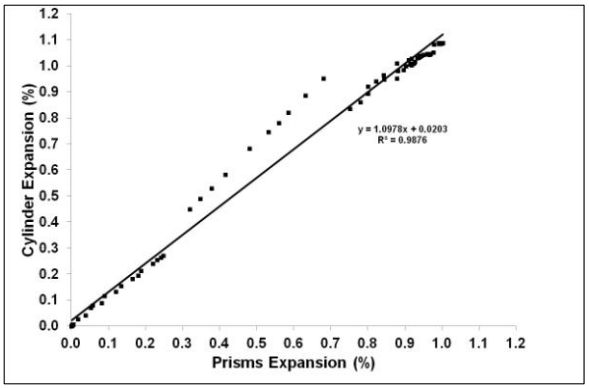

Figure (4.17) Expansion relationship between cylindrical and prismatic specimens

4.4.1.1.3 Effect of Casting Direction

The measurements of expansion were conducted on prismatic specimens cast in two different directions (i.e. vertically and horizontally) as illustrated in **Fig. (4.8)**. The prismatic specimens had the same dimensions and stored in an environmental chamber at 38 ^{o}C and 95±5% RH matching ASTM C1293 (2018) requirements. The prisms cast horizontally laying into the containers in the horizontal direction, while the prisms cast vertically laying in the vertical direction.

Figure (4.18) represents the expansion measurements as a function of time for all tested prismatic specimens comprising Spratt aggregate with and without different portions of FS. Mixtures exhibit an increase in expansion of the prisms cast vertically than the others cast horizontally. Up to 14 days, little difference was observed; however, after that age, the ratio increased in the range from 2.63% to 8.41% depending on the time of measurements and portion of replacement of FS.

For instance, at 56 days the expansion of specimens cast vertically had a higher increase than prisms cast horizontally by 6.9%, 7.52%, 7.86%, 8.19%, 8.23%, and 8.24% for mixtures incorporating Spratt aggregate with 0%, 5%, 7.5%, 10%, 15%, and 20% FS, respectively. The variation in expansion kept almost the same trend over time to be 5.24, 8.09, 7.63, 6.40, 7.34, and 7.59% at 548 days for the same specimens, respectively. From the above, the casting direction had an effect on the rate of expansion under the standard exposure conditions (i.e. 38 ^{o}C and 100% RH).

Finally, the correlation between the prismatic specimens cast vertically and horizontally for examined mixtures was represented in **Fig. (4.19)**. The coefficient of determination values for linear trend line is close to unity (i.e. R^2=0.999) at all level of replacement of FS and the slope of the linear trend line is 1.07. The relationship showed that the expansion measurements on the prism cast in a vertical and horizontal direction at different ages are well correlated linearly and confirming the ASR expansion is related to the cast direction of the tested specimens.

These results are counteracted with the results reported by (Smaoui et al., 2004). Where the average expansion measured on the prisms cast vertically and horizontally exhibit non significant effect (i.e. quite similar) on the average expansion, for example it where (0.48% versus 0.50% at 246 days) with Texas sand, (0.21% versus 0.21% at 270 days) with the new Mexico gravel, (0.09% versus 0.09% at 265 days) with potassium sandstone, and (0.17% versus 0.19% at 286 days) with the Quebec city limestone (Smaoui et al., 2004).

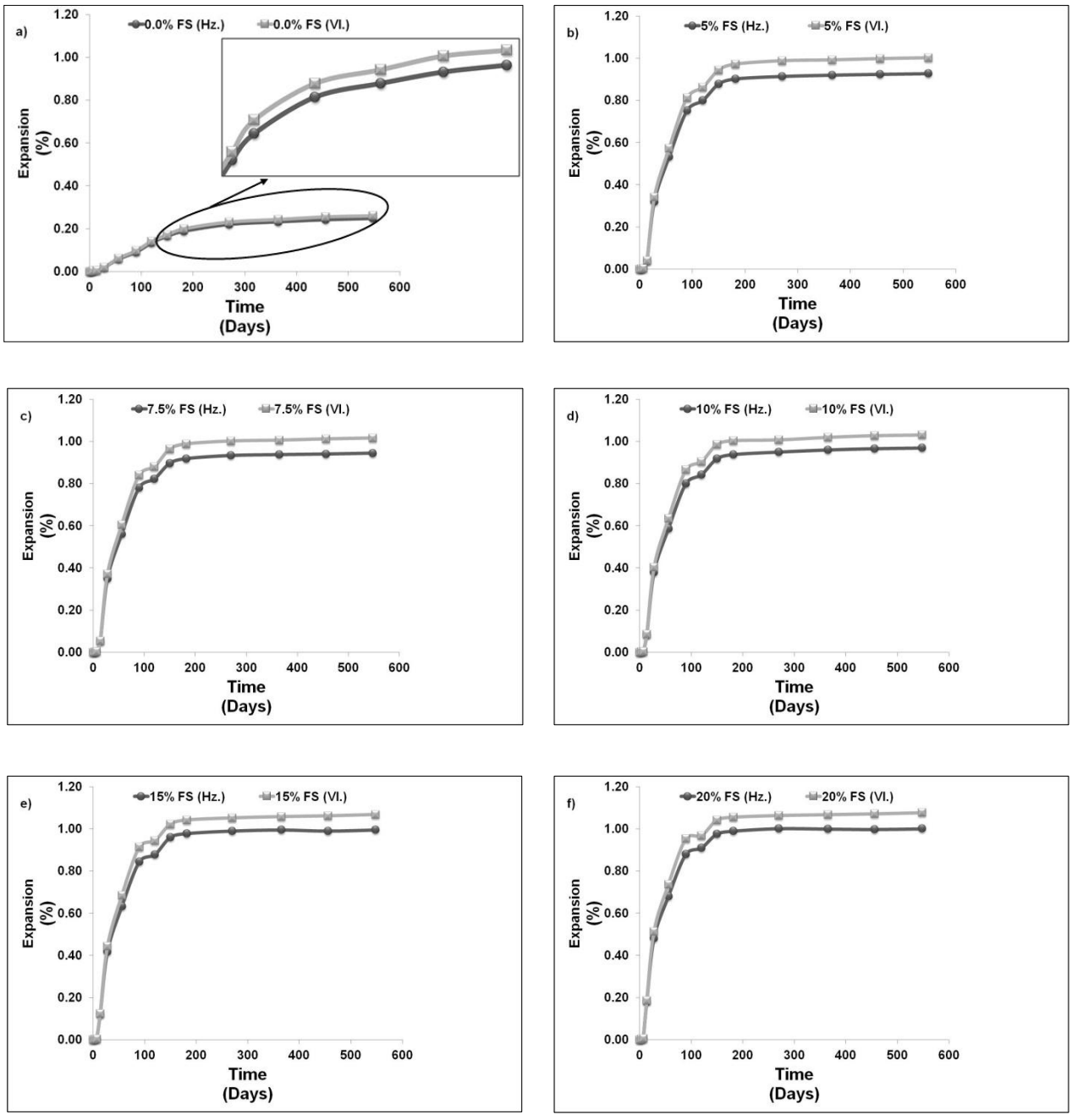

Figure (4.18) Expansion of prismatic specimens cast in vertical and horizontal direction contains Spratt aggregate with different portions of fused silica

(a) 0%, (b) 5%, (c) 7.5%, (d) 10%, (e) 15%, and (f) 20%

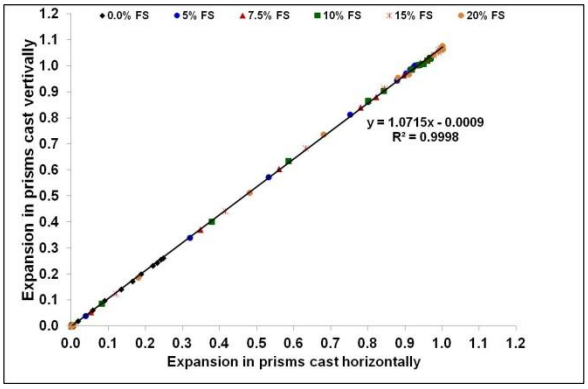

Figure (4.19) Expansion relationship between prismatic specimens cast vertically and horizontally

4.4.1.1.4 Effect of Specimen Size

The expansion measurements as a function of time for all tested cylindrical specimens incorporating Spratt aggregate with and without different portions of FS exhibited the larger diameter cylinders Ø100mm×200mm had lower expansion than the specimens Ø75mm×285mm. **Figure (4.20)** that represents the expansion up to 365 days for two different cylindrical sizes of mixture incorporated 15% FS; other mixtures gave similar results.

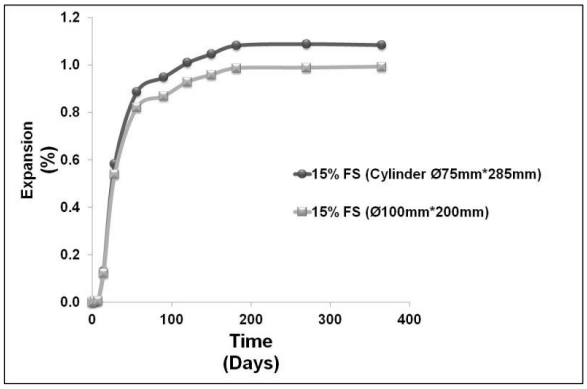

Figure (4.20) Expansion of concrete mixture contain 15% FS specimens Ø100×200mm Vs. Ø75×285m

For the cylindrical specimens, the results reveal an increase in concrete volume and decrease in lateral surface caused a significant reduction in expansion. For instance, the concrete containing reactive Spratt aggregate without adding FS, the expansion of specimens Ø100mm×200mm reduced by about 10% than the specimens Ø75mm×285mm at 356 days. Moreover, the concrete mixtures incorporating FS with different level of replacement followed a similar trend, where the expansion reduced in the range from 5.89% to 9.52% at the same duration. The relationship between the expansion of two cylindrical sizes can be plotted by a linear fit with an R^2 nearly at unity (i.e. R^2=0.999) at all level of replacement of FS and the slope of the linear trend line is 0.92 as shown in **Fig. (4.21)**. The relationship indicates that the expansion measurements on cylindrical specimens of two different size along one year are well correlated linearly.

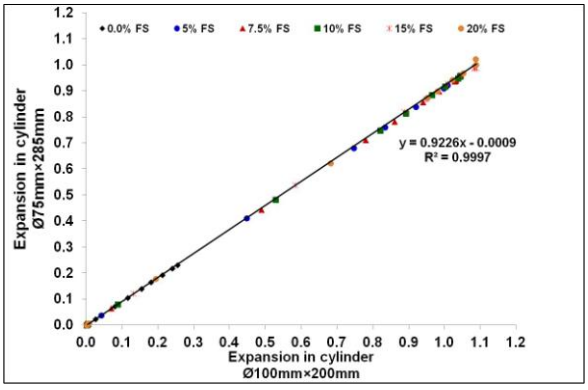

Figure (4.21) Expansion relationship between cylindrical specimens of sizes Ø75mm×285mm and Ø100mm×200mm

4.4.1.2 Mass Variation

The mass of all examined mixtures contains Spratt aggregate with and without different portions of FS were measured as a function of time. All measurements were conducted using a balance of 0.01gram accuracy and done at the same time of expansion measurements. **Figure (4.22)** represent the mass variation for all tested concrete mixtures. The standard deviation of the mass results was in the range of 3.9 to 7.8 gram.

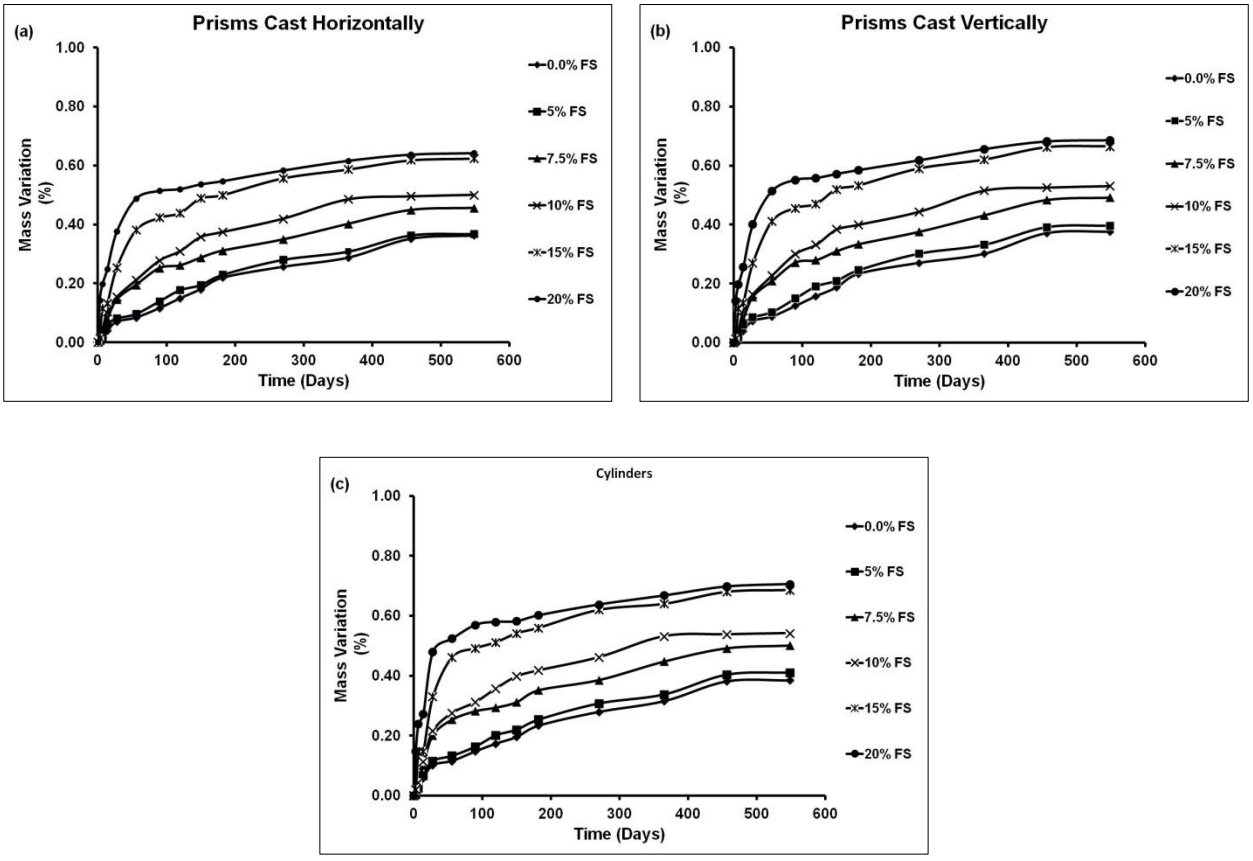

Figures (4.22) Mass variation of concrete specimens contains Spratt aggregate and a different portion of fused silica (FS)

(a) Prisms cast horizontally, (b) Prisms cast vertically, (c) Cylinders Ø75mm×285mm

Generally, up until 90 days, all specimens gain a significant increase in mass, then had a little mass variation until the end of the test duration following the same trend of expansion. Mixtures incorporating high portion FS (i.e. 7.5% FS and more) exhibited a higher increase in mass compared to that with Spratt reactive aggregate only and with less portion of FS (i.e. 5% FS).

Moreover, for the same mixture; the increase in mass was affected by the specimens geometry and the cast direction. Cylindrical specimens (i.e. Ø75mm×285mm) revealed a high increase in mass followed by the prismatic specimens cast vertically then the prismatic specimens cast horizontally. For example, at replacement portion of 15% FS, cylinders had an increase in mass over the prismatic specimens cast horizontally by about 30%, 16%, 11%, 9%, and 10% at 28, 90, 150, 356, and 548 days, respectively. These ratios decreased when compared with the prismatic specimens cast vertically to 22%, 8%, 4%, 3%, and 3% at the same measuring times. All mixtures have a similar trend with all replacement portion of FS at the same time. The relationships between the standard prismatic specimens (i.e. cast horizontally) with both cylindrical (i.e. Ø75mm×285mm) and prismatic (i.e. cast vertically) specimens was plotted by a linear fit as illustrated in **Fig. (4.23)** with a regression coefficient closed to unity (i.e. 0.99) and slope 1.08 approximately. Finally, the relationship between the expansion and mass variation for the tested concrete specimens (i.e. standard prism, prism cast vertically, and cylinders Ø75mm×285mm) were represented in **Fig. (4.24).** These relationships can be expressed by a exponential fit curve of regression coefficient in the range from 0.78 to 0.95 for the different specimens.

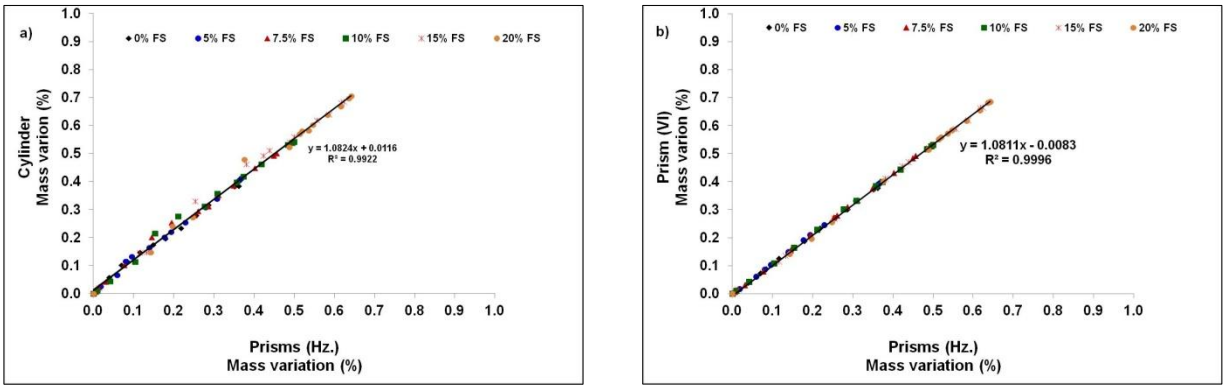

Figure (4.23) Weight variation relationship

(a) Cylindrical (Ø75mm×285mm) Vs. Prismatic (Hz.), (b) Prisms (Vl.) Vs. Prisms (Hz.)

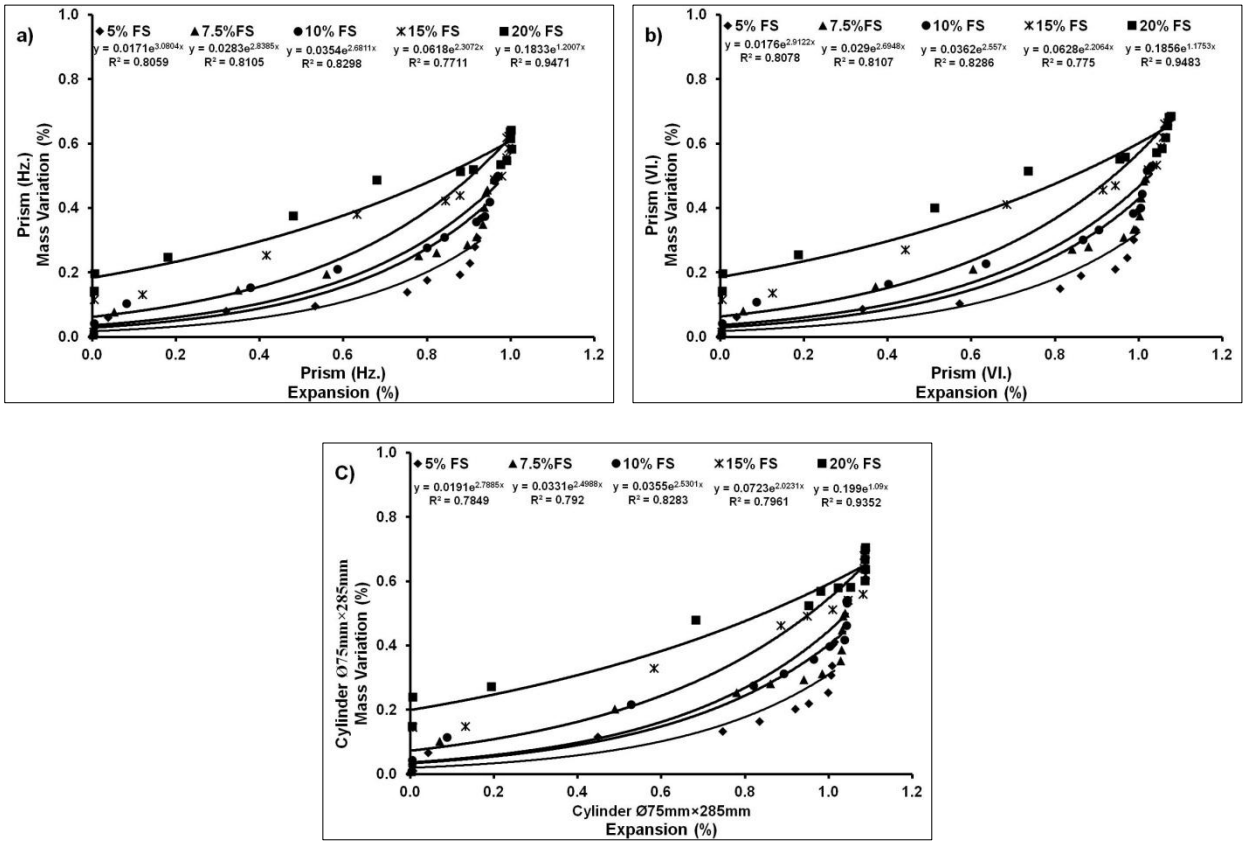

Figure (4.24) Relationship between weight variation and expansion

(a) Prisms (Hz.), (b) Prisms (Vl.), and (c) Cylinders (Ø75mm×285mm)

4.4.2 Category II - Changes in Mechanical Properties

4.4.2.1 Compressive and Tensile Strength

Compressive and tensile strengths results for all tested mixtures with time are represented in **Fig. (4.25)**. The standard deviation was in the range from 1.1 to 1.4 MPa and from 0.15 to 0.26 MPa for compressive and tensile strength, respectively. Generally, for all mixtures, strength decreased with time. For instance, the compressive strength of the mixture containing 15% FS decreased over time: 31.7, 26.0, 23.2, 18.2, and 15.5 MPa at 28, 90, 180, 270, and 365 days, respectively. In addition, a similar trend was obtained for tensile strength; the same mixture (i.e. 15% FS) decreased over time: 3.4, 2.9, 2.5, 2.4, and 2.3 MPa at 28, 90, 180, 270, and 365 days, respectively. The relationships between the strength (i.e. compressive and tensile) and time can be represented for all tested mixtures (i.e. six different level of replacement of FS) by linear fit lines with a regression coefficients in the range from 0.98 to 0.97 and from 0.99 to 0.82, respectively. (The trend lines are not shown on **Fig. (4.25)** for clarity.) Moreover, the slope of the linear trend line varies from -1.06 to -1.43 for compressive strength and from -0.1 to -0.08 tensile strength.

Mixtures incorporating high portion FS exhibited a higher decrease in strength over time compared to that of mixtures contains less portion FS as shown in **Table (4.3)**. For example, the mixture incorporating 10% FS showed a reduction in compressive strength by about 13.3%, 19.5%, and 38.8% and a reduction in tensile strength by about 12.2%, 19.6%, and 31.8% at 90 180, and 365 days, respectively compared to the strength at 28 days. In contrast, the reduction ratio changed mainly depending on the amount of FS replacement. For instance, compressive strengths for the mixture containing Spratt aggregate without FS at ages 28, 90, 180, 270, and 365 days were higher than that mixture containing 10% FS by about 19.5%, 28.4%, 30.3%,

33.6%, and 36.5%, respectively. According to Swamy and Asali (1988), this can be attributed to the hastening of ASR due to the replacement of FS that contains a high amount of reactive silica, which caused severe expansion and cracks over time. These results reinforce the previous research which found the mechanical properties of concrete were affected by the expansion rate whereas the cracking pattern depends mainly on the reactive aggregate used (Larive, et al., 1996, Fan and Hanson 1998, Multon, et al., 2004, Smaoui, et al. 2005, Giaccio et al., 2008, Yurtdas, et al., 2013, Esposito, et al., 2016, Barbosa, et al., 2018).

The tensile strength of mixtures incorporating FS exhibited a similar trend to the compressive strength by showing a higher decrease in strength than the control mixture containing Spratt reactive aggregate only. For instance, mixtures contain 10% FS exhibit a lower tensile strength than the mixture containing only Spratt aggregate by about 20.8%, 27.9% 30.1%, 32.4%, and 33% at age 28, 90, 180, 270, and 365 days, respectively. It is obvious concrete becomes more sensitive under tensile stresses produced from ASR (i.e. the extensive rate of expansion caused due to FS addition, where the reduction ratio changed to be higher mainly depends on FS replacement level at the same testing time. This highlights the role of FS in diminishing the tensile strength of concrete mixtures through increase cracks and decreases stiffness, also found by (Giaccio et al., 2008).

From the tests results, its clear the decrease in strengths confirm that the time and amount of hastening materials (i.e. FS) required to trigger ASR played a crucial role and had a significant potential to govern the mechanical properties of concrete. For instance, the compressive and tensile strengths at 90 days for concrete mixtures containing 5%, 7.5%, 10%, 15%, and 20% decreased over the control mixture by about 15%, 21.7%, 28%, 43%, 44% for compressive strength and 15.8%, 22.4%, 27.9%, 42.8%, and 44.4% for tensile strength, respectively. This can

be referred to as the negative effect of expansion due to high alkali content and crack growth, that reduces the continuous development of concrete durability before expansion takes place (Fan and Hanson 1998, and Smaoui, et al. 2005).

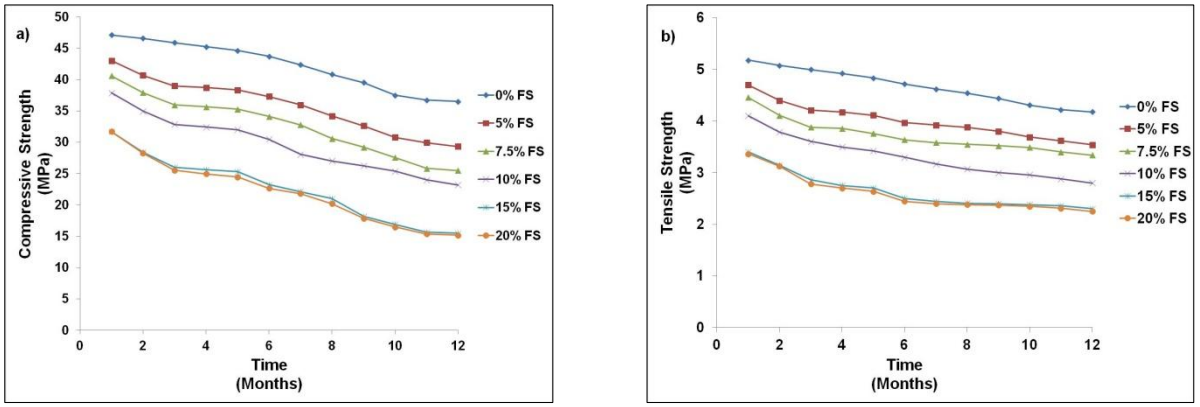

Figure (4.25) Strength versus time

(a) Compressive strength and (b) Tensile strength

Table (4.3) Reduction ratio in compressive and tensile strengths along time

Time (month)	Fused silica (%)											
	0.0		5		7.5		10		15		20	
	*CS	*TS	*CS	*TS	*CS	*TS	*CS	*TS	*CS	*TS	*CS	*TS
1	0.00	0.00	0.00	0.00	0.00	0.00	0.00	0.00	0.00	0.00	0.00	0.00
2	-1.12	-1.99	-5.42	-6.37	-6.65	-7.82	-7.76	-7.71	-10.33	-7.47	-10.89	-7.17
3	-2.54	-3.54	-9.30	-10.41	-11.45	-12.94	-13.28	-12.18	-17.93	-15.90	-19.41	-17.39
4	-3.92	-4.95	-9.92	-11.19	-12.17	-13.42	-14.42	-14.76	-19.21	-19.09	-21.22	-19.76
5	-5.23	-6.67	-10.87	-12.46	-13.08	-15.58	-15.50	-16.60	-20.11	-20.58	-22.83	-21.65
6	-7.18	-8.95	-13.29	-15.48	-15.94	-18.37	-19.53	-19.63	-26.69	-26.39	-28.46	-27.33
7	-10.05	-10.81	-16.36	-16.55	-19.30	-19.65	-25.96	-22.78	-30.20	-28.25	-31.18	-28.69
8	13.33	-12.35	20.44	-17.40	-24.66	-20.32	-28.66	-25.21	-33.69	-29.13	-36.28	-29.28
9	-16.06	-14.28	-24.12	-19.11	-27.99	-20.99	-30.71	-26.92	-42.66	-29.42	-43.68	-29.58
10	-20.43	-16.79	-28.40	-21.45	-32.07	-21.67	-33.07	-27.89	-46.70	-30.01	-47.95	-30.18
11	22.01	-18.53	-30.35	-22.94	-36.31	-23.69	-36.62	-29.84	-50.69	-30.60	-51.52	-31.36
12	-22.50	-19.30	-31.83	-24.64	-37.20	-25.04	-38.80	-31.79	-51.13	-32.37	-52.13	-33.15

***CS = Compressive strength and *TS =Tensile strength**

The relationship between the strengths and expansion of cylindrical specimens Ø100mm×200mm is represented in **Fig. (4.26)**. Both relationships showed that the strengths for all examined concrete mixtures decreased as expansion increased with similar trends. Up to a certain expansion, decreases in both compressive and tensile strength were within 10% of the 28 day strength. However, as expansion increased, a sharp drop in strength was observed. This is contrary to much of the published research that generally shows less drastic decreases. Esposito et al. (2016) obtained data from approximately a dozen published studies and analyzed both an S-shaped relationship and a piecewise linear function. The s-shaped curves fit the compressive strength with 15% standard deviation and the split tensile strength with 8%. However, this type of relationship yields an asymptotic strength decrease. For the case of compressive strength, their prediction indicated that the minimum strength would be 64% of the undeteriorated strength. In the current research, the strength drops at a very rapid rate and there is no indication that an asymptotic strength is likely. In fact, fitting the S-shaped curve of (Esposito et al., 2016) led to the prediction of negative strength. The obvious conclusion that the S-shaped relationship is faulted in that this prediction suggests continued expansion. Most specimens investigated here have reached a stable expansion at approximately six months, but continued to decrease in strength. It is apparent that deterioration continues well past the point that this deterioration manifests itself in the increased expansion. It is clear, from the results, the ASR resistance varied depending on the amount of FS, which affects the cement hydration and the concrete strength development. The high rate of ASR produced a high expansion that induced internal stress more significant than the concrete strength development, especially at early ages.

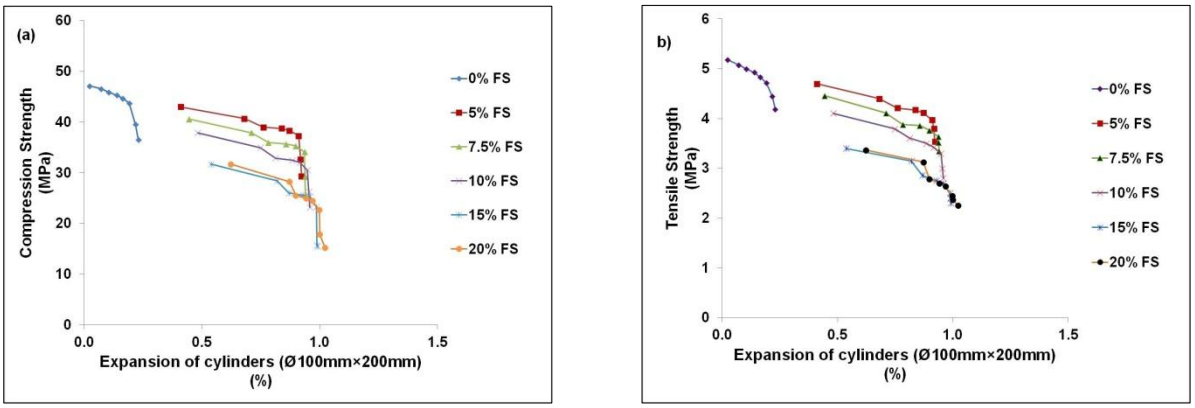

Figure (4.26) Relationship between expansion and strength

(a) Compressive strength and (b) Tensile strength

4.4.2.2 Modulus of Elasticity

Modulus of elasticity (MOE) is considered to be an effective indicator to the adverse effects of ASR (i.e. expansion) due its sensitivity to numerous micro-cracks and growth of cracks over time (Ahmed, et al., 2003, Smaoui et al., 2005, Giaccio et al., 2008, Sargolzahi et al., 2009, Hafçi, 2013, and Giannini et al., 2018). MOEs results represents the mean value of two specimens measured monthly until 12 months by using digital compresometer/extensometer according to ASTM C469 (2014). All specimens (Ø100mm×200mm cylinders) were subjected to uniaxial loads equivalent to 40% of the ultimate concrete compressive strength. The standard deviation of the MOE results was in the range of 0.65 to 1.2 MPa.

Generally, for all tested concrete mixtures (i.e. six mixtures), the MOE decreased over time with a varied ratio mainly depending on the replacement level of FS as represented in **Table (4.4)**. From the test results, MOEs were reduced dramatically with high rate within in the range of expansion from 0.00% to 0.76%. While MOEs continued reducing gradually with a slow rate with expansion in the range 0.76% to 1.022%. For instance, MOEs of the concrete mixture

containing Spratt aggregate without FS were 26.41 and 15.44 GPa at 28 and 365 days, respectively; a reduction of about 41%. On the other hand, for all mixtures containing FS, the MOE was in the range from 7.11 to 6.76 GPa at 28. As the expansion was high at 28 days (at least 0.4%), it is clear that significant damage occurred prior to the first test. Small reductions in modulus, 5.62% to 7.23% at 356 days, occurred for the concrete mixtures incorporating a different replacement level of FS.

Table (4.4) Modulus of elasticity, Poisson ratio and expansion with time on concrete specimens Ø100mm×200mm

Time (Month)	0.0% FS				5% FS				7.5% FS				10% FS				15% FS				20% FS			
	MOE (GPa)	*MOE (%)	υ	Exp. (%)	MOE (GPa)	*MOE (%)	υ	Exp. (%)	MOE (GPa)	*MOE (%)	υ	Exp. (%)	MOE (GPa)	*MOE (%)	υ	Exp. (%)	MOE (GPa)	*MOE (%)	υ	Exp. (%)	MOE (GPa)	*MOE (%)	υ	Exp. (%)
1	26.41	0.00	0.47	**0.023**	7.11	0.00	0.40	**0.410**	7.01	0.00	0.38	0.444	6.91	0.00	0.37	0.482	6.86	0.00	0.36	**0.538**	6.76	0.00	0.35	0.622
2	23.97	-9.24	0.47	**0.072**	6.96	-2.11	0.39	**0.680**	6.90	-1.57	0.37	0.710	6.80	-1.59	0.36	0.748	6.77	-1.31	0.35	**0.820**	6.71	-0.74	0.34	0.872
3	21.56	-18.36	0.42	**0.104**	6.85	-3.66	0.38	**0.760**	6.74	-3.85	0.36	0.782	6.70	-3.04	0.35	0.812	6.64	-3.21	0.35	**0.868**	6.60	-2.37	0.33	0.898
4	19.93	-24.54	0.39	0.140	6.78	-4.64	0.34	0.838	6.70	-4.42	0.33	0.856	6.59	-4.63	0.33	0.884	6.58	-4.08	0.33	**0.928**	6.57	-2.81	0.32	0.942
5	18.17	-31.20	0.39	0.164	6.72	-5.49	0.35	0.872	6.64	-5.28	0.33	0.898	6.54	-5.35	0.32	0.916	6.52	-4.96	0.31	**0.958**	6.50	-3.85	0.30	0.968
6	16.66	-36.92	0.36	0.192	6.67	-6.19	0.35	0.910	6.61	-5.71	0.32	0.936	6.52	-5.64	0.32	0.948	6.50	-5.25	0.31	**0.986**	6.49	-3.99	0.30	0.998
7	16.42	-37.83	0.35	--	6.66	-6.33	0.34	--	6.61	-5.71	0.32	--	6.52	-5.64	0.32	--	6.49	-5.39	0.31	--	6.48	-4.14	0.30	--
8	16.21	-38.62	0.35	--	6.66	-6.33	0.34	--	6.60	-5.85	0.32	--	6.52	-5.64	0.32	--	6.49	-5.39	0.31	--	6.48	-4.14	0.30	--
9	15.94	-39.64	0.34	**0.218**	6.64	-6.61	0.33	0.918	6.60	-5.85	0.32	0.938	6.50	-5.93	0.31	0.954	6.48	-5.54	0.30	**0.988**	6.47	-4.29	0.29	1.000
10	15.70	-40.55	0.34	--	6.63	-6.75	0.31	--	6.58	-6.13	0.31	--	6.50	-5.93	0.31	--	6.46	-5.83	0.30	--	6.42	-5.03	0.28	--
11	15.57	-41.05	0.31	--	6.62	-6.89	0.30	--	6.57	-6.28	0.30	--	6.49	-6.08	0.30	--	6.42	-6.41	0.28	--	6.40	-5.33	0.27	--
12	15.44	-41.54	0.30	0.230	6.61	-7.03	0.29	0.922	6.57	-6.28	0.29	0.940	6.48	-6.22	0.28	0.958	6.40	-6.71	0.27	**0.992**	6.38	-5.62	0.26	1.022

MOE= Modulus of Elasticity

*MOE= Reduction in MOEs along time for concrete mixtures incorporating Spratt aggregate with/without fused silica

υ:=Poisson Ratio

Exp.= Expansion

FS=Fused Silica

Bold underlined numbers refer to the expansion level used for SDT

The correlation between MOEs and time can be plotted with power trend curve with a regression coefficient (R^2) in the range from 0.93 to 0.97 which varied depending on the amount of FS as shown in **Fig. (4.27)**. This indicated that there is a robust correlation between these test results (i.e. degradation in MOEs) at different test ages for all tested mixtures in agreement with the majority of previously published studies.

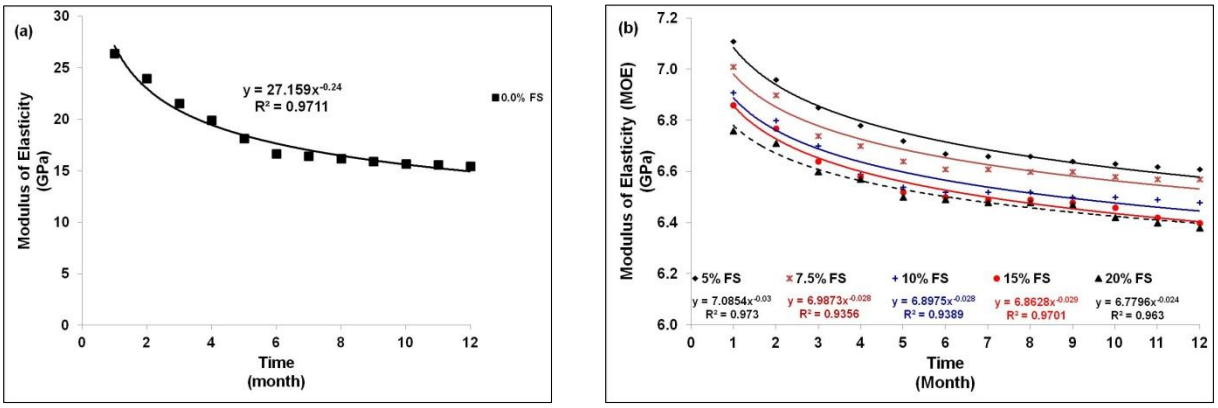

Figure (4.27) Relationship between modulus of elasticity and time

(a) Without FS, (b) With FS

The relationship between the MOEs and ASR expansion was plotted at ages 28, 56, 90, 180, 270, and 356 days for concrete mixtures contains Spratt aggregate with and without FS as shown in **Fig. (4.28)**. The relationship between concrete MOEs and expansion follow a different trend as that of concrete strength (i.e. compressive and tensile) versus expansion. In this case, the relationship in the mixture not containing FS showed a marked decrease in modulus with increased expansion. However, for all the mixtures containing FS, a less predominent behavior was observed. For these mixtures, significant expansion occurred within the first month that significantly decreased the modulus, but only small MOE decreases were during the 12 months. The relationship of all mixtures combined forms a bilinear relationship as suggested by (Eposito

et al., 2016). However, with the lack of data with expansion in the 0.2% to 0.4% range, it is not certain whether a single continuous bilinear relationship holds. As will be seen for other properties in this study, the FS mixtures performed notably different to the mixture only containing Spratt aggregate.

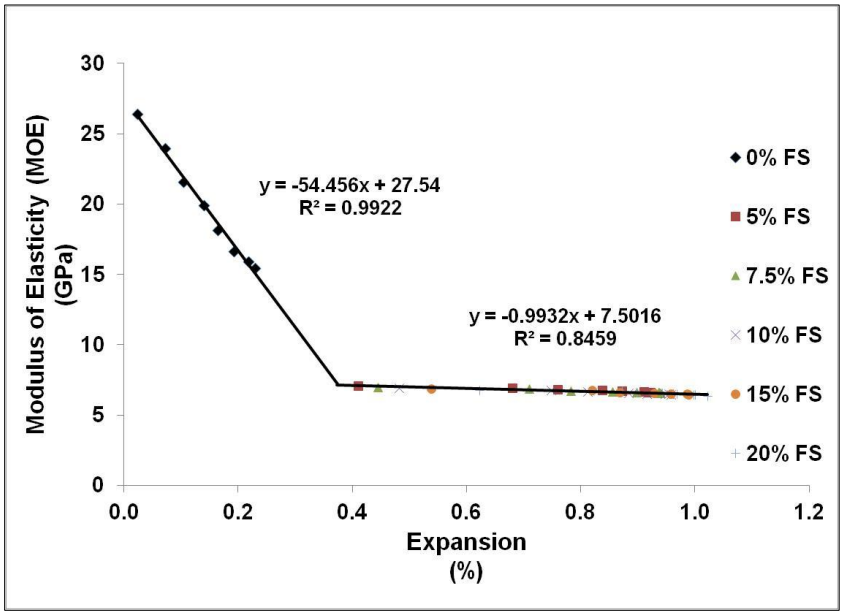

Figure (4.28) Relationship between modulus of elasticity and expansion

4.4.2.3 Poisson Ratio

The test was conducted on all tested mixtures contains Spratt aggregate with and without FS as a function of time (i.e. 12 months) according to ASTM C469 (2014). The standard deviation of the MOE results was in the range of 0.018 to 0.056.

Poisson ratio for all the examined mixtures decreased with time following the same general trend as MOEs as represented in **Table (4.4).** For instance, the Poisson ratio of the mixture containing Spratt aggregate without FS decreased by about 10%, 24%, and 36% at 3, 6, and 12 months, respectively. While, the concrete mixtures incorporating Sparrt aggregate with various

levels of FS replacement exhibited a lower (υ) to be in the range from 3% to 5%, from 12% to 16%, and from 23% to 26% at 3, 6, and 12 months, respectively. Moreover, the test results showed the adding of FS caused a significant reduction of (υ) as shown in **Table (4.4).** For example, (υ) was 0.47 and 0.36 at 28 days for concrete mixtures incorporating 0% and 15% FS respectively, while these values become lower at six months to be 0.36 and 0.31 for the same mixtures.

Figure (4.29) presents the relationship between the Poisson ratio and time over 12 months. It is clear there is a robust correlation between Poisson ratio and time at different test ages for all mixtures. The relationships between the Poisson ratio and ASR expansion was plotted at ages 28, 56, 90, 180, 270, and 356 days, respectively for concrete mixtures contains Spratt aggregate with and without FS as shown in **Fig. (4.30)**. The relationship between (υ) and expansion follow the same trend as that of concrete strengths and MOEs towards expansion. The coefficient of determination (R^2) value for the trend was 0.95 and 0.67 for the concrete mixture incorporated different portions of FS and the control mixture (i.e. 0% FS) respectively. However, in the case of Poisson's ratio, the linear trend for the mixture without FS was discontinuous with the other mixtures tested in this program. As the testing program terminated at 12 months, it is difficult to ascertain the validity of the linear relationship. As the FS specimens have reached terminal expansion, it is unknown whether the Poisson's ratio has also reached its minimum value.

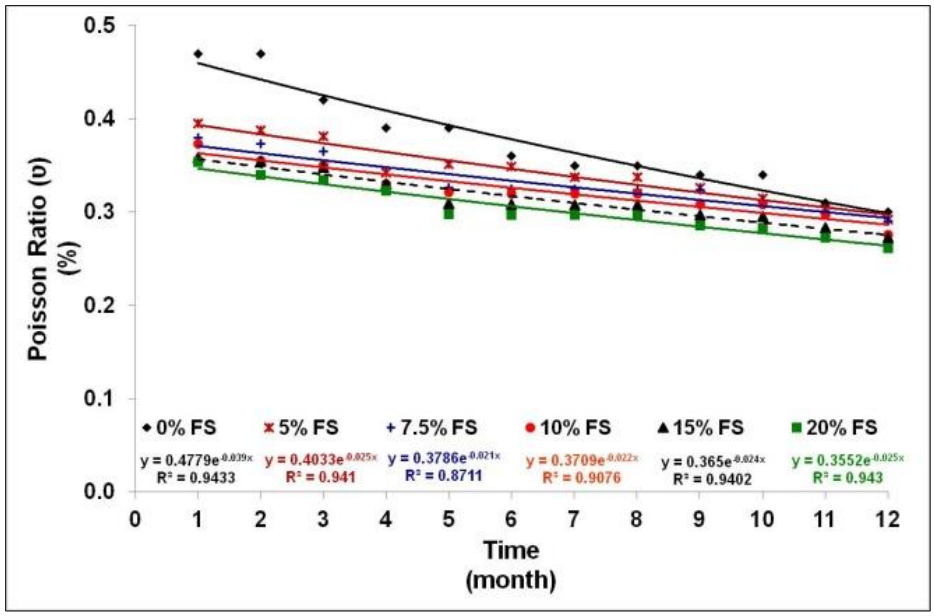

Figure (4.29) Relationship between Poisson ratio and Time

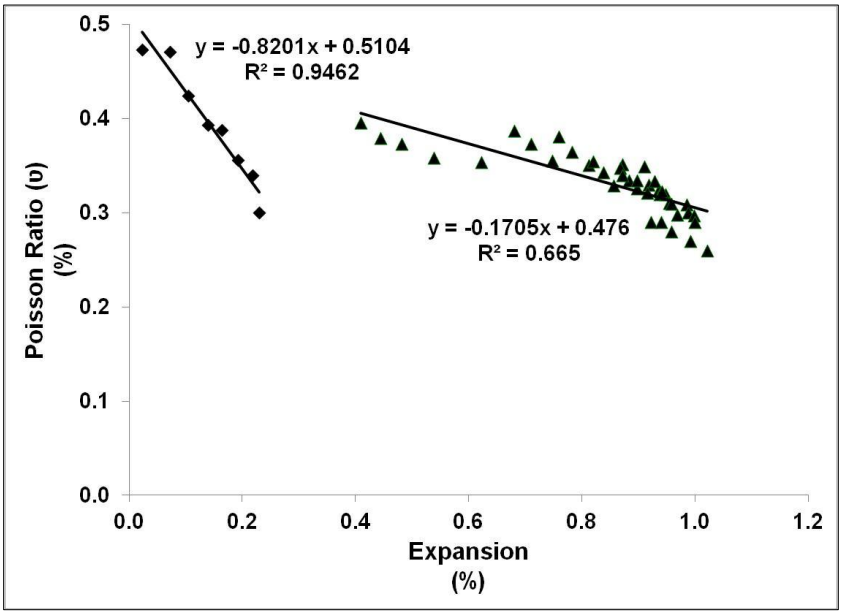

Figure (4.30) Relationship between Poisson ratio and expansion

4.4.2.4 Loss of Stiffness

Several different levels of expansion were selected to evaluate the degree of damage and effect of ASR performance on the concrete stiffness. The expansions selected were measured on Ø100mm×200mm specimens and covered the range of measured expansion; these are marked as underlined in **Table (4.4)**. At each expansion level, the stress-strain curve was plotted (examples are shown in **Fig. (4.31)**. Its obvious from the test results presented in **Table (4.5)** and the plots of stress-strain curves of the five loading cycles **Fig. (4.31)**, the calculated hysteresis areas (S1) of the first loading cycle, and the plastic deformation (D1) over the five loading cycles increased (i.e. stiffness decreased) as the expansion increased. For instance, the hysteresis area (S1) and plastic deformations (D1) were 800 J/m^3 and 110 µstrain, respectively at expansion level 0.023%. Both increased dramatically until expansion 0.538% to record 5861.4 J/m^3 and 880 µstrain, respectively. After that point, HA and D1 increased marginally with increased expansion.

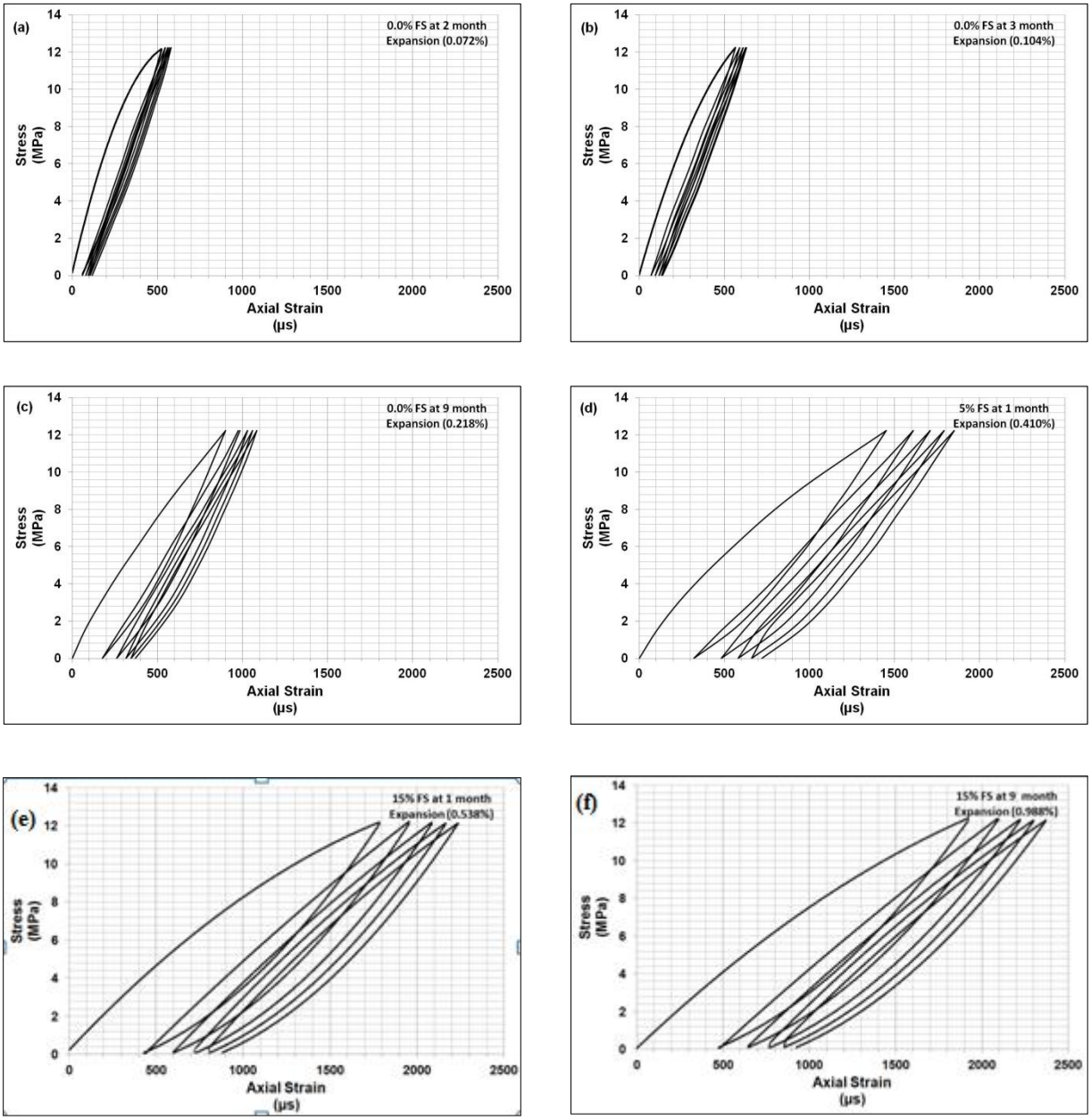

Figure (4.31) Stress-Strain curves of concrete mixtures contain Spratt aggregate with and without fused silica at different level of expansion

(a) 0.072%, (b) 0.104%, (c) 0.218%, (d) 0.410%, (e) 0.538%, and (f) 0.988%

Table (4.5) Hysteresis areas (S1), plasticity deformation (D1), stiffness damage index (SDI), plasticity deformation index (PDI) and expansion measured on specimens Ø100×200mm

Mixture	Expansion (%)	S1 (J/m^3)	D1 (µstrain)	SDI (%)	PDI (%)
0% FS	0.023	800	110	0.18	0.16
0% FS	0.072	1377.1	115	0.29	0.17
0% FS	0.104	1215.1	135	0.30	0.18
0% FS	0.218	2181.7	370	0.36	0.25
5% FS	0.410	4218.3	720	0.41	0.28
15% FS	0.538	5861.4	880	0.46	0.28
5% FS	0.680	5865.3	885	0.45	0.28
5% FS	0.760	5876.7	890	0.44	0.28
15% FS	0.820	5872.9	895	0.44	0.28
15% FS	0.868	5876.7	900	0.44	0.28
15% FS	0.928	5884.4	910	0.45	0.28
15% FS	0.958	5888.2	915	0.45	0.28
15% FS	0.986	5895.9	925	0.45	0.28
15% FS	0.988	5895.9	925	0.45	0.28
15% FS	0.992	5918.8	937	0.45	0.28

The relationships between the calculated HA (S1) after the first loading cycle and total plastic deformation (D1) after five loading cycles versus expansion are represented in **Fig. (4.32, 4.33)**, respectively. There is a very strong correlation between these test results (i.e. loss of stiffness) and ASR expansion. Both S1 and D1 increase as a function of increasing expansion. The best fit of the data is in the form of a Weibull distribution of the form $y = a - be^{-cx^{\wedge}d}$. For both these parameters, logarithmic equations fit with good correlation but tend to markedly overestimate S1 and D1 at low expansion levels and notably underestimate S1 and D1 at higher expansions. These conclusions reinforce the previous data reported by (Sanchez et al., 2014 and Giannini, et al., 2018).

Moreover, comparing the two different outputs (i.e. S1 and D1) showed the same trend with expansion, both increasing with high rate within the expansion in the range from 0% to 0.538%, while the behavior was fairly stable above that range. From the above, the relationships between HA (S1) plastic deformation (D1) versus expansion can be divided into two different parts: Initial part up to expansion range 0.538% and secondary part up to expansion 0.992%. This in agreement with the proposed value reported previously (Giannini et al., 2018) (i.e. excessive linear) trend until expansion 0.40% and slow rate after) these justify the relationship between S1 and D1 versus expansion.

On the other side, because the primary output of the SDT was affected by several parameters as mentioned above. The calculation of two different indices (SDI and PDI) due to its lower effectiveness by these parameters as proposed by (Sanchez et al., 2014, and 2016) were accomplished as represented in **Table (4.5)**. The relationships between indices SDI and PDI against expansion were plotted using logarithm fit of the coefficient of determination R^2=0.96 and 0.88 as shown in **Fig (4.34, 4.35)**, respectively. Its clear both relationships (i.e. SDI and PDI) against expansion exhibited a very similar trend. Moreover, by using the above two parts of relationship obtained from S1 and D1 against the expansion level (i.e. Initial and secondary parts), its clear the plotting SDI against expansion was in the range from 0.18% to 0.46% for the initial part of expansion (i.e. from 0.00% to 0.538%) and became stable at 0.45 along the secondary part of expansion (i.e. from 0.538% to 0.992%). The same trend obtained for PDI to be in the range 0.16% to 0.28 and became stable at 0.28 for the initial and secondary part respectively.

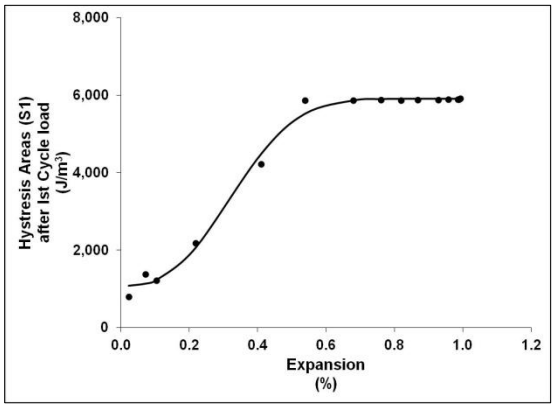

Figure (4.32) Relationship between hysteresis area (S1) and expansion

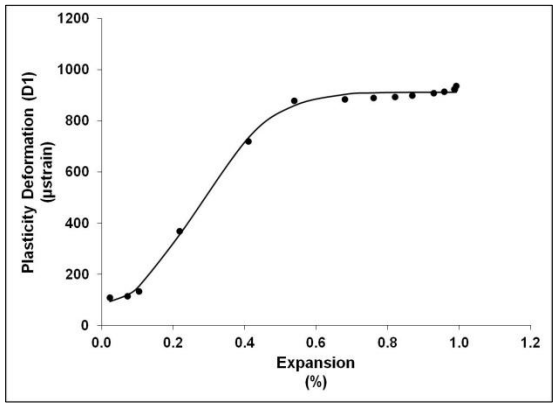

Figure (4.33) Relationship between plastic deformation (D1) and expansion

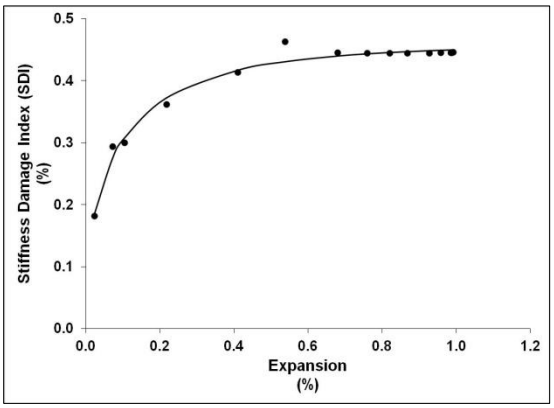

Figure (4.34) Relationship between stiffness damage index (SDI) and expansion

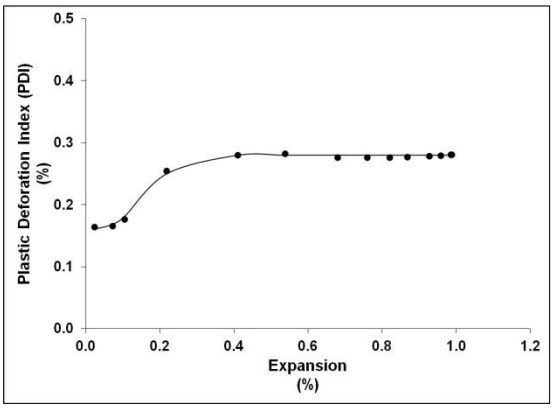

Figure (4.35) Relationship between plastic deformation index (PDI) and expansion

4.4.2.5 Ultrasonic Pulse Velocity

UPV evolution of all examined concrete mixtures containing Spratt aggregate with and without FS over time represented in Fig. (4.36). The standard deviation of the UPV results was in the range of 15 to 40 m/s. The velocities of concrete specimens incorporating Spratt aggregate without FS were higher than 4000m/s (i.e. 4550 m/s at 52 weeks). These velocities indicate the concrete until 52 weeks was of good quality based on ASTM C597 (2016) confirming with the

previous studies done on the same aggregate type (Saint-Pierre et al., 2007, and Sargolzahi et al., 2010). However, the velocities of all concrete specimens containing Spratt aggregate with FS of different ratios were in the range from 3950 to 3585 m/s (i.e. medium quality) varying mainly depending on the replacement level of FS.

It is clear the replacement level of FS had a crucial effect on decreasing the velocities. For all FS mixtures, UPV decreased following the same trend with high rate until 4 weeks due to an increase in expansion. These mixtures continued to decrease with slow rate until 365 days. This same behavior was seen in the compressive and tensile strength results. For instance, the velocities at 120 days were decreased by 5.45%, 17.81%, 19.01%, 19.99%, 22.04%, and 24.25% for mixtures incorporating Spratt aggregate with 0%, 5%, 7.5%, 10%, 15% and 20% FS respectively. While for the same mixtures, the velocities at 365 days were reduced by 8.17%, 20.04%, 21.23%, 22.89%, 24.80%, and 27.30% respectively. However, for the mixture without FS, UPV decreased at a steady rate in the one year of testing.

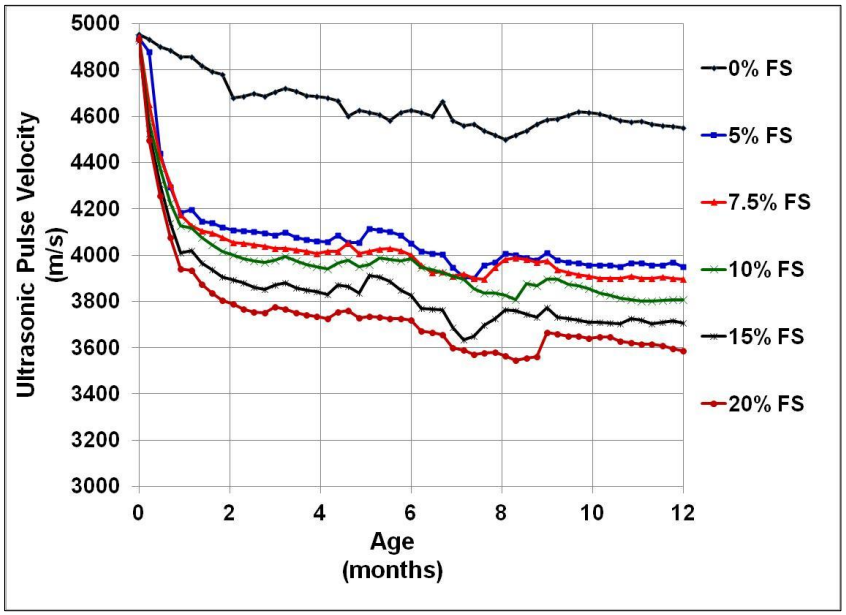

Figure (4.36) Ultrasonic pulse velocity of cylinders with time

The relationship between UPV and the expansion of cylindrical specimens (i.e. Ø100×200mm) for all tested concrete mixtures is presented in **Fig. (4.37).** A linear trend is apparent when considering all mixtures. However, deviations from the linear trend are amplified in the FS mixtures. At very low expansions (i.e. within the first week or two), there is a sharp drop in UPV. As well, a sharp drop in UPV can also be seen at high expansions. It is apparent that small microcracks are formed at early ages which affects the UPV results, but does not manifest in any notable expansion. At higher levels of expansion, the growing crack dimensions lead to a longer path and therefore lower velocity. From the above, these correlations indicate and confirm the sensitivity of UPV in assessing ASR over time at the different levels of expansion. However, that being said, the overall relationship is not as strong as other properties observed in this research. Previous studies have noted that UPV results are dependent on variables related to mixture design and no global relationship exists.

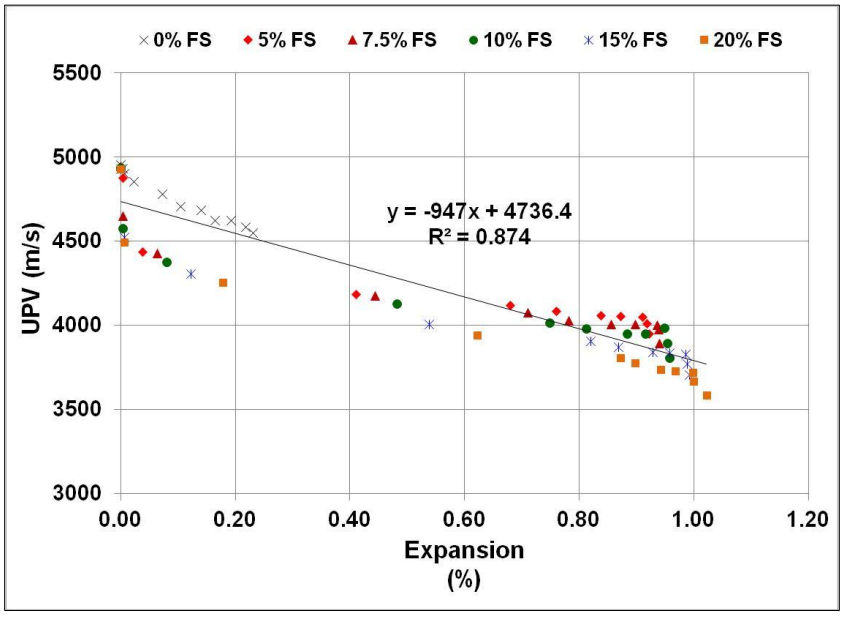

Figure (4.37) Relationship between ultrasonic pulse velocity and expansion

4.4.3 Category III - Durability Indices

The test was conducted at different intervals (i.e. 1, 2, 3, 6, and 12 months). All figures below represent the mean charge of three specimens. The standard deviation of the RCPT results was in the range of 100 to 175 coulomb. Generally, the total charge passed for all tested mixtures increased over time as concrete become more porous with more internal cracks due to the progression of ASR (i.e. expansion) as shown in **Table (4.6)** and **Fig. (4.38)**, respectively. For instance, the total charge passed at 3 months increased by 3.0%, 9.9%, 12.2%, 12.7%, 16.8%, and 18.4% for the mixtures incorporating 0%, 5%, 7.5%, 10%, 15%, and 20% FS, respectively. These variations continue to increase dramatically to reach 20.9%, 28.3%, 31.0%, 35.3%, 41.7%, and 44.4% at 12 months for the same mixtures, respectively.

Table (4.6) Variation of RCPT over time

Time (Month)	Variation a long time						Variation from Control mixture 0.0% FS					
	0% FS	5% FS	7.5% FS	10% FS	15% FS	20% FS	0% FS	5% FS	7.5% FS	10% FS	15% FS	20% FS
1	0.00	0.00	0.00	0.00	0.00	0.00	0.00	4.67	7.33	9.88	14.1	19.1
2	-3.33	5.91	7.50	7.74	8.90	9.09	0.00	14.6	19.3	22.4	28.6	34.4
3	3.05	9.90	12.2	12.7	16.8	18.4	0.00	11.6	16.8	20.1	29.5	36.9
6	8.10	14.4	17.1	19.2	25.9	27.9	0.00	10.7	16.2	21.1	33.0	40.9
12	20.9	28.3	31.0	35.3	41.7	44.4	0.00	11.0	16.3	22.9	33.8	42.3

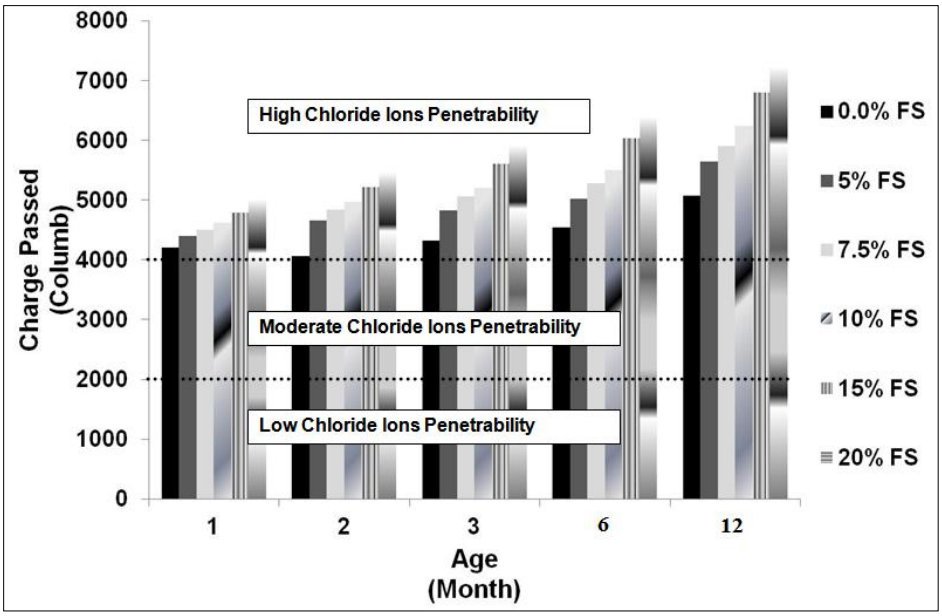

Figure (4.38) Chloride penetrability with time

From the above results, its obvious, the amount of FS had a significant effect on the total passed charge (i.e. all concrete mixtures classified in the "high" category according to ASTM C1202 (2017). The increase in expansion caused an increase in the internal micro-cracks. As the micro-cracks increased, the solution inside these micro-cracks produced a highly conductive medium and allowed the electrical charge transfer (Fournier and Bérubé, 2000, and Bérubé et al., 2002).

Although, all mixtures have the same behavior (i.e. increase the total charge passed as a function of time), the total charge passed of the mixture incorporating Spratt aggregate without FS decreased by 3.33% from 28 to 56 days. The reduction in total charge passing might be attributed to the slower development of the micro-cracks that can be blocked by the ASG at this age that causing an efficient seal to penetration (i.e. lower conductivity medium) (Smaoui et al., 2004). In addition, it might have occurred due to the concrete maturity, because this mixture does not contain the trigger material (i.e. FS) that increased the expansion at all ages.

The relationship between the total charge passed and expansion is shown in **Fig. (4.39)**. As can be seen in the figure, the charge passed begins to increase substantially with increased expansion. The mixture without FS shows that the increase begins at lower expansion than the other mixtures. The trend lines on the figures represent a hyperbolic relationship with high correlation ($R^2 > 0.95$). These correlations confirm adding of FS had a significant effect on the expansion, which caused an increase in cracks and moisture, producing higher conductivity and increasing the total charge passed.

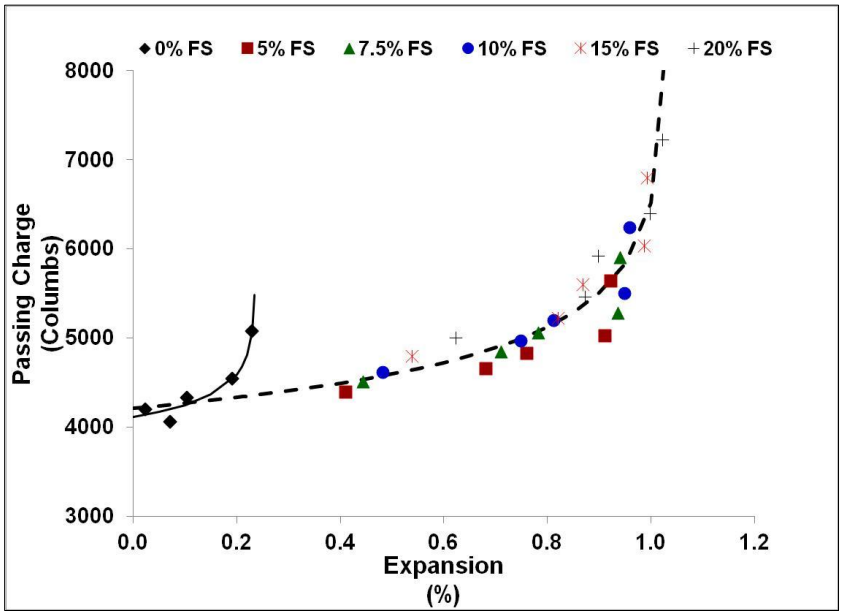

Figure (4.39) Relationship between total passing charge and expansion

4.5 Conclusion

This phase dealt with the evaluation of different parameters on ASR performance as specimen shape, size, and casting direction. In addition, evaluate effect of ASR expansion on concrete properties. Six concrete and mortar mixtures incorporating Spratt reactive aggregate and different replacement levels of hastening materials (i.e. 0%, 5%, 7.5%, 10%, 15%, and 20% FS) were cast and stored in conditions consistent with ASTM specifications.

- Generally, both concrete and mortar mixtures incorporating FS reveals a higher increase in expansion compared to that with reactive aggregate only. All concrete mixtures containing FS reveals a drastic increase in expansion until age 180 day, then the rate of expansion decreased until the end of the investigated period (i.e. 548 days). Moreover, Mortar mixtures exhibited an extreme increase in expansion with time followed the same trend of expansion in concrete mixtures. However, the optimum percentage of FS will differ from one type to another.
- Two different shapes of concrete specimens were cast to evaluate the effect of specimen geometry (i.e. prismatic specimens 75×75×285mm and cylindrical specimens Ø75×285mm). The results present evidence that the specimens geometry had a significant effect on the rate of expansion up to 56 days. The cylindrical specimens expanded more than prisms with all FS replacement portions. The increase in the expansion of cylinders continued at a higher rate than the prisms until 56 days between about 43% to 37% for all replacement portions of FS. From 90 days until test termination at 548 days, the expansion ratio was greater for cylinders than prisms within the range of 9% to 15%. The relationship between the cylindrical and prismatic specimens was plotted with a linear fit of R^2=0.98 and slope 1.09.

- Prismatic concrete specimens were cast in two different directions (i.e. vertically and horizontally) to evaluate the effect of casting direction on expansion rate. The casting direction had an effect on the rate of expansion under the standard exposure conditions. The specimens cast vertically exhibited an increase in expansion over the others cast horizontally in the range from 2.63% to 8.41% based on the time of measurements and portion of replacement of FS. The correlation between the prismatic specimens cast vertically and horizontally was plotted with a linear trend line close to unity (i.e. R^2=0.999 and slope1.07) at all level of replacement of FS.
- Concrete cylinders of two different sizes were cast to evaluate the effect of specimen size on the ASR rate (i.e. Ø75×285mm and Ø100×200mm). The results showed lower expansion for specimens Ø100×200mm than the specimens Ø75×285mm. Moreover, specimens Ø100×200mm showing the increase in the concrete volume caused lower expansion. The reduction ratio was in the range from 5.89% to 9.52%. The relationship between the expansion of two cylindrical sizes plotted by a linear fit with an R^2 nearly at unity (i.e. R^2= 0.999) and slope 0.92.
- The mass of all tested mixtures was measured as a function of time. Generally, the mass change followed the trend of expansion; all mixtures gain a higher increase in mass change at ages until 90 days then had a little mass variation to the end of the test duration. Moreover, for the same mixture; the increase in mass was affected by the specimen geometry and the casting direction. Cylindrical specimens reveal a high variation in weight followed by the prismatic specimens cast vertically then prismatic specimens cast horizontally. The relationship between the expansion and mass variation for the tested

concrete specimens expressed by a power fit curve of regression coefficient 0.79 for the different specimens.

- Compressive and tensile strengths decreased with time at similar linear rates for all mixtures tested. The level of FS replacement played a crucial role to govern the mechanical properties with increasing FS resulting in lower strength up to 15% FS. The correlation between strength and expansion did not result in a universal relationship. Instead, each mixture had a decrease in strength up to a critical expansion level, but significant drops in strength as the expansion reached its asymptotic maximum.
- All tested mixtures showed a reduction in the modulus as a function of time depends mainly on the replacement level of FS. MOEs were reduced dramatically with high rate during the first 6 months and continued reduction with a slow rate thereafter. Two strong linear relationships were observed between MOE and expansion. The mixture without FS showed a rapid drop in modulus throughout the 12 months; the FS mixtures exhibited a slight decrease in MOE as much of the expansion occurred in the first month.
- Poisson ratio exhibit some sensitivity to ASR expansion, where υ decreased over time following the same general trend as MOEs. The relationship between υ and expansion follow the same trend as MOEs, but in this case, the two linear relationships are not continuous.
- Stiffness damage test (SDT) was used to assess the ASR progression and detect the degree of damage in concrete mixtures at different levels of expansion. The test results revealed an increase in HA and D1 as the expansion increased. Both increased dramatically up to 0.538% expansion, then continued to increase gradually. The strong correlation between S1 and D1 versus expansion were found. S1 and D1 exhibited a similar trend with

expansion, both increasing with high rate within the expansion in the range from 0% to 0.538% (i.e. initial part), while the behavior was fairly stable above that range (i.e. secondary part from .538% up to 0.992%).

In addition, the relationships between indices SDI and PDI versus expansion exhibited a very similar trend and plotted using logarithm fit of the coefficient of determination R^2=0.96 and 0.88, respectively. SDI against expansion was in the range from 0.18% to 0.46% for the initial part of the expansion and became stable at 0.45 along the secondary part of the expansion. The same trend obtained for PDI to be in the range 0.16% to 0.28 and became stable at 0.28 for the initial and secondary parts, respectively.

- UPV for all examined mixtures decreased with time for all mixtures. The five mixtures containing FS had a sharp decrease in the first month followed by a lesser decrease thereafter. In general, there was a reasonable linear correlation between UPV and expansion.
- RCPT results exhibited and increased the total charge passed as a function of time due to an increase in the internal microcracks resulting from expansion. Hyperbolic relationships best decrease the correlation between the two properties.

Chapter

5

Evaluation Strengthening Materials (Phase Two)

5.1 Introduction

This chapter examines concrete mixtures incorporating four different types of fibre (i.e. conductive and non-conductive) with and without pozzolanic material (as silica fume, SF). In addition, concrete mixtures containing 10% replacement of sand with fine crumb rubber aggregate with and without SF were examined. Lastly, mortar mixture were examined at different exposure conditions (i.e. laboratory and harsh environmental conditions). These experimental works evaluated the mechanical properties along with the electrical resistivity, durability indices, water absorption, and ultrasonic pulse velocity for the concrete mixtures. In addition, mechanical properties of mortar under harsh environmental conditions were evaluated. This part is anticipated to provide site engineers with a guide to choosing suitable jacketing materials based on target performance rather than focusing only on the achieved strength.

5.2 Specimens, Mixtures, Casting, and Curing

5.2.1 Concrete and Mortar Specimens

A total of 444 concrete specimens were cast for Phase Two as detailed in **Chapter 3**, section 3.2 to evaluate mechanical properties and durability indices for Fibre Reinforced Concrete (FRC) and Crump Rubber Concrete (CRC). In addition, 54 mortar specimens were cast to evaluate the effect of exposure conditions as temperature and relative humidity on mechanical properties of mortar (i.e. compressive and tensile strength). The experimental work included three main parts (i.e. part A, B, and C) as represented in **Table (5.1, 5.2, and 5.3)**, respectively. Each table shows mixtures proportions, specimens (shape, dimension, and numbers), and tests performed (measurement, duration, and specification). All tests were conducted based on ASTM standards as detailed in **Chapter 3**.

5.2.2 Mixtures

Concrete mixtures of total density 2327 kg/m^3 as represented in **Table (5.1,5.2)** were cast with a ratio 1:1.44:1.25 (i.e. cement: fine agg.: coarse agg.). All mixtures had constant water to binder ratio of 0.40. High range water reducing (HRWRA) admixture with 42% solid content and specific gravity of 1.08 g/cm^3 was used to adjust the slump within a range from 90mm to 120mm. A proportion of 228 kg/m^3 water and 570 kg/m^3 GU cement was used as the main binder. Silica Fume (SF) with a purity of 93.8% was added to selected concrete mixtures at a rate of 10% partial replacement of cement by mass. The chemical and physical characteristics for the GU cement and SF are shown in **Chapter 3**, **Table 3.1**. In addition, 818 kg/m^3 natural sand with the fineness modulus of 2.70, the specific gravity of 2.51 and sorptivity of 2.73% was used as fine aggregate. Crushed stone with specific gravity, water absorption, and maximum nominal

size of 2.70, 1.3%, and 9.5 mm, respectively, was used as the coarse aggregate. Characteristics of aggregate were detailed in **Chapter 3**, **Sections 3.3.3.1** and **3.3.3.2**, respectively.

Fibre reinforced concrete "Part A", dealt with FRC mixtures incorporated various types of fibre: steel fibre, macro and micro polypropylene, and micro nylon fibres. The geometry and properties of fibres are given in **Chapter 3**, **Table 3.4 and Fig. 3.9**. The fibres were added to the dry concrete mixtures with small portions to avoid balling phenomena, prevent difficulty of fibre separation during the mixing process, allow good distribution within the mixtures, and enhance the concrete strength (Song and Hwang, 2004). To study FRC, concrete mixtures were divided into two groups: mixtures without silica fume and mixtures incorporating silica fume. Each group consisted of one plain control mixture, and four fibre reinforced mixtures as represented in **Table (5.1)**.

Rubberized concrete "Part B", dealt with one type of crumb rubber aggregate of size fraction as shown in **Chapter 3**, **Fig. (3.4)**. Fine rubber partially replaced 10% of the fine aggregate by mass. The mixtures differentiated based on the replacement portion of SF and FCRA as shown in **Table (5.2)**.

Finally, one mortar mixture mainly designed with high early strength to repair the vertical surfaces of the deteriorated concrete by specified weight ratio of 1A:4.8B where A is the liquid and B is cementitious materials (i.e. manufacturer's recommendation) as shown in **Table (5.3)**. In addition, The mix was modified by adding HRWRA to obtain an adequate flowability during the casting process.

Table (5.1) Phase Two -Part A "Fibre Reinforced Concrete", concrete mixture proportions, specimen (shape, dimensions, and number), and tests performed (measurements, duration, and specifications)

Mix No.	Mixture ingredients								Specimens		Test		
	Mix ID	W/B	Water (kg/m^3)	Cement (kg/m^3)	SF (kg/m^3)	Aggregate (kg/m^3) Fine	Aggregate (kg/m^3) Coarse	Fibre V_f(%)	HRWRA (%)	Dimension (mm)	No	Measurements	Duration (day/week)	Standard
1	MC	0.40	228	570	---	818	711	---	0.60	Ø100×200	12	Compression Strength	28 and 90 day	ASTM C39
												Tensile Strength	28 and 90 day	ASTM C496
												Surface Resistivity	28, 42, 56, 70, and 90 day	ASHTTO TP -95-11
												Bulk Resistivity	28, 42, 56, 70, and 90 day	ASTM C1760
												Ultrasonic Pulse Velocity	Weekly until 3 months	ASTM C597
										Ø100×50	9	Permeability	28, 56, and 90 day	ASTM C1202
										Ø100×50	9	Sorptivity	28, 56, and 90 day	ASTM C1585
2	MCS	0.40	228	570	---	818	711	2.00	0.75	As mentioned above in Mix#1 (MC)				
3	MCP	0.40	228	570	---	818	711	2.00	0.80					
4	MCMP	0.40	228	570	---	818	711	0.50	0.80					
5	MCMN	0.40	228	570	---	818	711	0.50	0.70					
6	MSF	0.40	228	513	57	818	711	---	0.90	Fibre code and properties were detailed in **Table (3.4)**				
7	MSFS	0.40	228	513	57	818	711	2.00	0.95	(i.e. S is Steel, P is macro polypropylene, MP is micro polypropylene, and MN is micro Nylon)				
8	MSFP	0.40	228	513	57	818	711	2.00	1.00					
9	MSFMP	0.40	228	513	57	818	711	0.50	0.85					
10	MSFMN	0.40	228	513	57	818	711	0.50	0.85					
Total number of concrete specimens										**<u>300</u> specimens of different size**				

Table (5.2) Phase Two -Part B "Crump Rubber Concrete", concrete mixture proportions, specimen (shape, dimensions, and number), and tests performed (measurements, duration, and specifications)

Mix No.	Mixture ingredients							Admixtures (ml/100kg of cementitious materials)			Specimens		Test		
	Mix ID	W/B	Water (kg/m^3)	Cement (kg/m^3)	SF (kg/m^3)	Aggregate (kg/m^3)									
						Fine		Coarse	HRWRA	AEA	Stabilizer				
						Natural	Rubber					Dimension (mm)	No	Measurements	Duration (day/week)	Standard
1	MC	0.40	228	570	---	818		711	130	30	65	Ø100×200	27	Compression Strength	28, 56, and 90 days	ASTM C39
														Tensile Strength	28, 56, and 90 days	ASTM C496
														MOE, υ, and SDT	28, 56, and 90 days	ASTM C469, and N.A.
														Surface Resistivity	28, 42, 56, 70, and 90 days	ASHTTO TP -95-11
														Bulk Resistivity	28, 42, 56, 70, and 90 days	ASTM C1760
														Ultrasonic Pulse Velocity	Weekly until 3 months	ASTM C597
												Ø100×50	9	Permeability	28, 56, and 90 day	ASTM C1202
2	MCR	0.40	228	570	---	740		711	285	75	130	As mentioned above in Mix#1 (MC)				
3	MSF	0.40	228	513	57	818		711	130	30	65					
4	MSFR	0.40	228	513	57	740		711	325	75	130					
Total number of concrete specimens												**<u>144</u> specimens of different size**				

Table (5.3) Phase Two -Part C "Mortar", mortar mixture proportions, specimen (shape, dimensions, number, and curing), and tests performed (measurements, duration, and specifications)

Mix No.	Mixture ingredients			Specimens		Curing		Test		
	Component (By weight)		HRWRA (ml/100kg of cement)	Dimension (mm)	No	23 °C & 50% RH	38 °C & 95±5% RH	Measurements	Duration (days)	Standard
	A (Liquid)	B (Powder)								
1	1	4.8	200	50×50×50	24	√	√	Compression Strength	3, 7, 28, and 90 days	ASTM C109
				Dog bone shape	30	√	√	Tensile Strength	3, 7, 21, 28, and 90 days	ASTM C307
Total number of specimens								**<u>54</u> specimens of different size**		

5.2.3 Mixing, Casting, and Curing

The mass of all concrete ingredients were batched by a balance of accuracy 5 grams, then mixed in the pan type small mixer of bowl capacity $0.1m^3$. Concrete mixtures were prepared and cast in accordance with ASTM C192 (2016). Initially, dry sand and crushed stone were introduced into the mixing bowl and mixed for 1 minute. Cement and silica fume was added to the dry mixture and mixed for an additional minute. This was followed by adding water and HRWRA and mixing continued for 2 minutes. Finally, the fibres were added to the mixture and mixed for an additional 3 minutes to ensure the adequate distribution of fibres.

In case of rubberized concrete mixtures, general use air-entraining admixture (AEA) and viscosity modifying admixture (stabilizer) of specific gravity 1.01 and 1.02 g/cm^3 were added to control air content, maintain proper distribution of FCRA particles, and to enhance the segregation resistance. Thereafter, all specimens were cast in the specified molds in two layers, vibrated for each layer, then the top surface finished smoothly before being covered with a cap. The cylinders were kept in the mold for 24 hours; after de-molding, all cylinders were continuously cured in a lime water tank until testing ages as shown in **Fig. (5.1)**.

Fresh properties for concrete mixtures including slump, air content, and unit weight were evaluated according to ASTM C143 (2015), ASTM C231 (2017), and ASTM C138 (2017), respectively as represented in **Table (5.4)**. For all mixtures; slump, air content, and unit weight were in the ranges of 90 to115mm, 1.9 to 3.1, and 2090 to 2380 kg/m^3, respectively.

Figure (5.1) Part of fibre reinforcement concrete (FRC) specimens of a different size after de-molding and during curing

Table (5.4) Fresh properties of FRC and CRC mixtures

Mix No.	Mix ID	Slump (mm) ASTM C143	Air Content (%) ASTM C231	Unit weight (kg/m^3) ASTM C138
		Fibre Reinforcement (FRC) mixtures		
1	MC	110	2.0	2300
2	MCS	100	2.1	2380
3	MCP	90	2.2	2340
4	MCMP	95	2.0	2330
5	MCMN	95	2.0	2310
6	MSF	100	1.9	2305
7	MSFS	95	2.0	2375
8	MSFP	90	2.1	2350
9	MSFMP	105	2.0	2325
10	MSFMN	105	2.1	2315
		Crumb Rubber Concrete (CRC) mixtures		
1	MC	90	2.0	2315
2	MCR	115	2.9	2125
3	MSF	95	1.9	2290
4	MSFR	110	3.1	2090

The mortar ingredients were measured by the balance of accuracy 0.01gram, and a small mortar mixer used to prepare all mixtures according to ASTM C305 (2014). Part A (i.e. liquid part) and admixture were introduced into the mixing bowl, then the designed amount of part B (i.e. cementitious material) was added slowly and mixed at a medium speed (i.e. 240±10 r/m) for 2 minutes. After oiling the specified molds, the mortar was cast in two layers and covered for 24 hours by plastic sheets. After de-molding, the mortar specimens were divided into two groups. First group stored under laboratory conditions (i.e. 23 ^{o}C and 50% RH) in plastic containers filled with lime water until testing age. While, the second group stored in an environmental chamber under 38 ^{o}C and 95±5% RH as shown in **Fig. (5.2)**.

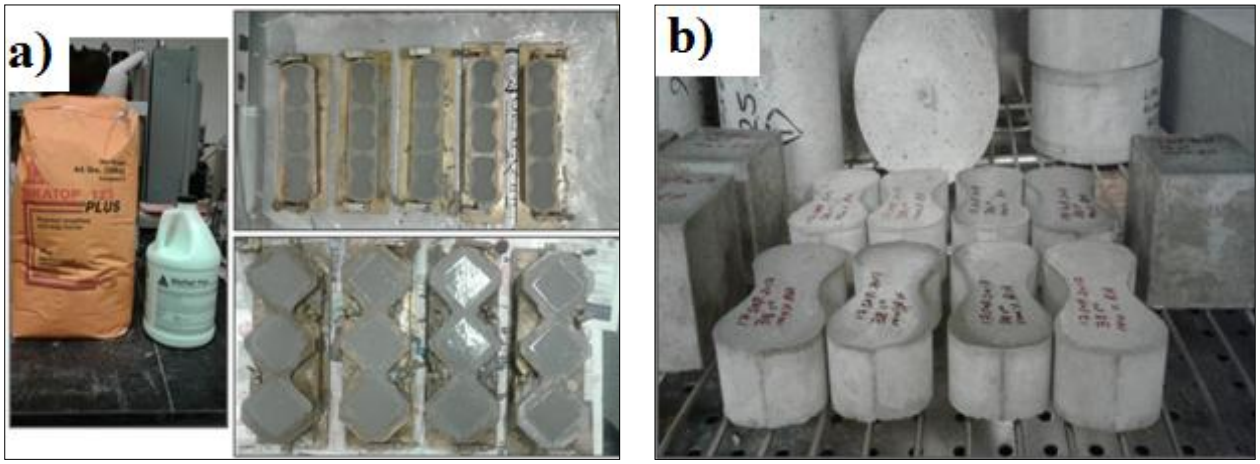

Figure (5.2) Mortar specimens

(a) Cubes 50×50×50mm and Dog bone shape, (b) Curing in an environmental chamber under 38^{o}C and 95±5% RH

5.3 Measurements and Results

The measurements and results are divided into three different parts based on the type of concrete mixtures (i.e. FRC and CRC) and mortar. The mechanical properties, durability indices, UPV, and electrical resistivity for each type are discussed individually to provide a better understanding of each mixture properties. Part A contains FRC incorporating four different type of fibre, Part B discusses CRC, and finally, Part C deals with mortar.

5.3.1 Part A- Fibre Reinforcement Concrete (Introduction)

Fibre reinforced concrete (FRC) is a widely used construction material within civil infrastructure (Narayanan et al., 1987, Zollo et al., 1997, Hensher et al., 2016, and Birol et al., 2016). FRC is favored for its beneficial mechanical properties and ability to restrain cracks (Jiang et al., 2016). The improvement in concrete properties due to fibre addition depends on many factors including fibre type, content, aspect ratio, and tensile strength of the fibre itself (Giaccio et al., 2015). Several types of fibre are commercially available such as steel, polypropylene, nylon, glass, and natural fibre. Among these types, steel fibre is the most commonly used and extensively examined by many researchers. This can be attributed to the fact that the majority of conducted studies have focused on enhancing the tensile behavior of concrete especially after the post-peak stage (Soroushian, et al., 1992, Song and Hwang, 2004, Holschemacher et al., 2010, Nili et al., 2010, and Behfarnia et al., 2014). Hence, adding steel fibres, which are characterized by high tensile strength, will definitely enhance the tensile strength of the composite. However, steel is a conductive material. Thus, concrete electric resistivity will decrease, increasing the reinforcement corrosion risk (Hornbostel et al., 2013, and Yu et al., 2017).

In addition, corrosion of steel reinforcement embedded in concrete is one of the major problems affecting the durability and sustainability of existed reinforced concrete (RC) structures. This can be ascribed to the cracking and spalling of concrete cover due to the expansive pressure associated with reinforcement corrosion (Broomfield et al., 2006, and Jang et al., 2010). This is usually combined with a reduction in the load-carrying capacity of RC structures due to the decrease in the effective cross section of the corroded embedded steel bars (Yu et al., 2017). Previous research has shown that corrosion risk of embedded steel reinforcement in concrete is highly correlated to concrete's electrical resistivity (Lopez and Gonzalez, 1993, Hornbostel et al., 2013, and Yu et al., 2017). Electrical resistivity reflects the ability of concrete to carry electrical charges within itself (Spragg et al., 2013). Hence, the concrete electric resistivity varies with its composition, moisture content, and maturity. For instance, dry cementitious materials have very high electrical resistivity due to their insulating nature (Fiala et al., 2016). Addition of supplementary cementitious materials (SCMs), especially silica fume, have been found to enhance significantly electric resistance of concrete (Papadakis, 2000). Conversely, incorporation of electrically conductive materials (such as steel fibre) in the concrete mixture will significantly decrease its electric resistivity (Lataste et al., 2008, and Solgaard et al., 2014).

5.3.1.1 Compressive Strength

Compressive strength results for all FRC tested mixtures are shown in **Fig. (5.3)**. For all mixtures, compressive strengths increased with time. Moreover, mixtures incorporating SF exhibited a higher increase in strength compared to that of mixtures without SF. For instance, compressive strengths for mixtures MC and MSF at age 90 days were around 9% and 15% higher than that at age 28 days, respectively. This can be attributed to the pozzolanic effect and

densification of the microstructure induced by SF addition (Poon et al., 2006, and Zhang et al., 2016).

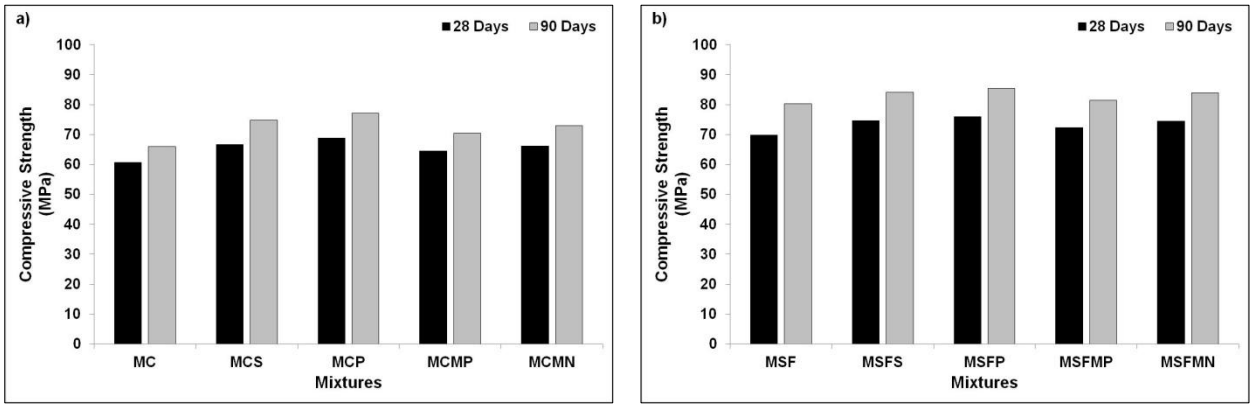

Figure (5.3) Compressive strength for FRC tested mixtures

a) Without SF and b) With SF addition

The average increases in the compressive strength due to the addition of various contents and types of fibres for concrete mixtures with and without SF compared to the respective control mixture are shown in **Fig. (5.4)**. Regardless of the type, addition of fibre increased the compressive strength. For the same volume content of 2%, mixtures without silica fume incorporating macro size polypropylene fibre (MCP) exhibited a slightly higher increase in strength compared to those mixtures incorporating macro size steel fibre (MCS). For example, mixtures MCP and MCS showed an increase in compressive strength around 13.47% and 9.87% at age 28 days, and 16.81% and 13.34% at age 90 days concerning the control mixture (MC), respectively. This higher achieved strength by MCP compared to that of MCS can be attributed to the lower density of polypropylene fibre compared to that of the steel fibre and thus higher mass for the same volume. Hence, at the same fibre volume content, more polypropylene fibres

are presently leading to a wide range of distribution in the mixture which increases fibre ability to interact with cracks (Song et al., 2005).

On the other hand, reducing the fibre content and size resulted in a lower increase in compressive strength as expected (Arafa et al., 2013). However, for the same relative size, it is seen that nylon fibre had a slightly higher potential to increase strength gain than that of micro polypropylene fibre. For instance, mixtures MCMN and MCMP showed an increase in compressive strength around 10.47% and 6.68% at age 90 days in relation to the control mixture (MC), respectively. This can be ascribed to the better dispersion and higher strength of nylon fibre compared to that of the polypropylene one (Song et al., 2005).

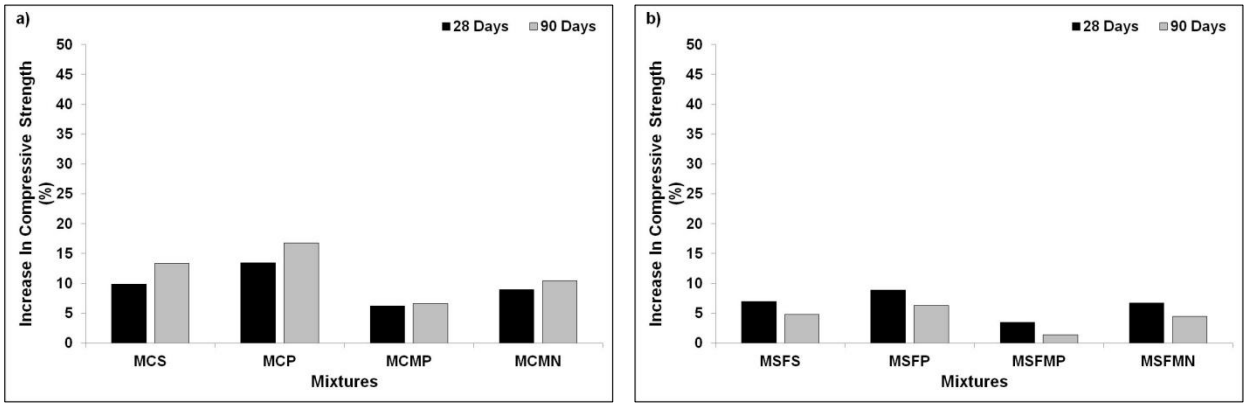

Figure (5.4) Increase in compressive strength for FRC tested mixtures

a) Without SF compared to control mixture MC and

b) With SF compared to control mixture MSF

One interesting point is the difference in the increase in compressive strength between fibre reinforced concrete mixtures with and without SF concerning that of the control mixtures without fibre. Generally, the increase in compressive strength in mixtures without SF is higher than that of mixtures with SF as shown in **Fig. (5.4)**. Moreover, the increases in compressive

strength for all mixtures without SF at age 90 days is higher than that at age 28 days. Conversely, for mixtures with SF, the increase in compressive strength at age 90 days is lower than that at age 28 days. For instance, mixtures MCP and MSFP showed an increase in compressive strength concerning the mixtures MC and MSF by about 13.47% and 8.87% at age 28 days, respectively. These ratios increased to be 16.81% and 6.35% at age 90 days for the same mixtures, respectively. From the above, Its clear, the enhancement in compressive strength is controlled by two factors: fibre addition and microstructure development with time (i.e. progress in hydration). Hence, it seems that the contribution of the microstructure development is higher in mixtures incorporating SF which is directly related to the pozzolanic effect and densification as mentioned earlier.

5.3.1.2 Tensile Strength

Splitting tensile test results for all FRC tested mixtures are shown in **Fig. (5.5)**. Tensile strength followed the same general trend of compressive strength. Tensile strength increased with time; mixtures incorporating SF exhibited a higher increase in strength than those mixtures without SF and addition of fibre had increased the tensile strength regardless of its type. For instance, the tensile strength at age 28 days was in the range from 11.3 up to 15.4 MPa for mixtures without SF and from 14.5 up to 18.1 MPa for mixtures with SF **Fig. (5.5)**.

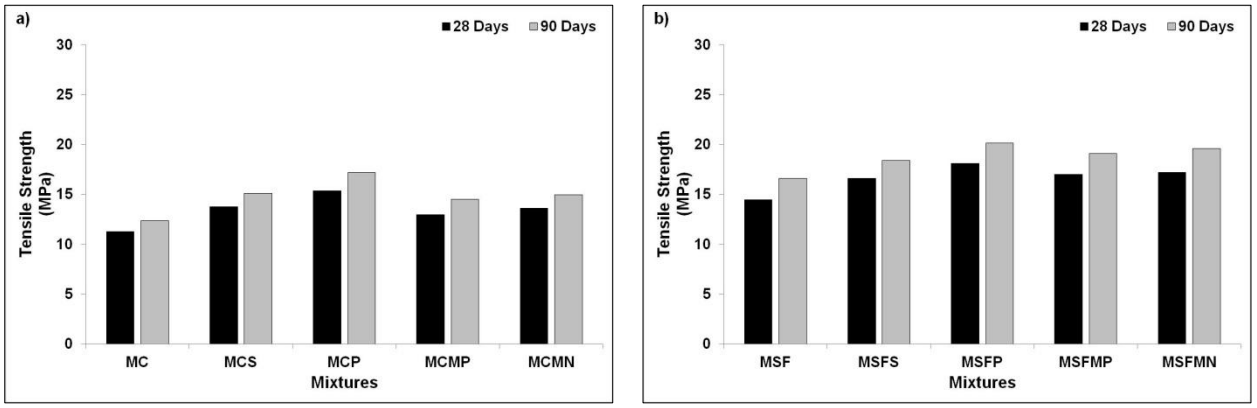

Figure (5.5) Tensile strength for FRC tested mixtures

a) Without SF and b) With SF addition

Figure (5.6) shows the average increase in tensile strength due to the addition of various contents and types of fibres for mixtures with and without SF. This highlights the role of fibre in enhancing the tensile strength of concrete mixtures through bridging cracks and increasing stiffness (Yap et al., 2013). Moreover, the pozzolanic effect and densification of the microstructure induced by SF addition are anticipated to increase the interfacial bond between fibres and surrounding cementitious matrix leading to a higher strength (Godman et al., 1989, Duan et al., 2013, and Çakır and Sofyanlı, 2015).

At the same volume content of 2%, mixtures incorporating macro size polypropylene fibre (MCP) exhibited a higher increase in tensile strength compared to that of mixture incorporating macro size steel fibre (MCS). For example, mixtures MCS and MCP showed an increase in tensile strength of around 22.22% and 36.71% at age 28 days in relation to the control mixture (MC), respectively. This can be attributed to the higher amount of polypropylene fibres in the failure section as explained previously (Song et al., 2005).

Similar to compressive strength results, it seems that micro size nylon fibre had a slightly higher potential to increase strength gain than that of micro size polypropylene fibre. For instance, mixtures MCMN and MCMP showed an increase in tensile strength of around 21.15% and 17.59% at age 90 days with respect to the control mixture (MC), respectively. Moreover, mixtures incorporating nylon fibre exhibited the same enhancement in tensile strength to that induced by steel fibre or even slightly higher in mixtures incorporating SF. For instance, at age 90 days, the differences between the increases in tensile strength for mixtures with steel and nylon fibres were 1.38% and 7.06% for mixtures without and with SF with respect to control mixtures (i.e. MC and MSF) without fibre, respectively. This can be ascribed to the effectiveness of nylon fibres which are smaller in size and characterized by a slightly lower tensile strength than steel fibre, especially in concretes with SF which are more brittle than other mixtures without SF (Tasdemir et al., 1996).

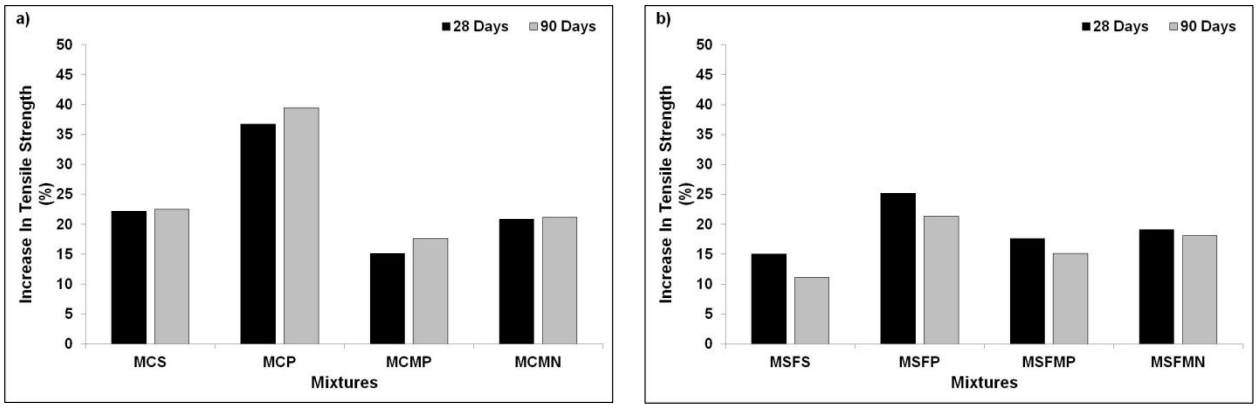

Figure (5.6) Increase in tensile strength for FRC tested mixtures

a) Without SF concerning control mixture MC and

b) With SF concerning control mixture MSF

5.3.1.3 Electrical Resistivity

The bulk electric resistivity of concrete specimens provides information on its ability to resist ionic species penetration through diffusion mechanism (Rupnow and Icenogle, 2011). The higher the bulk resistivity, the higher the resistance for ion penetration leading to higher durability (i.e. lower corrosion risk, sulfate attack, carbonation, and humidity). Generally, concrete electrical resistance is strongly influenced by capillary pore system and the presence of the conductive elements (Spragg et al., 2012, Layssi et al., 2015, and Kevern et al., 2015, Azarsa et al., 2017).

Figure (5.7) shows changes in bulk resistivity over time for the FRC tested mixtures. The standard deviation of the bulk resistivity results was in the range of 0.37 to 1.14 kOhm-cm. Regardless mixture type, bulk resistivity increased with time. From the capillary pore system point of view, comparing **Fig. (5.7)** shows that silica fume addition had a significant impact on the measured bulk resistivity. Adding 10% SF as a replacement of cement by mass increased the bulk resistivity of concrete by around 2.96 to 3.61 times that of the control mixture without SF over the investigated period and fibre type. Silica fume, as a very fine material, is known to densify the microstructure of concrete along with forming secondary calcium silicate hydrate (C–S–H) as a result of the pozzolanic reaction. This secondary C–S–H gel increases the volume of solid phases leading to high strength, low porosity concrete. Reducing concrete porosity will interrupt ionic transfer through concrete leading to a higher electrical resistivity and consequently a lower risk of deterioration rate.

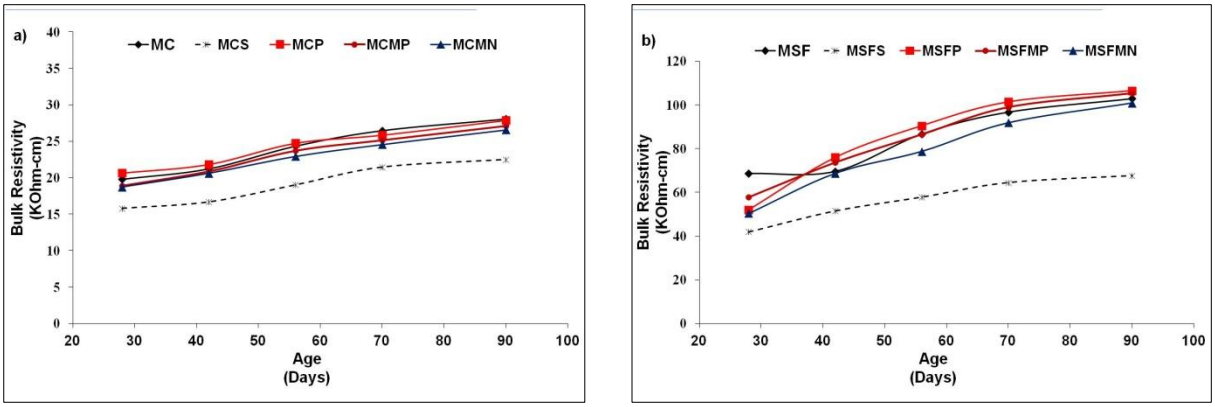

Figure (5.7) Bulk resistivity at various ages for FRC tested mixtures

a) Without SF and b) With SF addition

Moreover, results showed that the addition of non-conductive fibres (i.e. polypropylene and nylon) had slightly reduced concrete resistivity. For instance, MCP, MCMP, and MCMN exhibited about 0.76%, 3.52%, and 5.34% lower bulk resistivity that than of the control specimens (MC) at 90 days, respectively as shown in **Fig. (5.8**). This may be attributed to the fact that fibre inclusion increases concrete porosity as a result of possible fibre agglomeration and pore formation (Kakooei et al., 2012). The high porosity will increase concrete connectivity making ionic transport through concrete's pore system easier. This reduction in concrete resistivity was found to slightly decrease with time until 90 days. For example, reductions in the bulk resistivity of MCMP were 4.54% at age 28 days, and 3.52% at age 90 days compared to that of the control mixture (MC). This can be ascribed to the progress of the hydration process and formation of more hydration products which filled voids/pores.

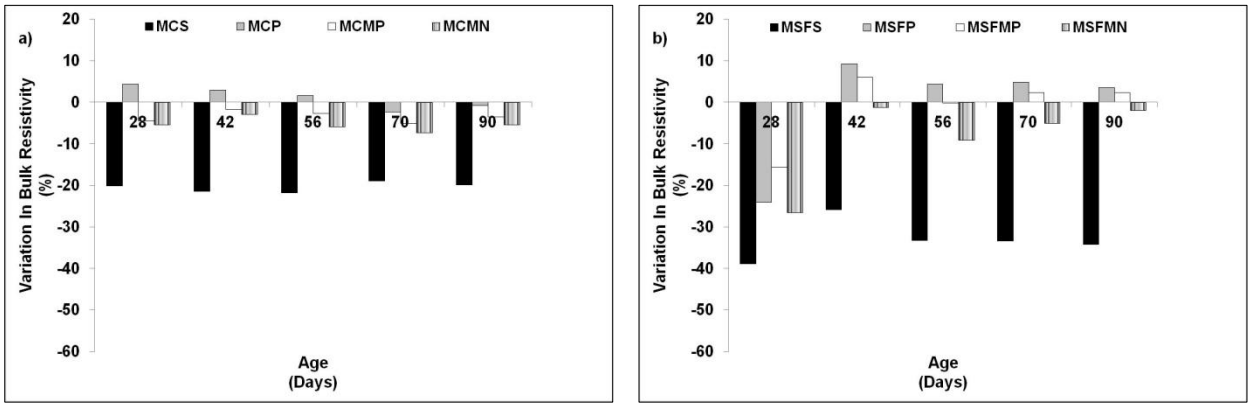

Figure (5.8) Effect of fibre addition on Bulk Resistivity at various ages for FRC tested mixtures

a) Without SF and b) With SF addition

A similar trend was found for silica fume mixtures incorporating non-conductive fibres. Moreover, it seems that silica fume was more effective in enhancing the bulk resistivity of fibre reinforced concrete at later ages. As shown in **Fig. (5.8b)**, at age 28 days, MSFP exhibited about 24.08% reduction in the bulk resistivity with respect to MSF mixture, while at age 90 days, it exhibited about 3.48% higher bulk resistivity than that of the MSF mixture. This can be attributed to the contribution of pozzolanic reactions and its rule in densifying, reducing the voids in concrete as mentioned earlier.

In the case of steel fibre-reinforced specimens, the presence of the conductive element (i.e. steel fibres) significantly reduced the bulk resistance of concrete **Fig. (5.7**). Addition of steel fibres reduced the electrical resistance of concretes up to 20.12% for MCS and 38.89% for MSFS at 28 days, compared to that of the plain concrete without SF (MC) and with silica fume (MSF), respectively. However, the bulk resistivity for mixtures incorporating steel fibre with SF was higher than that without silica fume. The addition of silica fume had reduced the adverse effect of steel fibre on the bulk resistivity of concrete. The bulk resistivity for concrete mixtures

incorporating silica fume and steel fibre (i.e. MSFS) was 2.65 and 3.01 times that of the plain concrete without SF (i.e. MCS) at ages 28 and 90 days, respectively. Therefore, it can be concluded that silica fume addition was sufficient to overcome the reduction in bulk resistivity resulted by steel fibres addition.

Figure (5.9) shows surface resistivity results for the tested mixtures. Surface resistivity results follow a similar trend to that of bulk resistivity. Surface resistivity increases over time for all FRC tested mixtures with and without silica fume. According to the AASHTO TP 95-11 (2011), all concrete mixtures without SF can be classified, based on surface resistivity results, in the range of High to Moderate as shown in **Fig. (5.9a**). On the other hand, other concrete mixtures with SF were in the range of Low to Very low as represented in **Fig. (5.9b**). These results illustrate the effects of age and SF addition on the surface resistivity. At later ages, the concrete microstructure becomes denser, less porous with lower conductivity as a result of hydration and pozzolanic reaction progress. Consequently, ionic transfer through the concrete network becomes more difficult leading to a higher electric resistivity. Moreover, the surface resistivity for MSFS mixture was the lowest compared to that of other silica fume mixtures, however, it still better than other mixtures without silica fume.

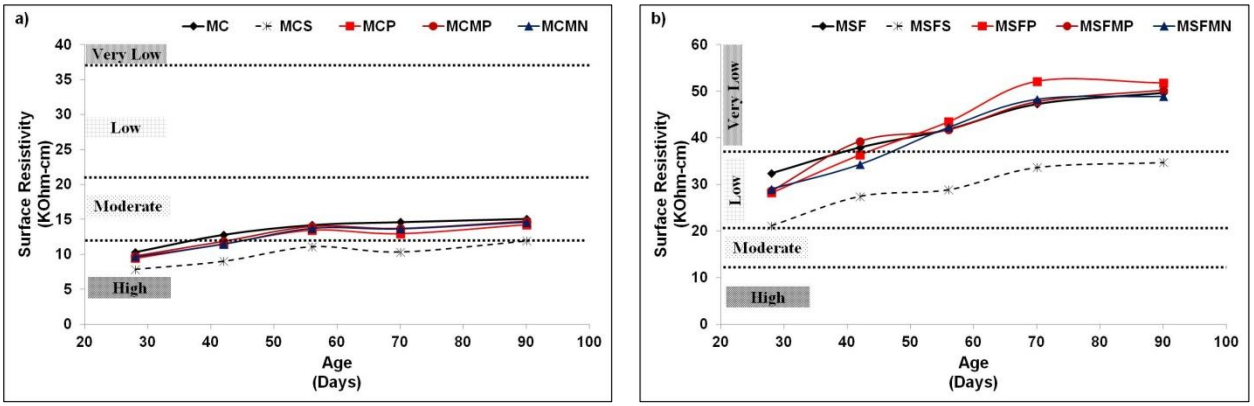

Figure (5.9) Surface resistivity at various ages for FRC tested mixtures

a) Without SF and b) With SF addition

Figure (5.10) shows the correlation between bulk and surface resistivity for tested mixtures. For all tested mixtures, the coefficient of determination values for the linear trend line is high (i.e. R^2=0.86 for concrete mixtures without SF, and 0.97 for concrete mixtures with SF). This indicates that the two electric resistivity measurements at different test ages for all tested mixtures are well correlated. Moreover, Morris et al. (1996) proposed a geometry correction factor that correlates the ratio between surface and bulk resistivity of approximately 1.9 for 100mm×200mm cylinder. From **Fig. (5.10)**, the slope of the linear trend line varies from around 2.15 to 1.52 with average 1.84. This in agreement with the proposed value and justifies the ratio between surface and bulk resistivity for all tested mixtures.

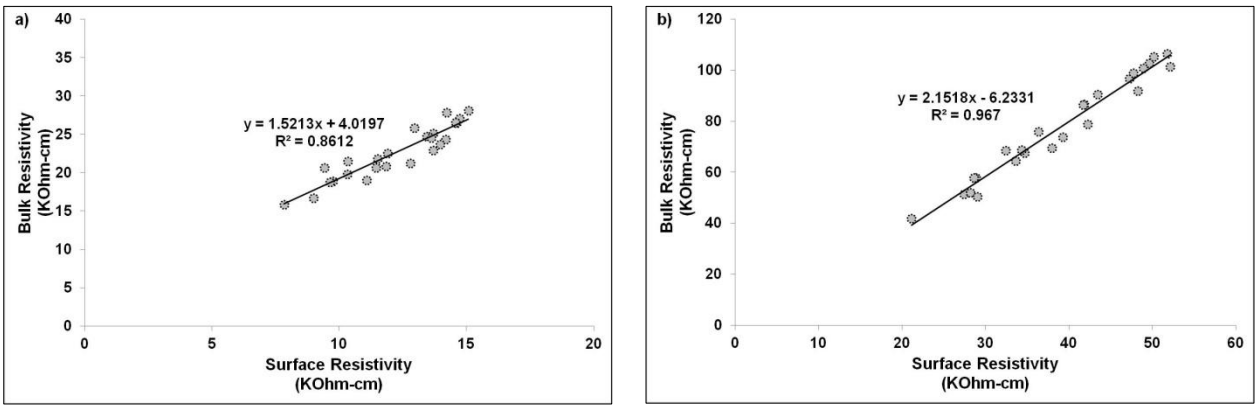

Figure (5.10) Correlation between bulk resistivity and surface resistivity for FRC tested mixtures

a) Without SF and b) With SF addition

Figure (5.11) presents the relationships between the compressive strength and concrete resistivity at ages 28 and 90 days. The results were analyzed in terms of: a) surface resistivity for mixtures with conductive and non-conductive fibre; b) bulk resistivity for mixtures with conductive and non-conductive fibre; c) surface resistivity for mixtures with non-conductive fibre only and; d) bulk resistivity for mixtures with non-conductive fibre only.

It is clear that for the relationship between the 90 day resistivity and compressive strength follows a parallel development to that of the 28 day readings. Regardless of age, the coefficient of determination (R^2) values for the trend was in the range between 0.812 and 0.834 for all mixtures (i.e. mixtures incorporating conductive and non-conductive fibre). This indicated that there is a good correlation between compressive strength and a concrete resistivity at different test ages for all tested mixtures (Piaw, 2006).

Individual assessments of **Fig. (5.11**) was suggest that conductivity of fibre has little influence on the relationship between the compressive strength and concrete resistivity. For instance, at

age 28 days, the difference in the estimated bulk resistivity for MCS and MSFS based on the proposed relationship between compressive strength and bulk resistivity for mixtures incorporating conductive and non-conductive fibres and the relationship when mixtures with conductive fibres were ignored were 4.8% and 6.4%, respectively. In addition, at 90 days, the R^2 for the relationship between compressive strength and bulk resistivity was 0.8168 for mixtures incorporating conductive and non-conductive fibres while it increased to 0.8934 when mixtures with conductive fibres were ignored. This indicated that fibre conductivity, known to have a significant influence on concrete resistivity, appear to have a marginal effect on the relationship between compressive strength and concrete resistivity. In other words, it seems that high strength concrete mixtures can be achieved while maintaining lower conductivity. Generally, electric conductivity for fibre reinforced concrete is highly affected by pore connectivity and fibre conductivity. On the other hand, fibre reinforced concrete strength will also be affected by fibre and porosity but in a different way. Strength will vary based on pore size either connected or not. Regardless of its conductivity, the addition of fibres is going to modify the achieved strength with variable values depending on many factors including fibre content, shape, size, stiffness, and material strength. Therefore, adding conductive or non-conductive fibre in dense concrete (i.e. mixtures with SF) would lead to a similar resistivity. This is confirmed with surface resistivity results shown in **Fig. (5.12b)** where all mixtures with conductive and non-conductive fibre exhibited very low chloride penetration (i.e. durable and low risk from attack materials and corrosion).

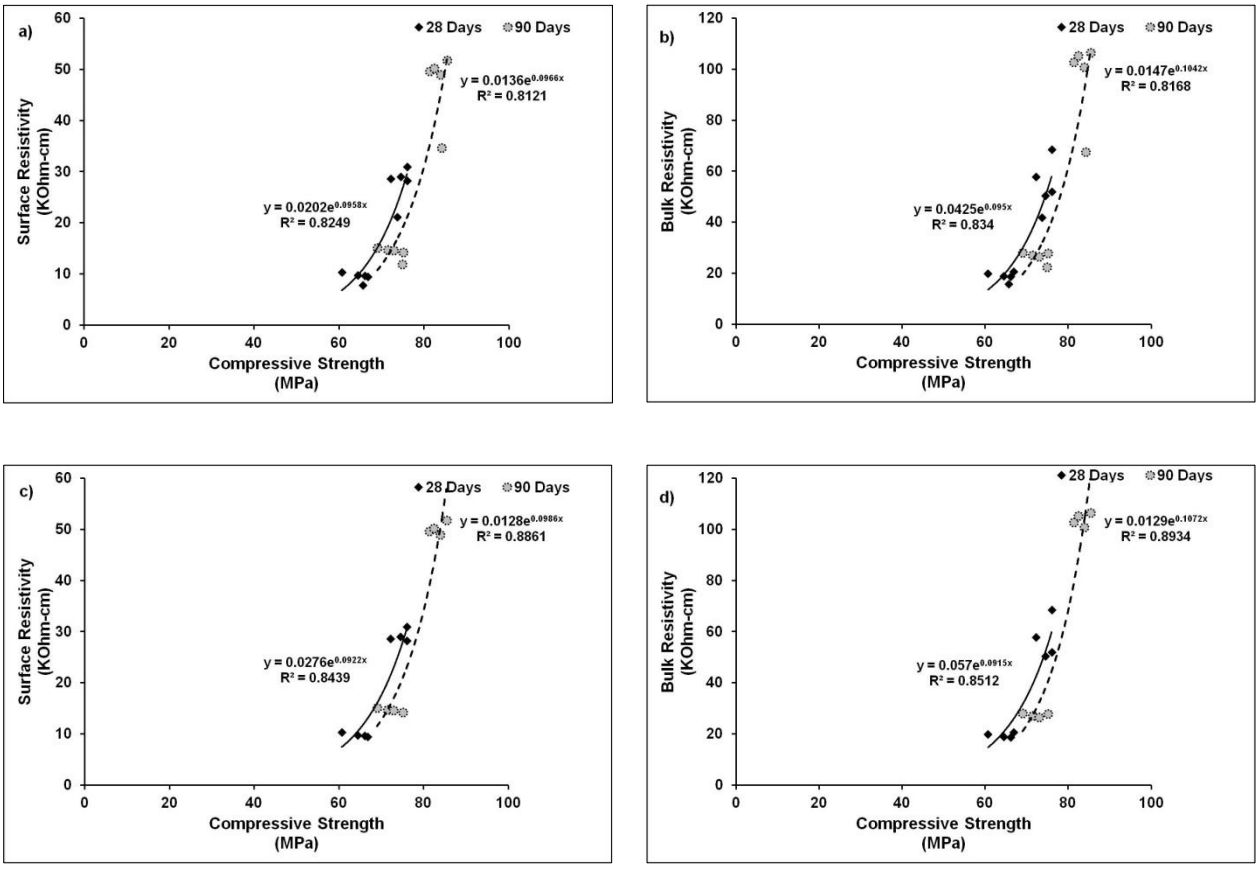

Figure (5.11) Correlation between compressive strength and electrical resistivity

a) Surface resistivity for all mixtures, b) Bulk resistivity for all mixtures, c) Surface resistivity for mixtures without steel fibre, and d) Bulk resistivity for mixtures without steel fibre

5.3.1.4 Durability Index

5.3.1.4.1 Rapid Chloride Permeability Test

Rapid chloride permeability test is the most commonly performed test to indicate a concrete's ability to resist chloride ion penetration. **Figure (5.12)** illustrates the total charge passing over 6 hours through the tested concrete specimens. Generally, the total charge passing decreased with time as concrete become less porous and denser due to the progress of hydration reactions. Moreover, it is clear that the total charge passing decreased with the addition of silica fume. This

can be attributed to the refinement of pores along with increasing its tortuosity leading to lower hydraulic conductivity and consequently interferes with ionic transfer through the concrete pore network (Zhong et al., 2016).

On the other hand, the addition of steel fibre was found to increase the total charge passing compared to all other samples. For instance, MCS showed higher total charge passing with about 37% increase than that of the control mixture (MC) at age 56 days. Also, it seems that other non-conductive fibres did not show a significant effect on the total charge passed.

Figure (5.13) illustrates the correlation of RCPT and surface resistivity for all FRC tested mixtures over the investigated period. For all tested mixtures, the coefficient of determination values for the trend was about 0.9 for concrete mixtures without SF and 0.97 for concrete mixtures with SF. This indicated that there is a very strong correlation between these test results at different test ages for all tested mixtures in agreement with the AASHTO (2011).

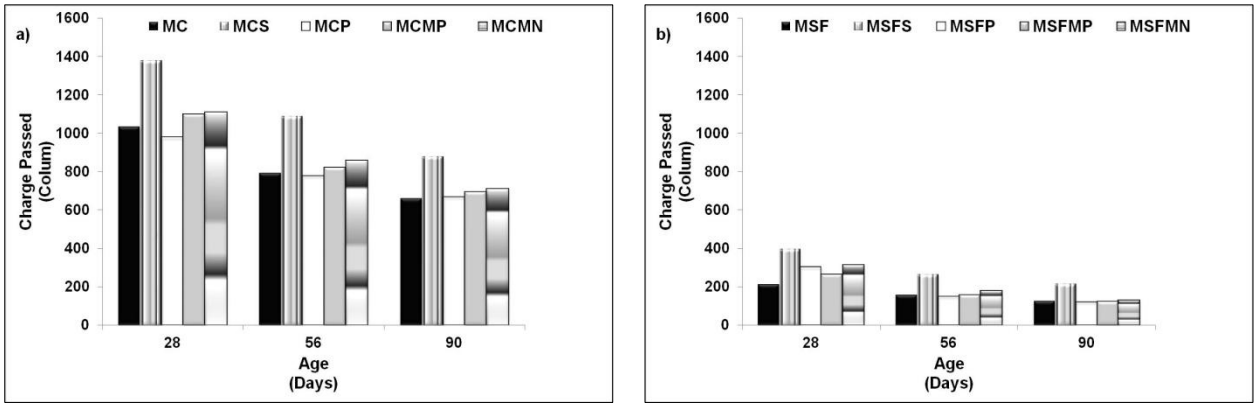

Figure (5.12) RCPT at various ages for FRC tested mixtures

a) Without SF and b) With SF addition

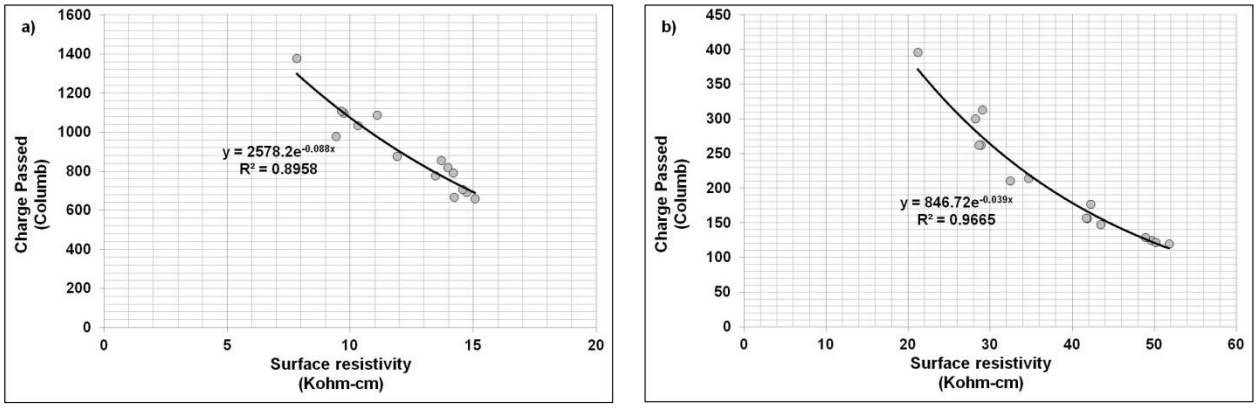

Figure (5.13) Correlation between RCPT and surface resistivity FRC tested mixtures

a) Without SF and b) With SF addition

5.3.1.4.2 Sorptivity

The characteristics of pores and their connectivity can be expressed by sorptivity to provide information concerning the permeable pores inside the concrete. The sorptivity results of different FRC tested mixtures are depicted in **Fig. (5.14)**. For all mixtures, accumulative sorptivity increased with time. Moreover, the results exhibited mixtures incorporating SF introduced a significant decrease in sorptivity compared to that of mixtures without SF. For instance, initial and secondary sorptivity (i.e. at six hours and nine days, respectively) for mixtures MSF was reduced by about 18.21% and 18.91%, respectively compared with control mixture MC.

The results reveal that the addition of various contents and types of fibre had a positive effect to decrease both initial and secondary sorptivity of concrete mixtures with and without SF as shown in **Fig. (5.15)**. For the same volume content of 2%, mixtures with and without silica fume incorporating macro size polypropylene fibre (MCP and MSFP) exhibited a higher reduction in sorptivity compared to those mixtures incorporating macro size steel fibre (MCS and MSFS). For

example, mixtures MCP and MCS showed a reduction in sorptivity by about 9.1% and 7.03% at 6 Hrs (i.e. Initial absorption) and 11.51% and 6.12% at age nine day (i.e. secondary absorption) concerning the control mixture (MC), respectively. Its clear and confirming with the data obtained from RCPT, the lower the fibre density, the higher the fibre mass, this can lead to a wide range of distribution of the macro polypropylene in the concrete mixture increases fibre ability to interact with cracks.

On the other hand, reducing the fibre content and size resulted in a higher decrease in water absorption. However, for the same relative size, it is seen that micro polypropylene fibre had a significant potential to decrease sorptivity than that of nylon fibre. For instance, mixture MCMP showed a higher reduction in sorptivity around 15.41% and 14.14% at age 6 hours and nine days concerning the control mixture (MC), respectively. While, MCMN exhibited an increase in sorptivity around 13.25% and 12.56% at the same age as depicted in **Fig. (5.16)**.

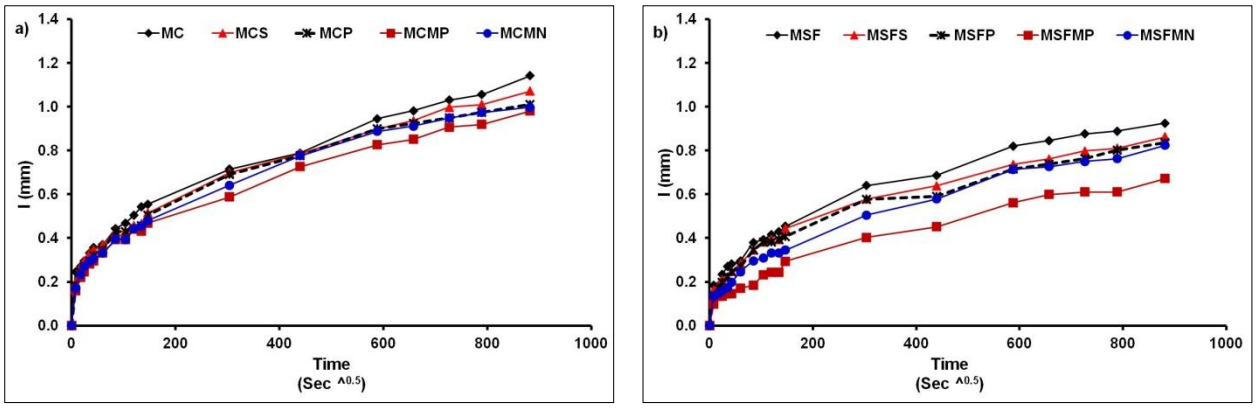

Figure (5.14) Sorptivity for FRC tested mixtures

a) Without SF and b) With SF addition

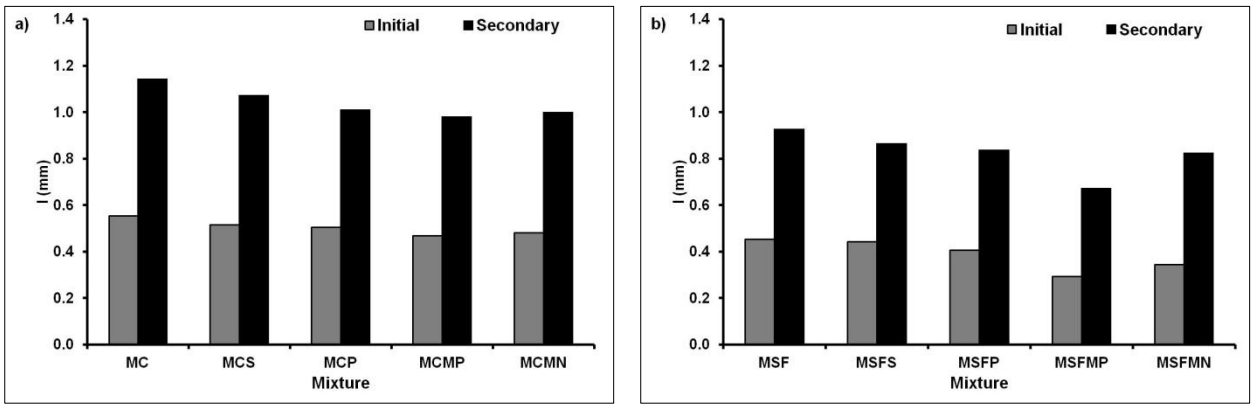

Figure (5.15) Initial and secondary sorptivity for FRC tested mixtures

a) Without SF and b) With SF addition

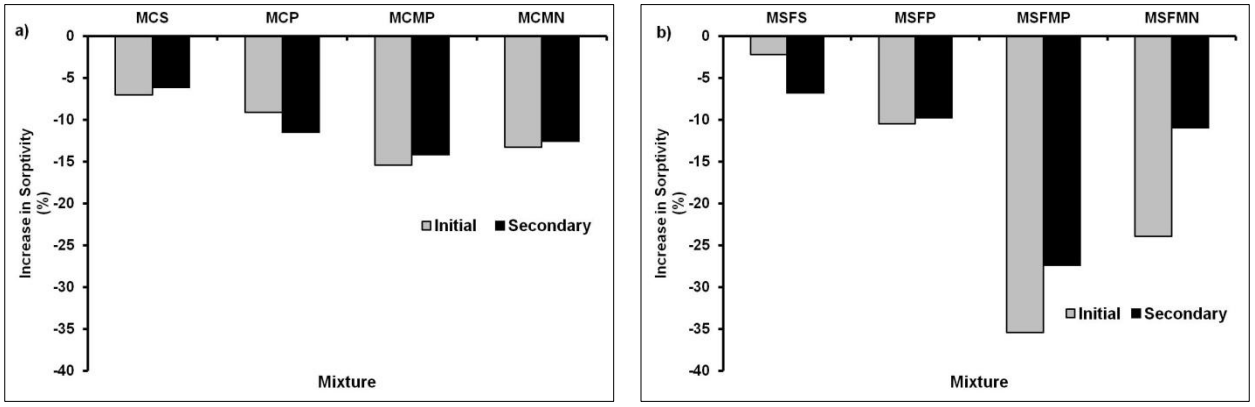

Figure (5.16) Increase in sorptivity for FRC tested mixtures

a) Without SF compared to the control mixture MC and b) With SF compared to the control mixture MSF

5.3.2 Part B - Crumb Rubber Concrete (Introduction)

Governments around the world are encouraging concrete manufactures to find substitutional materials instead of natural aggregate. Due to the environmental issues related to its safe disposal, waste tires are considered one of the alternatives to replace one or more of the concrete ingredients. The introduction of crumb rubber aggregate (CRA) into concrete mixtures had a dual action. It can reduce the amount of disposed waste tires along with produce greener concrete with a lower demand on natural materials (Azevedo et al., 2012, Najim et al., 2012, Onuaguluchiet al., 2014).

Generally, Crumb Rubber Aggregate (CRA) passes through steps before being added to concrete mixtures, including shredding and/or grinding (Karger-Kocsis et al., 2013). Various sizes can be produced and introduced into concrete mixtures as; shredded rubber in the range from 76 mm to 430 mm as a replacement to coarse aggregate, crumb rubber in the range from to 0.425 mm to 4.75 mm as a replacement to fine aggregate, and ground rubber in the range from 0.075mm to 0.475mm a a cement replacement (Ganjian et al., 2009).

Previous research studies on CRA showed an adverse effect for increasing its content on concrete fresh properties (i.e. workability). This was attributed to the irregular shape and rough surface of rubber particle which increase the inter-particle friction between rubber particles and concrete mixture ingredients (Turatsinze and Garros, 2008, Holmes et al., 2014, Kardos et al., 2015, Turatsinze et al., 2018, and Thomas and Gupta, 2016). The use of superplasticizer had a crucial role to overcome the CRA issues concerning the slump and to maintain slump within the specified range (Turatsinze and Garros, 2008, Kardos et al., 2015, Ganesan et al., 2013, Elchalakani et al., 2015). Moreover, other fresh properties such as air content was found to increase by about 48.4%, 100%, 132.3%, and 180.6% as CRA replaced coarse aggregate (i.e.

from 4mm to 10mm) by 10%, 15%, 20%, and 25%, respectively (Turatsinze and Garros, 2008). However, other studies showed only 7.5% increase in air content when CRA was used as a replacement for 30% of the fine aggregate (Kardos et al., 2015, and Thomas and Gupta, 2016). This was attributed to the rough surface and nonpolar property of fine CRA which fends off water and will adhere air on its surface. Generally, the air content issue can be overcome by utilizing air entrained admixture to adopt the air content of mixtures within the design limit.

The density and unit weight of concrete mixtures decreased as the replacement ratio of CRA increased into concrete mixtures (Pelisser et al., 2011, Sukontasukkul et al., 2012, Pacheco-Torgal et al., 2012, Gesoğlu et al., 2014b, and Holmes et al., 2014). Concrete unit weight is governed by low density components and the amount of air content entrapped into the concrete mixture. For instance, when CRA replaced coarse aggregate (i.e. from 4mm to 10mm) by 10%, 15%, 20%, and 25%, unit weight of fresh concrete decreased by about 3.7%, 6.8%, 9.5%, and 10.8%, respectively, and hardened concrete unit weight decreased by about 10.6%, 12.5%, 14.1%, and 16%, respectively (Turatsinze and Garros, 2008). In addition, adding CRA can increase the probability of segregation. Despite the use of a viscosity agent to control the appropriate distribution of CRA particles into the mixture, the segregation increased by about 14.3%, 28.6%, 20.4%, and 24.5% when CRA replaced coarse aggregate (i.e. 4mm-10mm) by 10%, 15%, 20%, and 25%, respectively (Turatsinze and Garros, 2008).

Moreover, many studies showed that mechanical properties and durability indices will be affected negatively due to the addition of rubber aggregate (Ganjian et al., 2009, and Gesoğlu et al., 2014a). For instance, compressive and tensile strengths at 28 days for rubberized concrete were decreased with about 29% to 71% as rubber aggregate content increased from 10% to 50% (Kardos et al., 2015). In the four-point flexure test, the peak load decreased by about 12.1% and

41.8% as CRA replacement of the coarse aggregate were 15% and 25%, respectively (Turatsinze and Garros, 2008, and Kardos et al., 2015). The achieved modulus of rupture for mixtures containing 10%, 20%, 30%, 40%, and 50% CRA as a replacement of fine aggregate were below the specified amount at 28 days (Kardos et al., 2015). Porosity for rubberized concrete also increased by about 8.5%, 17.7%, 23.1%, and 33.8% as CRA replaced coarse aggregate by 10%, 15%, 20%, and 25%, respectively (Turatsinze and Garros, 2008). Moreover, rubberized concrete mixtures incorporated 20% CRA and more reveals lower durability (i.e. durability factor is less than 60% after 324 freeze/thaw cycles) (Kardos et al., 2015). Moreover, penetration of water depth increased as CRA content increased (Ganesan et al., 2013).

Conversely, using CRA in ash form showed a different trend. Compressive strength for mortar mixtures incorporating CRA at rates 2.5%,5 %, 7.5%, and 10% as a replacement of fine aggregate increased by about 14%, 21%, 29%, and 45%, respectively (Al-Akhras et al., 2004). Moreover, utilization of coated CRA caused a significant increase in strength as a result of good bonding and enhancement for the interface around CRA (Dong et al., 2013, and Onuaguluchi et al., 2014). In addition, rubberized concrete reveals an increase in flexural strength and significant deformation (i.e. nonbrittle failure) compared with the control mixture as 20% CRA was used (Yilmaz and Degirmenci, 2009). Flexure strength for rubberized concrete was increased in the range from 9% to 15% in self-compacting mixtures (Onuaguluchi et al., 2014). For the durability properties, using CRA powder as partially replaced for cement caused a reduction in sorptivity (Ganjian et al., 2009). In addition, using granulated CRA particles as a replacement for sand reduced sorptivity (Oikonomou and Mavridou, 2009). The static flexural strengths for rubberized concrete mixtures incorporating 15% and 20% CRA were higher than that of the control specimens by about 15% and 9%, respectively (Ganesan et al., 2013). In addition, static flexure

strength for concrete mixtures contains 15% CRA with steel fibre by 0.5% and 0.75% was increased by about 26% and 35%, respectively (Ganesan et al., 2013).

Utilization of pozzolanic materials causes an improvement for the rubberized concrete. For example, 15% fly ash addition reduced the concrete permeability (Kardos et al., 2015). In addition, CRA could prevent the crack widening, but it cannot prevent the crack formation into concrete (Kardos et al., 2015). From the above, despite the introduction of CRA into the concrete, can adversely affect some of the concrete properties. Simultaneously, it can enhance other properties as ductility, insulation, and damping.

Due to several inconsistent information about effect of CRA on the concrete properties. This part presents the evaluation of rubberized concrete mixtures incorporating 10% FCRA partially replacing natural fine sand by volume with and without 10% silica fume that replaced cement by mass. Evalution was accomplished by applying standard test methods to laboratory concrete cylinders to evaluate mechanical properties, electrical resistivity, UPV, and durability indices. In addition, apply of SDT as a method to evaluate plasticity deformation and loss of stiffness.

5.3.2.1 Compressive and Tensile Strength

Compressive and tensile strength result at 28, 56, and 90 days for all tested mixtures are represented in **Fig. (5.17)**. Strengths increased for all mixtures with time. For instance, the compressive strength of the mixture containing 10% FCRA (MCR) increased over time: 33.5, 35.9, and 38.6 MPa at 28, 56 and 90 days, respectively. Tensile strength exhibited a similar trend. The relationships between compressive and tensile strength overtime showed linear trends with regression coefficients (i.e. R^2) around 0.9 to 0.99 as shown in **Fig. (5.18**). Moreover, results showed that mixtures containing SF showed a higher increase in strength compared to that of mixtures without SF. For instance, compressive strength for mixtures MSF and MSFR at age 90 days were around 17.35% and 22.28% higher than that compressive strength of mixtures MC and MCR, respectively. A similar trend was obtained for tensile strength. This can be attributed to the pozzolanic effect and densification of the microstructure induced by SF addition (Neville2002, Mehta and Montiero 2006, Poon et al., 2006, and Zhang et al., 2016).

On the other hand, average reductions in concrete strength due to FCRA addition are shown in **Fig. (5.19)**. For example, MCR mixtures showed a reduction in compressive strength with respect to the control mixture (MC) by about 29.5%, 28.4%, and 28.0% at 28, 56 and 90 days, respectively. In addition, tensile strength for the same mixture showed a similar trend. The tensile strength decreased by about 31.1%, 31.3%, and 28.0% at 28, 56, and 90 days, respectively. These reductions in compressive and tensile strengths can be attributed to the increase in air content, low FCRA stiffness, lower bond between cement paste and FCRA, and quick failure during loading process resulting from rapid development of cracks at the interfacial zone due to high softening of cement paste including FCRA surrounding the aggregate particles

(Ganjian et al., 2009, Issa et al., 2013, Ganesan et al., 2013, Kardos et al., 2015, and Gupta et al., 2016).

On the other hand, mixture incorporated SF and FCRA (MSFR) revealed a lower reduction in strengths compared to the control mixture. For instance, compressive and tensile strengths for mixture MSFR at 56 days showed lower values than that of the MCR by about 13.9%, and 24.4%, respectively. From the tests results, its clear that the target strength at 28 days was achieved with 10% SF partially replacing cement although the fine aggregate was replaced by 10% FCRA. It seems that the contribution SF (i.e. the pozzolanic effect and densification) had overcome the adverse effect of FCRA addition.

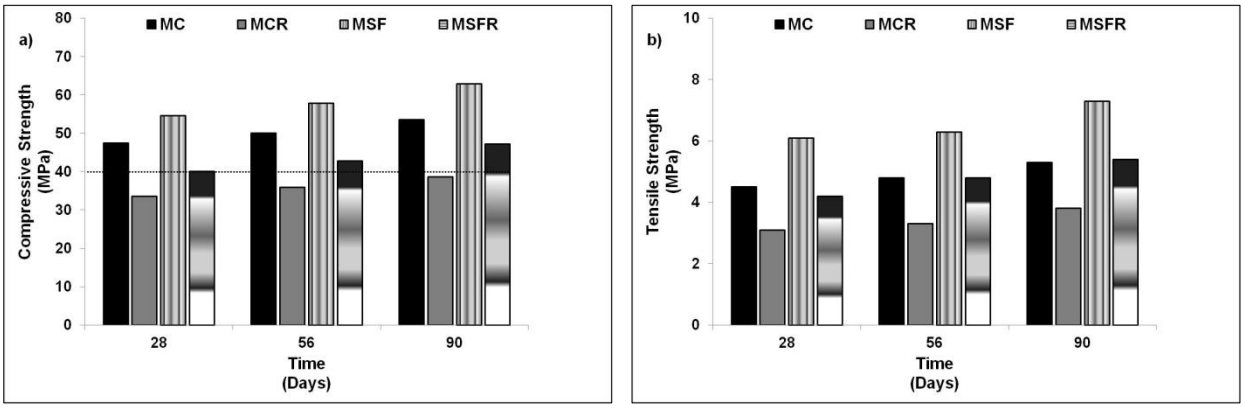

Figure (5.17) Strength for CRC tested mixtures with and without silica fume

a) Compressive Strength, and b) Tensile Strength

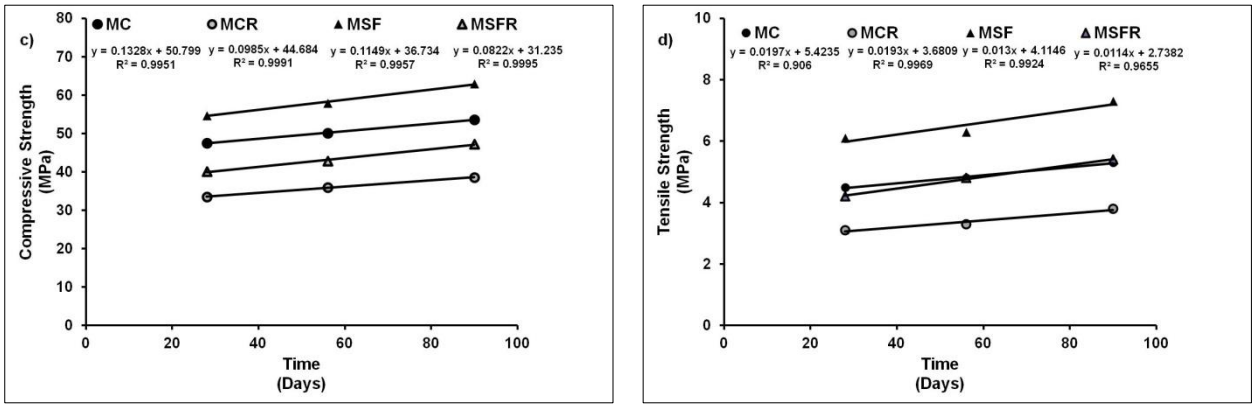

Figure (5.18) Relationship between strength for CRC tested mixtures with and without silica fume versus time

a) Compressive Strength, and b) Tensile Strength

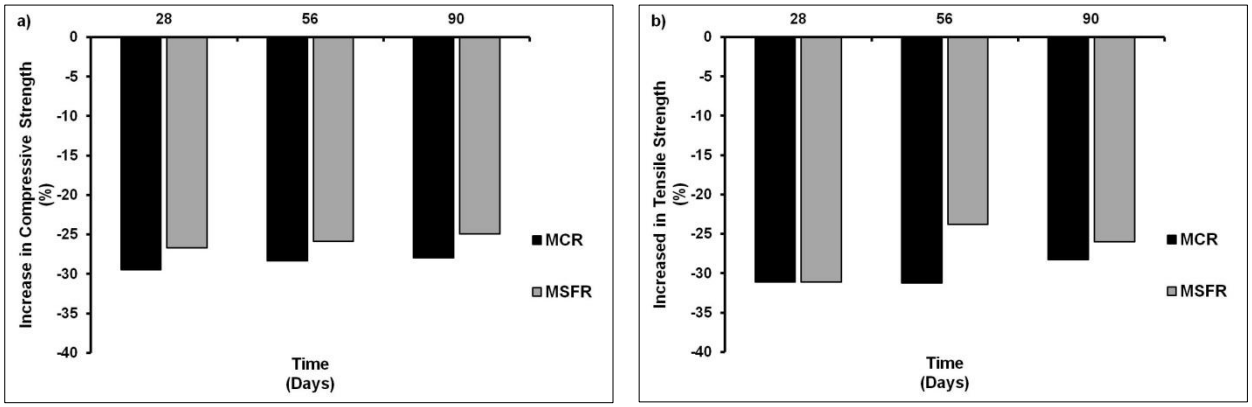

Figure (5.19) Increase in strength for CRC tested mixtures with and without silica fume

a) Compressive Strength, and b) Tensile Strength

5.3.2.2 Modulus of Elasticity and Poisson Ratio

Modulus of elasticity (MOE) and Poisson ration (υ) were used to evaluate the concrete response to load over time. Generally, for all tested concrete mixtures MOE and υ increased with varied ratios in the range from 5.6% to 19.6% and from 5.4% to 19.5%, respectively. This mainly depended on the testing time and concrete ingredients (i.e. FCRA with and without SF) as shown in **Fig. (5.20,5.21)**. For instance, MOE for MCR increased over time: 18.5, 20.0, and 21.3 GPa at 28, 56 and 90 days, respectively. In addition, a similar trend was obtained for υ. The relationships between the MOE and υ with time can be represented for all tested mixtures by linear fit lines with regression coefficients closed to unity (i.e. R^2=0.99).

Moreover, results showed that mixtures containing SF revealed an increase in both MOE and υ compared to that of mixtures without SF. For instance, MOE for mixtures MSF and MSFR at age 90 days were around 9.4% and 14.6% higher than that MOE of mixtures MC and MCR, respectively. A similar trend was obtained for υ. This can be attributed to the contribution of the pozzolanic effect of SF.

On the other hand, the average variations in the MOE and υ due to the addition of FCRA for concrete mixtures with and without SF are shown in **Fig. (5.22,5.23)**. For example, mixtures MCR showed a decrease in MOE with respect to MC by about 27.7%, 26.0%, and 25.5% at 28, 56 and 90 days, respectively. In addition, υ for the same mixture showed a contrary trend. It increased by about 34.7%, 31.3%, and 28.0% at 28, 56, and 90 days, respectively. This reduction and increase in MOE and υ due to addition of FCRA can be attributed to the addition of an elastic material into a rigid material. These results in agrement with previous researches (Ganjian et al., 2009, and Dong et al., 2013).

On the other hand, mixture incorporated SF and FCRA (MSFR) reveal a lower variation in MOE and υ compared to MC. For instance, the MOE and υ for mixture MSFR at 56 days showed a lower change than that of the MCR by about 8.0%, and 27.0%, respectively.

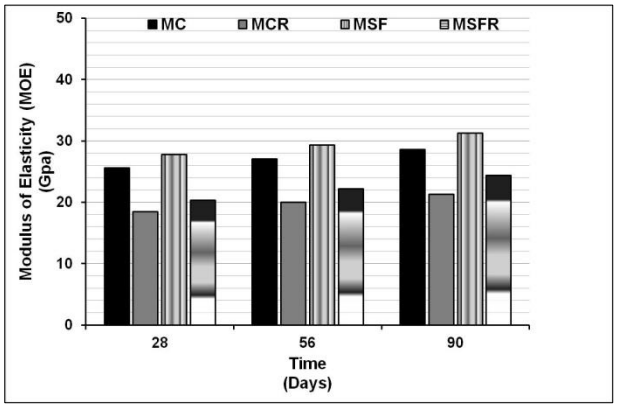

Figure (5.20) Modulus of elasticity for CRC tested mixtures with and without SF

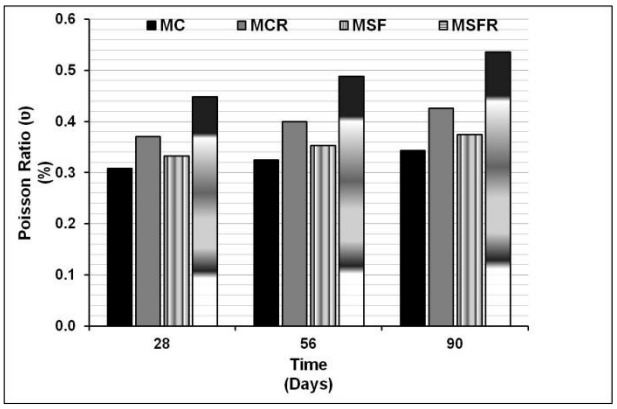

Figure (5.21) Poisson ratio for CRC tested mixtures with and without SF

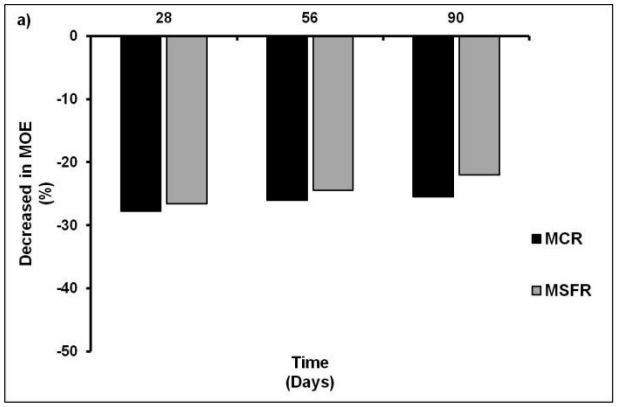

Figure (5.22) Reduction in MOE for CRC mixtures with and without SF

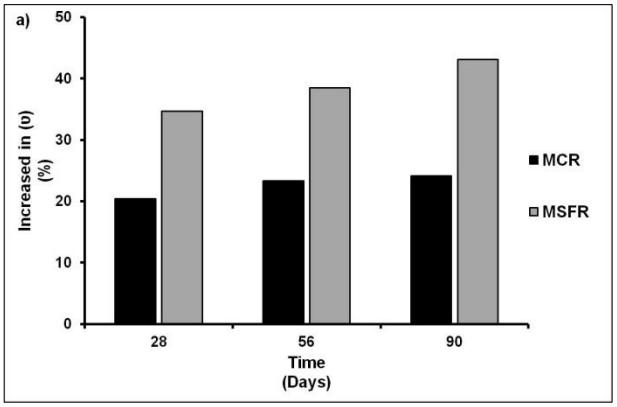

Figure (5.23) Increased in (υ) for CRC mixtures with and without SF

5.3.2.3 Loss of Stiffness

The stress-strain curves of the five loading cycles for all tested mixtures were plotted at 28, 56, and 90 days, respectively as shown in **Fig. (5.24)** as example. The plots of stress-strain curves and results showed that the hysteresis area (S1) of the first loading cycle decreased over time for all tested mixtures as shown in **(5.25)**. For instance, the hysteresis area (S1) were 190, 170, and 150 J/m^3 for MC mixture and 180, 160, and 140 J/m^3 for MSF mixture at 28, 56, and 90 days, respectively. In addition, plastic deformation (D1) calculated over the five loading cycles had decreased over time until age 56 days and then stabilized for control mixtures without FCRA. However, it continue decreasing for mixtures incorporating FCRA as shown in **Fig. (5.26)**. For instance, D1 were 60, 50, 50 and 60, 40, 40 μstrain for mixtures MC and MSF at 28, 56, and 90 days, respectively. While, D1 were 80, 70, 60 and 70, 60, 50 for mixtures MCR and MSFR at the ages.

Hence, it is clear that the stiffness for all tested mixtures increased over time. The correlation between calculated HA (S1) after the first loading cycle versus time were plotted for all tested mixtures at ages 28, 56, and 90 days, respectively as shown in **Fig. (5.27)**. The correlations reveal that all mixtures incorporated FCRA with and without SF followed a similar parallel power trend with coefficient of determinations (R^2) 0.98, 0.84, 0.98, and 0.99 for mixtures MC, MCR, MSF, and MSFR, respectively. On the other hand, plotting of the total plastic deformation (D1) after five loading cycles versus time showed a similar trend for all tested mixtures with different R^2 especially for mixture MC (i.e. R^2=0.83) as represented in **Fig. (5.28)**.

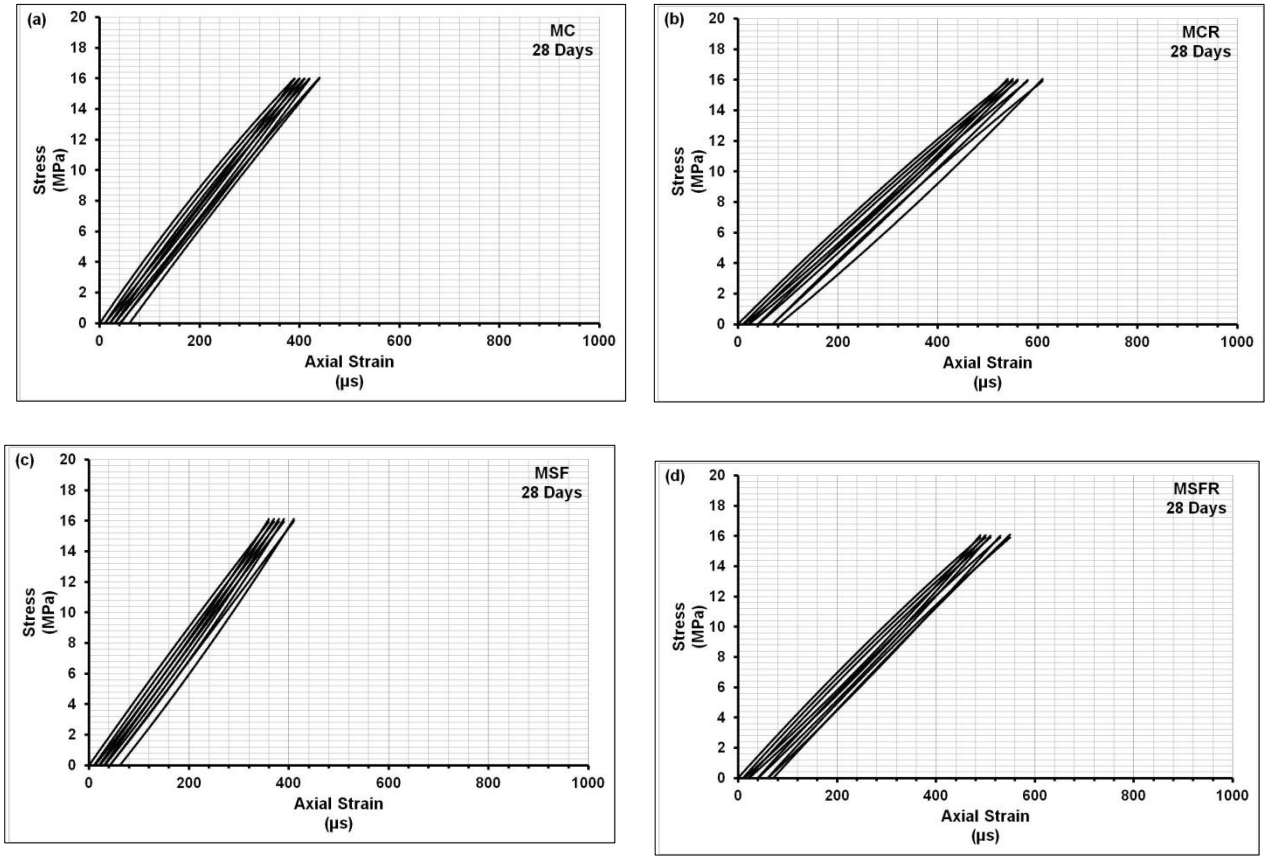

Figure (5.24) Stress-Strain curves of CRC mixtures with and without SF at 28 days

(a) MC, (b) MCR, (c) MSF, and (d) MSFR

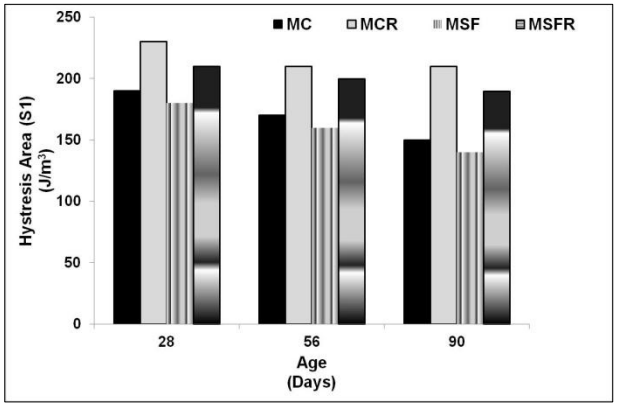

Figure (5.25) Hysteresis areas (S1) for tested mixtures at different ages

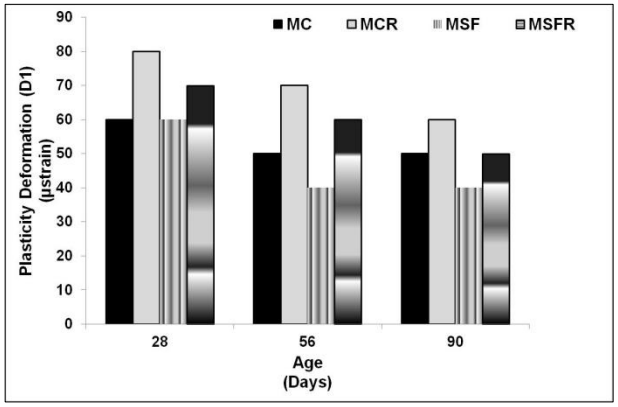

Figure (5.26) Plastic deformation (D1) for tested mixtures at different ages

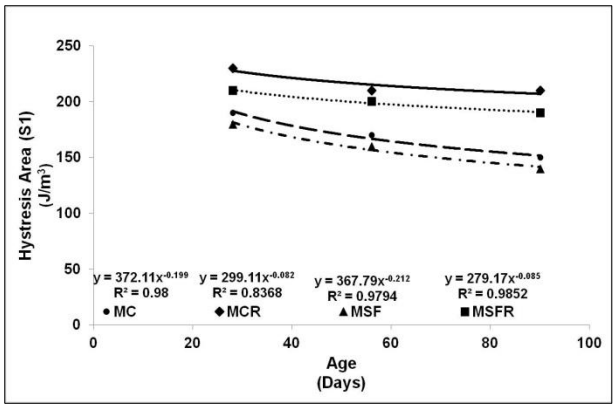

Figure (5.27) Relationship between hysteresis area (S1) and time

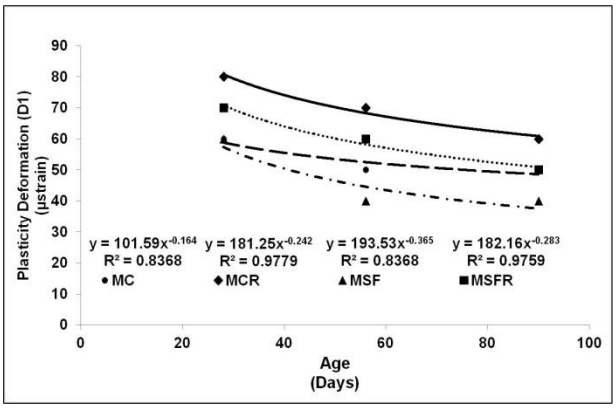

Figure (5.28) Relationship between plastic deformation (D1) and time

Moreover, results showed a reduction in S1 for mixtures containing SF with and without FCRA in the range from 4.8% to 9.5% and from 5.3% to 6.7% compared to mixtures MC and MCR, respectively. In addition, total deformation after 5 loading cycles (D1) was decreased by about 17% and 20% at 90 days for the same mixtures compared to mixtures MC and MCR, respectively. This can be ascribed to the pozzolanic effect and densification of the microstructure induced by SF addition (Neville 2002, Mehta and Montiero 2006, Poon et al., 2006, and Zhang et al., 2016).

On the other hand, the average increase in both S1 and D1 due to the addition of FCRA for concrete mixtures with and without SF are shown in **Figs. (5.29,5.0)**. For example, mixture MCR showed an increase in hysteresis area (S1) by about 21.1%, 23.5%, and 40.0% at 28, 56 and 90 days compared to that of the MC, respectively. In addition, the total deformation after 5 cycles (D1) for the same mixture showed a similar trend. An increase in D1 by about 33.3%, 40.0%, and 20.0% at 28, 56, and 90 days, respectively. This increase in hysteresis area and total deformation can be attributed to the rubber properties (i.e. more softener than fine aggregate).

However, mixture incorporated FCRA at the presence of SF exhibited an increase in both S1 and D1 due effect of SF. For instance, S1and D1 increased by about 36% and 25% at age 90 days compared with mixture MSF as shown in **Fig. (5.29,5.30)**.

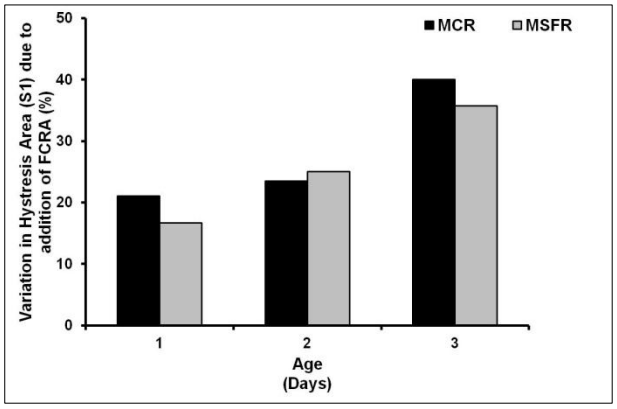

Figure (5.29) Variation in hysteresis area (S1) for CRC tested mixtures with and without Silica Fume

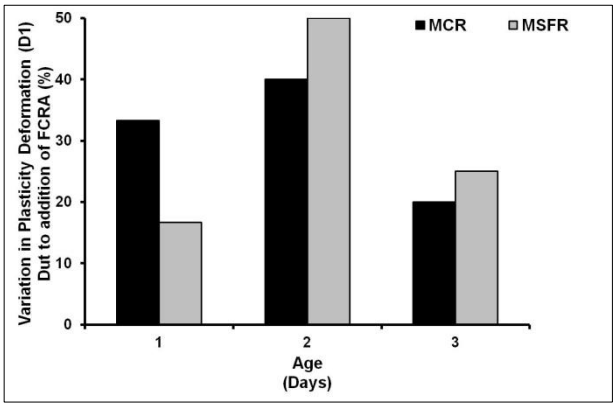

Figure (5.30) Variation in between plastic deformation (D1) for CRC tested mixtures with and without Silica Fume

On the other hand, two different indices stiffness damage index (SDI) and plasticity deformation index (PDI) were calculated as proposed by (Sanchez et al., 2014, and 2016). The relationships between indices SDI as a function of time were plotted using logarithm fit with regression coefficients R^2= 0.998, 0.962, 0.996, and 0.731 for mixtures MC, MCR, MSF, and MSFR, respectively as shown in **Fig. (5.31)**. It is clear that SDI decreased with time for all tested mixtures. Moreover, the relationships between indices PDI as a function of time were plotted for the same mixtures at the same testing ages. The relationship between PDI versus time showed a similar trend of SDI versus time, where PDI decreased with time for all tested mixtures as represented in **Fig. (5.32)**. The results showed SDT output (i.e. S1, D1, SDI, and PDI) are sensitive to quantify and assess the the change in properties (i.e. stiffness and deformation) of

the rubberized concrete mixtures incorporating FCRA replacing FA at a rate of 10% by volume with and without SF cement replacement at a rate of 10% by mass. The SDT output parameters reveal that the hysteresis area, stiffness, plasticity deformation, and elasticity as a function of time. In addition, replacing 10% of fine aggrgate with FCRA had increased the plasticity deformation and elasticity at testing ages compared with the control mixtures.

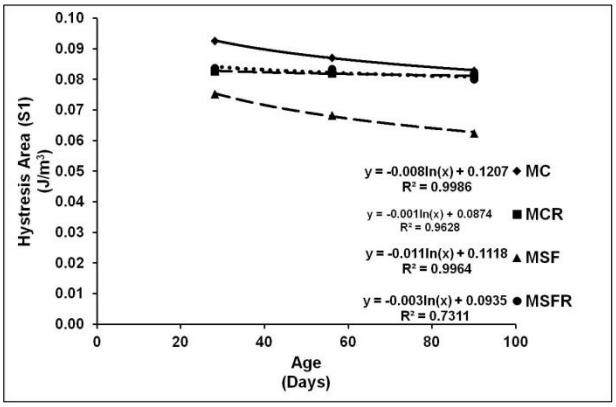

Figure (5.31) Correlation between stiffness damage index (SDI) and time

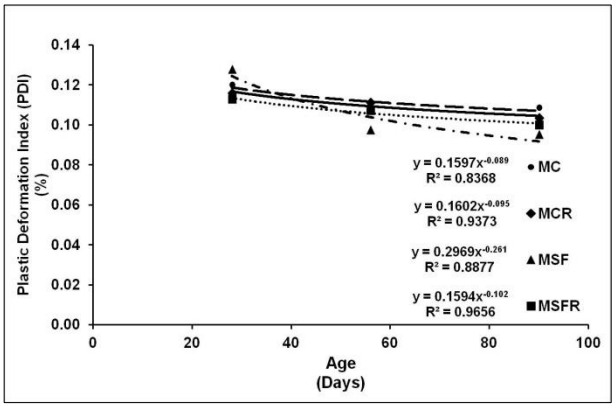

Figure (5.32) Correlation between plastic deformation index (PDI) and time

5.3.2.4 Ultrasonic Pulse Velocity (UPV)

In this part, UPV was conducted as a function of time over a period of 12 weeks to explore its correlation with time and strength due to FCRA addition with and without SF. **Figure (5.33)** represents the UPV evolution of all examined concrete mixtures. The velocities for concrete specimens without FCRA reached 4000m/s and higher at ages 7 and 14 days, respectively. This indicates the good quality of concrete based on ASTM C597 (2016). However, the velocities of concrete specimens containing 10% FCRA were laying in the ranges from 3100 to 3580m/s for mixtures without SF, and from 3418 to 3788m/s for mixtures with SF. Hence, theses mixtures are classified as a medium quality. These reductions can be ascribed to the increase in air

content, presence of cracks around FCRA particles, presence of high level of carbon which have soft element, and increase in concrete porosity (Ganjian al., 2009, Turatsinze and Garros, 2008, Gesoğlu and Güneyisi, 2011, Bravo et al., 2012, Onuaguluchi et al., 2014).

Correlation between UPV and concrete strengths were plotted for all tested mixtures at ages 28, 56, and 90 days as shown in **Fig. (5.34)**. It is clear that the relationship between UPV and compressive strength of mixtures containing FCRA without SF follows a parallel development to that of the mixtures incorporating FCRA with SF. Regardless of FCRA, the coefficient of determination (R^2) values for the trend were in the range between 0.94 and 0.97 for mixtures with and without SF. This indicated that there is a very good correlation between UPV and compressive strength. On the other hand, the relationship between UPV and tensile strength showed a similar trend but with a lower R^2 (i.e. 0.86 and 0.93 for mixtures incorporated FCRA with and without SF, respectively). The reduction in R^2 might be due to the high sensitivity of UPV to the formation and growing of nonconnected cracks than strengths.

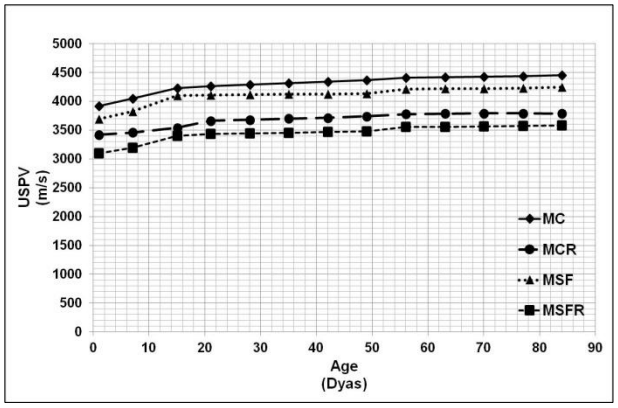

Figure (5.33) Ultrasonic pulse velocity of cylinders with time

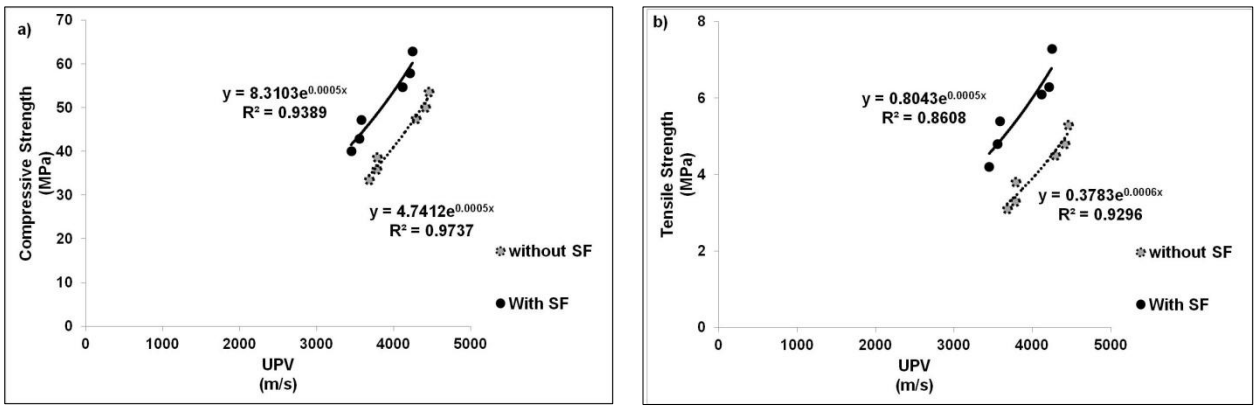

Figure (5.34) Relationship between ultrasonic pulse velocity and strength

a) Compressive Strength, and b) Tensile Strength

5.3.2.5 Electrical Resistivity

Changes in electrical resistivity (i.e. surface (SR) and bulk resistivity (BR)) over time for all tested mixtures are represented in **Figs. (5.35, 5.36)**. Regardless of mixture type, surface, and bulk resistivity increased with time. For instance, the surface resistivity values at four weeks were 10.4, 11.1, 33.6, and 26.1 kOhm-cm, while at 12 weeks were 15.1, 16.4, 51.6, and 48.1 kOhm-cm for mixtures MC, MCR, MSF, and MSFR, respectively. According to the AASHTO TP 95-11 (2011) and based on surface resistivity results, concrete mixtures without SF can be classified in the range of High to Moderate as shown in **Fig. (20)**. Other concrete mixtures with SF were in the range of Low to Very low after the second week as shown in **Fig. (5.35)**. A similar trend was found for bulk resistivity. The BR had increased at 12 weeks compared with four weeks by about 41%, 43%, 50%, and 93% for mixtures MC, MCR, MSF, and MSFR, respectively. This can be attributed to the increase in density and reduction in voids and pores of concrete over time due to the hydration process.

Moreover, SF addition to mixtures with and without FCRA had significantly increased the measured resistivity. For example, after 12 weeks, the surface resistivity increased by about 242%, 193% for mixtures MSF and MSFR compared to mixtures MC and MCR, respectively. In other words, surface resistivity for mixtures MSF and MSFR increased by about 3.42, and 2.9 times compared to control mixtures. A similar trend was found for the bulk resistivity. Mixtures MSF and MSFR had increases in BR values by about 265% and 243% compared to control mixtures MC and MCR after 12 weeks. This significant amelioration in the resistivity of concrete mixtures incorporated SF was due to the pozzolanic reaction producing more dense microstructure as a result calcium silicate hydrate formation.

Results showed that the addition of FCRA without SF had slightly increase concrete resistivity. Surface and bulk resistivity increased in the range from 7% to 8.8% and from 1% to 7.6% along time, respectively. For instance, at six weeks, surface resistivity values for concrete mixtures MC and MCR were 12.9 and 13.8 and bulk resistivity values were 22.5 and 24.2, respectively. These results are in agreement with findings of the recent studies (Mohammed et al., 2012, Yung et al., 2013, and Issa et al., 2013). The increase in resistivity of concrete mixtures incorporated rubber may be attributed to the high electrical insulation property of crumb.

On the contrary, the addition of fine rubber with SF had significantly decreased the concrete resistivity. For example, concrete mixtures MSFR exhibited lower surface and bulk resistivity values over the investigated time in the ranges of 6.8% to 22.3% and from 6.3% to 27.8% compared with control MSF, respectively. One interesting point that was noticed from the test results, the effect of fine rubber addition with SF was reduced with time to be 6.8% and 6.3% at 12 weeks for surface and bulk resistivity, respectively. This can be attributed to the progress of the hydration process and formation of more hydration products which filled micropores.

The relationship between surface and bulk resistivity for tested mixtures is shown in **Fig. (5.37)**. A linear trend is apparent when considering all mixtures. It is clear that there is a robust correlation between the two types of resistivity over time. The coefficient of determination (R^2) values for all tested mixtures were high for the linear trend (i.e. R^2=0.96 for mixtures without SF and R^2=0.99 for mixtures with SF). As shown in **Fig. (5.36)**, the slope of the trend line was 2.03 and 1.68 with an average 1.86 for rubberized concrete mixtures with and without SF. These results were in agreement with the geometry correction factor that correlates the ratio between a surface and bulk resistivity for 100mm×200mm cylinder (i.e. 1.9) (Morris et al. 1996).

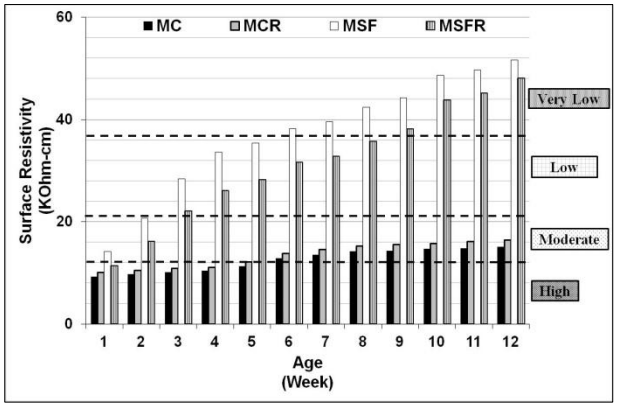

Figure (5.35) Surface resistivity of cylinders with time

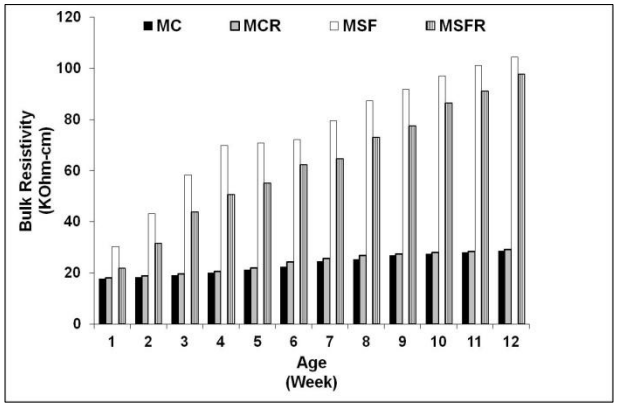

Figure (5.36) Bulk resistivity of cylinders with time

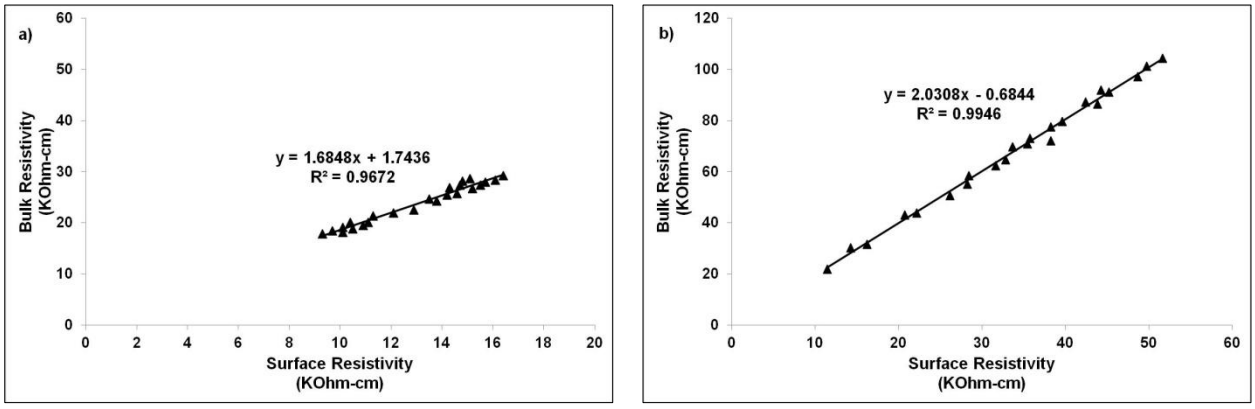

Figure (5.37) Correlation between bulk and surface resistivity for rubberized concrete

a) Without SF and b) With SF addition

5.3.2.6 Durability Index

5.3.2.6 Rapid Chloride Permeability Test

The test was conducted at different intervals (i.e. 28, 56, and 90 days) on the standard specimens over 6 hours. All figures shown below represent the mean charge of three specimens. The standard deviation of the total charge passing results was in the range of 15 to 125 Coulombs. the total charge passed decreased with age for all tested mixtures due to development of hydration and concrete becoming more dense with less porous as shown in **Fig. (5.38)**. For instance, mixture MC showed a reduction in the total charge passed by about 23.4% and 37% at 56 and 90 days, respectively. In addition, it is clear that the addition of SF caused a significant reduction in total charge passing with time (about 78%) due to its pozzolanic reaction.

On the other hand, the addition of FCRA was found to increase total charge passing compared to all samples as shown in **Fig. (5.39)**. For instance, the total charge passing values were increased with about 51.8%, 58.7%, and 44.9% for mixture MCR compared to the control mixture MC at 28, 56, and 90 days, respectively. Moreover, the total charge passing was increased with about 51.9%, 72%, and 53.6% for mixture MSFR compared to that of the control mixture MSF at 28, 56, and 90 days, respectively.

Results reveal that mixtures incorporating SF exhibited a lower increase in the total charge passing compared to those mixtures without SF after 28 days. For instance, the total charge passing for mixture MSFR showed a lower reduction than the mixture MCR by about 13% and 9% at 56 and 90 days, respectively. This contribution may be due to the improvement of microstructure due to the addition of SF.

From the above, it is obvious that although the addition of FCRA had a significant effect on the total passed charge, but all concrete mixtures classified in the "low" category according to ASTM C1202 (2017).

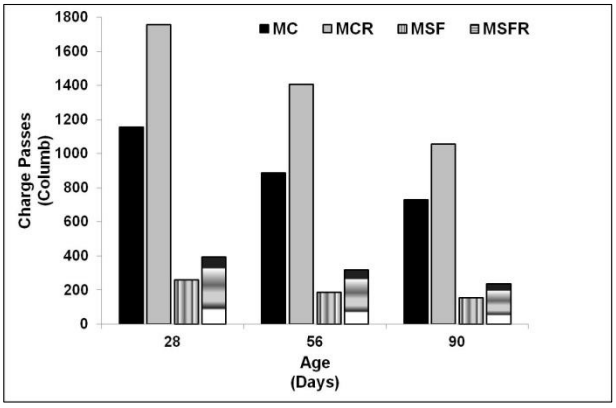

Figure (5.38) Chloride penetrability with time

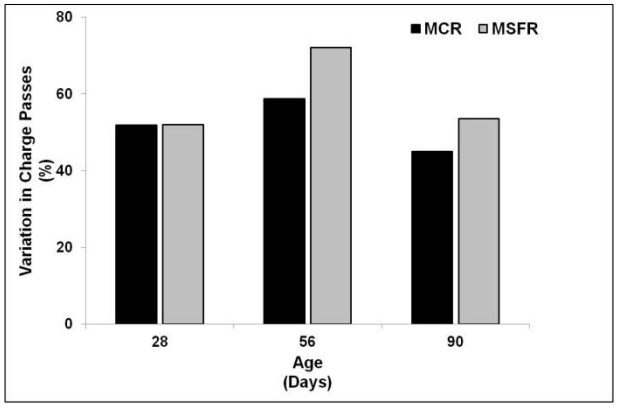

Figure (5.39) Variation in RCPT of Rubberized mixtures with time

5.3.3 Part C - Mortar

Mortar mixture consists of two ingredients (i.e. liquid (A), and cementitious (B)) designed by the manufacture with specified ratio (i.e. 1A:4.8B) to meet high early strength was prepared. Mortar mainly used as a repair material for the vertical surfaces as bridges, tunnels, parking structures, dams, and industrial plants. This mortar is applied on SSD concrete surface by trowel after surface preparation (i.e. remove all debris materials and deteriorated parts). In this research, the mortar mix was modified by adding HRWRA to obtain an adequate flowability during the casting process. In addition, mortar were kept in environmental room (i.e. 38^{o}C and 95±5% RH). So that compressive and tensile strengths at different ages were evaluated and compared with the manufacturer's test results.

5.3.3.1 Strength

Compressive and tensile strengths results at 3, 7, 28, and 90 days for all tested mixtures cured in the lab (i.e. 22^{o}C and 50% RH) and in environmental room (i.e. 38^{o}C and 95±5% RH) are represented in **Fig. (5.40)**., Its observed that the strengths increased for all examined mortar mixtures cured at different conditions with time as shown in **Fig. (5.40)**. For instance, the compressive strength of the mixture cured in lab conditions increased over time: 20.8, 38.6, 52.1, and 53.2 MPa 3, 7, 28, and 90 days, respectively. In addition, a similar trend was obtained for tensile strength; the same mixture increased over time: 2.4, 3.9, 4.9, 5.0, and 5.1 MPa at 3, 7, 21, 28, and 90 days, respectively. Moreover, the results showed HRWRA has no negative effect on the compressive strength at all ages compared with the manufacturer's results of mixtures cast without HRWRA. For instance, compressive strength were 38.6, and 37.6 MPa for mixtures treated in 22^{o}C & 50% RH and 38^{o}C & 95±5% RH, respectively at 7 days as shown in **Fig. (5.40a)**. On the other side, tensile strength was reduced by about 2.4% for the same mixture compared with 21 days results available from the manufacture as shown in **Fig. (5.40b).**

At 3 days, its noticed the compressive strength of mortar mixtures cured in 38^{o}C & 95±5% RH was higher by about 5.7% than that cured in 22^{o}C & 50% RH. While, the same mixtures showed a reduction in the strength development by about 2.5%, 6.7% and 2.7% at 7, 28, and 90 days, respectively. A similar trend was exhibited with the tensile strength. It's clear the strength at early ages was affected by the elevated temperature and relative humidity. Elevated Temperature had a crucial effect on the hydration process that accelerate the formation of hydration product at the early age (Price 1951, Elkhadiri et al., 2009, and Pimenta Teixeira et al., 2016). The relationships between the strengths (i.e. compressive and tensile) and time can be

represented for all tested mixtures (i.e. four mixtures) by linear fit lines with regression coefficients (i.e. R2) 0.997 as shown in **Fig. (5.41**).

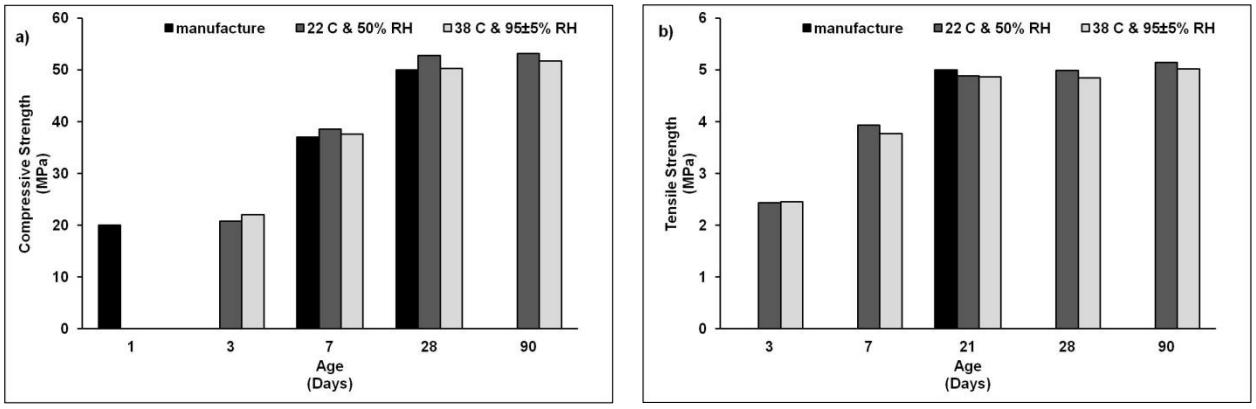

Figure (5.40) Strength for mortar tested mixtures

a) Compressive Strength, and b) Tensile Strength

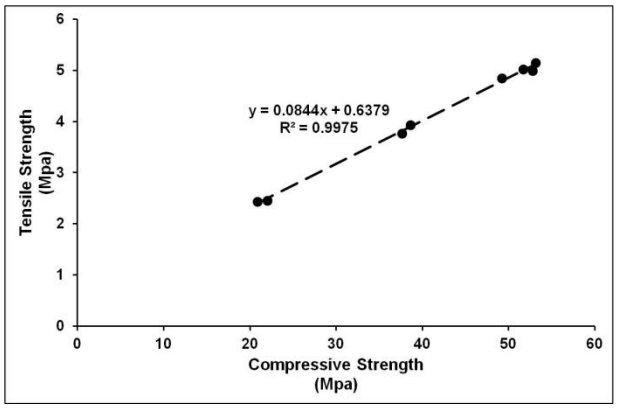

Figure (5.41) Correlation between compressive and tensile strength of mortar mixtures cured in 22°C & 50% RH and 38°C & 95±5% RH

5.4 Conclusion

Different mixtures incorporating four different types of fibre and fine crumb rubber aggregate with and without SF were tested to evaluate properties to select the proper mixtures used as a concrete jacketing. In addition, the mechanical properties of mortar mixture at harsh environmental condition were evaluated. The following conclusions can be drawn:

1. Addition of silica fume significantly enhances mechanical properties and electrical resistance of concrete through densifying concrete microstructure and increasing the fibre matrix bond.
2. Polypropylene fibre enhances good comparative for steel fibre to provide adequate mechanical strengths (i.e. High bulk and surface resistivity).
3. Fibre conductivity has a lower influence on the electric resistivity of concrete with silica fume compared to concrete mixtures without SF.
4. Fibre conductivity had a marginal effect on the relationship between concrete mechanical properties and electrical resistivity.
5. FCRA addition with and without SF decreases strengths at all testing ages. Compressive strength decreased by about 29.47%, 28.38%, and 27.99%, and tensile strength decreased by about 31.11%, 31.25%, and 28.03% compared with control specimens at 28, 56, and 90 days, respectively.
6. FCRA addition decreases MOE by about 27.7%, 26%, and 25.5% at 28, 56 and 90 days, respectively. In addition, FCRA increases υ by about 34.7%, 31.3%, and 28% at 28, 56, and 90 days, respectively.
7. FCRA addition increased S1 and D1 for concrete mixtures with and without SF.

8. The correlations between S1 and time reveal all mixtures incorporated FCRA with and without SF follows a similar parallel power trend with a coefficient of determination (R^2) 0.98, 0.84, 0.98, and 0.99 for mixtures MC, MCR, MSF, and MSFR, respectively. The similar trend between total plastic deformation (D1) and time obtained.
9. FCRA addition with and without SF reduced UPV by about 15% and 6% at 12 weeks.
10. FCRA addition with SF decreased surface and bulk resistivity by about 6.8% to 22.3% and from 6.3% to 27.8%, respectively.
11. RCPT results exhibited an increase the total charge passed as a function of time due to the replacement of FCRA.
12. From test results, FRC incorporated 2% micro fibre with SF and CRC incorporated 10% FCRA as a replacement of fine aggregate with SF were used as a concrete jacketing to strengthening ASR damaged concrete specimens.

Chapter

6

Evaluation Strengthening Types & Time (Phase Three)

6.1 Introduction

This chapter examines concrete specimens after strengthening. The primary goal of this part of the dissertation is the evaluation of six different strengthening techniques and materials used to mitigate deleterious effects in ASR-damaged concrete specimens as well as evaluation of the sensitivity of strengthening time and testing time for the selected strengthening types. One concrete mixture incorporating Spratt reactive aggregate with 15% fused silica was selected from Phase-One as detailed in **Chapter 4**. Deteriorated concrete specimens were subjected to strengthening at six different times (i.e. monthly from 1 to 6 months). The ASR performance and mechanical properties of concrete specimens as compressive strength, modulus of elasticity, Poisson ratio, and stiffness were evaluated after strengthening at three different times (i.e. at 2, 4, and 6 months from the strengthening date).

6.2 Specimens, Mixtures, Cast, and Curing

A total of 432 specimens were cast in Phase three to evaluate the effectiveness of six strengthening techniques as a function of strengthening material type, time of strengthening, and time of testing based on ASTM standards as represented in **Table (6.1)**.

The concrete mixture was selected from Phase one (i.e. mixture No.# 5 incorporating 15% FS with Spratt reactive aggregate) to prepare the deteriorated specimens Ø100mm×200mm. This mix provides the highest expansion level and loss of concrete properties as a function of time. A mixture of total density 2329 kg/m^3 was cast with 0.45W/C, and proportions of 189 kg/m^3 water, 420 kg/m^3 GU cement with total alkali content 0.87% Na_2O equivalent. In addition, 927 kg/m^3 reactive coarse aggregate of nominal maximum size 19mm, and 793 kg/m^3 natural fine aggregate of fineness modulus 2.7. Fused silica replaced 15% of the total weight of fine aggregate. Finally, the total alkali content was raised to the level 1.25% Na_2O equivalent by adding NaOH solution to the mixing water, the solution prepared according to ASTM C1293 (2018). The concrete was prepared, mixed, cast, cured, and stored in the environmental room (i.e. 38 ^oC and 95±5% RH) as detailed in **Section 4.3.3 - Chapter 4** until the time of strengthening.

Table (6.1) Phase Three - Strengthening method, and tests performed (measurements, duration, and specifications)

Strengthening Type	Strengthening Time (Month)	Test	
		Measurements	Duration (Week/Month)
1- <u>Strengthening</u>			
a- Uni-Directional CFRP-one layer applied to the deteriorated samples			
b- Uni-Directional BFRP-one layer applied to the deteriorated samples			
c- Basalt fabric mesh and mortar	1, 2, 3, 4, 5, and 6	Expansion (ASTM C1293)	Weekly
d- Glass Grid mesh and mortar		Compression (ASTM C39)	2, 4, and 6 Months
2- <u>Jacketing</u>		MOE and υ (ASTM C496)	2, 4, and 6 Months
a- Concrete jacketing contain micro polypropylene fibres and silica fume,		SDT (N.A)	2, 4, and 6 Months
b- Concrete jacketing contain fine crumb rubber aggregate and silica fume, then strengthened by basalt fibre fabric			

6.3 Specimens Preparation and Strengthening Application

The concrete specimens were strengthened at various times, monthly starting at 28 days until 182 days (i.e. monthly at six different times). At the time of strengthening, the concrete cylinders were taken out from the environmental room and subjected to the following steps:

- Clean the concrete surface from the residual hydroxide, debris, and dust materials by using a duster and air compressor.
- Epoxy demec points at a distance 150±3mm fixed linearly in the casting direction by two different methods based on the strengthening type:
    1. For CFRP and BFRP - Fix demec directly on the surface of the specimens as shown in **Fig. (6.1a)**.
    2. For mortar and concrete jacketing - Prepare two holes, and clean all dust and debris by using an air compressor. Then fix demec of length 30mm inside the holes to be flush with the surface after complete strengthening using concrete and mortar jacketing (i.e. 25mm from the surface before strengthening) as shown in **Fig. (6.1b)**.

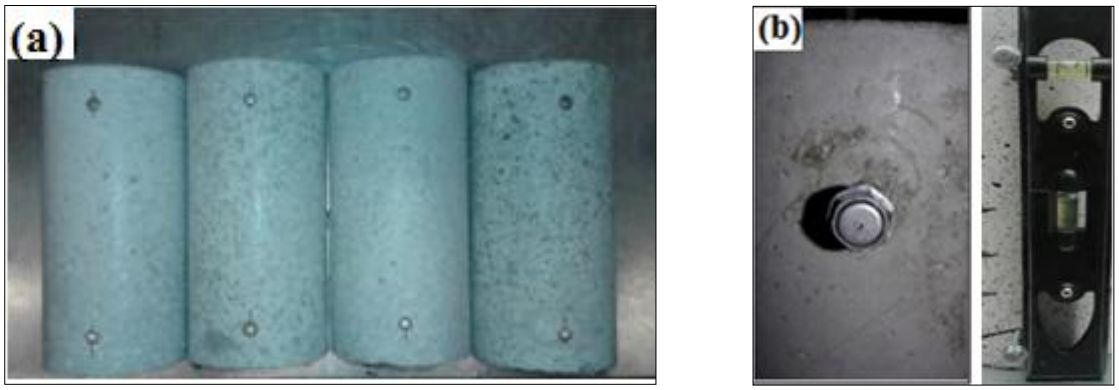

Figure (6.1) Demec installation

(a) Directly on the concrete surface, and (b) Inside two linear holes

- Roughen the surface of the concrete specimens, clean, and remove debris, and dust materials by using a duster and an air compressor.
- The strain gauge sensors of length 60mm (i.e. sensors type PL-60-11-5L) were fixed by PR-2 adhesive on the surface of the specimen along the casting direction. Sensors were protected from the harsh environmental conditions and the process of strengthening by using SB rubber tape (i.e. 1274SB strain gauge coating) of 10mm wide and 3mm thickness as shown in **Fig. (6.2a,b)**.

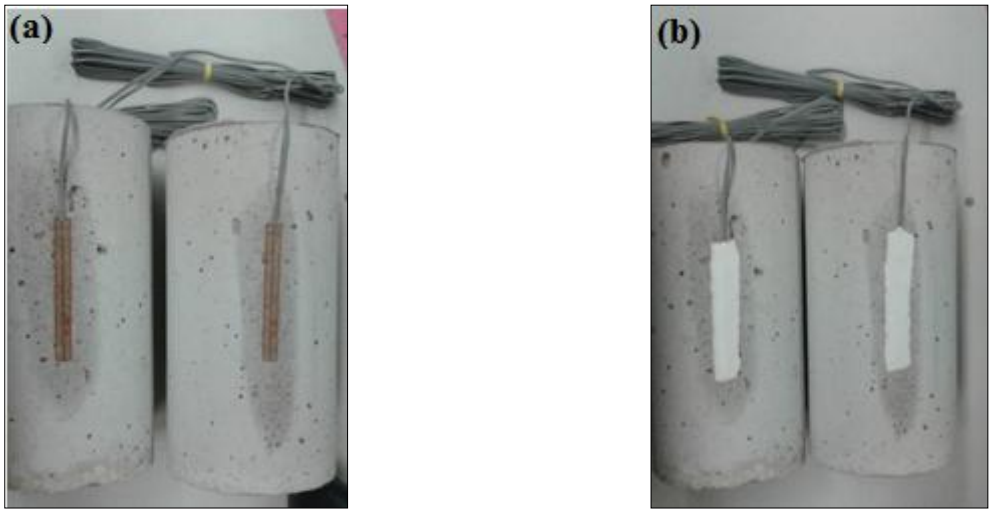

Figure (6.2) Strain gauge installation

(a) Fix strain gauge using PR-2 adhesive, and (b) Protection of strain gauge from damage during repair procedure using tap 10mm wide and 3mm thickness

- Prior to starting the strengthening steps, the top and bottom surfaces of all specimens were covered by a plastic cover and tape to protect from the applied materials as shown in **Fig. (6.3)**.
- The strengthening was started by the application of lithium nitrate ($LiNO_3$) on the surface of all deteriorated concrete specimens as a first barrier before applying the

strengthening materials to minimize future distress and expansion. Lithium nitrate of 30% solution was applied by "topical application" at rates in the range from 0.12 to 0.24 L/m^2 as shown in **Fig. (6.4)**.

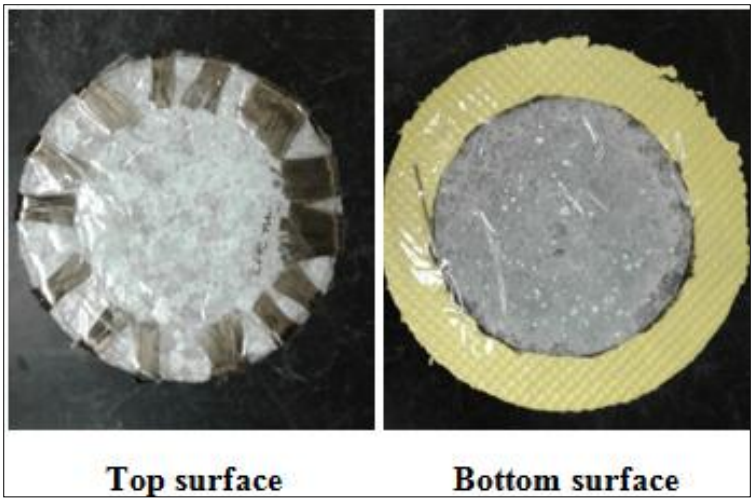

Figure (6.3) Protection of the top and the bottom surface of specimens using plastic cover and tap

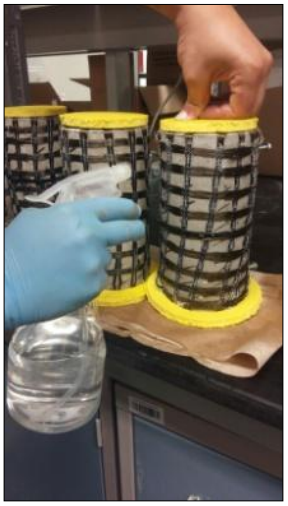

Figure (6.4) Application of lithium nitrate on the specimens surface using topical application

- Specimens were subjected to strengthening using six different materials as illustrated in **Fig. (6.5a)** at 28, 56, 90, 120, 150, and 182 days from casting date, respectively.
- One-third of the specimens coated with epoxy resin adhesive (Sikadur 330) at a rate of 0.7-1.2 kg/m^2 by using a roller brush as shown in **Fig. (6.5b)**. The adhesive contains two components that mixed mechanically in a ratio 4A:1B using a drill at low speed for a continuous three minutes until obtaining a homogenous color without colored streaks. It was then remixed for one minute to minimize the air entrained. Thereafter, these specimens were wrapped by two different types of fibres after cutting to the desired dimensions (i.e. 190mm in height and length with overlapping 100mm in the same direction of the fibres ~345mm total length) as follows;

1. Uni-Directional Carbon Fibre Fabric "SikaWrap Hex 230C", one layer applied directly on the surface of deteriorated specimens as shown in **Fig. (6.5c)**.
2. Uni-Directional Basalt Fabric "UD-300-60", one layer applied directly on the surface of deteriorated specimens as shown in **Fig. (6.5d)**.

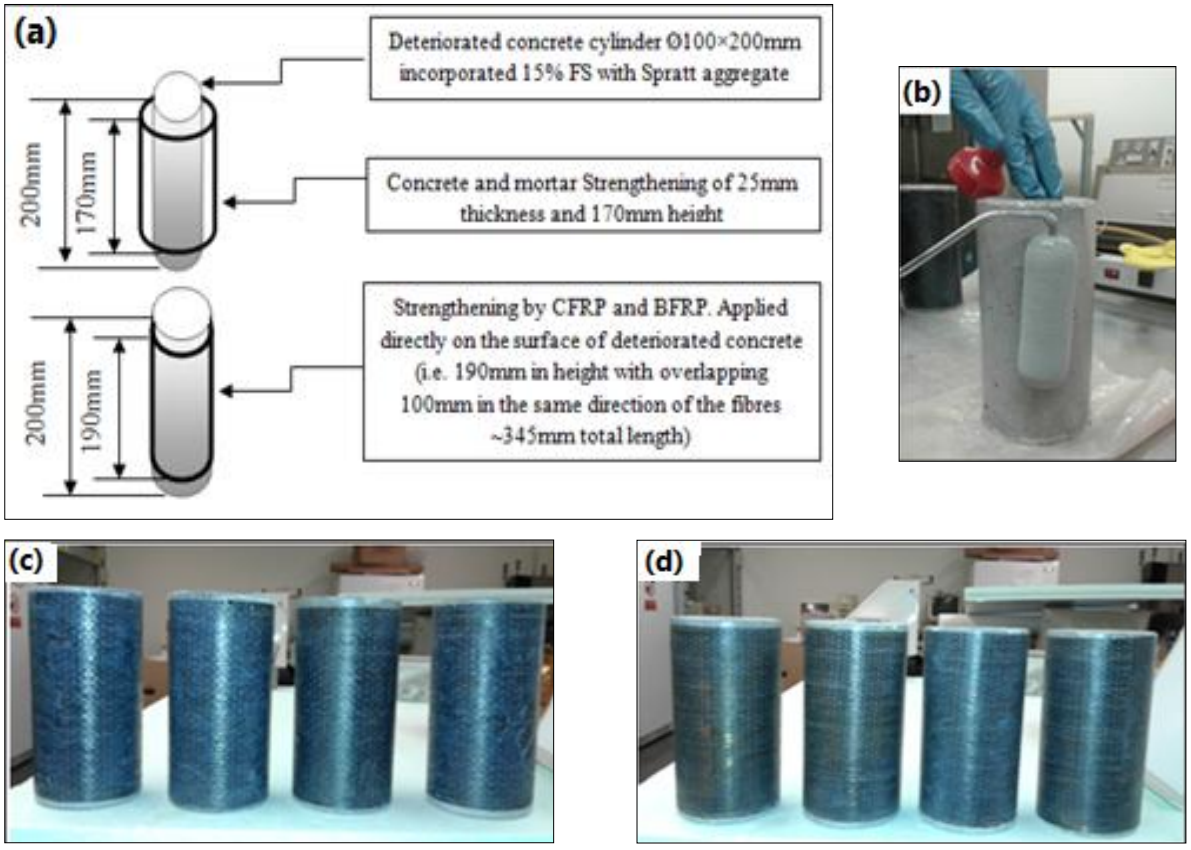

Figure (6.5) Wrapping using different types of FRP

(a) Illustration of strengthening, (b) Application of the epoxy resin adhesive, (c) CFRP wrapping, and (D) BFRP wrapping

- The second third of the specimens were coated with the bonding material Sika Top Armtec 110 EpoCem as shown in **Fig. (6.6a)**. The bonding material incorporated three components (A, B, and C) was prepared by mixing component A and B mechanically using a low-speed drill (300-450 rpm) for 30 seconds. Then component C was added slowly and remixed mechanically for a continuous 3 minutes. Finally, this bonding

slurry was applied on the concrete surface using a paintbrush to cover all surface with a thickness greater than 0.5mm. The wrapping was achieved by:

1. Glass Grid Mesh as shown in **Fig. (6.6b)**.
2. Basalt Fabric Mesh as shown in **Fig. (6.6c)**.

For these specimens, strengthening also included casting 25mm freshly mixed epoxy mortar at laboratory temperature (i.e. 21°C) within the service life of the bonding slurry (i.e. 12 hours). Mortar was prepared by using Sika Top 13 Plus incorporating two components (A and B) mixed mechanically using a drill at low speed (i.e. 300-450 rpm) with a mixing paddle with a specified weight ratio of 1A:4.8B. Mixing the ingredients was continued for 3 minutes to have a uniform consistency. The mortar mixture was applied on the surface of concrete specimens after mixing by about 15 minutes as shown in **Fig. (6.6d)**.

- Last third of specimens were subjected to applying the same bonding material Sika Top Armtec 110 EpoCem. After this step, two jacketing techniques were used.
  1. Fibre reinforced concrete (FRC) jacketing of 25mm thickness incorporating micro polypropylene fibres and silica fume selected from **Phase Two** (i.e. mixture No.#4 MSFMP) as shown in **Fig. (6.7a)**.
  2. Crumb rubber concrete (CRC) jacketing of thickness 25mm incorporating fine crumb rubber aggregate and silica fume selected from **Phase Two** (i.e. mixture No.#4 MSFR), then strengthened by one layer uni-directional BFRP as shown in **Fig. (6.7b)**.

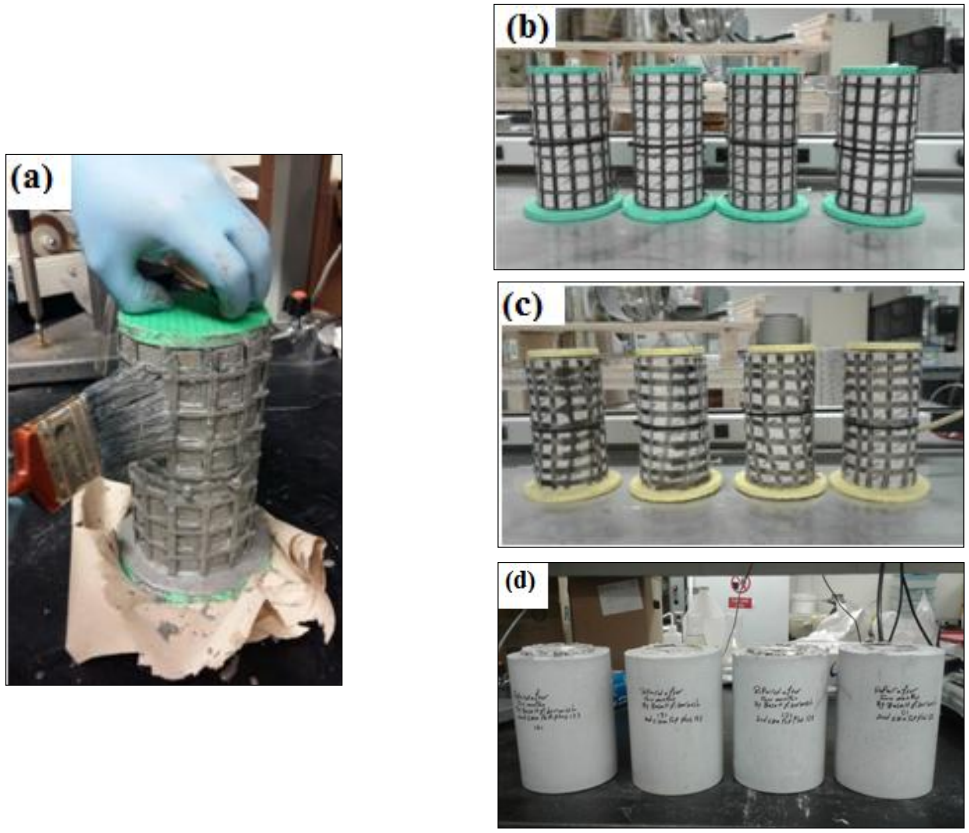

Figure (6.6) Strengthening using different types of FRP

(a) Application of the bonding material, (b) Strengthening using Basalt Fabric Mesh, (c) Strengthening using Glass Grid Mesh, (d) cast of mortar with 25mm thickness.

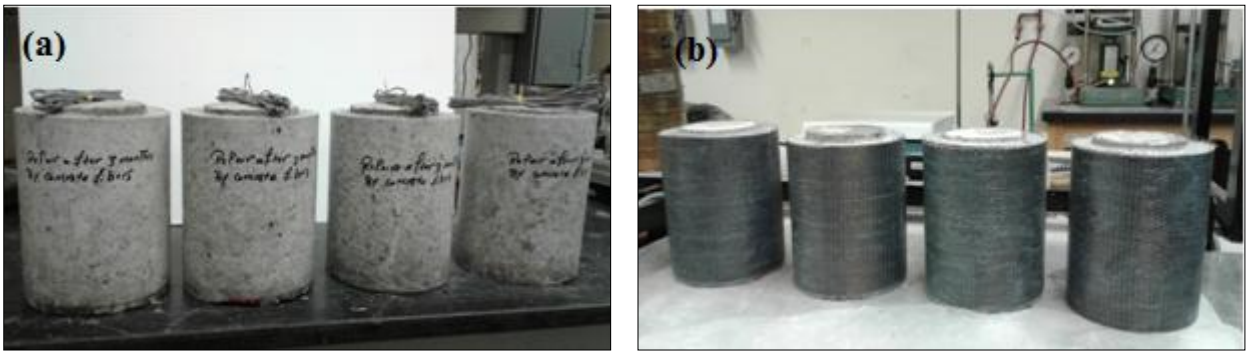

Figure (6.7) Concrete jacketing

(a) with FRC, and (b) with CRC and BFRP

- As per ACI 308 (2016) "Guide to curing concrete" to achieve the performance of mortar and concrete, the specimens were cured using wet burlap for a continuous 24

hours. In addition, the specimens wrapped using CFRP and BFRP were allowed to cure at laboratory temperature for 24 hours as shown in **Fig. (6.8)**.

- The strain gauge sensors were connected to a data acquisition system (DAS) to record the expansion.
- After completing the strengthening methods and curing, the concrete specimens were placed back into the environmental room until the testing time. Tests were conducted at three different ages from the date of strengthening (i.e. after 2, 4, and 6 months) to measure the mechanical properties of concrete at each age. Steps from casting until testing was illustrated in **Fig. (6.9)**.

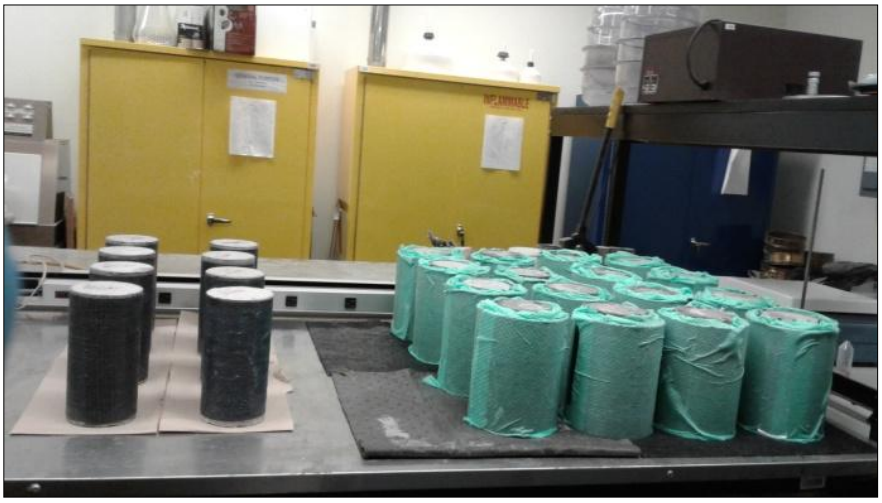

Figure (6.8) Curig of specimens after complete repair methods

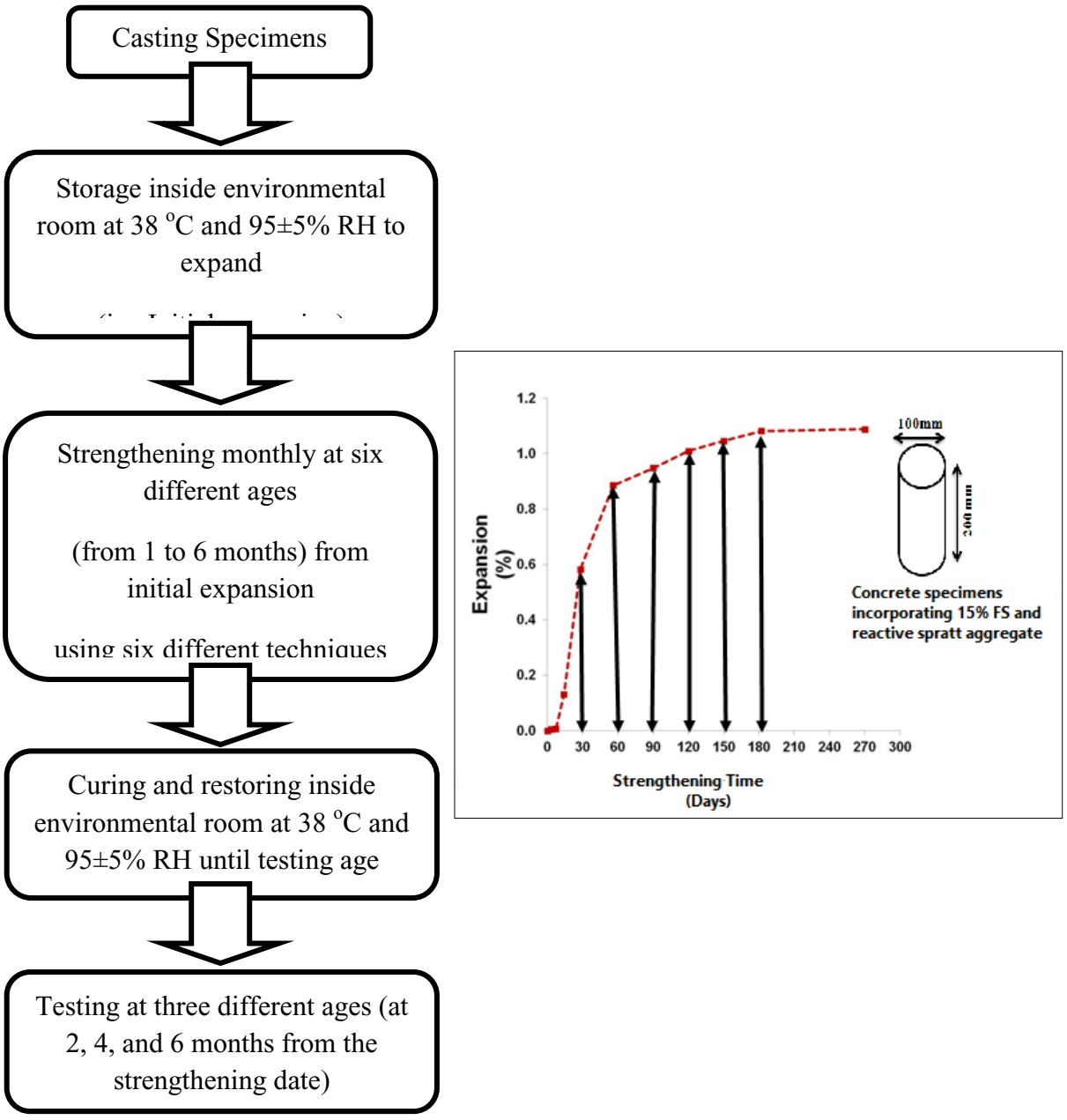

Figure (6.9) Steps from castimg specimens until testing

6.4 Measurements and Results

The results of tests after applying the six different strengthening materials were analyzed with respect to; a) Strengthening type; b) Time of strengthening and testing

6.4.1 Expansion

6.4.1.1 Effect of Strengthening Type

The crack propagation produced from ASR expansion on the concrete surface for all tested specimens was inspected before applying the strengthening materials. Both length and width of cracks increased extensively over time as a result of the increase in the internal stresses produced from adding reactive aggregates (i.e. 15% FS and Spratt) and the exposure condition (i.e. 38 ^{o}C and 100% RH). The cracks propagate over time from hair cracks to cracks of length in the range from 40mm to 75mm and width in the range from 0.5mm to 1.8mm as the example shown in **Fig. (6.10)**. These cracks provide easy access to high moisture content and increase the rate of deterioration.

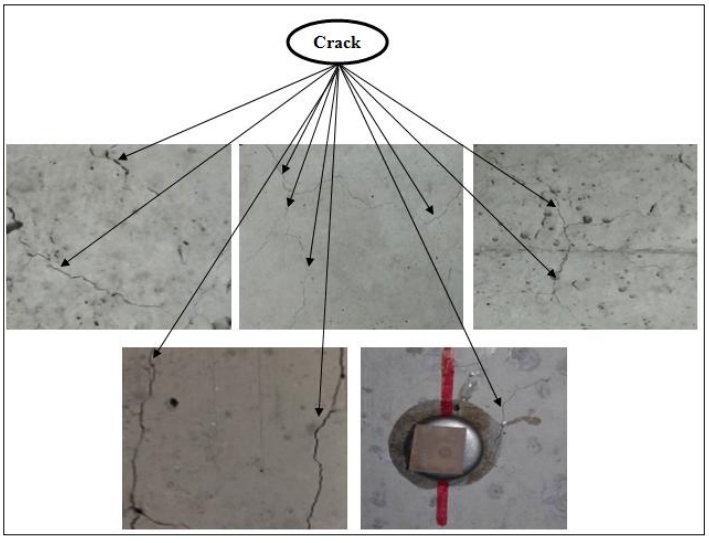

Figure (6.10) Cracks development on the concrete surface before applying strengthening materials at age three months

The expansion measurements as a function of time for all tested concrete specimens after applying the strengthening materials at one month are shown in **Fig. (6.11)**. The figures represent an average of two specimens of the same type. With all types of strengthening, the expansion was lower than the control specimens (i.e. no strengthening) and increased gradually at a different rate over time for all tested specimens depending mainly on the strengthening type. For instance, the expansion of the control specimens at age of two months was 0.820%, while, the expansion were 0.562%, 0.601%, 0.603%, 0.607%, 0.609%, and 0.614% at the same age (i.e. two months) for specimens strengthened after one month with CFRP, BFRP, CRC + BFRP, Mortar + GG, Mortar + BFRP, and FRC, respectively.

It is clear, at all times of strengthening the specimens strengthened with CFRP exhibited a reduction in expansion compared to the control specimens and followed by BFRP, CRC + BFRP, Mortar + GG, Mortar + BFRP, and FRC, respectively as represented in **Table (6.2)**. For instance, the specimens strengthened after one month showed a significant reduction in expansion within the range from 31.44% to 34.56%, from 26.75% to 28.05%, from 26.36% to 27.47%, from 25.96% to 27.31%, from 25.67% to 26.84%, and from 25.08% to 25.80% for specimens strengthened with CFRP, BFRP, CRC + BFRP, Mortar + GG, Mortar + BFRP, and FRC, respectively.

The above results confirm the previous studies. Linear expansion of AAR specimens (i.e. Ø80mm×160mm specimens incorporating siliceous limestone of 20% reactive silica and opal sand as reactive materials and cured in NaCl solution at 50 ^{o}C) wrapped with carbon fibre reduced expansion by 52% over unwrapped specimens at the end test duration (i.e. 35 days) (Mohamed et al., 2001). Moreover, wrapping of concrete cylinder (i.e. Ø160mm×320mm incorporating opal as a reactive aggregate) with unidirectional CFRP reduced the longitudinal

and transverse expansion in comparison with unwrapped reactive specimens by about 21% and 75%, respectively (i.e. longitudinal expansion 3 times higher than transverse expansion because fibres act better in the circumferential direction of the test) (Mohamed et al., 2005). Expansion measured on the bottom face of beams 100mm×150mm×1220mm after applied FRP was slow down to exceeds maximum limit after 100 days, while control beams exceeds limit after 150 days (Lacasse et al., 2003). This shows that FRP slows down the effects of the AARs. FRPs limit the concrete expansion on the face on which they were installed. In addition, it is appears that the effects of the AARs are "migrating" to areas that present less resistance to their actions (Lacasse et al., 2003).

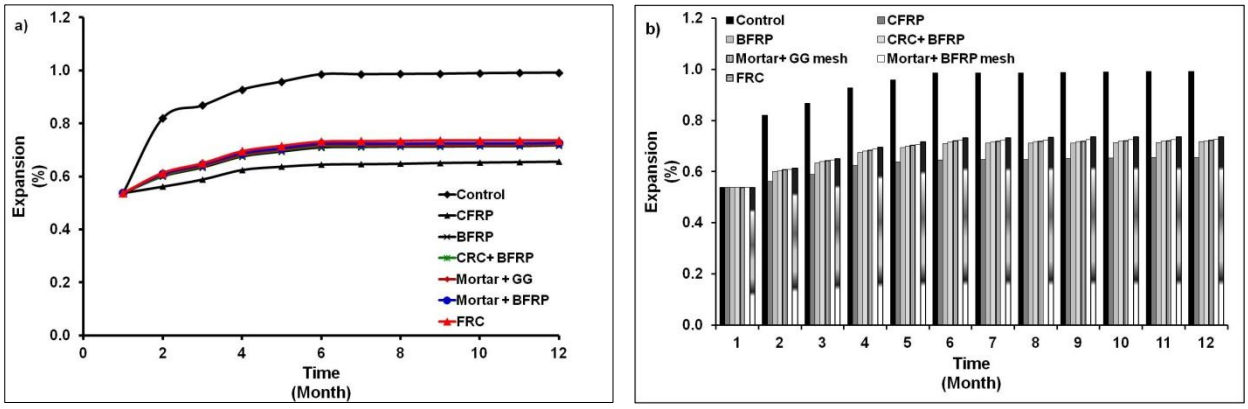

Figure (6.11) Expansion of concrete specimens after applying strengthening materials after one month

Table (6.2) Reduction ratio in expansion compared with control specimens along time after applying strength materials at different ages

Strengthening Type	Total Reduction in Expansion (%)											
	Time of applying Strengthening											
	1 Month		2 Months		3 Months		4 Months		5 Months		6 Months	
	Min.	Max.	Min.	Max.	Min.	Max.	Min.	Max.	Min.	Max.	Min.	Max.
CFRP	31.4	34.6	4.2	10.8	4.8	8.1	2.7	4.9	2.2	2.7	0.0	0.4
BFRP	26.8	28.1	2.8	5.9	3.9	5.5	2.1	4.7	2.0	2.4	0.0	0.4
CRC + BFRP	26.4	27.5	2.5	5.3	3.5	4.9	1.9	4.3	1.8	2.2	0.0	0.4
Mortar + GG	25.9	27.3	2.1	5.1	3.2	4.5	1.7	4.1	1.6	2.0	0.0	0.4
Mortar + BFRP	25.7	26.8	1.9	4.7	3.1	3.9	1.5	3.9	1.6	2.0	0.0	0.4
FRC	25.1	25.8	1.4	4.3	2.2	3.6	1.5	3.5	1.2	1.8	0.0	0.4

Moreover, all specimens showed the rate of expansion increased gradually after applying the strengthening materials until it reached the steady state at 6 months with all types of strengthening materials until the end of the investigation period (i.e. 12 months after casting) as represented in **Fig. (6.11)**. In addition, the expansion level became stable at a different level lower than the expansion level of the control specimens mainly depending on the strengthening material and the residual expansion even when the strengthening was applied at a later age. For instance, expansion of control specimens increased by about 52.42%, 83.27%, and 84.39% at 2, 6, and 12 months, respectively. While, after applying strengthening materials at one month, these ratios changed at the same measuring ages mainly depending on the type of strengthening materials as shown in **Table (6.3)** and **Fig. (6.12)** as follows: 4.5%, 19.92%, and 21.96% for CFRP, 11.64%, 31.86%, 33.31% for BFRP, 12.12%, 33.02%, 33.90% for CRC + BFRP,

12.85%, 33.76%, 34.19% for Mortar + GG, 13.23%, 34.48%, 35.06% for Mortar + BFRP, and 14.10%, 35.93%, 36.81% for FRC, respectively. One interesting point, the type of strengthening materials had a less significant effect on expansion rate when applied on the deteriorated specimens after 5 months; this can be attributed to the residual expansion as shown in **Fig. (6.13)**. After 5 months, the residual expansion reached the minimum level so that all types of strengthening showed a similar effect. In addition, the efficacy of all strengthening materials did not affect when applied after 6 months because the residual expansion is almost null as shown in **Fig. (6.13f)**.

From the above and test results, it is apparent the expansion after strengthening increased gradually until 6 months and then became stable until the end of the test duration (i.e. 12 months). In addition, the selection of strengthening materials plays a crucial role to suppress the ASR expansion (i.e. the increase in the expansion was minimum with CFRP, and maximum with FRC jacketing).

Table (6.3) Increase in expansion with time after applying strength materials at different times

Strengthening Type	Increase in Expansion from initial expansion at one month (%)																	
	Strengthening Applying after																	
	1 Month			2 Months			3 Months			4 Months			5 Months			6 Months		
	2m	6m	12m	3m	6m	12m	4m	6m	12m	5m	6m	12m	6m	6m	12m	7m	6m	12m
Control	52.42	83.27	84.39	61.34	83.27	84.39	72.49	83.27	84.39	78.07	83.27	84.39	-	83.27	84.39	83.27	-	84.39
CFRP	4.50	19.92	21.96	54.65	63.57	66.91	64.27	68.49	71.38	73.30	74.35	75.46	-	78.39	80.30	83.27	-	83.64
BFRP	11.64	31.86	33.31	56.88	72.55	76.21	65.80	73.23	76.95	74.35	74.72	77.70	-	78.81	80.67	83.27	-	83.64
CRC + BFRP	12.12	33.02	33.90	57.25	73.61	77.02	66.54	74.35	77.70	74.72	75.46	78.44	-	79.18	81.04	83.27	-	83.64
Mortar + GG	12.85	33.76	34.19	57.99	73.98	77.32	66.91	75.01	78.44	75.09	75.84	78.81	-	79.55	81.41	83.27	-	83.64
Mortar + BFRP	13.23	34.48	35.06	58.28	74.72	78.81	67.29	76.21	79.93	75.46	76.21	79.55	-	79.55	81.41	83.29	-	83.64
FRC	14.10	35.93	36.81	59.11	75.46	79.18	68.77	76.95	80.30	75.46	76.95	79.93	-	79.93	82.16	83.27	-	83.64

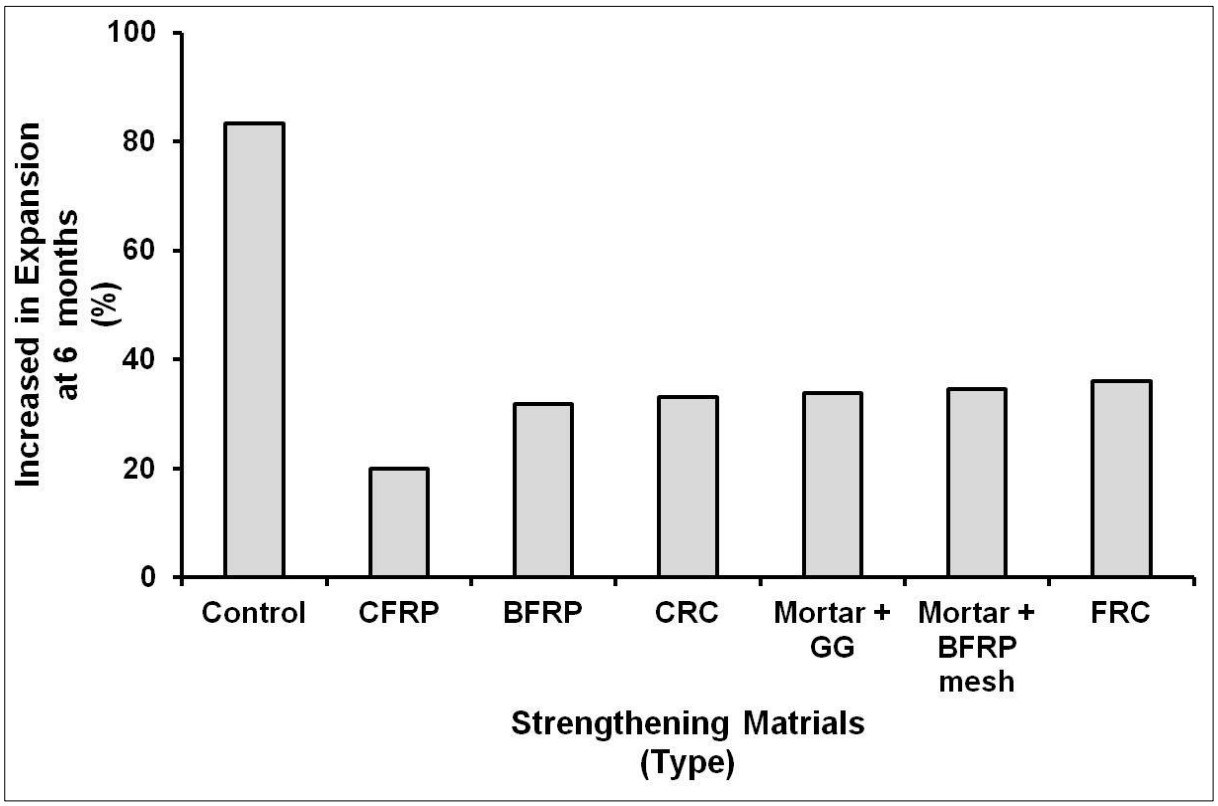

Figure (6.12) Increased in the expansion for concrete specimens measured at 6 months after applying strengthening materials at one month

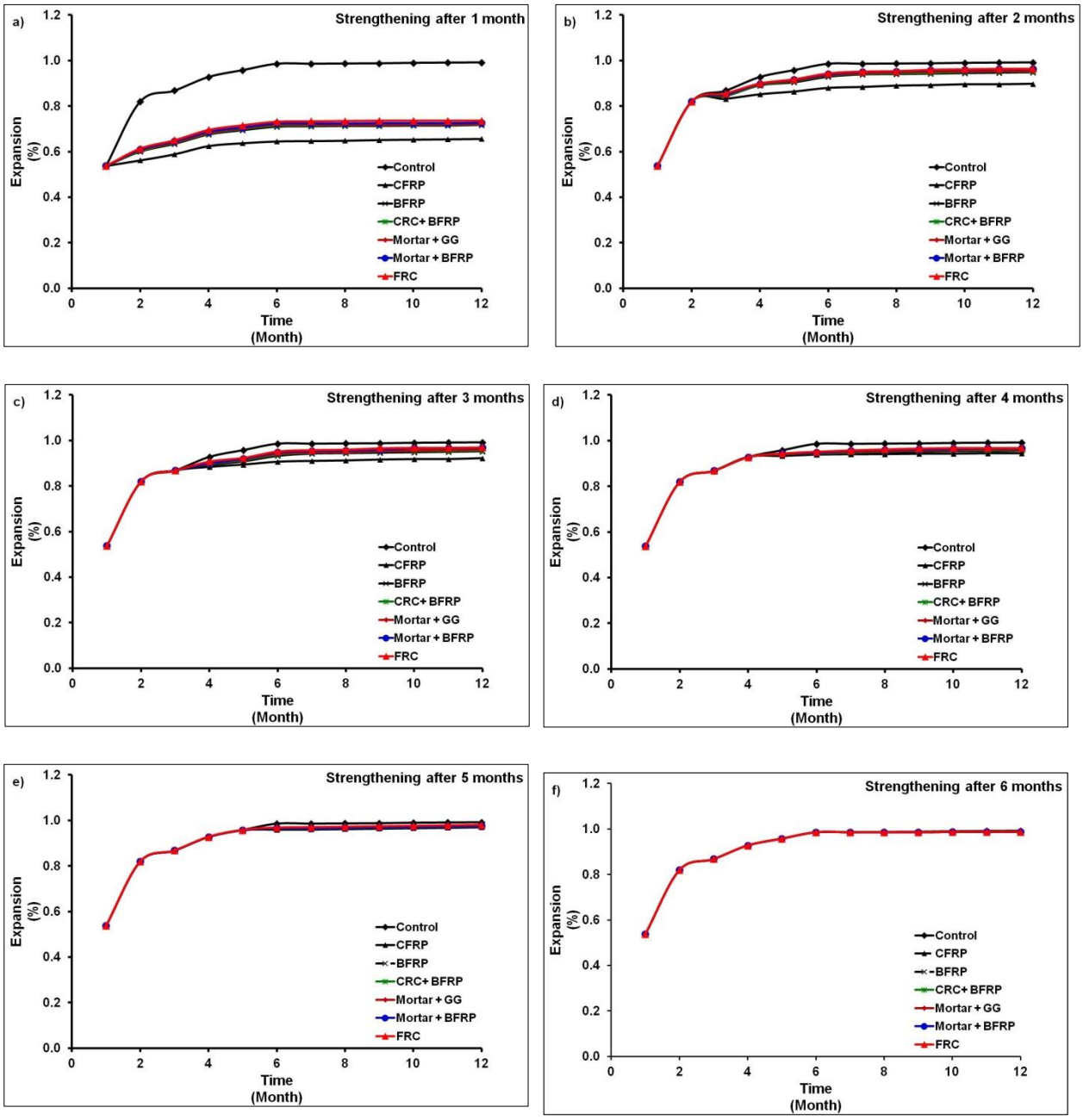

Figure (6.13) Expansion with time for concrete specimens after applying strengthening materials

6.4.1.2 Effect of Strengthening and Testing Time

The expansion measurements for all tested concrete specimens after applying the same strengthening material at different times (i.e. monthly from 1 to 6 months) as a function of time are shown in **Fig. (6.14)**. Generally, the expansion of concrete specimens after applying different strengthening materials reveal the same trend with different level of reduction. Expansion at an early age (i.e. after 1 month) showed a lower level of expansion compared with the control specimens. For instance, the expansion of the control specimens were 0.820%, 0.868%, 0.928%, 0.958%, 0.986%, and 0.986% at 2, 3, 4, 5, 6, and 7 months, respectively. While, the expansion of specimens strengthened by CFRP at 1, 2, 3, 4, 5, and 6 months were 0.562%, 0.832%, 0.884%, 0.932%, 0.960%, and 0.986% at the same ages.

On the other hand, the strengthening after two months and more using the same material showed less effectiveness as represented in **Table (6.2)** (i.e. expansion was lower than control specimens with low variation depending on the type of strengthening material). This can be attributed to the expansion of the concrete specimens had reached to a stable maximum level before applying strengthening materials (i.e. residual expansion was lower).

For example, expansion of concrete specimens strengthened with CRC + BFRP was lower than the expansion of control specimens over time in the range 26.44% to 27.42%, from 2.53% to 5.27%, from 3.45% to 4.87%, from 1.88% to 4.26%, from 1.81% to 2.23%, and from 0.00% to 0.40% after 1, 2, 3, 4, 5, and 6 months, respectively. From test results, it is apparent the strengthening time is important to control the residual expansion in the deteriorated concrete.

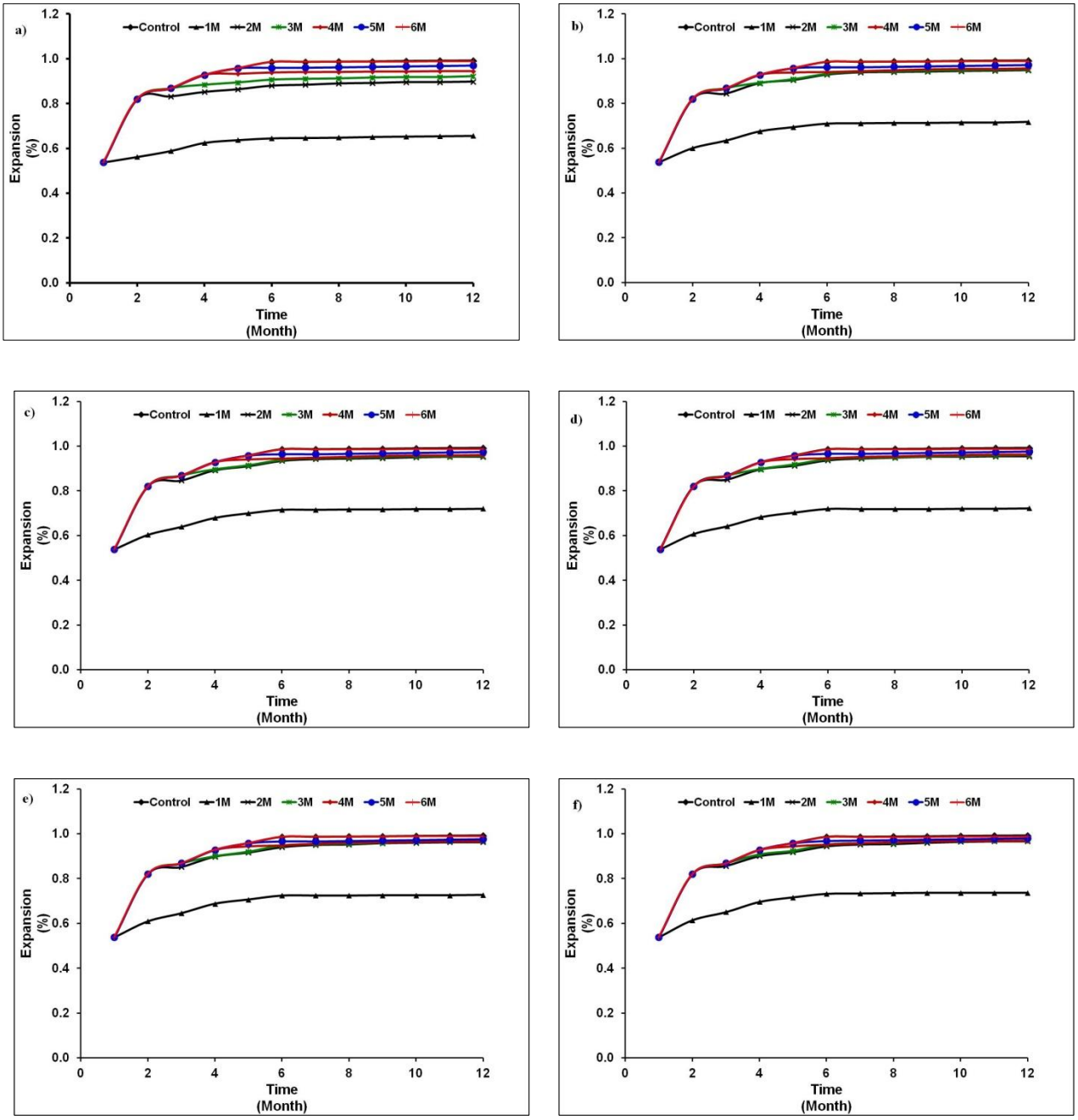

Figure (6.14) Expansion of concrete specimens after applying strengthening materials at different times

(a) CFRP, (b) BFRP, (c) CRC+ BFRP, (d) Mortar + GG, (e) Mortar + BFRP, and (f) FRC

The expansion for all examined specimens after completing strengthening using six different materials was recorded to evaluate the sensitivity of testing time (i.e. tests performed after 2, 4, and 6 months from the strengthening date), that can expressed the effect of exposure conditions on the efficacy of strengthening materials. Generally, the increase in the testing age, the higher the expansion for all tested specimens strengthened with the same material at the same age. This can be attributed to the long duration of exposure to harsh environmental conditions plus residual expansion effect on the strengthening materials.

For instance, for specimens strengthened after one month with CFRP, BFRP, CRC + BFRP, Mortar + GG, Mortar + BFRP, and FRC, the expansion for specimens tested after 4 months from the strengthening date was higher than expansion for same specimens tested after 2 months from the strengthening date by about 8.24%, 9.41%, 9.52%, 9.52%, 9.44%, and 10.12%, respectively, as shown in **Fig. (6.15)**. These ratios increased for the same specimens strengthened with the same materials at the same time (i.e. 1 month) when tested at 6 months from the strengthening date to recorded 9.84%, 12.10%, 11.97%, 11.97%, 12.14%, 12.77%, respectively, as shown in **Fig. (6.15)**.

The test results reveal the sensitivity of the testing age (exposure conditions) decreased as the strengthening applied; after 2 and 3 months it was found to be within a range from 3.27% to 6.01%, and can be neglected as the strengthening applied at 4, 5, and 6 months (i.e. was in the range from 0.19% to 1.48%) confirming with the above results (i.e. the lower the residual expansion, the less effect on the strengthening materials) and the exposure conditions had less effect on the strengthening materials. The relationship between the reduction ratio in expansion for concrete specimens after applying strengthening materials at six different ages and tested at 4 and 6 months compared with specimens tested at 2 months was illustrated in **Fig. (6.16)**. The

relationships were found to be an exponential fit curve with a regression coefficient in the range from 0.91 to 0.97 for all strengthening materials. The relations exhibited testing time had a significant effect on the measured expansion only when the residual expansion is higher (i.e. at early ages) and no significant effect at later ages as the residual expansion reached lower levels. In addition, indicated that there is a robust correlation between these test results.

On the other hand, reduction in expansion for all tested specimens after strengthening using the same strengthening materials at the same time and tested after 2, 4, and 6 months from the strengthening date as compared with the control specimens exhibited lower sensitivity of the testing time (i.e. no significant effect). For instance, **Fig. (6.17)** shows the reduction in the expansion of specimens strengthened with CFRP at six different ages and tested after 2, 4, 6 months from the strengthening date. Reduction in expansion for specimens strengthened after 1 month and tested after 2, 4, 6 months from the strengthening date compared with control specimens was 32.16%, 33.47%, and 34.41%, respectively (i.e. no significant difference).

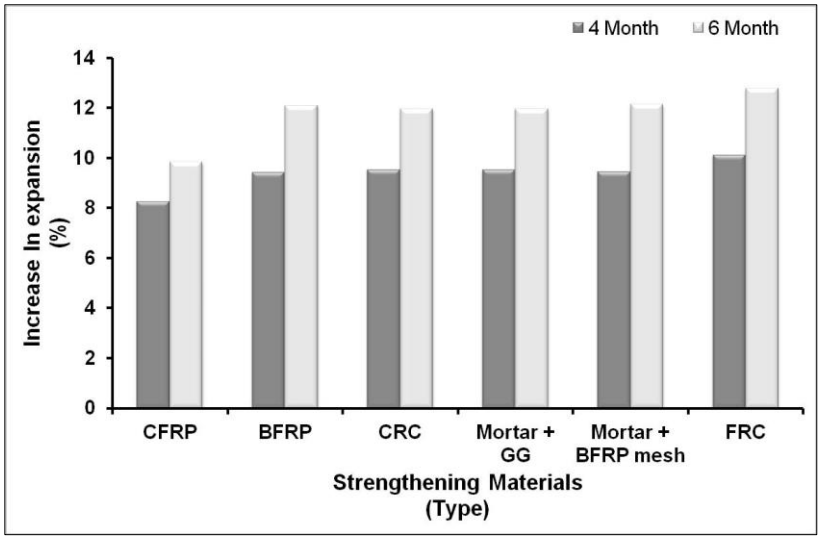

Figure (6.15) Increase in expansion of concrete specimens strengthened after 1 month and tested after 4 and 6 months from the strengthening date compared to the specimens tested after 2 months from the strengthening date

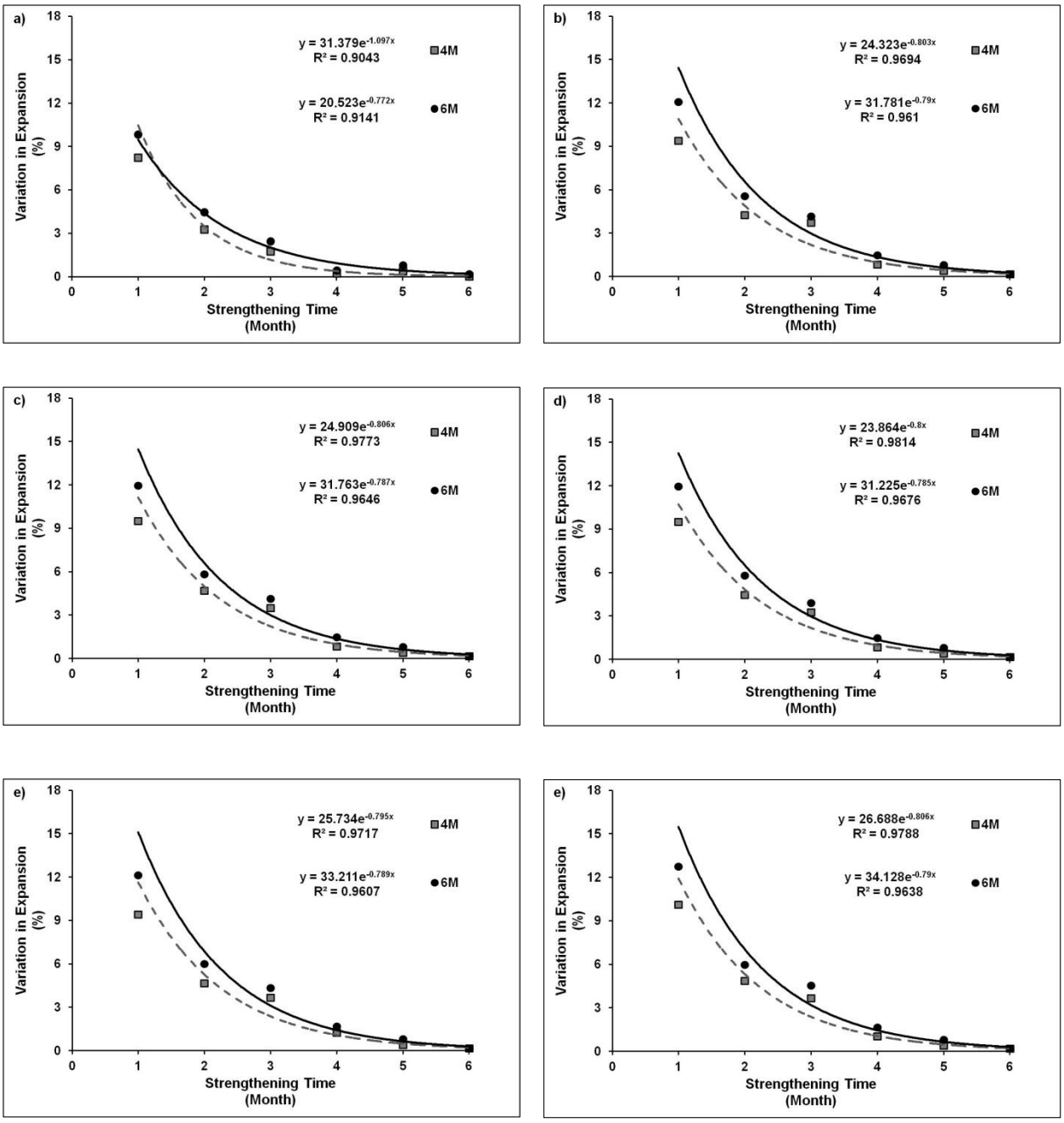

Figure (6.16) Variation in the expansion of concrete specimens after applying strengthening materials at different ages and testing at different ages compared with specimens tested at 2 months

(a) CFRP, (b) BFRP, (c) CRC+ BFRP, (d) Mortar + GG, (e) Mortar + BFRP, and (f) FRC

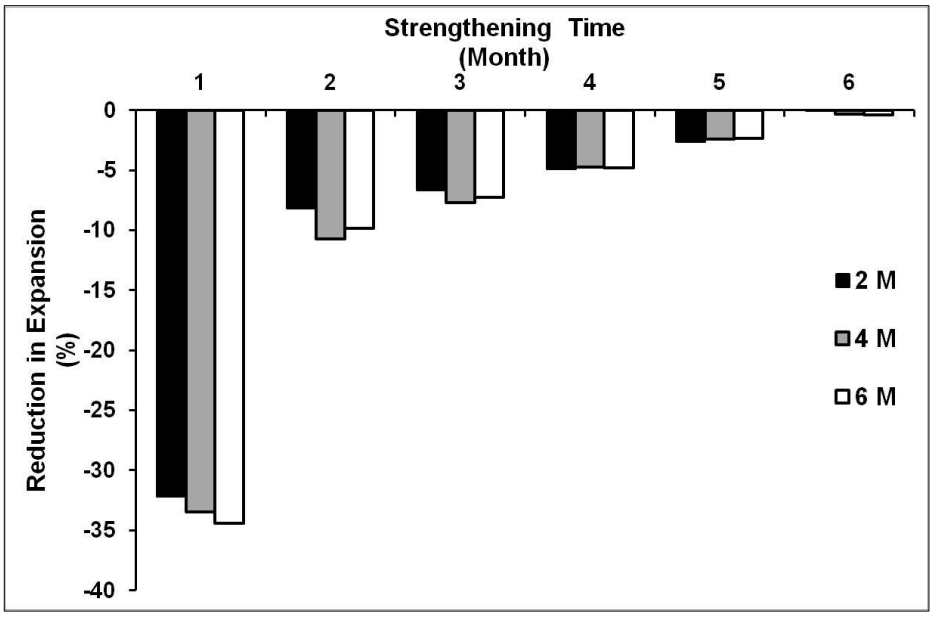

Figure (6.17) Reduction in expansion of concrete specimens after applying CFRP at different ages and testing at different ages compared with control specimens

6.4.2 Compressive Strength

6.4.2.1 Observation and Inspection

Uniaxial compression testing according to ASTM C39 (2018) was performed at three different ages (2, 4 and 6 months after strengthening). Specimens showed a different mode of failure mainly depending on the strengthening materials. According to the six typical fracture patterns described in ASTM C39 (2018), specimens strengthened with CFRP and BFRP can be classified as "cone" as shown in **Fig. (6.18)**. Specimens exhibited the failure starting with tearing of the FRP in the same direction of the fibre at the middle height of the specimens, and occurred away from the overlapping area (i.e. no failure occurred at the overlapping area). Failure of specimens strengthened with CFRP ruptured explosively (i.e. sudden failure without signs), while specimens strengthened with BFRP ruptured less violent and suddenly. In addition, after

the test was completed, thin parts from the concrete cover were adhered to the FRP indicating sufficient bonding (due to the epoxy). Thereafter, the concrete showed a cone failure (i.e. referring to good test) with some cracks at the top surface.

Figure (6.18) Specimens strengthened at 1, 2, 3, and 4 months and tested after 2 months from the strengthening date

(a) CFRP, and (b) BFRP

On the other hand, specimens strengthened with CRC + BFRP exhibited three different fracture patterns as "side fracture at the top", "cone at both ends with well formation", and "columnar" as shown in **Fig. (6.19a,b,c)**. In addition, failure occurred without any sound and normally started with tearing the fibre in three different shapes mainly depending on the type of fracture as shown in **Fig. (6.19a,e,f)**. The adhesion between deteriorated concrete and the

strengthening materials showed three different forms as shown in **Fig. (6.19d,f,g)**; good adhesion between deteriorated concrete and CRC+BFRP (i.e. epoxy and bonding agent working well), good adhesion between deteriorated concrete and CRC only (i.e. a bonding agent working better than the epoxy), and poor adhesion between deteriorated concrete and CRC+BFRP (i.e. epoxy working better than bonding agent). All of the above behaviors can be attributed to the properties of fine crumb rubber added to concrete (i.e. nonpolar property, fend off the water, and adhere air on its surface).

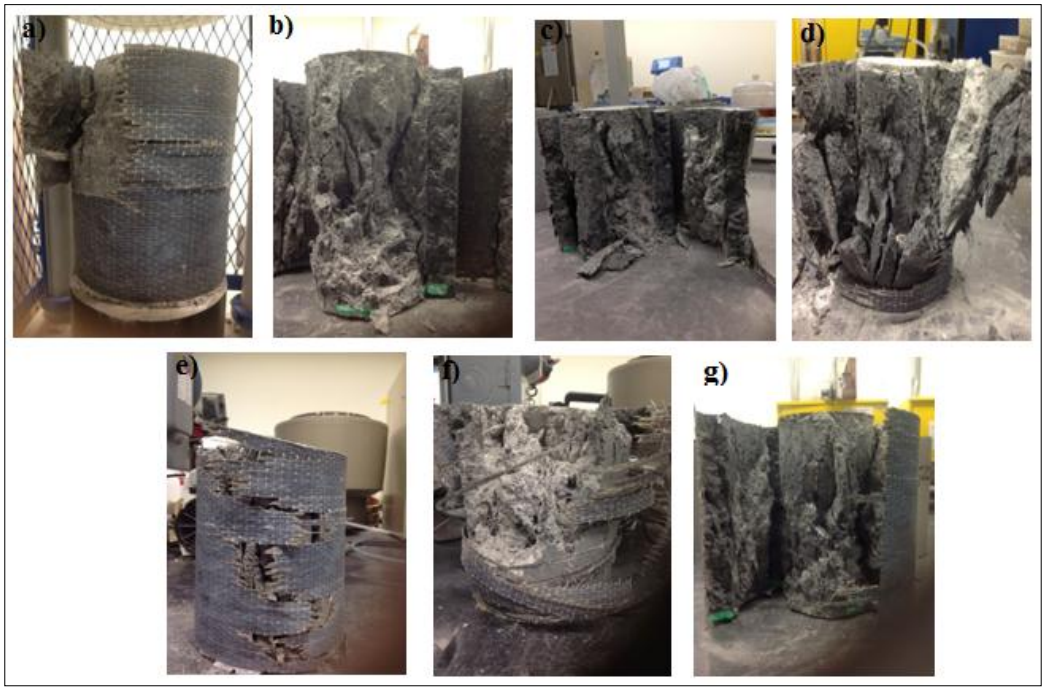

Figure (6.19) Specimens strengthened with CRC + BFRP at 1, 2, 3, 4, 5, and 6 months and tested after 2, 4, and 6 months from the strengthening date

The majority of the specimens strengthened with Mortar + GG, and Mortar + BFRP mesh exhibited a similar pattern of fracture as "cone at one end with vertical cracks" and "diagonal shear cracks with cone" as shown in **Fig. (6.20a,b)**. The tests revealed good adhesion between the deteriorated concrete and both strengthening materials (i.e. proofed well bonding). Finally, the specimens strengthened with FRC jacketing reveals two different patterns of fracture as "shear" and "columnar" with longitudinal cracks at outer the surface as shown in **Fig. (6.21).** Moreover, the majority of specimens revealed the good bond between the deteriorated concrete and FRC jacketing concrete.

Figure (6.20) Specimens strengthened at 1, 2, 3, and 4 months and tested after 2 months from the strengthening date

(a) Mortar + GG, and (b) Mortar + BFRP mesh

Figure (6.21) Specimens strengthened with FRC jacketing at 1, 2, 3, 4, and 5 months and tested after 4 months from the strengthening date

6.4.2.2 Effect of Strengthening Type

Compressive strength results for all tested concrete specimens after strengthening with the six different materials and tested at the same time (i.e. tested after 2, 4, and 6 months from the strengthening date) as well as the control specimens (i.e. specimens incorporated 15% FS and Spratt agg.) are shown in **Fig. (6.22)**. Generally, all concrete specimens after strengthening exhibited compressive strength higher than the control specimens except specimens strengthened with FRC after 1, 2, and 3 months, respectively as shown in **Fig. (6.22)**.

For instance, the compressive strength of the control specimens at age of three months was 26.0 MPa, while, the compressive strength of specimens strengthened after 1 month with CFRP, BFRP, CRC + BFRP, Mortar + GG, Mortar + BFRP, and FRC, and tested after 2 months were 60.4, 41.1, 36.2, 27.7, 27.2, and 23.0 MPa, respectively, as shown in **Fig. (6.23a)**. The reduction in compressive strength for the specimens strengthened with FRC after 1 and 2 months might be due to high residual expansion at early ages that induced high internal stress resulting in a more internal cracking.

At all times of strengthening, the specimens strengthened with CFRP exhibited a significant increase in compressive strength compared with the control specimens, followed by BFRP, CRC + BFRP, Mortar + GG, Mortar + BFRP, and FRC, respectively as represented in **Fig. (6.24)**. For example, the specimens strengthened after four months and tested after 2 months from the strengthening date showed an increase in compressive strength by about 178.45%, 88.20%, 72.58%, 28.68%, 24.38%, and 7.16% for specimens strengthened with CFRP, BFRP, CRC + BFRP, Mortar + GG, Mortar + BFRP, and FRC, respectively as shown in **Fig. (6.24)**. These results confirm the previous studies conducted on AAR damaged concrete; for RC columns incorporating FS, strengthening with one and two layers CFRP increased ultimate load capcity of RC circular columns in comparison with unwrapped columns by 50% - 75% and 109% - 120%, respectively. While, these ratios became 21% - 48% and 52% - 69% with RC square columns (Abdullah, 2013). In addition, strength of concrete cylinders (i.e. 160mm×320mm incorporating opal as a reactive aggregate) wrapped with unidirectional CFRP was four times as high as the failure strength of reactive concrete and almost equal the strength on non reactive specimens after 8 months (Mohamed et al., 2005).

In addition, all tested specimens exhibited a progressive increase in the compressive strength as represented **Fig. (6.24)**. For instance, the compressive strength increased for tested specimens in the range from 132.22% to 217.37%, from 58.01% to 120.78%, from 39.18% to 107.46%, from 6.50% to 49.88%, from 4.57% to 38.94%, and from -11.57% to 29.90% for CFRP, BFRP, CRC + BFRP, Mortar + GG, Mortar + BFRP, and FRC, respectively.

One interesting point, test results showed the efficacy of strengthening with FRC jacketing when the strengthening was applied at least after 3 months or more as shown in **Fig. (6.24a)**. Moreover, the efficacy of mortar with GG and BFRP mesh had a similar effect on increasing the

compressive strength. From the above and test results, its apparent the selection of strengthening material is significant for enhancement and achieve the target compressive strength for the deteriorated concrete suffering from ASR.

The relationship between compressive strength and expansion for all examined specimens after application of the strengthening materials at six different ages and tested at 2,4, and 6 months from the strengthening date are represented in **Fig. (6.25)**. The relationship showed that the compressive strength for the same specimens increased after applying the strengthening materials with increases in expansion with similar trends. This is can be attributed to the properties of strengthening materials to enhance the mechanical properties of ASR damaged concrete. Up to a certain expansion (i.e. from 0.852% to 0.900%), compressive strength for specimens strengthened with CFRP, BFRP, CRC + BFRP, Mortar + GG, Mortar + BFRP, and FRC increased in comparison with the strength of control specimens within 141%, 62%, 49%, 16%, 8%, and -9%, respectively. However, as expansion increased, a significant increase in strength was observed as a result of lower residual expansion.

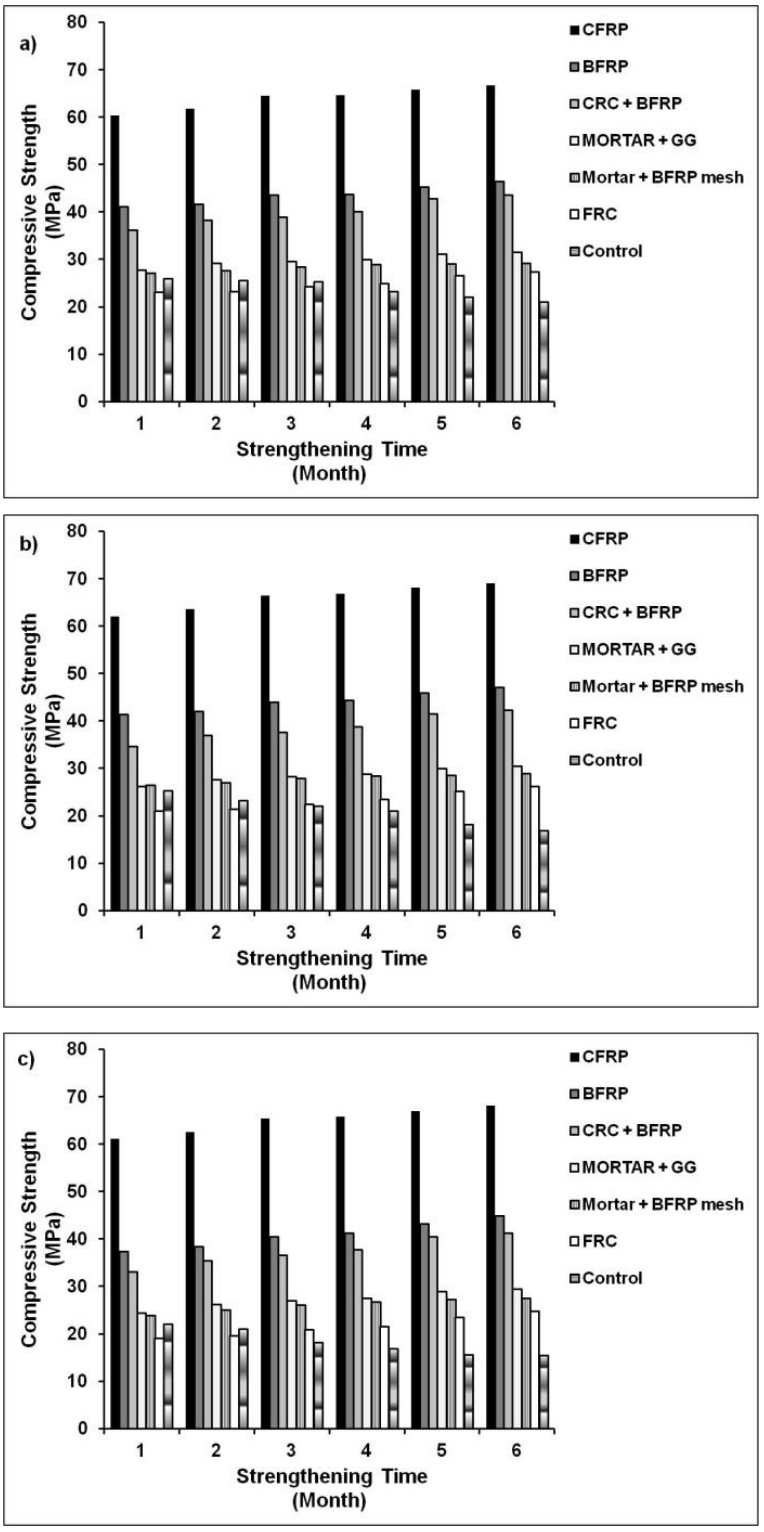

Figure (6.22) Compressive strength versus strengthening time and testing at different times from strengthening date

(a) 2M, (b) 4M, and (c) 6M

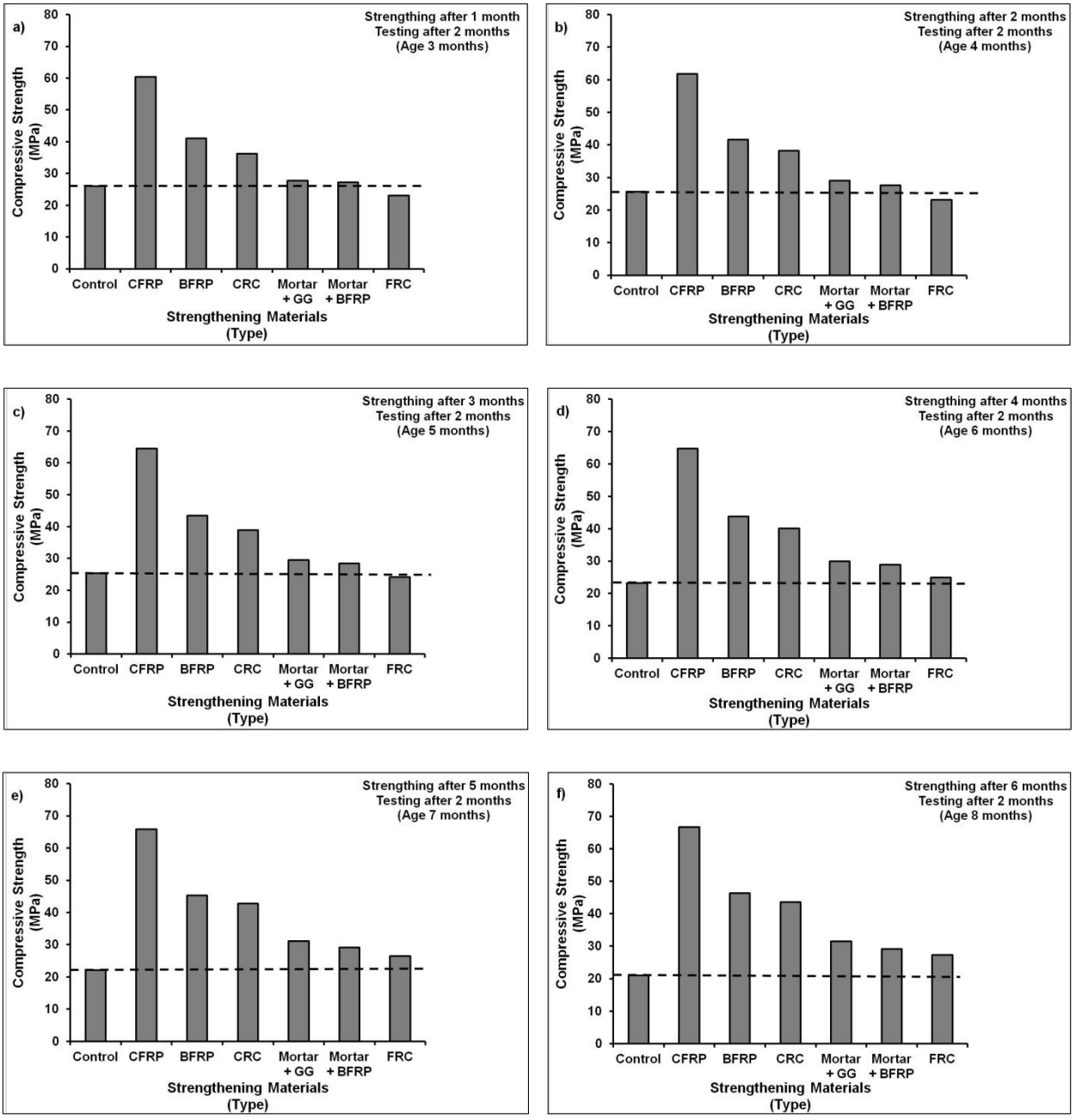

Figure (6.23) Compressive strength for specimens tested at 2 months from the strengthening date and strengthening at different times

(a) 1M, (b) 2M, (c) 3M, (d) 4M, (e) 5M, and (f) 6M

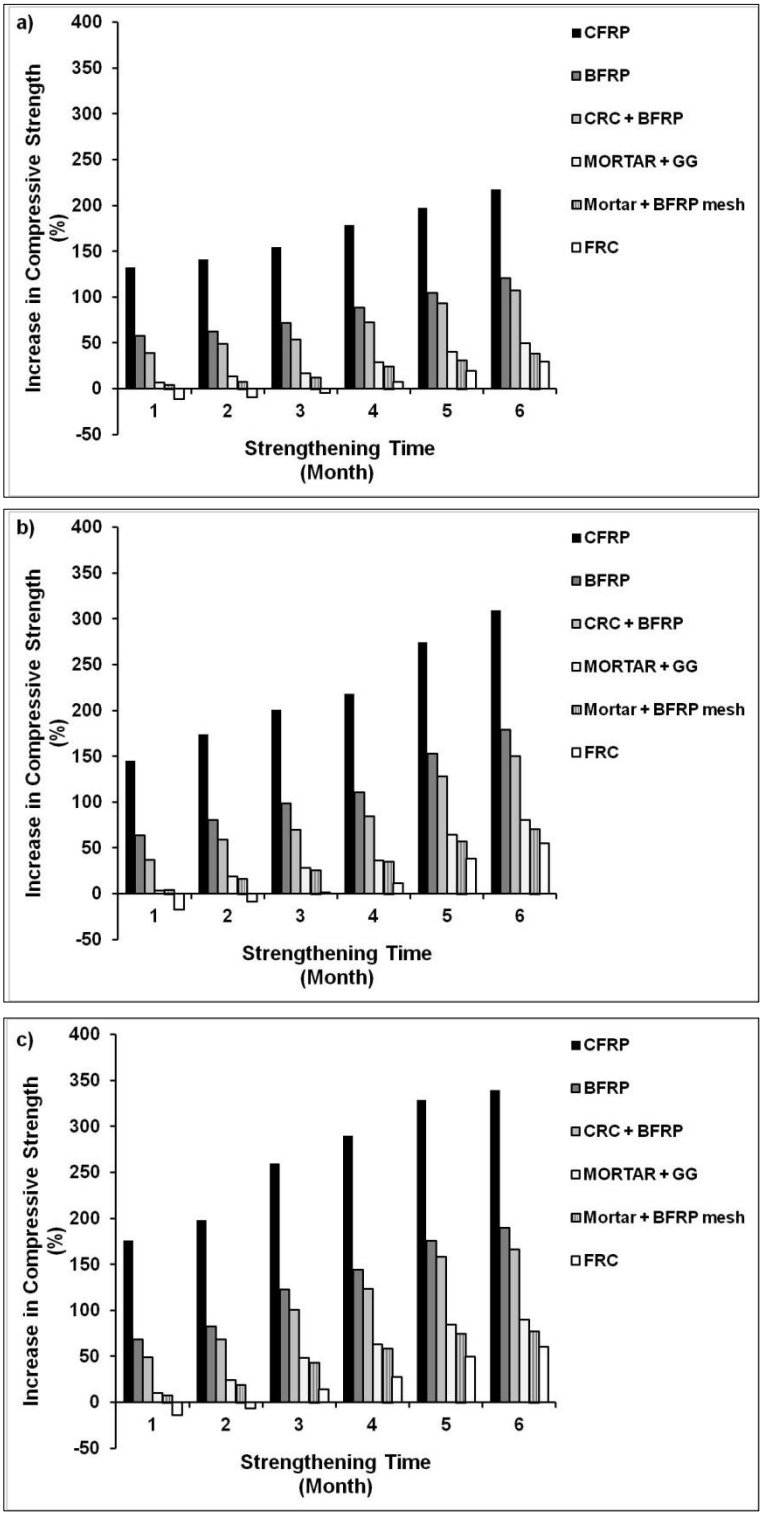

Figure (6.24) Increase in compressive strength for specimens strengthening at different times w.r.t control specimens

(a) 2M, (b) 4M, and (c) 6M

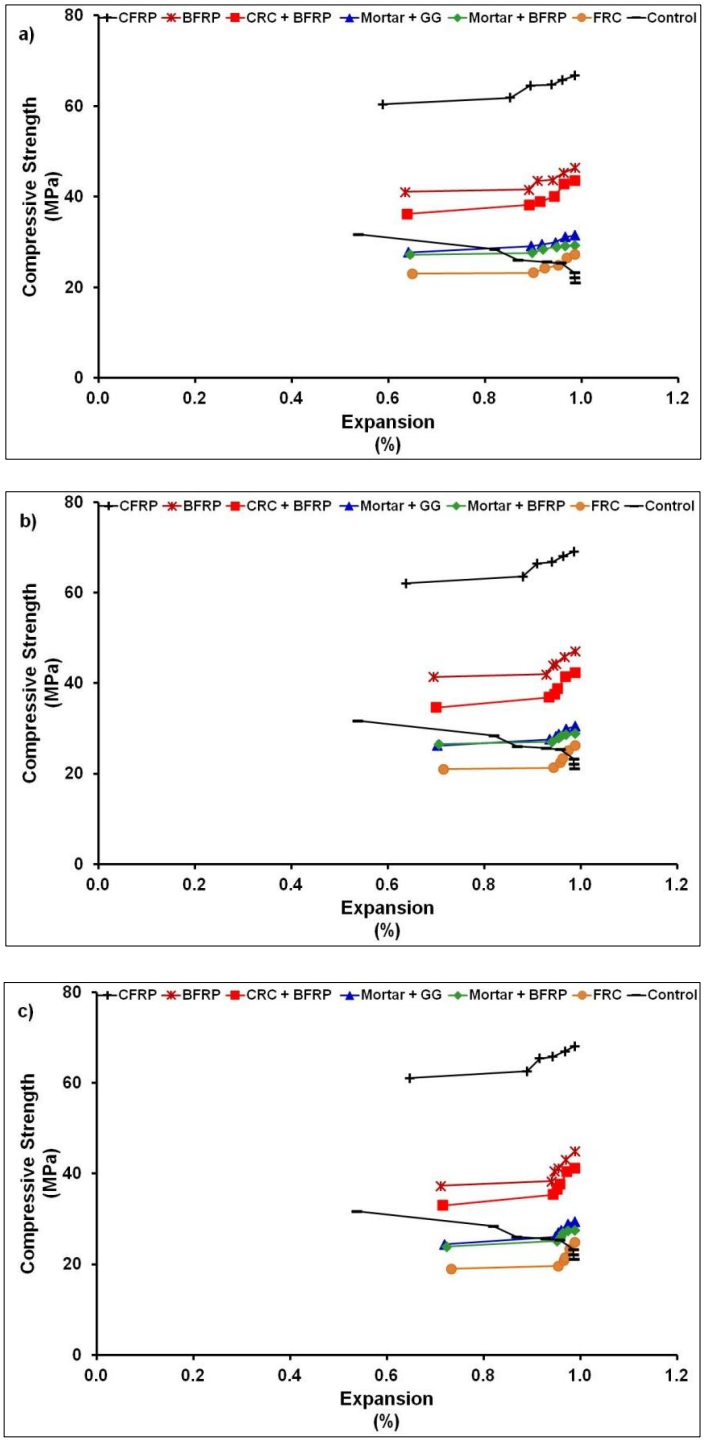

Figure (6.25) Relationship between compressive strength and expansion for examined specimens before and after applying strengthening materials at different times and tested at different times

(a) 2M, (b) 4M, and (c) 6M

6.4.2.3 Effect of Strengthening and Testing Time

The compressive strength for all examined specimens after applying the same strengthening material at 6 different ages was recorded to evaluate the sensitivity of the strengthening time as shown in **Fig. (6.22)**. For the same strengthening material, the compressive strength increased as the strengthening time increased. For instance, the compressive strength of specimens strengthened with BFRP after 1, 2, 3, 4, 5, and 6 months were 41.1, 41.6, 43.5, 43.7, 45.3, 46.4 MPa, respectively. In addition, for all tested specimens, the relationship between the increased ratio in compressive strength for the same strengthening material as a function of time were found to have a logarithmic trendline with regression coefficients (R^2) in the range from 0.9493 to 0.9647, from 0.9523 to 0.9567, from 0.8926 to 0.9229, from 0.8943 to 0.9478, from 0.9617 to 0.991, and from 0.9462 to 0.9241 for specimens strengthened with CFRP, BFRP, CRC+ BFRP, Mortar + GG, Mortar + BFRP, and FRC, respectively as shown in **Fig. (6.26)**. These relationships highlighted the link between the situation of the strengthened concrete, strengthening techniques and time of application to achieve the required strength after apply strengthening material. In addition, a robust correlation between these test results was found.

The relationship between the increased ratios in compressive strength of all tested specimens after applying different strengthening materials and the strengthening time (i.e. 6 different times) showed a similar trend as compared with the compressive strength of control specimens. These relationships can be expressed linearly with different regression coefficients and slopes as represented in **Table (6.4)**. For example, the relationship between increased ratio in compressive strength compared with control specimens and strengthening time of specimens strengthening with BFRP and tested 2 months from the strengthening date can be plotted linearly with R^2 =0.9665.

Regardless of the strengthening time using the same material, it is clear, CFRP, BFRP, and CRC + BFRP were effective at all times of strengthening. The compressive strength increased by about 132.22%, 58.01%, and 39.18%, respectively compared with control specimens when the strengthening was applied at 1 month and more (i.e. effective even the residual expansion was maximum). On the other hand, specimens strengthened with Mortar + GG showed a significant increase in compressive strength when the strengthening was applied at 2 months and more (i.e. compressive strength increased in the range from 13.65% to 49.88%). In addition, Mortar + BFRP mesh exhibited considerable increase when strengthening was applied at 3 months and more (i.e. compressive strength increased in the range from 12.16% to 38.94%). Finally, FRC became more effective as strengthening achieved at 4 months and more (i.e. compressive strength increased in the range from 7.16% to 29.19%)

From above, it is clear, the selection of the strengthening time plays a crucial role to achieve the target strength. For the same type of strengthening, the compressive strength increased as the strengthening time increased (i.e. the later the strengthening time, the higher the strength). This can be attributed to lower residual expansion at later ages.

The above conclusion is contrary with the conclusion repotted by Abdullah (2013) (i.e. early CFRP application on AAR damaged concrete RC columns incorporated FS as a fastening material produced higher ultimate load capacity). Strengthening after one month of exposure using one and two layers CFRP exhibited an increase in the ultimate load capacity for RC circular columns in comparison with unwrapped columns by 66% and 119%, respectively. While, these ratios decreased with RC square columns (i.e. 34% and 56%). On the other hand, strengthening after two months of exposure using one and two layers CFRP exhibited an increase in the ultimate load capacity for RC circular columns in comparison with unwrapped columns by

72% and 94%, respectively. While, these ratios decreased with RC square columns (i.e. 32% and 64%) (Abdullah, 2013).

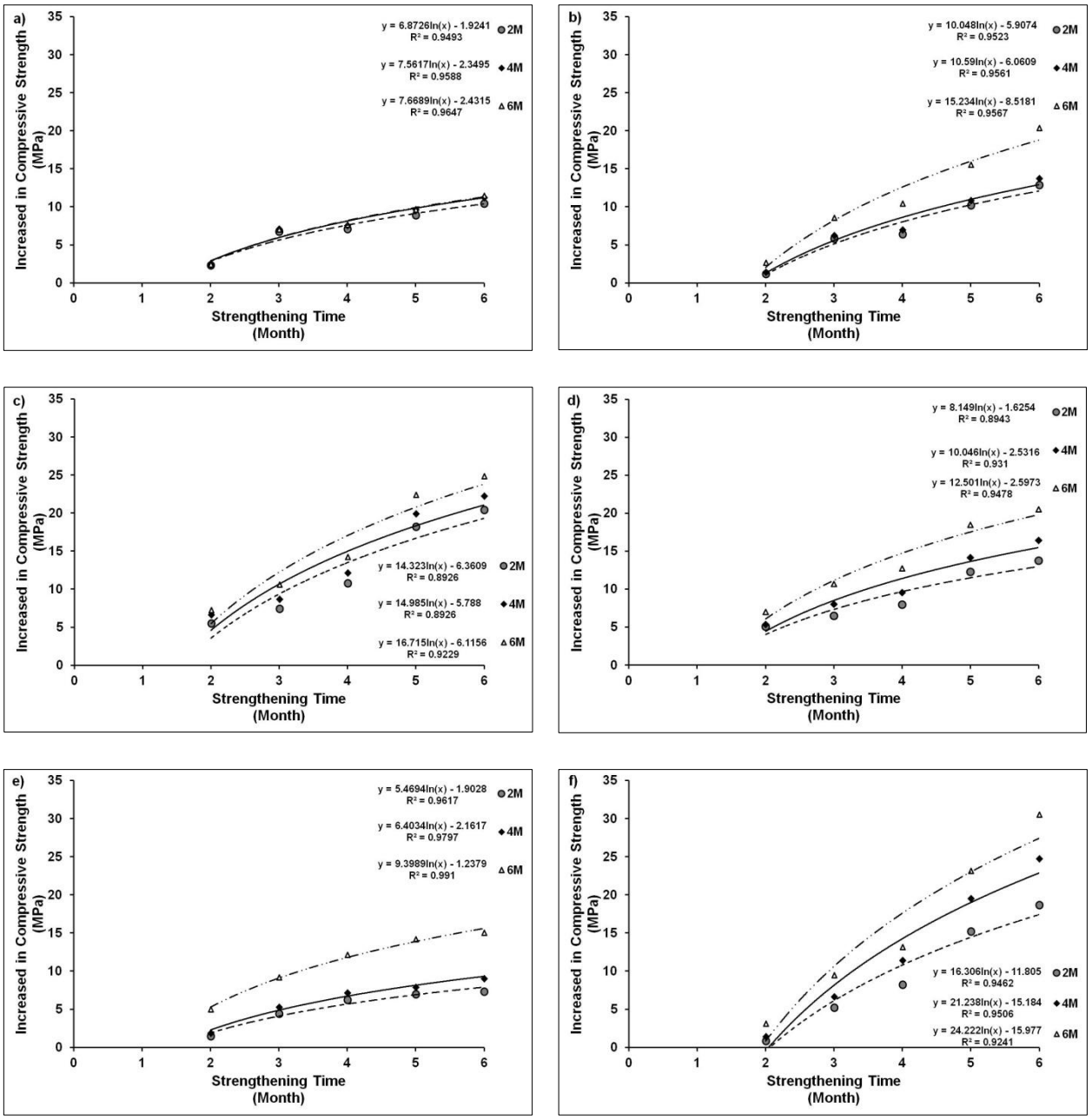

Figure (6.26) Relationship between increase in compressive strength and strengthening time for specimens tested at different times

(a) CFRP, (b) BFRP, (c) CRC+ BFRP, (d) Mortar + GG, (e) Mortar + BFRP, and (f) FRC

Table (6.4) Relationship between increased ratio in compressive strength and strengthening time for specimens tested different times compared with control specimens

Strengthening Type	Testing Time (Month) 2		4		6	
	Linear Equation	R^2	Linear Equation	R^2	Linear Equation	R^2
CFRP	y = 17.649x + 108.49	0.9824	y = 32.552x + 106.27	0.9741	y = 35.394x + 141.38	0.969
BFRP	y = 13.061x + 38.625	0.9665	y = 22.97x + 33.826	0.9635	y = 25.93x + 39.762	0.9838
CRC + BFRP	y = 14.091x + 19.93	0.963	y = 22.632x + 8.9203	0.9587	y = 25.034x + 23.378	0.9833
Mortar + GG	y = 8.8543x - 5.0243	0.9708	y = 15.18x - 14.492	0.9653	y = 16.962x - 5.955	0.9804
Mortar + BFRP	y = 7.2939x - 5.6317	0.9704	y = 13.276x - 11.374	0.9775	y = 15.087x - 5.8261	0.9669
FRC	y = 8.7568x - 25.406	0.9493	y = 14.578x - 37.623	0.9532	y = 15.803x - 33.538	0.9862

The sensitivity of testing time (i.e. 2, 4, and 6 months) for the specimens after completing strengthening with six different materials and subjected to compression test were evaluated. Generally, for the same strengthening materials and at all strengthening times with an increase in the testing age, the lower the compressive strength except with CFRP and BFRP (i.e. slightly increased) as shown in **Fig. (6.27)**. For instance, compressive strength for specimens strengthened with mortar + GG were 36.2, 34.6, 33.0 MPa as tested at 2, 4, and 6 months, respectively.

The test results showed, the reduction ratio in compressive strength measured after 4 and 6 months compared with compressive strength measured after 2 months from the strengthening

date mainly depends on the strengthening materials. For instance, specimen strengthened with CFRP showed an increase in compressive with maximum variation of 3.6% (i.e. no significant effect for testing date). In addition, specimens strengthened with BFRP showed an increase in compressive with max. variation 1.51%, and showed a reduction in strength with max. variation by about 9.25% (i.e. no effect as the test done at 4 months, and significant effect as the test done at 6 months). However, a reduction in compressive with maximum variation reached by about 8.84%, 11.91%, 12.13%, and 17.39% with CRC + BFRP, mortar + GG, mortar + BFRP mesh, and FRC (i.e. significant effect) at 6 months as shown in **Fig. (6.27)**. This can be attributed to CFRP is more durable than the other materials to withstand the harsh environmental conditions (i.e. 38 ^{o}C & 95±5% RH).

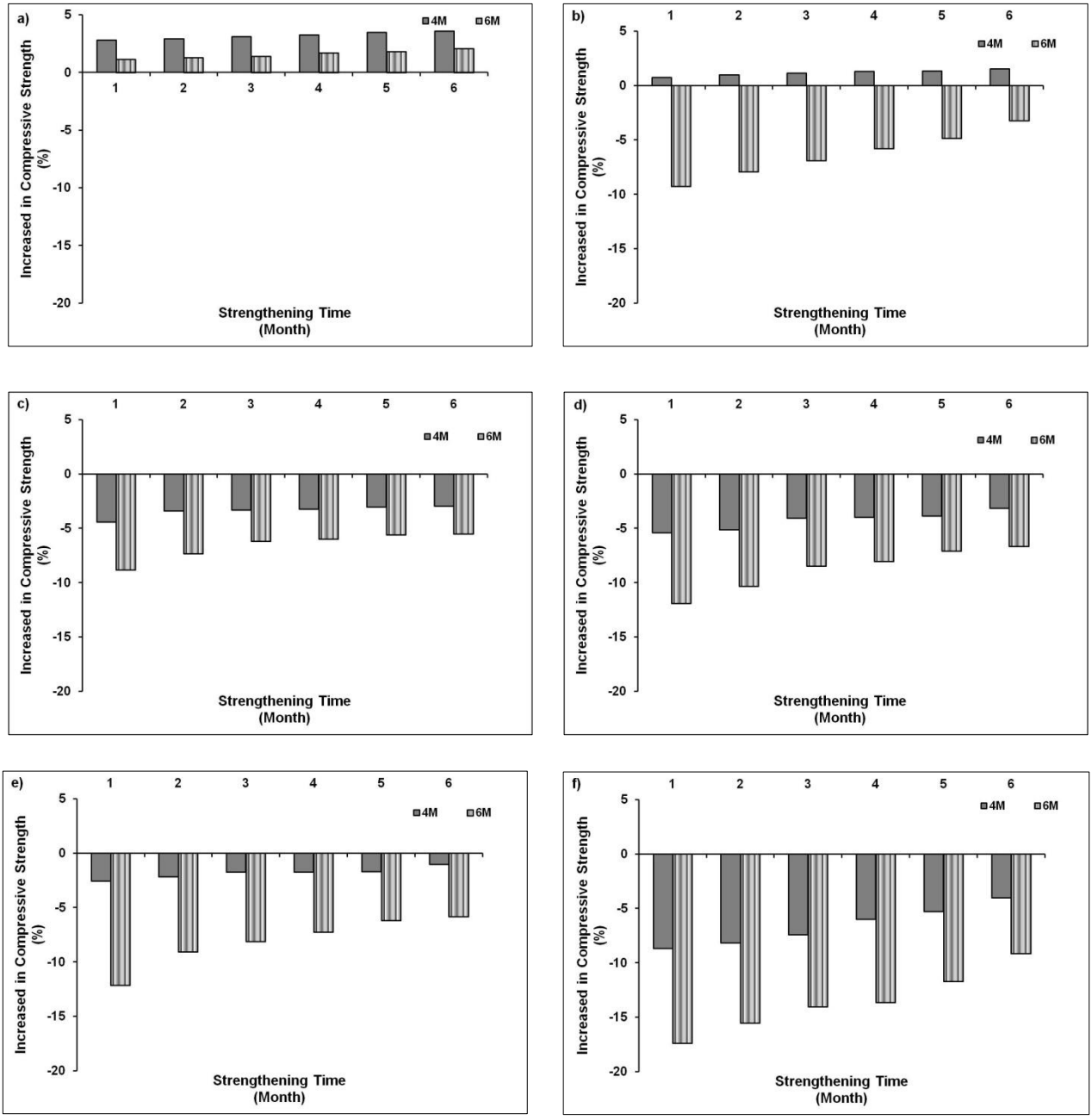

Figure (6.27) Increase in compressive strength for specimens strengthening at different time and tested at different times compared with specimens tested at 2 months;

(a) CFRP, (b) BFRP, (c) CRC+ BFRP, (d) Mortar + GG, (e) Mortar + BFRP, and (f) FRC

6.4.3 Modulus of Elasticity and Poisson Ratio

Generally, MOE increased for all concrete specimens after strengthening with six different materials tested at the same time (i.e. tested after 2, 4, and 6 months from the strengthening date) in comparison with the control specimens as shown in **Fig. (6.28).** In addition, for the same specimens at the same conditions, Poisson's ratios decreased as shown in **Fig. (6.29)**. For instance, MOE of the control specimens at age of four months was 6.58 GPa, while, MOE of specimens strengthened after 2 months with CFRP, BFRP, CRC + BFRP, Mortar + GG, Mortar + BFRP, and FRC, and tested after 2 months were 8.81, 7.96, 7.61, 7.41, 7.47, and 6.95 GPa, respectively, as shown in **Fig. (6.30d)**. The same specimens showed a reduction in Poisson's ratio compared with control specimens (i.e. υ was 0.33 for control, and 0.207, 0.268, 0.209, 0.242, 0.263, and 0.210 for specimens strengthened with CFRP, BFRP, CRC + BFRP, Mortar + GG, Mortar + BFRP, and FRC, respectively) as shown in **Fig. (6.31d)**.

The test results exhibited increased/decreased in MOE and υ mainly depending on the type of the strengthening materials as represented in **Table (6.5, 6.6)**. For MOE, at all strengthening times and testing time, CFRP showed the highest level of increase followed by BFRP, CRC + BFRP, Mortar + BFRP, Mortar + GG, and FRC, respectively. However, the same strengthening materials showed a different classification concerning the reduction in υ. The lowest value of υ obtained with CFRP and followed by CRC + BFRP**,** FRC, Mortar + GG, and Mortar + BFRP.

For example, specimens strengthened after two months and tested after 6 months from the strengthening date showed an increase in MOE by about 34.44%, 19.83%, 15.49%, 12.65%, 13.71%, and 6.01% for specimens strengthened with CFRP, BFRP, CRC + BFRP, Mortar + GG, Mortar + BFRP, and FRC, respectively. At the same time of strengthening and testing, the same specimens showed a reduction in Poisson's ratio by 38.28%, 22.73%, 32.95%, 24.57%, 18.75%,

and 34.48%. From MOE and υ results, It is apparent the concrete specimens had different behavior mainly depending on the strengthening materials. As the uniaxial loads (i.e. stress) increase, the linear strain increases due to formation and integration of internal cracks, and the resistance of concrete to restrain deformation changed based on the strengthening materials (i.e. concrete became stronger and more ductile).

The relationship between MOE versus ASR expansion for all examined specimens after applying strengthening materials at six different ages and tested at 2,4, and 6 months from the strengthening date was found to behave linearly with a regression coefficient in the range from 0.92 to 0.99 for all strengthening materials as shown in **Fig. (6.32)**. It is clear there is a robust correlation between MOE versus ASR expansion for all examined strengthening materials (i.e. similar trend) where MOE decreased as the expansion increase in agreement with the majority of previously published studies. As well, the relationship between υ and ASR expansion for the same specimens showed linear correlation with varied R^2 0.99, 0.95, 0.9, 0.71, 0.65, 0.55 for the strengthening materials Mortar + GG, CRC + BFRP, CFRP, BFRP, FRC, respectively, as shown in **Fig. (6.33)**. It is clear, υ is sensitive enough and affected by the properties of the final composite product after apply strengthening materials.

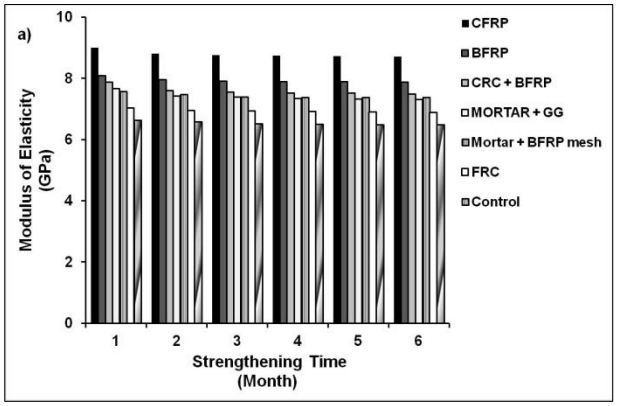

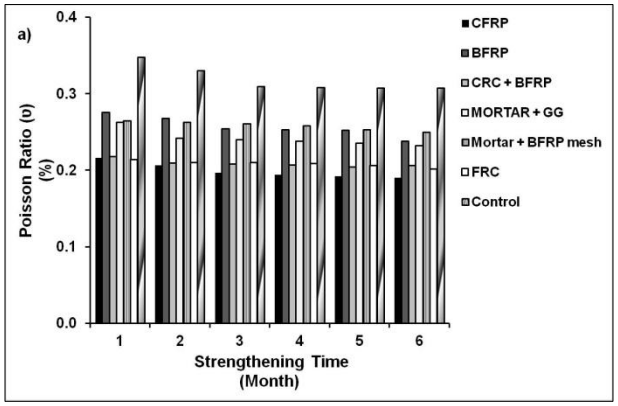

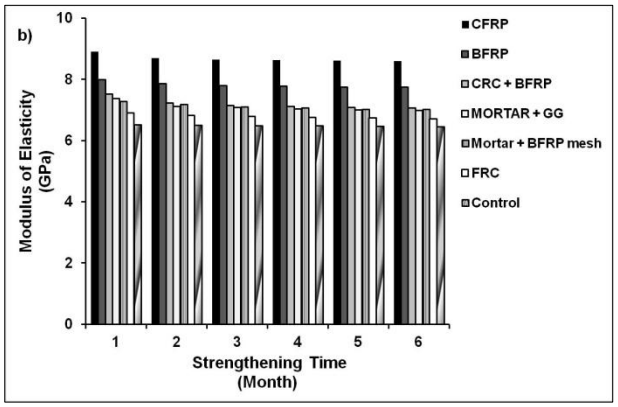

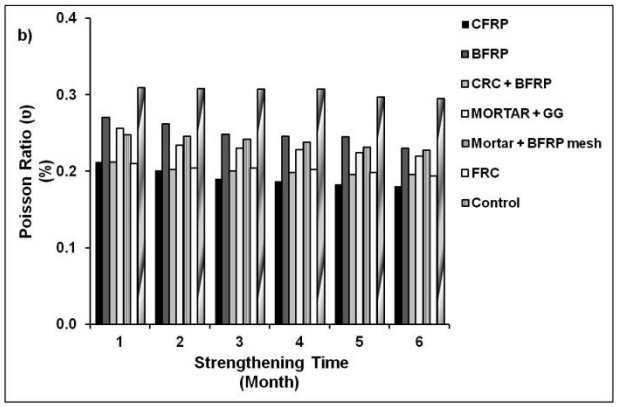

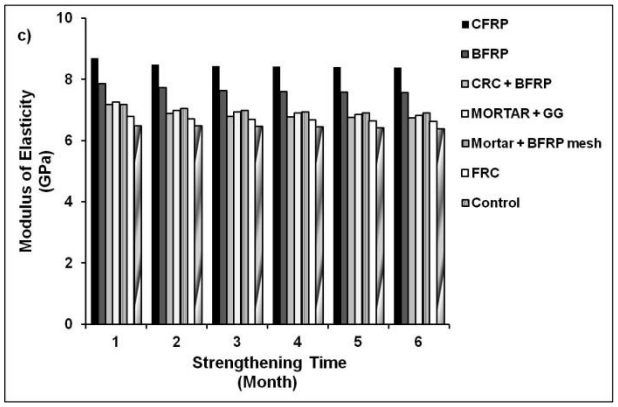

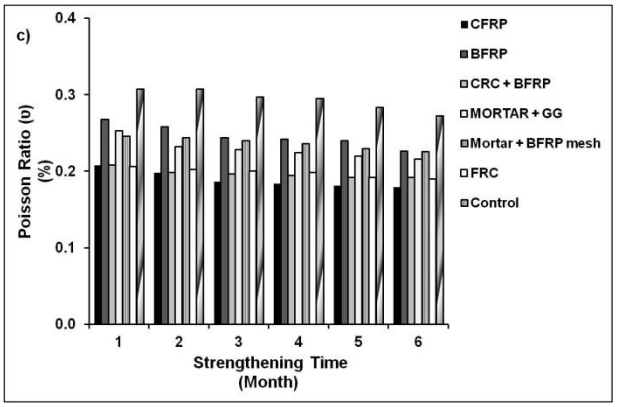

Figure (6.28) Modulus of elasticity at different strengthening time

(a) 2M, (b) 4M, and (c) 6M

Figure (6.29) Poisson ratio at different strengthening time

(a) 2M, (b) 4M, and (c) 6M

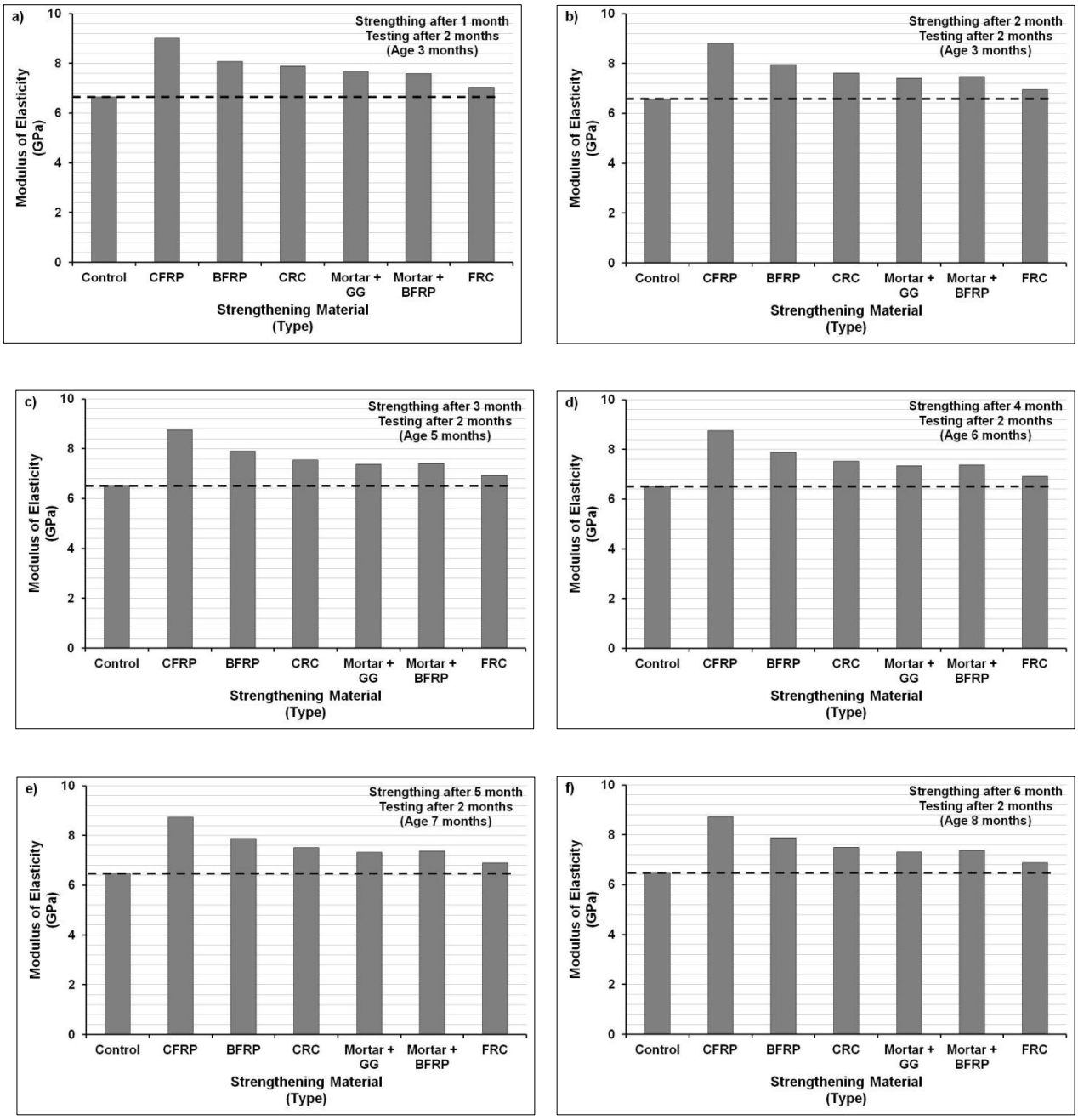

Figure (6.30) Modulus of Elasticity for specimens tested at 2 months from the strengthening date and strengthening at different times

(a) 1M, (b) 2M, (c) 3M, (d) 4M, (e) 5M, and (f) 6M

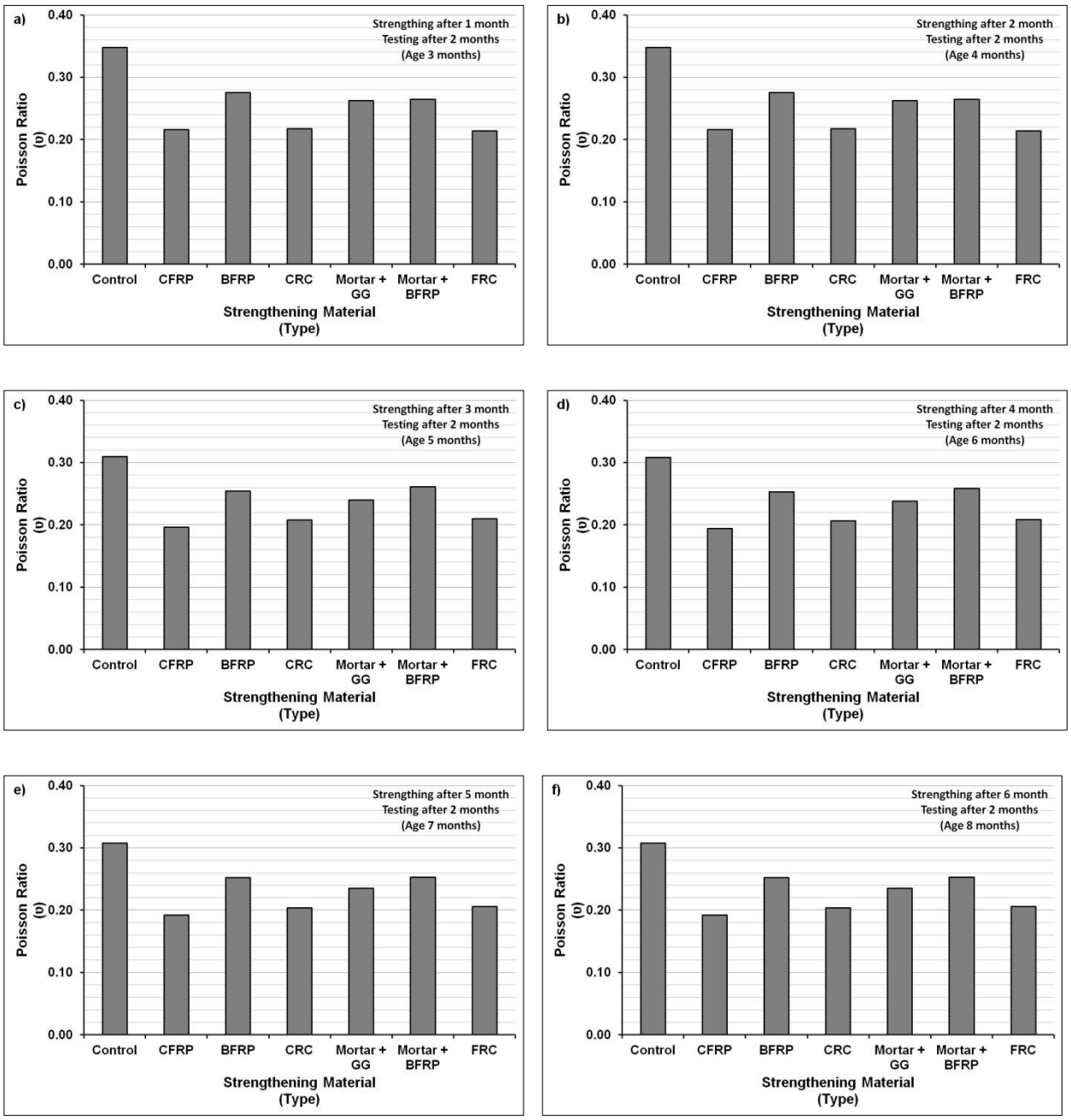

Figure (6.31) Poisson ratio for specimens tested at 2 months from the strengthening date and strengthening at different times

(a) 1M, (b) 2M, (c) 3M, (d) 4M, (e) 5M, and (f) 6M

Table (6.5) Increase in modulus of elasticity for specimens after strengthening with different materials at different times and tested at different times compared with control specimens (percent change)

Strengthening Age (Month)	CFRP			BFRP			CRC			Mortar + GG			Mortar + BFRP mesh			FRC		
	2 M	4 M	6 M	2 M	4 M	6 M	2 M	4 M	6 M	2 M	4 M	6 M	2 M	4 M	6 M	2 M	4 M	6 M
1	35.69	36.56	34.04	21.69	22.59	21.16	18.67	15.36	10.63	15.36	13.02	11.89	14.16	11.84	10.72	5.87	5.83	4.64
2	33.82	33.83	30.81	20.94	20.97	19.07	15.64	11.29	6.00	12.69	9.49	7.55	13.58	10.50	8.84	5.62	4.92	3.38
3	34.29	33.20	30.20	21.19	20.11	17.79	15.78	10.05	4.84	13.26	9.09	7.10	13.58	9.44	7.81	6.44	4.62	3.38
4	34.55	33.05	30.40	21.44	19.90	17.73	15.80	9.73	4.76	13.01	8.47	6.81	13.54	8.87	7.59	6.46	4.16	3.25
5	34.53	32.98	30.83	21.51	19.67	18.04	15.83	9.25	5.15	12.76	8.02	6.85	13.71	8.48	7.72	6.32	4.01	3.58
6	34.33	33.14	31.00	21.41	19.83	18.20	15.49	9.27	5.32	12.65	8.05	6.56	13.71	8.70	7.88	6.01	3.87	3.59

Table (6.6) Decreased in Poisson ratio for specimens after strengthening with different materials at different times and tested at different times compared with control specimens (percent change)

Strengthening Age (Month)	CFRP			BFRP			CRC			Mortar + GG			Mortar + BFRP mesh			FRC		
	2 M	4 M	6 M	2 M	4 M	6 M	2 M	4 M	6 M	2 M	4 M	6 M	2 M	4 M	6 M	2 M	4 M	6 M
1	-37.93	-31.47	-32.40	-20.87	-12.62	-12.90	-37.42	-31.47	-32.40	-24.47	-17.24	-17.79	-23.89	-19.94	-20.05	-38.49	-32.11	-33.05
2	-37.38	-34.85	-35.65	-18.84	-15.04	-16.15	-36.62	-34.52	-35.65	-26.65	-24.15	-24.60	-20.30	-20.26	-20.70	-36.46	-33.88	-34.35
3	-36.51	-38.25	-37.39	-17.79	-19.39	-17.87	-32.76	-35.00	-33.98	-22.41	-25.25	-23.25	-15.70	-21.35	-19.21	-32.11	-33.70	-32.68
4	-37.04	-39.16	-37.74	-18.09	-20.07	-18.11	-33.07	-35.65	-34.19	-22.86	-25.90	-24.20	-16.37	-22.65	-20.14	-32.44	-34.35	-33.00
5	-37.59	-38.29	-36.15	-17.96	-17.54	-15.33	-33.70	-34.03	-32.27	-23.52	-24.60	-22.39	-17.78	-21.91	-18.86	-33.05	-33.35	-32.33
6	-38.28	-38.93	-34.25	-22.73	-22.14	-16.99	-32.95	-33.68	-29.48	-24.57	-25.55	-20.66	-18.75	-22.85	-16.99	-34.48	-34.35	-30.21

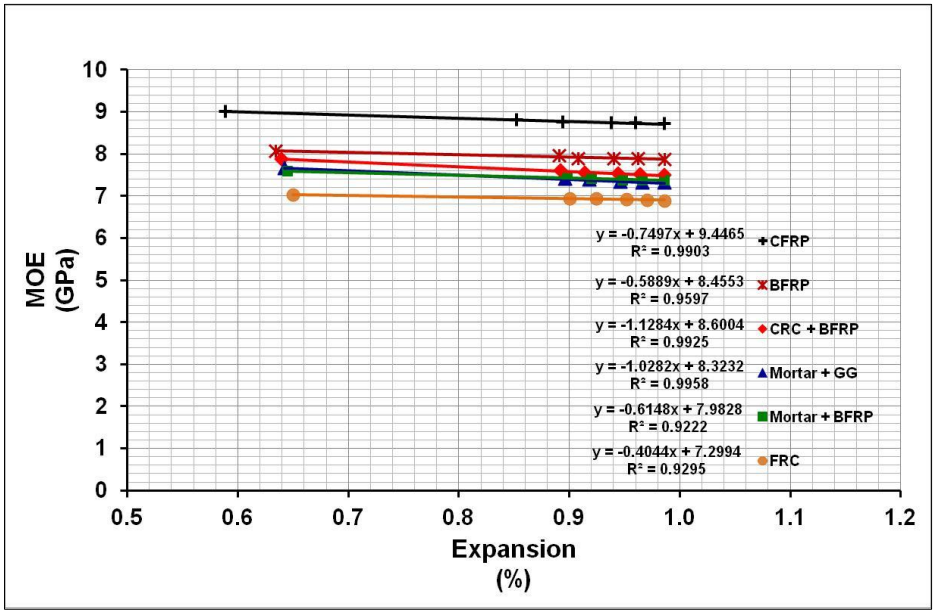

Figure (6.32) Relationship between Modulus of Elasticity and expansion for examined specimens after applying strengthening materials at different times and tested at 2 months

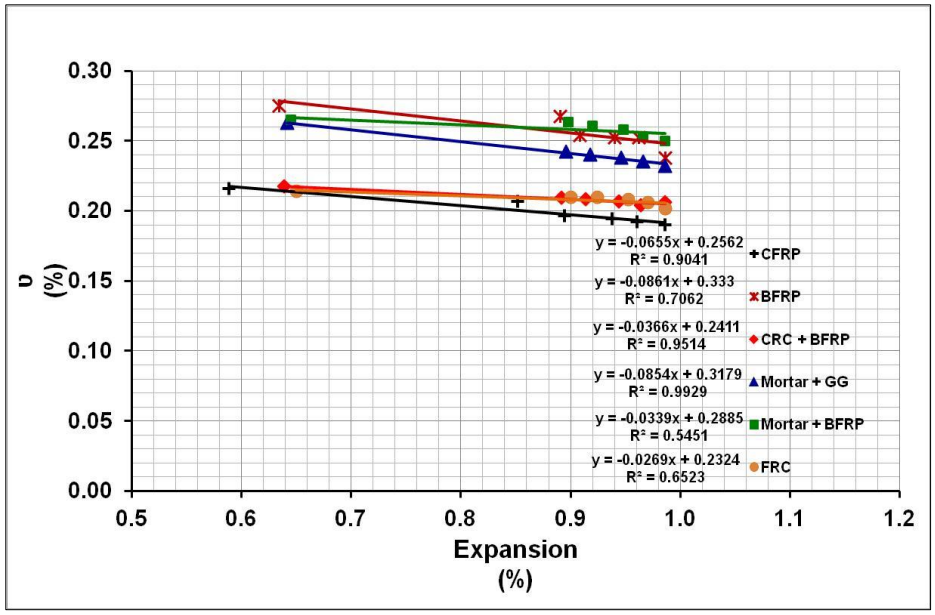

Figure (6.33) Relationship between Poisson Ratio and expansion for examined specimens after applying strengthening materials at different times and tested at 2 months

6.4.3.2 Effect of Strengthening and Testing Time

Modulus of elasticity and Poisson's ratio for all examined specimens after applying the same strengthening material at 6 different ages were calculated to evaluate the sensitivity of the strengthening time as shown in **Fig. (6.34,6.35)**. Generally, for the same strengthening material, MOE and υ decreased as the strengthening time increased as a result of the reduction in residual expansion.

MOEs reduced gradually with minimal rate in the range from 2.27% to 3.62%, from 1.51% to 3.79%, from 3.44% to 6.12%, from 3.2% to 6.08%, from 1.40% to 3.92%, and 1.14% from to 2.37% for CFRP, BFRP, CRC+ BFRP, Mortar + GG, Mortar + BFRP, and FRC, respectively indicating the lower sensitivity of the strengthening time on MOEs than compressive strength. The logarithmic correlation between MOEs and strengthening time was determined with high regression coefficient differentiated based on the strengthening type (i.e. max. R^2=0.9935, min. R^2=0.8763) as shown in **Fig. (6.34).**

On the other hand, Poisson's ratio decreased gradually as the strengthening time increased at a higher rate than MOEs in the range from 4.29% to 13.94%, from 2.69% to 15.67%, from 3.92% to 7.69%, from 7.86% to 14.61%, from 0.66% to 8.13%, and from 1.99% to 7.77%, for CFRP, BFRP, CRC+ BFRP, Mortar + GG, Mortar + BFRP, and FRC, respectively. These results indicated the sensitivity of the strengthening time on (υ) depends on the material type. Moreover, the logarithmic correlation between (υ) and strengthening time was determined with high regression coefficients differentiated based on the strengthening type (i.e. max. R^2=0.9892, min. R^2=0.8262) as shown in **Fig. (6.35).** This indicated that there is a robust correlation between these test results. From the correlations shown in **Fig. (6.34,6.35)**, it is clear, the relationship

between reduction ratios in MOEs and (υ) and strengthening time for all tested specimens showed a similar trend.

The sensitivity of testing time on MOEs and υ (i.e. testing after 2, 4, and 6 months from the strengthening date) for specimens after application of strengthening materials were evaluated. Generally, for the same strengthening materials and at all strengthening times, as the testing age increased, the lower the MOEs and υ as shown in **Fig. (6.34,6.35)**. For instance, MOEs for specimens strengthened with mortar + GG were 7.66, 7.37, 7.26 GPa as tested at 2, 4, and 6 months, respectively. Moreover, Poisson ratio followed the same trend of MOEs and recorded 0.263%, 0.256%, and 0.253% for the same specimens at the same of testing.

The test results showed the reduction ratio in MOEs and υ measured after 4 and 6 months compared with MOEs and υ measured after 2 months from the strengthening date did not reveal a significant sensitivity as represented in **Table (6.7)**. For instance, specimens strengthened at different age (i.e. monthly from 1 to 6 months) and tested after 4 months showed a reduction ratio in MOEs as compared with specimens tested after 2 months in the range from 1.18% to 1.34%, from 1.08% to 1.76%, from 4.55% to 5.83%, from 3.80% to 4.52%, from 3.80% to 4.85%, and from 1.85% to 2.47% for the strengthening materials CFRP, BFRP, CRC+ BFRP, Mortar + GG, Mortar + BFRP, and FRC, respectively.

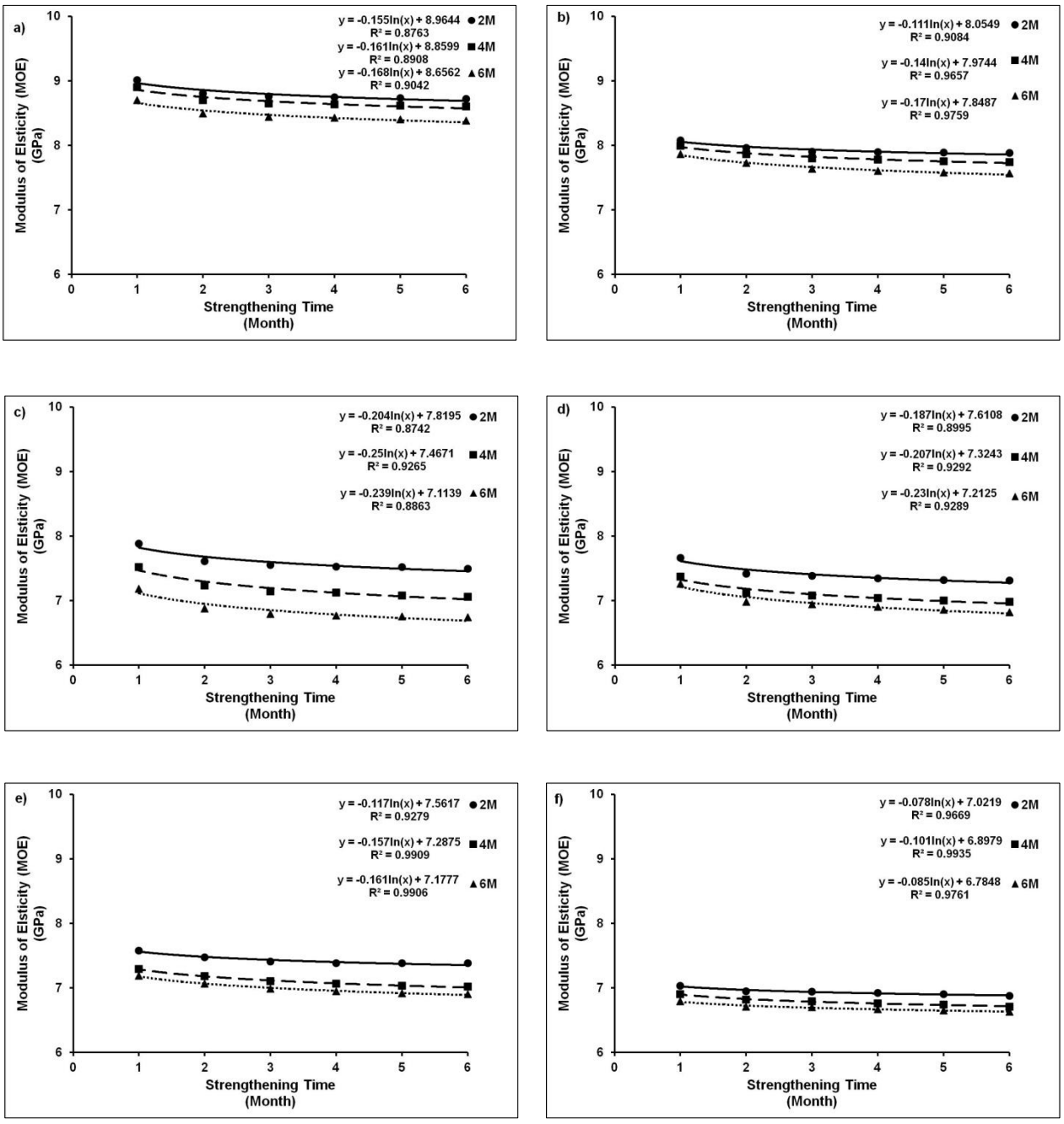

Figure (6.34) Modulus of elasticity versus strengthening time for different strengthening materials

(a) CFRP, (b) BFRP, (c) CRC+ BFRP, (d) Mortar + GG, (e) Mortar + BFRP, and (f) FRC

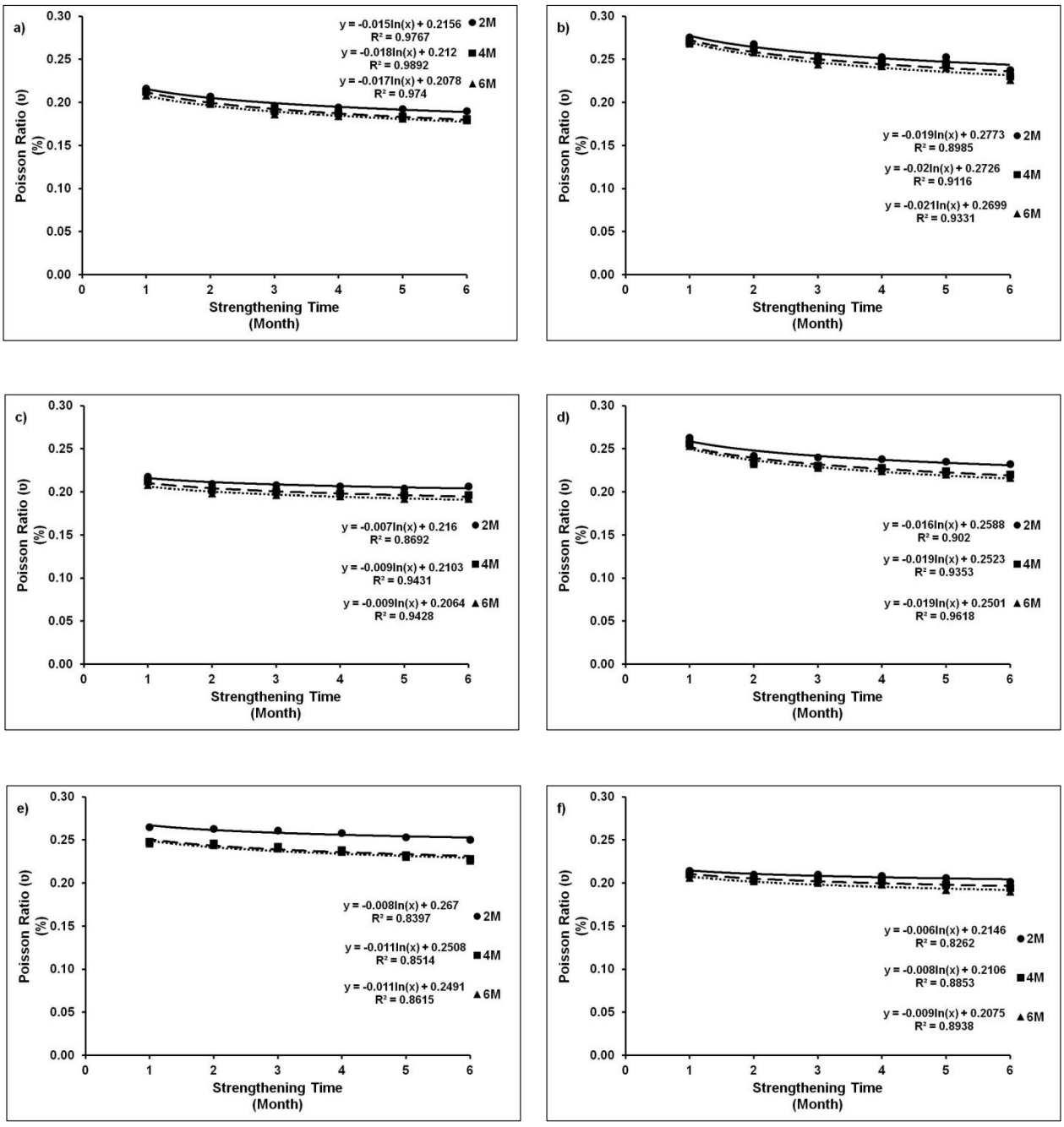

Figure (6.35) Poisson ratio at different strengthening time versus strengthening time for different strengthening materials

(a) CFRP, (b) BFRP, (c) CRC+ BFRP, (d) Mortar + GG, (e) Mortar + BFRP, and (f) FRC

Table (6.7) Decrease in Modulus and Poisson's ratio for specimens after strengthening with different materials at different times and tested at 4 and 6 months from the strengthening date compared with specimens tested after 2 months from the strengthening date

(percent change)

Strengthening Material	MOE				υ			
	4 months		6 months		4 months		6 months	
	Min.	Max.	Min.	Max.	Min.	Max.	Min.	Max.
CFRP	1.18	1.34	3.45	3.83	1.81	4.98	3.66	5.75
BFRP	1.08	1.76	2.68	3.99	1.80	3.22	2.63	4.94
CRC	4.55	5.83	8.89	10.07	2.61	4.99	5.45	6.93
Mortar + GG	3.80	4.52	5.20	6.71	2.55	5.21	3.71	6.93
Mortar + BFRP	3.80	4.85	5.20	6.45	6.46	8.80	7.08	6.90
FRC	1.85	2.47	3.40	3.63	1.85	3.78	3.72	5.76

6.4.4.4 Stiffness

The effect of strengthening materials on stiffness and deformation of ASR-damaged concrete was evaluated by calculating hysteresis area (S1) of the first loading cycle and plastic deformation (D1) over the five loading cycles as detailed in sec.3.4.1.2- Chapter 3. S1 and D1 for all strengthening materials decreased for all tested specimens compared with the control specimens as shown in **Fig. (6.36,6.37)**. For instance, the hysteresis area (S1) was 5877 J/m^3 for control specimen at 3 months. However, S1 were 3526, 4108, 4325, 4484, 4813, and 5336 J/m^3 for specimens strengthened after 1 month and tested after 2 months with CFRP, BFRP, CRC + BFRP, Mortar + GG, Mortar + BFRP, and FRC, respectively.

In addition, plastic deformation (D1) calculated over the five loading cycles decreased for all strengthening materials compared to the control specimen. For instance, D1 was 900 μstrain for control specimen at 3 months, and 480, 595, 645, 675, 725, and 805 μstrain for specimens strengthened with the same materials and tested at the same age as shown in **Fig. (6.37)**. Hence,

it is clear that the stiffness for all tested specimens increased after application of the strengthening materials. The stiffness increased (i.e. S1 decreased) with variable rate mainly depending on the strengthening material type as represented in **Fig. (6.38, 6.39)**. CFRP showed the highest level of decrease in S1 and D1 followed by BFRP, CRC + BFRP, Mortar + BFRP, Mortar + GG, and FRC, respectively. For example, specimens strengthened after 1 month using CFRP, BFRP, CRC + BFRP, Mortar + BFRP, Mortar + GG, and FRC and tested after 2 months showed a reduction in S1 as compared with the control specimen by about 40%, 30.1%, 26.4%, 23.7%, 18.1% and 9.2%, respectively. In addition, the same specimens exhibited a similar behavior with deformation, D1 was decreased by about 46.7%, 33.9%, 28.3%, 25.0%, 19.4%, 10.6%, respectively.

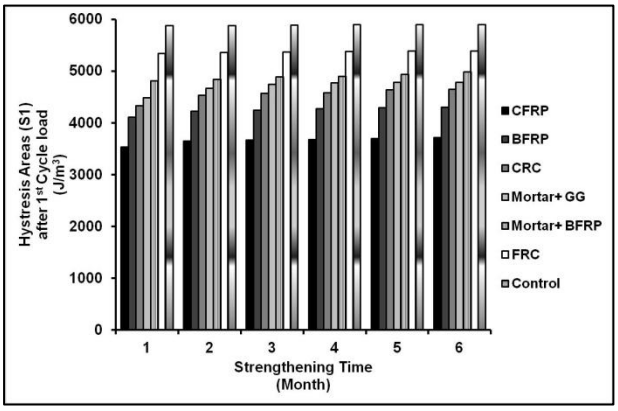

Figure (6.36) Hysteresis areas (S1) for specimens strengthened with different materials

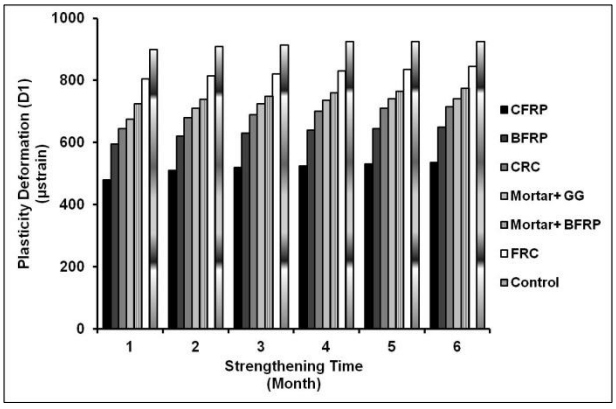

Figure (6.37) Plastic deformation (D1) for specimens strengthened with different materials

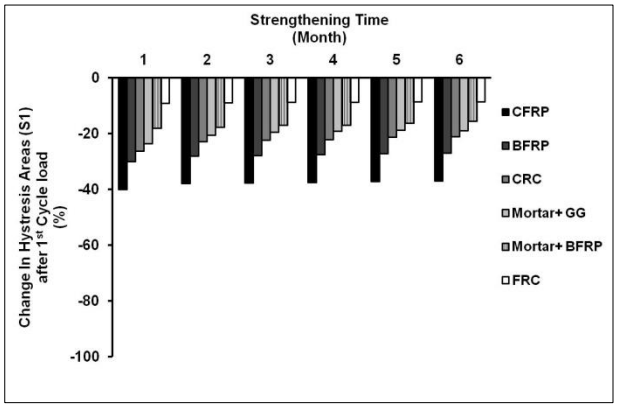

Figure (6.38) Change In hysteresis areas (S1) of specimens strengthened with different materials

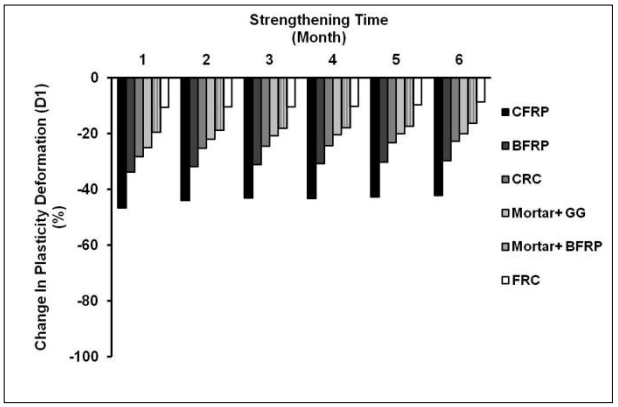

Figure (6.39) Change in plastic deformation (D1) for specimens strengthened with different materials

As well, stiffness damage index (SDI) and plasticity deformation index (PDI) were calculated for all tested specimens. SDI and PDI with all strengthening materials as compared with the control specimens with no significant increase as shown in **Fig. (6.40,6.41).** For instance, SDI was 0.445 for control specimen at 3 months. However, SDI were 0.453, 0.448, 0.448, 0.447, 0.448, and 0.446 for specimens strengthened after 1 month and tested after 2 months with CFRP, BFRP, CRC + BFRP, Mortar + GG, Mortar + BFRP, and FRC, respectively. In addition, PDI calculated over the five loading cycles had increased with all strengthening materials. For instance, PDI were 0.277 for control specimen at 3 months, and 0.284, 0.280. 0.280, 0.280, 0.280, and 0.279 for specimens strengthened with the same materials and tested at the same age.

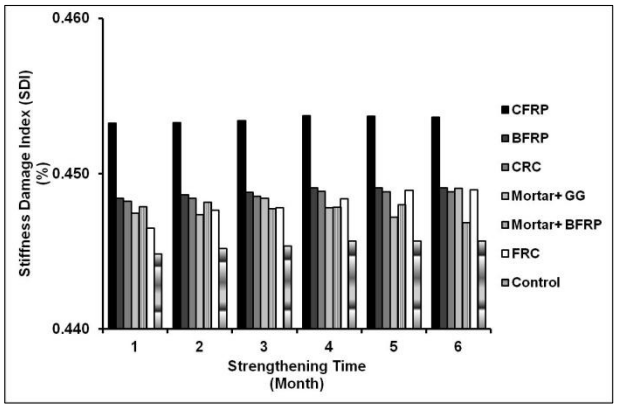

Figure (6.40) Stiffness damage index (SDI) of specimens strengthened with different materials

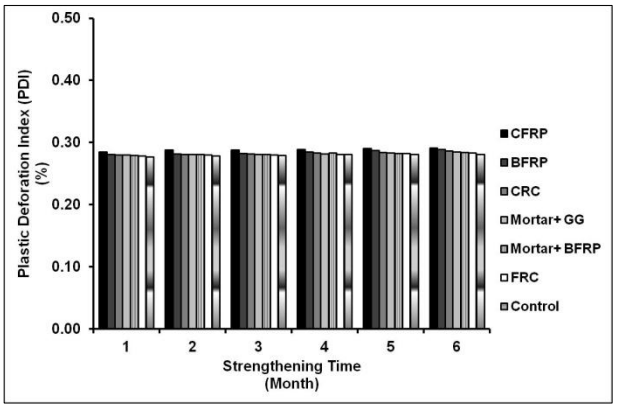

Figure (6.41) Plasticity deformation index (PDI) of specimens strengthened with different materials

The correlation between calculated HA (S1) after first loading cycle versus strengthening time (i.e. monthly from 1 to 6 months) was plotted for all tested specimens after applied strengthening materials and tested after 2 months as shown in **Fig. (6.42**). Generally, for the same strengthening material, S1 increased with a minimal rate as the strengthening time increased. For instance, S1 was increased in the range from 3.47% to 5.34%, from 2.85% to 4.63%, from 4.76% to 7.42%, from 4.07% to 6.51%, from 0.6% to 3.51%, and from 0.35% to 0.89% for CFRP, BFRP, CRC+ BFRP, Mortar + GG, Mortar + BFRP, and FRC, respectively indicating the less sensitivity of the strengthening time on HA (S1). The correlations reveal that all specimens after strengthening followed a similar parallel logarithm trend with a coefficient of determinations (R^2) 0.922, 0.9479, 0.9257, and 0.9122, 0.9078, and 0.9872 as shown in **Fig. (6.42)**.

Moreover, D1 followed the same trend of S1 and increased gradually as the strengthening time increase with an insignificant rate in the range from 6.25% to 11.46%, from 4.22% to 9.26%, from 5.43% to 10.85%, from 5.19% to 9.63%, from 2.07% to 6.90%, and from 1.24 to

4.97% for CFRP, BFRP, CRC+ BFRP, Mortar + GG, Mortar + BFRP, and FRC, respectively. These results indicating the sensitivity of the strengthening time on D1 depends on the strengthening of material types. Moreover, the correlation between D1 and strengthening time was plotted with algorithm fit curve of regression coefficient differentiated based on the strengthening type (i.e. Max. R^2=0.99, min. R^2=0.93) as shown in **Fig. (6.43).** This indicated that there is a well correlation between these test results.

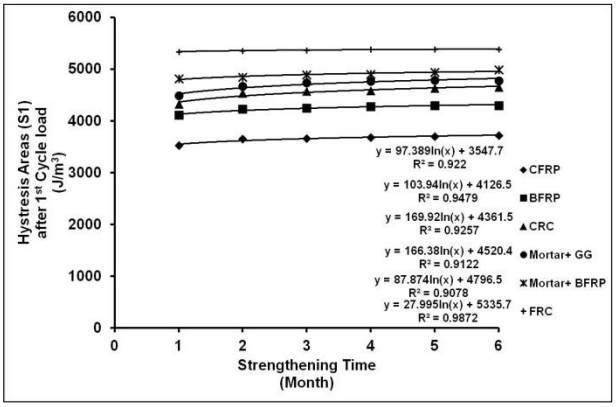

Figure (6.42) Correlation between hysteresis areas (S1) and strengthening time

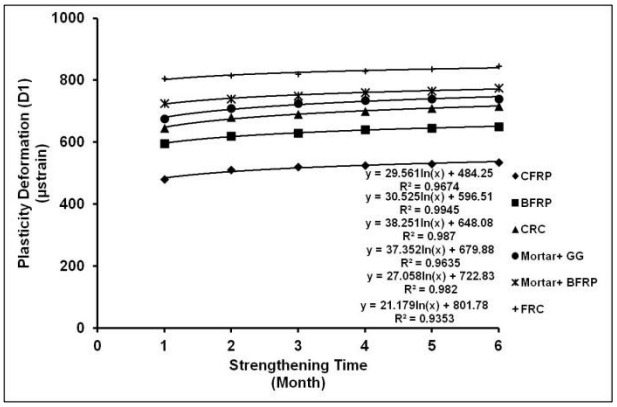

Figure (6.43) Correlation between plastic deformation (D1) and strengthening time

6. 5 Conclusion

This part included the evaluation of the remedy methods applied on the ASR-damaged damaged concrete at different time to suppress further expansion. In addition, the sensitivity of both strengthening time and testing time were evaluated after applying strengthening materials. Strengthening materials involved CFRP, BFRP, mortar with GG mesh, mortar with BFRP mesh, FRC, and CRC with BFRP.

- All types of the strengthening materials selected in this research caused a reduction in expansion compared to the control specimens. After applying strengthening, the expansion increased gradually until 6 months then became stable until the end of the test duration (i.e. 12 months) at a levels lower than the control specimens mainly depending on the strengthening material. CFRP exhibited a significant reduction in expansion compared to with the control specimens and followed by BFRP, CRC + BFRP, Mortar + GG, Mortar + BFRP, and FRC, respectively.
- The strengthening time had a significant effect to control the residual expansion in the deteriorated concrete. Moreover, testing time is sensitive as strengthening applied after 1, 2, and 3 months, while sensitivity was reduced over time to be eliminated after 6 months.
- The selection of strengthening material and time plays a crucial role for enhancement and achieve the target mechanical properties for ASR damaged concrete.
- CFRP, BFRP, CRC with BFRP, Mortar with GG, Mortar with BFRP, and FRC reveals an increase in compressive strength in the range from 132.22% to 217.37%, from 58.01% to 120.78%, from 39.18% to 107.46%, from 6.50% to 49.88%, from 4.57% to 38.94%, and from -11.57% to 29.90%, respectively. Strong correlation between compressive strength

and expansion was found and expressed with polynomial fit curve of R^2 in the range from 0.91 to 0.98 for all strengthening materials.

- MOE increased for all concrete specimens after strengthened. While, Poisson's ratios decreased. Specimens strengthened after two months and tested after 6 months from the strengthening date showed an increase in MOE by 34.44%, 19.83%, 15.49%, 12.65%, 13.71%, and 6.01% for specimens strengthened with CFRP, BFRP, CRC + BFRP, Mortar + GG, Mortar + BFRP, and FRC, respectively. At the same time of strengthening and testing, the same specimens showed a reduction in Poisson's ratio by 38.28%, 22.73%, 32.95%, 24.57%, 18.75%, and 34.48%.
- Linear correlation between MOE and expansion with a regression coefficient in the range from 0.92 to 0.99 for all strengthening materials was obtained.
- Specimens strengthened after 1 month using CFRP, BFRP, CRC with BFRP, Mortar with BFRP, Mortar with GG, and FRC and tested after 2 months showed a reduction in S1 as compared with the control specimen by 40%, 30.1%, 26.4%, 23.7%, 18.1% and 9.2%, respectively. In addition, the same specimens exhibited a similar behavior with deformation, D1 was decreased by 46.7%, 33.9%, 28.3%, 25.0%, 19.4%, 10.6%, respectively.

Chapter

7

Summary & Conclusions
Contribution
Future Work
List of publications

7.1 Summary and Conclusion

Despite the current knowledge and specifications for the alkali silica reactions of concrete and various strengthening techniques, numerous expansion cracking problems in various concrete structures have been reported, indicating the insufficiently or low efficiency of existing strengthening techniques. Yet, the issue of alkali silica reaction and how to sufficiently resist it has not been fully resolved and there are clear gaps between theory, research and practice. This dissertation attempted to overcome some of these gaps through providing a series of fundamental investigations related to volume changes in concrete due to alkali silica reaction and strengthening techniques used, taking into consideration the current situation of the concrete element (i.e. degree of deterioration and progress of alkali silica reaction). Moreover, new strategies for strengthening concrete through combining more than one strengthening technique were investigated.

This dissertation initially uses a first-principles approach to understand the interrelation mechanisms between concrete deterioration (i.e. ASR) and the role of various strengthening techniques and materials. The ultimate goal of the dissertation is to achieve a sustainable strengthening technique (including the method and materials) for concrete suffering of alkali silica reactions along with identifying the ideal time for its applications. This will extend concrete service life with minimal maintenance leading to both environmental and economic benefits.

At the start of this research, Chapter 2 provides a comprehensive review for the alkali silica reaction of concrete. It was found that reported results showed contradictory data about alkali silica reaction and efficiencies of different strengthening techniques. Many factors had contributed to this discrepancy including type of reactive materials (i.e. natural aggregates or artificial materials), properties of strengthening materials, method of application, testing duration, degree of concrete deterioration and method of evaluation. Thus, this dissertation focuses on investigating each of these parameters individually and combined with others to capture a realistic performance. All experimental work and different phases were explained in Chapter 3.

Chapter 4 adopted a more fundamental approach based on the effect of reactive aggregate and fused silica content in an attempt to capture their effects along with identifying the optimum concrete mixture that possess the highest level of expansion within a reasonable timeframe. Fused silica was added at rates 0%, 5%, 7.5%, 10%, 15%, and 20%. In addition, casting direction (same or perpendicular to measuring direction) and specimen shape (cylindrical and prismatic) were also investigated. Results show that the optimum percentage of FS will differ from one type to another depending on degree of fineness and other physical properties. For example, in this

study the 15% FS was the optimum, while the one recommended by the literature (i.e. 7.5%) exhibited lower expansion. Moreover, the cylindrical specimen exhibited higher expansion than that of the prismatic one. In addition, experimental work proved the existence of direct liner relationship between the expansions measured on both shapes. This suggested changing the standard testing procedure to test cylindrical specimens rather than prismatic one in order to shorten the testing time (i.e. one year) which is one of the main disadvantages of the current procedure. These finding was also confirmed by conducting the mortar bar test on the same mixtures. Furthermore, specimens cast vertically exhibited an increase in expansion over the others cast horizontally. One interesting finding that the degradation in mechanical properties is directly linked to the achieved expansion regardless the mixture composition.

The findings from Chapter 4 motivated research on investigating the roles and efficiencies of different strengthening materials, with a special focus on two indirect techniques namely, fibre reinforcement (i.e. increasing tensile capacity and consequently increase resisting confinement pressure) and crumb rubber concrete (i.e. relieving expansion stresses through the compressibility of rubber materials) in Chapter 5. Several sizes (i.e. micro and macro) and types of fibres (i.e. steel, polypropylene and Nylon) were tested. Results show that the addition of fibre will enhance cementitious material's mechanical performance. Combining two different sizes of fibre is more beneficial than using each type separately. Besides improving mechanical performance, the used of non-conductive fibre (i.e. polypropylene and Nylon) will enhance the durability for the used cementitious materials through reducing its conductivity. However, its addition had reduced the mechanical properties; crumb rubber was found to increase concrete deformability while dissipating stresses and associated energy. This indicates its high potential to act as a stress relieving material in concrete.

Chapters 4 and 5 provided fundamental knowledge for the interaction mechanisms between reactive materials (i.e. optimum fused silica content) and measured expansion, along with identifying the effects of different parameters including specimens shape, casting direction and properties of various materials (i.e. fibre reinforced and crumb rubber). In Chapter 6, the second level of the fundamental investigation that covers the behaviour of concrete suffering of ASR (i.e. the optimum concrete mixtures based on Chapter 4) strengthened with different repair techniques (i.e. common techniques and combined with material tested in Chapter 5) was investigated. All specimens were exposed to the recommended standard curing condition to accelerate concrete deterioration. Furthermore, all strengthening were applied for concrete at different ages from the start date of deterioration. Results show that efficiency of any strengthening material will significantly be affected by the deterioration degree of concrete at time of application.

7.2 Contribution

This research introduces a series of fundamental investigations related to the strengthening of concrete suffering of alkali silica reaction and the role of different parameters. These parameters included reactive aggregate and artificial reactive materials content, specimen shape and casting direction, properties of strengthening materials and techniques, situation/degree of deterioration of concrete at strengthening time. Specific original contributions of this dissertation include:

1. Developing a large and comprehensive database on existing research on different techniques strengthening of concrete suffering from alkali silica reaction.

2. Identifying the interaction mechanisms between different parameters related to ASR development and evaluation. Specifically, it was revealed that: (i) the optimum fused silica content that induces the highest expansion will differ depending on its physical properties such as fineness; (ii) Cylindrical specimens will exhibit higher expansion than that of prismatic specimens, (iii) Casting specimens in the same direction of measuring showed higher expansion, (iv) mechanical property degradation will mainly depend on achieving certain degree of expansion rather than the concrete composition.

3. Evaluating the performance and efficiency of different indirect strengthening techniques based on their properties and functions. Specifically, it was found that: (i) adding fibre will increase the strengthening material's tensile capacity leading to a higher confinement pressure; (ii) Incorporating of crumb rubber will reduce the level of stress developed in concrete due ASR expansion; (iii) the non-conductive fibre will have a dual effect: enhancing the tensile strength and increase durability of the strengthening materials.

4. Providing for the first time data about time sensitivity and efficiency for the application of various commonly used types of strengthening techniques. This highlighted the link between the

situation of the strengthened concrete, strengthening techniques and time of application. It is anticipated that this data would assist engineers in selecting suitable strengthening technique based on the concrete deterioration degree.

5. Stiffness damage test is a very useful technique for measuring the degree of deterioration of concrete and how its mechanical properties were affected. However, this technique is not suitable for strengthened materials as the monitored changes will be insignificant.

7.3 Future Work

For long term studies, the behavior of ASR damaged concrete after applying the selected strengthening materials at an early age (i.e. high residual expansion) at different exposure conditions should be evaluated. These could be: lab conditions, harsh environmental condition (38 ^{o}C % 95±5% RH), and actual weathering conditions as shown in **Fig (7.1)**.

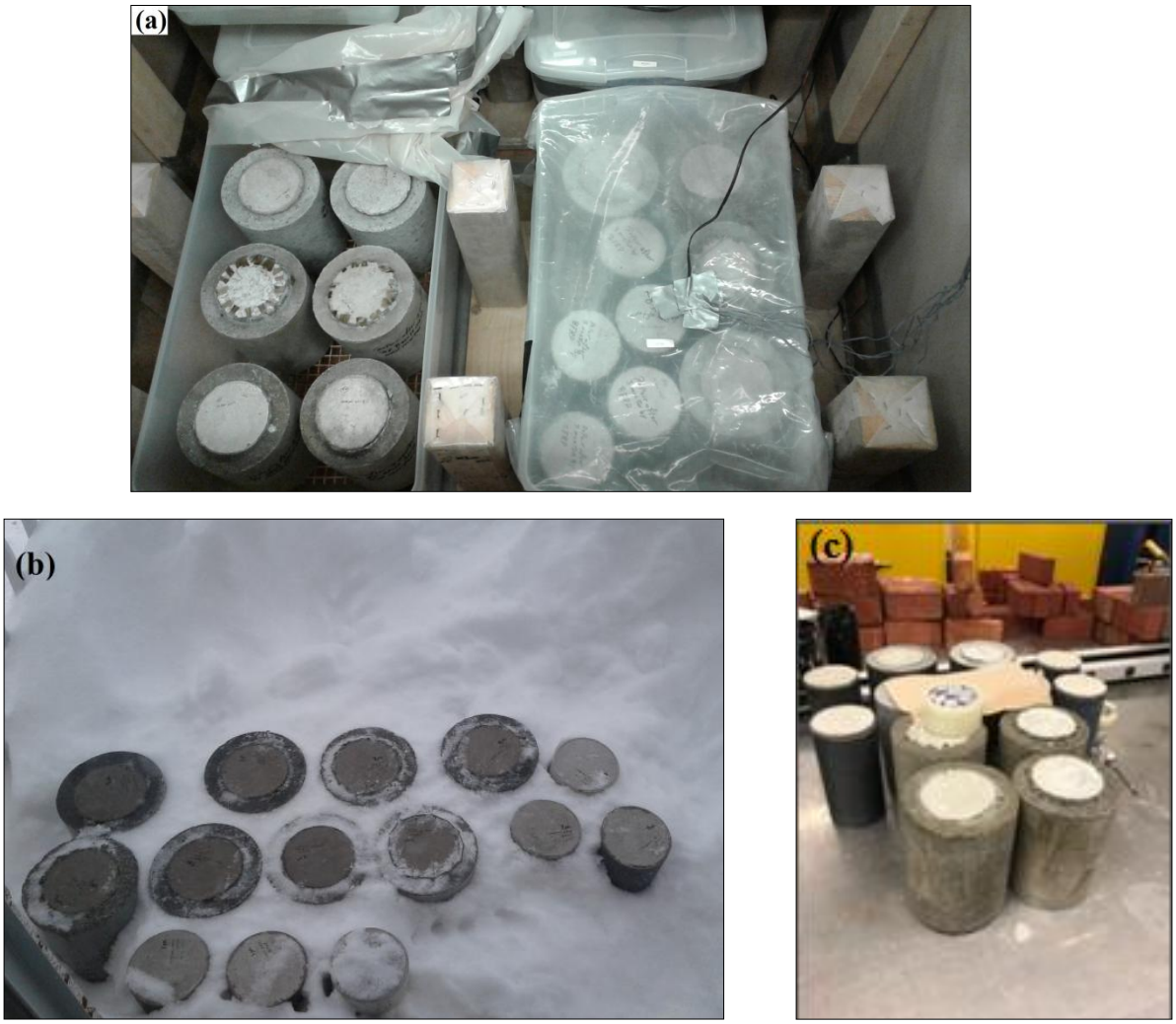

Figure (7.1) Long term exposure condition
(a) At 38 ^{o}C % 95±5% RH, (b) Actual weathering conditions,

7.4 Limitations

1. In order to reach a high degree of deterioration, the experimental lab work conducted in this research focused on accelerating ASR. This was accomplished by combining FS with Spratt reactive aggregate into small plain concrete specimens under different parameters as shape, size, and casting direction. However, these results not adequately related to actual degree of deterioration into concrete structures. In addition, under filed condition, sizes, types and weathering effects are different than the lab specimens and conditions. For that reason, it would be helpful to assess the actual performance of concrete elements, and investigate the correlations between laboratory test results and actual concrete specimens after the application of strengthening materials and being subjected to a harsh environmental condition.
2. The sensitivity of the strengthening materials after applying on RC columns of different shapes (i.e. square and circular) deteriorated by ASR and subjected to long term conditions as; harsh environmental conditions and actual weathering conditions should be evaluated.
3. The sensitivity of strengthening concrete affected by ASR using other materials should be evaluated.
4. Modeling behavior of PC and RC concrete affected by ASR before and after applying different strengthening materials at different ages.

References

AASHTO (2006). 194M/M 194-06,". Standard Specification for Chemical Admixtures for Concrete," American Association of State and Highway Transportation Officials, Washington, DC.

AASHTO (2009). 132-87 Standard Method of Test for Tensile Strength of Hydraulic Cement Mortars. American Association of State and Highway Transportation Officials.

AASHTO (2011). Standard Method of Test for Surface Resistivity of Concrete's Ability to Resist Chloride Ion Penetration, American Association of State Highway and Transportation Officials, Washington, DC.

Abdullah, S. R. (2012). Experimental Investigation of CFRP Confined Columns Damaged by Alkali Aggregate Reaction. International Journal of Integrated Engineering, 4(2), pp.(49-52).

Abdullah, S. R. (2013). Fibre Reinforced Polymer Rehabilitation of Alkali-Aggregate Reaction-Damaged Concrete Structures (Doctoral dissertation, Monash University, Australia).

Abdullah, S., Al-Mahaidi, R., & Shayan, A. (2010). CFRP confinement of RC Columns Damaged by Alkali Aggregate Reaction. In 5th Civil Engineering Conference in the Asian Region and Australasian Structural Engineering Conference 2010, (pp.773), Engineers Australia.

ACI 211, American Concrete Institute, & International Organization for Standardization (1998). Guide for Selecting Proportions for High-Strength Concrete Using Portland Cement & Other Cementitious Material (ACI 211.4R), ISBN: 9780870313141

ACI 308, American Concrete Institute, & International Organization for Standardization (2011). Specification for Curing Concrete (ACI 308.1-11), ISBN: 9780870314391

ACI 544, American Concrete Institute, & International Organization for Standardization (2002). Specification for Curing Concrete (ACI 544.1R). (Reapproved 2009), ISBN: 9780870315282

Ahmed, T., Burley, E., & Rigden, S. (1999). Effect of Alkali-Silica Reaction on Bearing Capacity of Plain and Reinforced Concrete. ACI Structural Journal, 96(4), pp.(557-570).

Ahmed, T., Burley, E., Rigden, S., & Abu-Tair, A. I. (2003). The Effect of Alkali Reactivity on The Mechanical Properties of Concrete. Construction and Building Materials, 17(2), pp.(123-144).

Al-Akhras, N. M., & Smadi, M. M. (2004). Properties of Tire Rubber Ash Mortar. Cement and Concrete Composites, 26(7), PP.(821-826).

Alderman, A. R. A review of the evidence concerning expansive reaction between aggregate and cement in concrete. Bulletin - Council for Scientific and Industrial Research, Australia. 1943; PP.(161:1-19).

Alotaibi, K. S. S. (2018). Axial-Flexural Behaviour of Reinforced Concrete Masonry Columns Confined by FRP Jackets (Doctoral dissertation, Concordia University, Canada).

Andiç, Ö., Yardımcı, M. Y., & Ramyar, K. (2008). Performance of Carbon, Polyvinylalcohol and Steel Based Microfibres on Alkali–Silica Reaction Expansion. Construction and Building Materials, 22(7), pp.(1527-1531).

Arafa, M. H., Alqedra, M. A., & Almassri, H. G. (2013). Effect of Forta-Ferro Fibres on Fresh and Mechanical Properties of Ultra High-Performance Self Compacting Concrete. Int. J. Eng. Tech. Res, 1(7), pp.(43-47).

ASTM C1064 / C1064M-17, Standard Test Method for Temperature of Freshly Mixed Hydraulic-Cement Concrete, ASTM International, West Conshohocken, PA, 2017, www.astm.org

ASTM C109/C109M-16, Standard Test Method for Compressive Strength of Hydraulic Cement Mortars (Using 2-in. or [50-mm] Cube Specimens), ASTM International, West Conshohocken, PA, 2016, www.astm.org

ASTM C1202-17, Standard Test Method for Electrical Indication of Concrete's Ability to Resist Chloride Ion Penetration, ASTM International, West Conshohocken, PA, 2017, www.astm.org

ASTM C1260-14, Standard Test Method for Potential Alkali Reactivity of Aggregates (Mortar-Bar Method), ASTM International, West Conshohocken, PA, 2014, www.astm.org

ASTM C127-15, Standard Test Method for Relative Density (Specific Gravity) and Absorption of Coarse Aggregate, ASTM International, West Conshohocken, PA, 2015, www.astm.org

ASTM C128-15, Standard Test Method for Relative Density (Specific Gravity) and Absorption of Fine Aggregate, ASTM International, West Conshohocken, PA, 2015, www.astm.org

ASTM C1293-18, Standard Test Method for Determination of Length Change of Concrete Due to Alkali-Silica Reaction, ASTM International, West Conshohocken, PA, 2018, www.astm.org

ASTM C136 / C136M-14, Standard Test Method for Sieve Analysis of Fine and Coarse Aggregates, ASTM International, West Conshohocken, PA, 2014, www.astm.org

ASTM C138 / C138M-17, Standard Test Method for Density (Unit Weight), Yield, and Air Content (Gravimetric) of Concrete, ASTM International, West Conshohocken, PA, 2017, www.astm.org

ASTM C143 / C143M-15, Standard Test Method for Slump of Hydraulic-Cement Concrete, ASTM International, West Conshohocken, PA, 2015, www.astm.org

ASTM C1585-13, Standard Test Method for Measurement of Rate of Absorption of Water by Hydraulic-Cement Concretes, ASTM International, West Conshohocken, PA, 2013, www.astm.org

ASTM C1760-12, Standard Test Method for Bulk Electrical Conductivity of Hardened Concrete, ASTM International, West Conshohocken, PA, 2012, www.astm.org

ASTM C192 / C192M-16, Standard Practice for Making and Curing Concrete Test Specimens in the Laboratory, ASTM International, West Conshohocken, PA, 2016, www.astm.org

ASTM C231 / C231M-17, Standard Test Method for Air Content of Freshly Mixed Concrete by the Pressure Method, ASTM International, West Conshohocken, PA, 2017, www.astm.org

ASTM C260 / C260M-10 (2016), Standard Specification for Air-Entraining Admixtures for Concrete, ASTM International, West Conshohocken, PA, 2016, www.astm.org

ASTM C29 / C29M-17, Standard Test Method for Bulk Density ("Unit Weight") and Voids in Aggregate, ASTM International, West Conshohocken, PA, 2017, www.astm.org

ASTM C305-14, Standard Practice for Mechanical Mixing of Hydraulic Cement Pastes and Mortars of Plastic Consistency, ASTM International, West Conshohocken, PA, 2014, www.astm.org

ASTM C307-18, Standard Test Method for Tensile Strength of Chemical-Resistant Mortar, Grouts, and Monolithic Surfacings, ASTM International, West Conshohocken, PA, 2018, www.astm.org

ASTM C33 / C33M-18, Standard Specification for Concrete Aggregates, ASTM International, West Conshohocken, PA, 2018, www.astm.org

ASTM C39 / C39M-18, Standard Test Method for Compressive Strength of Cylindrical Concrete Specimens, ASTM International, West Conshohocken, PA, 2018, www.astm.org

ASTM C469 / C469M-14, Standard Test Method for Static Modulus of Elasticity and Poisson's Ratio of Concrete in Compression, ASTM International, West Conshohocken, PA, 2014, www.astm.org

ASTM C494 / C494M-17, Standard Specification for Chemical Admixtures for Concrete, ASTM International, West Conshohocken, PA, 2017, www.astm.org

ASTM C496 / C496M-17, Standard Test Method for Splitting Tensile Strength of Cylindrical Concrete Specimens, ASTM International, West Conshohocken, PA, 2017, www.astm.org

ASTM C597-16, Standard Test Method for Pulse Velocity Through Concrete, ASTM International, West Conshohocken, PA, 2016, www.astm.org

ASTM D5603-01 (2015), Standard Classification for Rubber Compounding Materials—Recycled Vulcanizate Particulate Rubber, ASTM International, West Conshohocken, PA, 2015, www.astm.org

Azarsa, P., & Gupta, R. (2017). Electrical Resistivity of Concrete for Durability Evaluation: A review. Advances in Materials Science and Engineering**;** New York Vol. 2017, DOI:10.1155/2017/8453095

Azevedo, F., Pacheco-Torgal, F., Jesus, C., De Aguiar, J. B., & Camões, A. F. (2012). Properties and Durability of HPC with Tyre Rubber Wastes. Construction and Building Materials, 34, pp.(186-191).

Bakis, C. E., Ganjehlou, A., Kachlakev, D. I., Schupack, M., Balaguru, P. N., Gee, D. J.,& Kliger, H. S. (2002). Guide for The Design and Construction of Externally Bonded FRP Systems for Strengthening Concrete Structures. Reported by ACI 440 (2002).

Barborak, R. (2005). Using Lithium Compounds as an Admixture in New Concrete and as a Post-Treatment for Existing Concrete Affected by Alkali-Silica Reaction. M. Sc. Eng., University of Texas, Austin, TX, pp.(129).

Barbosa, R. A., Hansen, S. G., Hansen, K. K., Hoang, L. C., & Grelk, B. (2018). Influence of Alkali-Silica Reaction and Crack Orientation on The Uniaxial Compressive Strength of Concrete Cores from Slab Bridges. Construction and Building Materials, 176, pp.(440-451).

Behfarnia, K., & Behravan, A. (2014). Application of High-Performance Polypropylene Fibres in Concrete Lining of Water Tunnels. Materials & Design, 55, pp.(274-279).

Ben Haha, M. (2006). Mechanical Effects of Alkali Silica Reaction in Concrete Studied by SEM-Image Analysis, DOI 10.5075/epfl-thesis-3516.

Bencardino, F., Rizzuti, L., Spadea, G., & Swamy, R. N. (2010). Experimental Evaluation of Fibre Reinforced Concrete Fracture Properties. Composites Part B: Engineering, 41(1), pp.(17-24).

Bentz, D. P., Ehlen, M. A., Ferraris, C. F., & Garboczi, E. J. (2001, September). Sorptivity-Based Service Life Predictions for Concrete Pavements. In 7th International Conference on Concrete Pavements, Orlando, Florida, pp.(181-193).

Berra, M., Faggiani, G., Mangialardi, T., & Paolini, A. E. (2010). Influence of Stress Restraint on the Expansive Behaviour of Concrete Affected by Alkali-Silica Reaction. Cement and Concrete Research, 40(9), pp.(1403-1409).

Bérubé, M. A., Duchesne, J., Dorion, J. F., & Rivest, M. (2002). Laboratory Assessment of Alkali Contribution by Aggregates to Concrete and Application to Concrete Structures Affected By Alkali-Silica Reactivity. Cement and Concrete Research, 32(8), pp.(1215-1227).

Bérubé, M. A., Durand, B., Vézina, D., & Fournier, B. (2000). Alkali-Aggregate Reactivity in Quebec (Canada). Canadian Journal of Civil Engineering, 27(2), pp.(226-245).

Birol, T., Hasgul, U., Terzi, M., Yavas, A., Turker, K., & Yazici, H. (2016). Effect of Different Steel Fibre Type and Content in Flexural Behavior of Ultra-High-Performance Fibre Reinforced Concrete. 3rd International Balkans Conference on Challenges of Civil Engineering, 3-BCCCE, 19-21 May 2016, Epoka University, Tirana, Albania, pp.(263-272).

Bouikni, A., Swamy, R. N., & Bali, A. (2009). Durability Properties of Concrete Containing 50% and 65% Slag. Construction and Building Materials, 23(8), pp.(2836-2845).

Bravo, M., & de Brito, J. (2012). Concrete Made with used Tyre Aggregate: Durability-Related Performance. Journal of Cleaner Production, 25, pp.(42-50).

Broomfield, J. P. (2006). Corrosion of Steel in Concrete: Understanding, Investigation, and Repair. CRC Press.

Çakır, Ö., & Sofyanlı, Ö. Ö. (2015). Influence of Silica Fume on Mechanical and Physical Properties of Recycled Aggregate Concrete. HBRC Journal, 11(2), pp.(157-166).

CAN/CSA-A23.2-14A-14 (2014) "Potential Expansivity of Aggregates; Procedure for Length Change Due to Alkali-Aggregate Reaction in Concrete Prisms"

CAN/CSA-A3001-13, CSA (2013) "Cementitious Materials Used in Concrete. Canadian Standard Association".

Castro, J., Bentz, D., & Weiss, J. (2011). Effect of Sample Conditioning on The water absorbtion of Concrete. Cement and Concrete Composites, 33(8), pp.(805-813).

Chhabra, Y. (2013). Bridge Rehabilitation Techniques. The DS Brown Company, Singapore.

Chrisp, T. M., Waldron, P., & Wood, J. G. M. (1993). Development of a Non-Destructive Test to Quantify Damage in Deteriorated Concrete. Magazine of Concrete Research, 45(165), pp.(247-256).

Chrisp, T. M., Wood, J., & Norris, P. (1989). Towards Quantification of Microstructural Damage in AAR Deteriorated Concrete. Fracture of Concrete and Rock: Recent Developments.

Collins, C. L., Ideker, J. H., Willis, G. S., & Kurtis, K. E. (2004). Examination of the Effects of LiOH, LiCl, and LiNO 3 on Alkali–Silica Reaction. Cement and Concrete Research, 34(8), pp.(1403-1415).

Collins, C. L., Ideker, J. H., Willis, G. S., Jessica Hurst Alkali-Silica Reaction: "The Cancer of Concrete" ppt Slides Published 2015.

Crouch, R. S. (1987). Specification for The Determination of Stiffness Damage Parameters from the Low Cyclic Uniaxial Compression of Plain Concrete Cores. Revision A, Mott, Hay & Anderson, Special services division, internal technical note.

de Carvalho, M. R. P., Fairbairn, E. D. M. R., Toledo Filho, R. D., Cordeiro, G. C., & Hasparyk, N. P. (2010). Influence of Steel Fibres on the development of Alkali-Aggregate Reaction. Cement and Concrete Research, 40(4), pp.(598-604).

De Lorenzis, L., & Teng, J. G. (2007). Near-Surface Mounted FRP Reinforcement: An Emerging Technique for Strengthening Structures. Composites Part B: Engineering, 38(2), pp.(119-143).

DeSouza, S. J., Hooton, R. D., & Bickley, J. A. (1997). Evaluation of Laboratory Drying Procedures Relevant to Field Conditions for Concrete Sorptivity Measurements. Cement, Concrete, and Aggregates, 19(2), pp.(59-63).

Dong, Q., Huang, B., & Shu, X. (2013). Rubber Modified Concrete Improved by Chemically Active Coating and Silane Coupling Agent. Construction and Building Materials, 48, pp.(116-123).

Duan, P., Shui, Z., Chen, W., & Shen, C. (2013). Effects of Metakaolin, Silica Fume, and Slag on Pore Structure, Interfacial Transition Zone and Compressive Strength of Concrete. Construction and Building Materials, 44, pp.(1-6).

Elchalakani, M. (2015). High Strength Rubberized Concrete Containing Silica Fume for the Construction of Sustainable Road Side Barriers. In Structures, Vol. 1, pp.(20-38).

Elkhadiri, I., Palacios, M., & Puertas, F. (2009). Effect of curing temperatura on hydration process of different cement. Ceramics – Silikáty, 53 (2), pp.(65-75).

Esposito, R., Anaç, C., Hendriks, M. A., & Çopuroğlu, O. (2016). Influence of the alkali-Silica Reaction on the Mechanical Degradation of Concrete. Journal of Materials in Civil Engineering, 28(6), DOI: 10.1061/(ASCE) MT.1943-5533.0001486.

Fan, S., & Hanson, J. M. (1998). Effect of Alkali Silica Reaction Expansion and Cracking on Structural Behavior of Reinforced Concrete Beams. ACI Structural Journal, 95, pp.(498-505).

Fares, G., & Khan, M. I. (2014). The Effect of Curing Time on the ASR Expansion of Different HPC Composites. Construction and Building Materials, 72, pp.(124-132).

Feng, X., Thomas, M. D. A., Bremner, T. W., Balcom, B. J., & Folliard, K. J. (2005). Studies on Lithium Salts to Mitigate ASR-Induced Expansion in New Concrete: A critical review. Cement and Concrete Research, 35(9), pp.(1789-1796).

Feng, X., Thomas, M. D. A., Bremner, T. W., Folliard, K. J., & Fournier, B. (2010). New Observations on the Mechanism of Lithium Nitrate Against Alkali Silica Reaction (ASR). Cement and Concrete Research, 40(1), pp.(94-101).

Fiala, L., Toman, J., Vodička, J. & Ráček, V. (2016) "Experimental Study on Electrical Properties of Steel-Fibre Reinforced Concrete," Procedia Engineering, Vol. 151, pp.(241-248).

Folliard, K. J., Thomas, M. D., Ideker, J. H., East, B., & Fournier, B. (2008, June). Case studies of treating ASR-affected structures with lithium nitrate. In Proc. of the 13th International Conference on Alkali-Aggregate Reaction in Concrete, Trondheim, Norway, pp.(90-99).

Forster, S. W., Akers, D. J., Lee, M. K., Pergalsky, A., Arrand, C. D., Lewis, D. W., & Boone, R. L. (1998). State-of-the-art report on alkali-aggregate reactivity. ACI, 221, pp.(1-23).

Fournier, B., & Bérubé, M. A. (2000). Alkali-Aggregate Reaction in Concrete: A review of Basic Concepts and Engineering Implications. Canadian Journal of Civil Engineering, 27(2), pp.(167-191).

Fournier, B., & Malhotra, V. M. (1997). CANMET/Industry Research Consortium on Alkali-Aggregate Reactivity in Concrete. Interim report (No. EPRI-TR-109132). Electric Power Research Inst., Palo Alto, CA (United States); Canada Centre for Mineral and Energy Technology, Ottawa, Ontario (Canada).

Fournier, B., Ferro, A., & Sivasundaram, V. (2001). CANMET/Industry Research Consortium on Alkali Aggregate Reactivity in Concrete. In Technical Report, 1004031.

Fournier, B., Ideker, J. H., Folliard, K. J., Thomas, M. D., Nkinamubanzi, P. C., & Chevrier, R. (2009). Effect of Environmental Conditions on Expansion in Concrete Due to Alkali–Silica Reaction (ASR). Materials Characterization, 60(7), pp.(669-679).

Ganesan, N., Raj, J. B., & Shashikala, A. P. (2013). Flexural Fatigue Behavior of Self Compacting Rubberized Concrete. Construction and Building Materials, 44, pp.(7-14).

Ganjian, E., Khorami, M., & Maghsoudi, A. A. (2009). Scrap-Tyre-Rubber Replacement for Aggregate and Filler in Concrete. Construction and Building Materials, 23(5), pp.(1828-1836).

Gaskin, A. J., Jones, R. H., Vivian, H. E. (1955). Studies in Cement-Aggregate Reaction. 21. The Reactivity of Various Forms of Silica in Relation to the Expansion of Mortar Bars. Australian Journal of Applied Science. 1955; 6, pp.(78-87).

Gautam, B. P., & Panesar, D. K. (2017). The Effect of Elevated Conditioning Temperature on the ASR Expansion, Cracking and Properties of Reactive Spratt Aggregate Concrete. Construction and Building Materials, 140, pp.(310-320).

Gesoğlu, M., & Güneyisi, E. (2011). Permeability Properties of Self-Compacting Rubberized Concretes. Construction and Building Materials, 25(8), pp.(3319-3326).

Gesoğlu, M., Güneyisi, E., Khoshnaw, G., & İpek, S. (2014a). Abrasion and Freezing–Thawing Resistance of Pervious Concretes Containing Waste Rubbers. Construction and Building Materials, 73, pp.(19-24).

Gesoğlu, M., Güneyisi, E., Khoshnaw, G., & İpek, S. (2014b). Investigating Properties of Pervious Concretes Containing Waste Tire Rubbers. Construction and Building Materials, 63, pp.(206-213).

Giaccio, G., Bossio, M. E., Torrijos, M. C., & Zerbino, R. (2015). The Contribution of Fibre Reinforcement in Concrete Affected by Alkali-Silica Reaction. Cement and Concrete Research, 67, pp.(310-317).

Giaccio, G., Zerbino, R., Ponce, J. M., & Batic, O. R. (2008). Mechanical Behavior of Concretes Damaged by Alkali-Silica Reaction. Cement and Concrete Research, 38(7), pp.(993-1004).

Giannini, E. R., Sanchez, L. F., Tuinukuafe, A., & Folliard, K. J. (2018). Characterization of Concrete Affected by Delayed Ettringite Formation Using the Stiffness Damage Test. Construction and Building Materials, 162, pp.(253-264).

Giannini, E., & Folliard, K. (2012). Stiffness Damage and Mechanical Testing of Core Specimens for the Evaluation of Structures Affected by ASR. In Proceedings of the 14th International Conference on Alkali–Aggregate Reaction in Concrete, Austin, (Texas).

Godman, A., & Bentur, A. (1989). Bond Effects in High-Strength Silica Fume Concrete. ACI Materials Journal, 86(5), PP.(440-449).

Gupta, T., Chaudhary, S., & Sharma, R. K. (2016). Mechanical and Durability Properties of Waste Rubber Fibre Concrete With and Without Silica Fume. Journal of Cleaner Production, 112, PP.(702-711).

Haddad, R. H., & Qudah, A. (2005). Alkali-Silica Reaction Expansions in High-Performance and Normal-Strength Cement Grouts Reinforced With Steel and Synthetic Fibres. Mechanics of Composite Materials, 41(1), PP.(87-94).

Haddad, R. H., Shannag, M. J., & Al-Hambouth, M. T. (2008). Repair of Reinforced Concrete Beams Damaged by Alkali-Silica Reaction. ACI Structural Journal, 105(2), PP.(145).

Hafçi, A. (2013). Effect of Alkali–Silica Reaction Expansion on Mechanical Properties of Concrete (Master's Thesis, Middle East Technical University. http://etd. lib. metu. edu. tr/upload/12616369/index. pdf).

Hattori, A., Yamamoto, S., Miyagawa, T., & Kubo, Y. (2003). ASR Expansion Reduction and Ductility Improvement by CFRP Sheet Wrapping. In Fibre-Reinforced Polymer Reinforcement for Concrete Structures: (In 2 Volumes) (pp. 815-822), pp.(815-822), Singapore, June 2003.

Hensher, D. A. (2016). Fibre-reinforced-plastic (FRP) Reinforcement for Concrete Structures: Properties and Applications, Vol. 42. Elsevier, Jan. 22, 2016 - Technology & Engineering - 459 pages.

Holmes, N., Browne, A., & Montague, C. (2014). Acoustic Properties of Concrete Panels With Crumb Rubber as a Fine Aggregate Replacement. Construction and Building Materials, 73, pp.(195-204).

Holschemacher, K., Mueller, T., & Ribakov, Y. (2010). Effect of Steel Fibres on Mechanical Properties of High-Strength Concrete. Materials & Design, 31(5), pp.(2604-2615).

Hornbostel, K., Larsen, C. K., & Geiker, M. R. (2013). The Relationship Between Concrete Resistivity and Corrosion Rate: A literature review. Cement and Concrete Composites, 39, pp.(60-72).

Hoseini, M., Bindiganavile, V., & Banthia, N. (2009). The Effect of Mechanical Stress on Permeability of Concrete: A review. Cement and Concrete Composites, 31(4), pp.(213-220).

Hou, X., Struble, L. J., & Kirkpatrick, R. J. (2004). Formation of ASR Gel and the Roles of CSH and Portlandite. Cement and Concrete Research, 34(9), pp.(1683-1696).

Ideker, J. H., East, B. L., Folliard, K. J., Thomas, M. D., & Fournier, B. (2010). The Current State of the Accelerated Concrete Prism Test. Cement and Concrete Research, 40(4), pp.(550-555).

ISIS educational module (6), (2006): "Application and Handling of FRP Reinforcements for Concrete", www.isiscanada.com.

Issa, C. A., & Salem, G. (2013). Utilization of Recycled Crumb Rubber as Fine Aggregates in Concrete Mix Design. Construction and Building Materials, 42, pp.(48-52).

Issa, M. A., Ovitigala, T., & Westin, N. (2014). Durability of Reinforced Concrete Beams Strengthened with CFRP Sheets. Concrete International, 36(11), pp.(43-48).

Jang, B. S., & Oh, B. H. (2010). Effects of Non-Uniform Corrosion on the Cracking and Service Life of Reinforced Concrete Structures. Cement and Concrete Research, 40(9), pp.(1441-1450).

Jiang, C., Huang, S., Zhu, Y., Lin, Y., & Chen, D. (2016). Effect of Polypropylene and Basalt Fibre on the Behavior of Mortars for Repair Applications. Advances in Materials Science and Engineering, Volume 2016, Article ID 5927609, 11 pages, doi.org/10.1155/2016/5927609.

Kakooei, S., Akil, H. M., Jamshidi, M., & Rouhi, J. (2012). The Effects of Polypropylene Fibres on the Properties of Reinforced Concrete Structures. Construction and Building Materials, 27(1), pp.(73-77).

Kandasamy, S., & Shehata, M. H. (2014). The Capacity of Ternary Blends Containing Slag and High-Calcium Fly Ash to Mitigate Alkali Silica Reaction. Cement and Concrete Composites, 49, pp.(92-99).

Kardos, A. J., & Durham, S. A. (2015). Strength, Durability, and Environmental Properties of Concrete Utilizing Recycled Tire Particles for Pavement Applications. Construction and Building Materials, 98, pp.(832-845).

Karger-Kocsis, J., Mészáros, L., & Bárány, T. (2013). Ground Tyre Rubber (GTR) in Thermoplastics, Thermosets, and Rubbers. Journal of Materials Science, 48(1), pp.(1-38).

Kelly, T. M., Schuman, L., & Hornibrook, F. B. (1948, September). A study of alkali-silica reactivity by means of mortar bar expansions. In ACI J Proc (Vol. 45, No. 1, pp.(57-80).

Kevern, J. T., Halmen, C., & Hudson, D. P. (2015). Evaluation of Resistivity Meters for Concrete Quality Assurance (No. cmr 16-001). Missouri Department of Transportation.

Khitab, A., Arshad, M. T., Hussain, N., Tariq, K., Ali, S. A., Kazmi, S. M. S., & Munir, M. J. (2013). Concrete Reinforced with 0.1 Vol% of Different Synthetic Fibres. Life Science Journal, 10(12s), pp.(934-939).

Kirchhof, L. D., Lorenzi, A., & Silva Filho, L. C. P. (2015). Assessment of Concrete Residual Strength at High Temperatures Using Ultrasonic Pulse Velocity. The E-Journal of Nondestructive Testing, 20 (7).

Kubat, T., Al-Mahaidi, R., & Shayan, A. (2014). Effect of CFRP Wrapping Time on Rehabilitation of Concrete Damaged by Alkali-Aggregate Reaction, in ST Smith (ed.), 23rd Australasian Conference on the Mechanics of Structures and Materials (ACMSM23), Vol. I, Byron Bay, NSW, 9-12 December, Southern Cross University, Lismore, NSW, pp.(471-476). ISBN: 9780994152008.

Kubat, T., Al-Mahaidi, R., & Shayan, A. (2016). CFRP Confinement of Circular Concrete Columns Affected by Alkali-Aggregate Reaction. Construction and Building Materials, 116, pp.(98-109).

Lacasse, C., Labossiere, P., & Neale, K. W. (2003). On Fibre-Reinforced Polymer Rehabilitation of Alkali-Aggregate Reaction-Damaged Beams. Structural Journal, 100(1), pp.(66-74).

Larive, C. (1997). Apports Combinés de L'expérimentation et de la Modélisation à la Compréhension de L'alcali-Réaction et de Ses Effets Mécaniques (Doctoral dissertation, Ecole nationale des ponts et chaussees).

Larive, C., Laplaud, A., & Joly, M. (1996). Behavior of AAR-Affected Concrete: Experimental Data. In Proc. 10th Int. Conf. AAR, Melbourne, Australia, pp.(670-677).

Lataste, J. F., Behloul, M., & Breysse, D. (2008). Characterisation of Fibres Distribution in a Steel Fibre Reinforced Concrete with Electrical Resistivity Measurements. NDT&E International, 41(8), pp.(638-647).

Latifee, E. R., & Rangaraju, P. R. (2014). Miniature concrete prism test: rapid test method for evaluating alkali-silica reactivity of aggregates. Journal of Materials in Civil Engineering, 27(7), DOI: 10.1061/ (ASCE)MT.1943-5533.0001183.

Layssi, H., Ghods, P., Alizadeh, A. R., & Salehi, M. (2015). The Electrical Resistivity of Concrete. Concrete International, 37(5), pp.(41-46).

Lindgård, J., Thomas, M. D., Sellevold, E. J., Pedersen, B., Andiç-Çakır, Ö., Justnes, H., & Rønning, T. F. (2013). Alkali-Silica Reaction (ASR) - Performance Testing: Influence of Specimen Pre-Treatment, Exposure Conditions and Prism Size on Alkali Leaching and Prism Expansion. Cement and Concrete Research, pp.(68-90).

Lopez, W., & Gonzalez, J. A. (1993). Influence of the Degree of Pore Saturation on the Resistivity of Concrete and the Corrosion Rate of Steel Reinforcement. Cement and Concrete Research, 23(2), pp.(368-376).

Malhotra, V. M., & Carino, N. J. (2003). Handbook on Nondestructive Testing of Concrete Second Edition. CRC press.

Markus, R. P. (2013). An investigation of means of mitigating alkali-silica reaction in hardened concrete. Master of Science in Engineering, Texas University, Austin, May 2013.

Marzouk, H., & Langdon, S. (2003). The Effect of Alkali-Aggregate Reactivity on the Mechanical Properties of High and Normal Strength Concrete. Cement and Concrete Composites, 25(4), pp.(549-556).

Masahiro N., Akinori K., Kazunari F., Kazuyuki T. (2013). Evaluation of Maintenance Methods for ASR-Damaged Structures in Hokuriku District, Japan. 3rd International Conference on Sustainable Construction Materials & Technologies, pp.(19-21), August 2013.

McConnell, D., & Irwin, W. H. (1945). Notes on Cement-Aggregate Reaction in Concrete. American Mineralogist, 30(1-2), PP.(78-80).

McCoy, W. J., & Caldwell, A. G. (1951). New approach to inhibiting alkali-aggregate expansion. ACI Journal Proceedings, Vol. 47, Issue 5, pp.(693-706).

Mehta, P. K., & Monteiro, P. J. (2006). Concrete: Microstructure, Properties, and Materials. 2006. 3rd edition, McGraw-Hill Publishing.

Mielenz, R. C., Greene, K. T., & Benton, E. J. (1947, November). Chemical Test for Reactivity of Aggregates with Cement Alkalies; Chemical Processes in Cement-Aggregate Reaction. In Journal Proceedings. Vol. 44, No. 11, pp.(193-222).

Mo, X. (2005). Laboratory Study of LiOH in Inhibiting Alkali–Silica Reaction at 20 ^{o}C: a Contribution. Cement and Concrete Research, 35(3), pp.(499-504).

Mo, X., Zhang, Y., Yu, C., Deng, M., Tang, M., Hünger, K. J., & Fournier, B. (2010). Investigation of Alkali-Silica Reaction Inhibited by New Lithium Compound. ACI Materials Journal, 107(1), pp.(37-41).

Mohamed, I., Curtil, L., Ronel-Idrissi, S., & Hamelin, P. (2005). Influence of Composite Materials Confinement on Alkali Aggregate Expansion. Materials and Structures, 38(3), pp.(387-394).

Mohamed, I., Ferrier, E., Curtil, L., Hamelin, P. (2001). The Role of Composite Materials in Concrete Durability. Case Study of Alkali Aggregate Reaction. FRPRCS-5, Fibre Reinforced Plastics For Reinforced Concrete Structures, Thomas Telford , London 2001, pp.(45-52).

Morris, W., Moreno, E.I. and Sagues, A.A. (1996): Practical Evaluation of Resistivity of Concrete in Test Cylinders Using a Wenner Array Probe, Cement, and Concrete Research, Vol. 26, pp.(1779–1787).

Multon, S. (2003). Evaluation Expérimentale et Théorique des Effets Mécaniques de L'alcali-Réaction sur des Structures Modèles. Doctoral dissertation, Université de Marne-la-Vallée, France.

Multon, S., Leclainche, G., Bourdarot, E., & Toutlemonde, F. (2004). Alkali-silica reaction in specimens under multi-axial mechanical stresses. In Proc. 4th Int. Conf. CONSEC, Vol. 4, Seoul, Korea, 2004, pp.(2004-2011).

Multon, S., Seignol, J. F., & Toutlemonde, F. (2005). Structural Behavior of Concrete Beams Affected by Alkali-Silica Reaction. ACI Materials Journal, 102(2), pp.(67-76).

Musaoglu, O., Turanli, L., & Saritas, A. (2014). Assessing the Effects of Mechanical Preventive Measures on Alkali-Silica Reaction Expansion with Accelerated Mortar Bar Test. Journal of Testing and Evaluation, 42(6), pp.(1520-1529).

Na, O., Xi, Y., Ou, E., & Saouma, V. E. (2016). The Effects of Alkali-Silica Reaction on the Mechanical Properties of Concretes with Three Different Types of Reactive Aggregate. Structural Concrete, 17(1), pp.(74-83).

Nadeem, A., Memon, S. A., & Lo, T. Y. (2013). Evaluation of Fly Ash and Metakaolin Concrete at Elevated Temperatures Through Stiffness Damage Test. Construction and Building Materials, 38, pp.(1058-1065).

Najim, K. B., & Hall, M. R. (2012). Mechanical and Dynamic Properties of Self-Compacting Crumb Rubber Modified Concrete. Construction and Building Materials, 27(1), pp.(521-530).

Narayanan, R., & Darwish, I. Y. S. (1987). Use of Steel Fibres as Shear Reinforcement. ACI Structural Journal, 84(3), pp.(216-227).

Neville, A. M. (2002). Properties of Concrete–Fourth and Final Edition. Harlow, England.

Nili, M., & Afroughsabet, V. (2010). The Combined Effect of Silica Fume and Steel Fibres on the Impact Resistance and Mechanical Properties of Concrete. International Journal of Impact Engineering, 37(8), pp.(879-886).

Oikonomou, N., & Mavridou, S. (2009). Improvement of Chloride Ion Penetration Resistance in Cement Mortars Modified with Rubber from Worn Automobile Tires. Cement and Concrete Composites, 31(6), pp.(403-407).

Onuaguluchi, O., & Panesar, D. K. (2014). Hardened Properties of Concrete Mixtures Containing Pre-Coated Crumb Rubber and Silica Fume. Journal of Cleaner Production, 82, pp.(125-131).

Pacheco-Torgal, F., Ding, Y., & Jalali, S. (2012). Properties and Durability of Concrete Containing Polymeric Wastes (Tyre Rubber and Polyethylene Terephthalate Bottles): An overview. Construction and Building Materials, 30, pp.(714-724).

Pan, J. W., Feng, Y. T., Wang, J. T., Sun, Q. C., Zhang, C. H., & Owen, D. R. J. (2012). Modeling of Alkali-Silica Reaction in Concrete: A review. Frontiers of Structural and Civil Engineering, 6(1), pp.(1-18).

Papadakis, V. G. (2000). Effect of Supplementary Cementing Materials on Concrete Resistance Against Carbonation and Chloride Ingress. Cement and Concrete Research, 30(2), pp.(291-299).

Pelisser, F., Zavarise, N., Longo, T. A., & Bernardin, A. M. (2011). Concrete Made with Recycled Tire Rubber: Effect of Alkaline Activation and Silica Fume Addition. Journal of Cleaner Production, 19(6-7), pp.(757-763).

Piaw, CY. 2006. Basic research statistics. McGraw-Hill Education; 2 edition, 396 p.

Piersanti, M (2015). Testing Recycled Concrete Aggregate Suffering Different Levels of Alkali-Silica Reaction for Use in New Structures of Alkali-Silica Reaction for Use in New Structures. (Master of Applied Science, Ryerson University).

Pimenta Teixeira, K., Perdigão Rocha, I., De Sá Carneiro, L., Flores, J., Dauer, E. A., & Ghahremaninezhad, A. (2016). The Effect of Curing Temperature on the Properties of Cement Pastes Modified with TiO2 Nanoparticles. Materials, 9(11), pp.(952).

Poon, C. S., Kou, S. C., & Lam, L. (2006). Compressive Strength, Chloride Diffusivity and Pore Structure of High-Performance Metakaolin and Silica Fume Concrete. Construction and Building Materials, 20(10), pp.(858-865).

Price, W. H. (1951, February). Factors Influencing Concrete Strength. ACI Journal Proceedings. Vol. 47, No. 2, pp.(417-432).

Qian, C., Chen, C., & Gao, J. (2003). Restrained Alkali-Aggregate Expansion of Concrete Due to External Wrapping and its Mechanism. In High Performance Materials in Bridges, pp.(397-405).

Ramlochan, T., Thomas, M., & Gruber, K. A. (2000). The Effect of Metakaolin on Alkali–Silica Reaction in Concrete. Cement and Concrete Research, 30(3), PP.(339-344).

RILEM, (2000). 106-3,"RILEM Recommended Test Method AAR-3. Detection of Potential Alkali-Reactivity of Aggregates - Method for Aggregate Combinations Using Concrete Prisms,". Materials and Structures, 33, PP.(283-293).

Roy, S. T. R., & Morrison, J. A. (2000). Experience with Alkali-Aggregate Reaction in the Canadian Prairie Region. Canadian Journal of Civil Engineering, 27(2), pp.(261-276).

Rupnow, T., and Icenogle, P. (2011). Evaluation of Surface Resistivity Measurements as an Alternative to the Rapid Chloride Permeability Test for Quality Assurance and Acceptance. Publication FHWA/LA.11/479. Louisiana Department of Transportation, Baton Rouge, Louisiana, 2011, pp.(68).

Rupnow, T., and Icenogle, P. (2012). Surface Resistivity Measurements Evaluated as Alternative to Rapid Chloride Permeability Test for Quality Assurance and Acceptance. Transportation Research Record: Journal of the Transportation Research Board, (2290), pp.(30-37).

Saafi, M. (2000). Design and Fabrication of FRP Grids for Aerospace and Civil Engineering Applications. Journal of Aerospace Engineering, 13(4), pp.(144-149).

Saint-Pierre, F., Rivard, P., & Ballivy, G. (2007). Measurement of Alkali–Silica Reaction Progression by Ultrasonic Waves Attenuation. Cement and Concrete Research, 37(6), pp.(948-956).

Sanchez, L. F. M., Fournier, B., Jolin, M., & Bastien, J. (2014). Evaluation of the stiffness Damage Test (SDT) as a Tool for Assessing Damage in Concrete due to ASR: Test Loading and Output Responses for Concretes Incorporating Fine or Coarse Reactive Aggregates. Cement and Concrete Research, 56, pp.(213-229).

Sanchez, L. F. M., Fournier, B., Jolin, M., & Bastien, J. (2015). Evaluation of the Stiffness Damage Test (SDT) as a Tool for Assessing Damage in Concrete due To Alkali-Silica Reaction (ASR): Input Parameters and Variability of the Test Responses. Construction and Building Materials, 77, pp.(20-32).

Sanchez, L. F. M., Fournier, B., Jolin, M., Bastien, J., & Mitchell, D. (2016). Practical Use of the Stiffness Damage Test (SDT) for Assessing Damage in Concrete Infrastructure Affected by Alkali-Silica Reaction. Construction and Building Materials, 125, pp.(1178-1188).

Sargolzahi, M. (2009). Evaluation of alkali-silica reaction evolution in concrete using ultrasonic tests. Ph.D Thesis, Université de Sherbrooke, Canada, isbn 9780494641965.

Sargolzahi, M., Kodjo, S. A., Rivard, P., & Rhazi, J. (2010). Effectiveness of Nondestructive Testing for the Evaluation of Alkali–Silica Reaction in Concrete. Construction and Building Materials, 24(8), pp.(1398-1403).

Shahroodi, A. (2010). Development of Test Methods for Assessment of Concrete Durability for Use in Performance-Based Specifications. Master's of Applied Science, University of Toronto.

Shayan, A., Xu, A., & Hii, A. (2006). Causes of Deterioration of Precast Bridge Piles: An Experimental Study. In Austroads Bridge Conference, 6th, 2006, Perth, Western Australia.

Shayan, A., Xu, A., & Olasiman, R. (2008). Factors Affecting the Expansion and Cracking of Model Bridge Piles in Seawater, and the Effects of Mechanical Confinement. Road & Transport Research: A Journal of Australian and New Zealand Research and Practice, 17(3), pp.(23).

Shayan, A., Xu, A., & Salamy, R. (2009, May). Effectiveness of CFRP Wrapping in Confining the Expansion of AAR-Affected Concrete. In Austroads 7th Bridge Conference, Auckland, New Zealand, May, pp.(24-26).

Smaoui, N., Bérubé, M. A., Fournier, B., & Bissonnette, B. (2004). Influence of Specimen Geometry, Orientation of Casting Plane, and Mode of Concrete Consolidation on Expansion due to ASR. Cement, Concrete and Aggregates, 26(2), pp.(1-13).

Smaoui, N., Bérubé, M. A., Fournier, B., Bissonnette, B., & Durand, B. (2004). Evaluation of the Expansion Attained to Date by Concrete Affected by Alkali–Silica Reaction. Part I: Experimental study. Canadian Journal of Civil Engineering, 31(5), pp.(826-845).

Smaoui, N., Bérubé, M. A., Fournier, B., Bissonnette, B., & Durand, B. (2005). Effects of Alkali Addition on the Mechanical Properties and Durability of Concrete. Cement and Concrete Research, 35(2), pp.(203-212).

Smaoui, N., Bissonnette, B., Bérubé, M. A., & Fournier, B. (2007). Stresses Induced by Alkali–Silica Reactivity in Prototypes of Reinforced Concrete Columns Incorporating Various Types of Reactive Aggregates. Canadian Journal of Civil Engineering, 34(12), pp.(1554-1566).

Solgaard, A. O. S., Geiker, M., Edvardsen, C., & Küter, A. (2014). Observations on the Electrical Resistivity of Steel Fibre Reinforced Concrete. Materials and Structures, 47(1-2), pp.(335-350).

Song, P. S., & Hwang, S. (2004). Mechanical Properties of High-Strength Steel Fibre-Reinforced Concrete. Construction and Building Materials, 18(9), pp.(669-673).

Song, P. S., Hwang, S., & Sheu, B. C. (2005). Strength Properties of Nylon-and Polypropylene-Fibre-Reinforced Concrete. Cement and Concrete Research, 35(8), pp.(1546-1550).

Soroushian, P., Khan, A., & Hsu, J. W. (1992). Mechanical Properties of Concrete Materials Reinforced with Polypropylene or Polyethylene Fibres. ACI Materials Journal, 89, pp.(535-535).

Spragg, R. P., Castro, J., Nantung, T., Paredes, M., & Weiss, J. (2012). Variability Analysis of the Bulk Resistivity Measured using Concrete Cylinders. Advances in Civil Engineering Materials, 1(1), pp.(1-17).

Spragg, R., Y. Bu, K. Snyder, D. Bentz, and J. Weiss. Electrical Testing of Cement-Based Materials: Role of Testing Techniques, Sample Conditioning, and Accelerated Curing. Publication FHWA/IN/JTRP-2013/28. Joint Transportation Research Program, Indiana Department of Transportation and Purdue University, West Lafayette, Indiana, 2013. https://doi.org/10.5703/1288284315230.

Stanton, T. E. (1940): Expansion of Concrete Through Reaction Between Cement and Aggregate. In Proceedings of the American Society of Civil Engineers (Vol. 66, No. 10, pp.(1781-1812). ASCE.

Sukontasukkul, P., & Tiamlom, K. (2012). Expansion Under Water and Drying Shrinkage of Rubberized Concrete Mixed with Crumb Rubber with Different Size. Construction and Building Materials, 29, pp.(520-526).

Swamy, R. N. (Ed.). (2002). The Alkali-Silica Reaction in Concrete. CRC Press.

Swamy, R. N., & Al-Asali, M. M. (1988). Engineering properties of concrete affected by alkali-silica reaction. ACI Materials Journal, 85(5), pp.(367-374).

Tabatabaei, Z. S., Volz, J. S., Keener, D. I., & Gliha, B. P. (2014). Comparative Impact Behavior of Four Long Carbon Fibre Reinforced Concretes. Materials & Design, 55, pp.(212-223).

Täljsten, B., & Blanksvärd, T. (2008). Strengthening of Concrete Structures with Cement Based Bonded Composites. Nordic Concrete Research, 2(38), pp.(133-153).

Talley, K. G. (2009). Assessment and strengthening of ASR and DEF Affected Concrete Bridge Columns. Doctor of Philosophy, Texas University, Austin.

Tasdemir, C., Tasdemir, M. A., Lydon, F. D., & Barr, B. I. (1996). Effects of Silica Fume and Aggregate Size on the Brittleness of Concrete. Cement and Concrete Research, 26(1), pp.(63-68).

Thomas, B. S., & Gupta, R. C. (2016). A comprehensive Review on the Applications of Waste Tire Rubber in Cement Concrete. Renewable and Sustainable Energy Reviews, 54, pp.(1323-1333).

Thomas, M. (2011). The Effect of Supplementary Cementing Materials on Alkali-Silica Reaction: A review. Cement and Concrete Research, 41(12), pp.(1224-1231).

Thomas, M. D., Fournier, B., Folliard, K. J., Ideker, J. H., & Resendez, Y. (2007). The Use of Lithium to Prevent or Mitigate Alkali-Silica Reactions in Concrete Pavements and Structures, (No. FHWA-HRT-06-133).

Thomas, M., Dunster, A., Nixon, P., & Blackwell, B. (2011). Effect of Fly Ash on the Expansion of Concrete due to Alkali-Silica Reaction–Exposure Site Studies. Cement and Concrete Composites, 33(3), pp.(359-367).

Thomas, M., Fournier, B., Folliard, K., Ideker, J., & Shehata, M. (2006). Test Methods for Evaluating Preventive Measures for Controlling Expansion due to Alkali–Silica Reaction in Concrete. Cement and Concrete Research, 36(10), pp.(1842-1856).

Toutanji, H. (2000). Ultrasonic Wave Velocity Signal Interpretation of Simulated Concrete Bridge Decks. Materials and Structures, 33(3), pp.(207).

Toutanji, H. A., & Gomez, W. (1997). Durability Characteristics of Concrete Beams Externally Bonded with FRP Composite Sheets. Cement and Concrete Composites, 19(4), pp.(351-358).

Toutanji, H., & Balaguru, P. (1998). Durability Characteristics of Concrete Columns Wrapped with FRP Tow Sheets. Journal of Materials in Civil Engineering, 10(1), pp.(52-57).

Toutanji, H., & Ortiz, G. (2001). The Effect of Surface Preparation on the Bond Interface Between FRP Sheets and Concrete Members. Composite Structures, 53(4), pp.(457-462).

Turatsinze, A., & Garros, M. (2008). On the Modulus of Elasticity and Strain Capacity of Self-Compacting Concrete Incorporating Rubber Aggregates. Resources, Conservation and Recycling, 52(10), pp.(1209-1215).

Turatsinze, A., Measson, M., & Faure, J. P. (2018). Rubberised Concrete: from Laboratory Findings to Field Experiment Validation. International Journal of Pavement Engineering, 19(10), pp.(883-892).

Ukita, K. (1989). Effect of Classified Fly Ash on Alkali Aggregate Reaction. In Proceedings of 8th International Symposium of Alkali Aggregate Reaction in Concrete, Kyoto, Japan, 1989, pp.(259-264).

US. (FHWA) (Federal Highway Administration) Department of Transportation (2013): "Alkali-Aggregate Reactivity (AAR) Workshops for Engineers and Practitioners" - Reference Manual, January 2013.

US. Federal Aviation Administration (2004). Handbook for Identification of Alkali-Silica Reactivity in Airfield Pavements. US Department of Transportation, Federal Aviation Administration.

Walsh, J. B. (1965). The Effect of Cracks on the Uniaxial Elastic Compression of Rocks. Journal of Geophysical Research, 70(2), pp.(399-411).

Yang, Z., Weiss, W. J., & Olek, J. (2006). Water Transport in Concrete Damaged by Tensile Loading and Freeze–Thaw Cycling. Journal of Materials in Civil Engineering, 18(3), pp.(424-434).

Yap, S. P., Alengaram, U. J., & Jumaat, M. Z. (2013). Enhancement of Mechanical Properties in Polypropylene–and Nylon–Fibre Reinforced Oil Palm Shell Concrete. Materials & Design, 49, pp.(1034-1041).

Yazıcı, H. "The Effect of Steel Micro-Fibres on ASR Expansion and Mechanical Properties of Mortars." Construction and Building Materials 30 (2012), pp.(607-615).

Yi, C. K., & Ostertag, C. P. (2005). Mechanical Approach in Mitigating Alkali-Silica Reaction. Cement and Concrete Research, 35(1), pp.(67-75).

Yilmaz, A., & Degirmenci, N. (2009). Possibility of Using Waste Tire Rubber and Fly Ash with Portland Cement as Construction Materials. Waste Management, 29(5), pp.(1541-1546).

Yu, B., Liu, J., & Chen, Z. (2017). Probabilistic Evaluation Method for Corrosion Risk of Steel Reinforcement Based on Concrete Resistivity. Construction and Building Materials, 138, pp.(101-113).

Yung, W. H., Yung, L. C., & Hua, L. H. (2013). A study of the Durability Properties of Waste Tire Rubber Applied to Self-Compacting Concrete. Construction and Building Materials, 41, pp.(665-672).

Yurtdas, I., Chen, D., Hu, D. W., & Shao, J. F. (2013). Influence of Alkali Silica Reaction (ASR) on Mechanical Properties of Mortar. Construction and Building Materials, 47, pp.(165-174).

Zhang, Z., Zhang, B., & Yan, P. (2016). Comparative Study of Effect of Raw and Densified Silica Fume in the Paste, Mortar and Concrete. Construction and Building Materials, 105, pp.(82-93).

Zhong, R., Xu, M., Netto, R. V., & Wille, K. (2016). Influence of Pore Tortuosity on Hydraulic Conductivity of Pervious Concrete: Characterization and Modeling. Construction and Building Materials, 125, pp.(1158-1168).

Zollo, R. F. (1997). Fibre-Reinforced Concrete: An Overview After 30 Years of Development. Cement and Concrete Composites, 19(2), pp.(107-122).